UNDERSTANDING BACTERIAL CELL DIVISION PROTEINS USING NOVEL NANOENCAPSULATION METHODS

by

ZOE STROUD

A thesis submitted to the University of Birmingham for the degree of
DOCTOR OF PHILOSOPHY

School of Biosciences
College of Life and Environmental Sciences
University of Birmingham

September 2019

Abstract

The proteins of the *Escherichia coli* divisome are essential for bacterial viability, and have attracted increasing interest as potential targets for new antibiotics. Despite this, very little is known about the structure and function of the FtsBLQ divisomal complex, due to the complexities of studying integral membrane proteins. The development of the use of styrene-maleic acid (SMA) as a solubilisation technique over the past decade offers an alternative strategy for the solubilisation of the complex. SMA solubilises proteins with intact transmembrane regions and the surrounding native lipid environment.

This thesis aimed to establish whether SMA is an effective method for the solubilisation of the FtsBLQ complex. Using SMA, the individual proteins of the FtsBLQ complex were solubilised successfully and characterised by a range of methods. Additionally, the FtsB/FtsL subcomplex was co-expressed and purified, and a model of the association of these proteins was supported with biophysical studies. These results demonstrate that SMA supports the solubilisation of divisomal proteins in the native lipid environment and maintains protein-protein interactions. The application of analytical ultracentrifugation to SMA-solubilised proteins was also investigated, demonstrating the applicability of SMA to a wide range of downstream techniques.

For Grandpa

Acknowledgements

First and foremost, I would like to thank my supervisor, Professor Tim Dafforn, not only for his support and advice during my PhD but also for his continued belief in me for the past six years.

This thesis would not have been possible without the help of all the collaborators I have had the pleasure of working alongside. I firstly thank Professor David Roper, for routinely taking me under his wing and assisting with the cloning presented in this thesis. I also thank Dr Bertrand Raynal, for hosting me in Paris and teaching me everything I know about AUC, and ABRE-MOBIEU for funding the visit. I also cannot forget to thank my funding body, the BBSRC, and the MIBTP training partnership for making this project possible.

After a wonderful six years on the seventh floor, I have so many people to thank. To Dr Sarah Lee, Dr Naomi Pollock and Dr Deborah Ricci, I am so grateful to have had your support throughout my PhD, and I could not ask for better role models as a woman and as a scientist. I am also very grateful to Dr Timothy Knowles and Pooja Sridhar, who have always treated me like one of their own group and have often gone above and beyond to help me. A special thanks goes to Dr Aysha Ali, for keeping me smiling and laughing through the bad days. To the rest of the seventh floor, old and new: Rachael Grime, Stephanie Nestorow, Peter Wotherspoon, Dr Gareth Hughes, Hannah Walters-Morgan, Amber Wilson, Jake Carter, Dr Stephen Hall, Dr Ian Cadby, Dr Richard Logan and of course Rosemary Parslow, you have all been the best co-workers someone could ask for, and I will miss you all terribly.

Finally, I must of course thank my family and friends for their support during this time. Mum and Matt, Dad and Lisa, you've been by my side every step of the way and I can't thank you enough for everything you do. To my wonderful friends, both at home and in Birmingham, thank you for sticking with me even when I only talk about science and cancel on plans because I've got to finish an experiment. Last but definitely not least, to Lewis, thank you for your unwavering love and support through the toughest thing I've ever done, for all the late night lab visits, and for believing in me every single day.

Table of Contents

List of Figures

List of Abbreviations

ABC	ATP-binding cassette
APS	Ammonium persulfate
AUC	Analytical ultracentrifugation
BN-PAGE	Blue native polyacrylamide gel electrophoresis
bp	Base pairs
BSA	Bovine serum albumin
CD	Circular dichroism
CL	Cardiolipin
CV	Column volume
DM	n-Decyl-β-d-Maltopyranoside
DDM	n-Dodecyl-β-D-Maltopyranoside
DLS	Dynamic light scattering
DMPC	1,2-dimyristoyl-sn-glycero-3-phosphocholine
DMSO	Dimethyl sulfoxide
DNA	Deoxyribonucleic acid
DUE	DNA unwinding element
E. coli	*Escherichia coli*
EDTA	Ethylenediaminetetraacetic acid
FRET	Förster resonance energy transfer
FT	Flow-through
Fts	Filamentous temperature sensitive
GPCR	G-protein-coupled receptor
GTase	Glycosyltransferase
HRP	Horseradish peroxidase
IMAC	Immobilized metal affinity chromatography
IPTG	Isopropyl-β-D-thiogalactoside
KOPS	FtsK orienting polar sequences
LB	Luria Bertani
MD	Macrodomain
MSP	Membrane scaffold proteins
Ni-NTA	Nickel- nitrilotriacetic acid
NMR	Nuclear magnetic resonance

OD	Optical density
OG	n-Octyl-β-d-Glucopyranoside
PAGE	Polyacrylamide gel electrophoresis
PBP	Penicillin binding protein
PBS	Phosphate buffered saline
PCR	Polymerase chain reaction
PE	Phosphatidylethanolamines
PG	Phosphatidylglycerol
POTRA	Polypeptide-transport-associated
SAXS	Small angle X-ray scattering
SCE	Sister chromatid exchange
SDS	Sodium dodecyl sulfate
SEC	Size exclusion chromatography
SEDS	Shape, elongation, division and sporulation
SMA	Styrene–maleic acid
SMAnh	Styrene–maleic anhydride
SMALP	Styrene-maleic acid-lipid particle
SMC	Structural maintenance of chromosomes
TEMED	Tetramethylethylenediamine
TLC	Thin-layer chromatography
TM	Transmembrane
TPase	Transpeptidase

CHAPTER 1: INTRODUCTION

The focus of this thesis is the FtsB/FtsL/FtsQ sub-complex of the *Escherichia coli* divisome. To better understand how this complex fits into the broader context of cell division, this introduction will first discuss the *E. coli* cell cycle and its control, and the divisome as a whole. This introduction will then cover the FtsBLQ proteins in detail, and finally, discuss how novel solubilisation methods may be used to assist the study of the FtsBLQ complex and membrane proteins in general.

1.1 *Escherichia coli* Cell Cycle

Unlike in eukaryotes, where the cell cycle can be separated into discrete stages, the process of binary fission in *E. coli* involves many overlapping processes (figure 1.1).

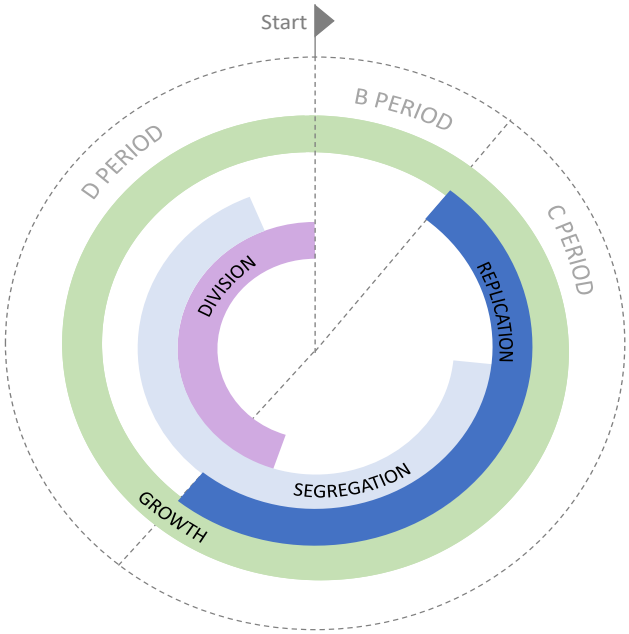

Figure 1.1. **The *E. coli* cell cycle**. The cell cycle is divided into three stages: B, C and D. The B period is a gap phase between division and replication, where no major events take place. The C period is characterised by DNA replication, and D period by division into two daughter cells.

Therefore, to describe the stages of the cell cycle in bacteria, there are three periods: B period, the gap phase between cell division and DNA replication; C period, the period of replication of the chromosome; and D period, where division into two daughter cells takes place (Cooper and Helmstetter, 1968). Fast-growing bacteria with a replication time of fewer than 60 minutes skip the B period, and the next round of DNA replication begins before division is fully completed (Michelsen, 2003).

During these periods, four main processes must be carried out; cell growth, DNA replication, DNA segregation and cell division, as discussed in the next sections.

1.1.1 Cell Growth

Before division can take place, the cylindrical part of the cell must first be elongated to ensure that cell length remains consistent throughout each round of division. Elongation requires the addition of new material to the peptidoglycan sacculus, a layer of peptide cross-linked glycan chains forming a mesh-like structure between the inner and outer membrane which maintains cell shape (reviewed by Vollmer, Blanot and De Pedro, 2008).

The existing links between peptidoglycan chains must first be hydrolysed to allow room for the insertion of new peptidoglycan. Per division, *E. coli* can turn over 40-50% of its existing peptidoglycan (Kraft *et al.*, 1999). *E. coli* has at least 12 periplasmic peptidoglycan hydrolases, however, the structure of the resultant products of hydrolysis implies that lytic transglycosylases, endopeptidases and amidases are involved (Vollmer *et al.*, 2008).

Once these cross-links have been hydrolysed, newly synthesised peptidoglycan can be integrated into the resulting gaps. Peptidoglycan biosynthesis and cross-linking has been

extensively reviewed by publications such as Typas *et al.* (2012) and will only be outlined here in brief (see figure 1.2). Peptidoglycan biosynthesis begins in the cytoplasm, where D-fructose-6-phosphate is converted to UDP-GlcNAc by four successive reactions catalysed by three enzymes; GlmS, GlmM and GlmU (Rodríguez-Díaz, Rubio-Del-Campo and Yebra, 2012). MurA and MurB then catalyse its conversion to UDP-MurNAc, and amino acid ligases MurC, MurD, MurE, MurF catalyse the addition of the pentapeptide sidechain (El Zoeiby, Sanschagrin and Levesque, 2003). MraY then catalyses the transfer of the UDP-MurNAc-pentapeptide to the membrane lipid undecaprenyl phosphate (C55-P), also known as bactoprenol, to form lipid I. The GlcNAc moiety from the previously synthesised UDP-GlcNAc is then transferred to lipid I by MurG to form the peptidoglycan precursor Lipid II (Bouhss *et al.*, 2008).

Lipid II must then be transported across the periplasmic membrane to be polymerised into peptidoglycan. The identity of the Lipid II flippase has been highly debated. Using a bioinformatics approach, Ruiz (2008) identified the membrane-anchored MurJ as a potential flippase, demonstrating its essentiality in *E. coli* and that its depletion inhibited peptidoglycan biosynthesis. However, this was challenged by studies from Mohammadi *et al.* (2011), which instead identified FtsW as the flippase. Using a FRET-based assay, they demonstrated that FtsW in proteoliposomes was able to translocate Lipid II from the inner to the outer leaflet. Further light was shed on this by the development of an *in vivo* flippase activity assay, which found that while MurJ was able to flip Lipid II *in vivo* and that this activity was essential for cell survival, FtsW depleted strains showed no loss of flippase function (Sham *et al.*, 2014). These results suggested that MurJ is the central flippase in *E. coli*.

With FtsW no longer a candidate for a role as a flippase, its role in *E. coli* peptidoglycan synthesis was still yet to be elucidated. FtsW belongs to the shape, elongation, division and sporulation (SEDS) family of proteins along with RodA, and these SEDS proteins are now known to have glycosyltransferase (GTase) activity, polymerising Lipid II monomers in the periplasm into glycan strands (Meeske *et al.*, 2016). FtsW and RodA both complex with a class B penicillin-binding protein (PBP), which can then be cross-linked through the pentapeptides by the PBP's D,D transpeptidase activity (TPase), integrating the newly synthesised peptidoglycan into the sacculus. The RodA/PBP2 pair is a subcomplex of the Rod system, important in the elongation of rod-shaped cells (Rohs *et al.*, 2018), while the FtsW/PBP3 subcomplex makes up a portion of the divisome, which controls cell division (discussed in section 1.2.5). Both GTase and TPase activity can also be carried out by bifunctional class A PBPs such as PBP1A, which is integral for cell elongation (Spratt, 1975).

To direct peptidoglycan assembly to effectively maintain rod-shaped growth, the actin-like protein MreB and its associated proteins MreC and MreD are required. It was originally believed that MreB formed helical "tracks" that guided peptidoglycan insertion through polymerisation treadmilling, however current models suggest that peptidoglycan insertion actually drives MreB polymerisation, and MreB filaments instead may act to impose the direction of insertion perpendicular to the long axis of the cell (Lovering, Safadi and Strynadka, 2012).

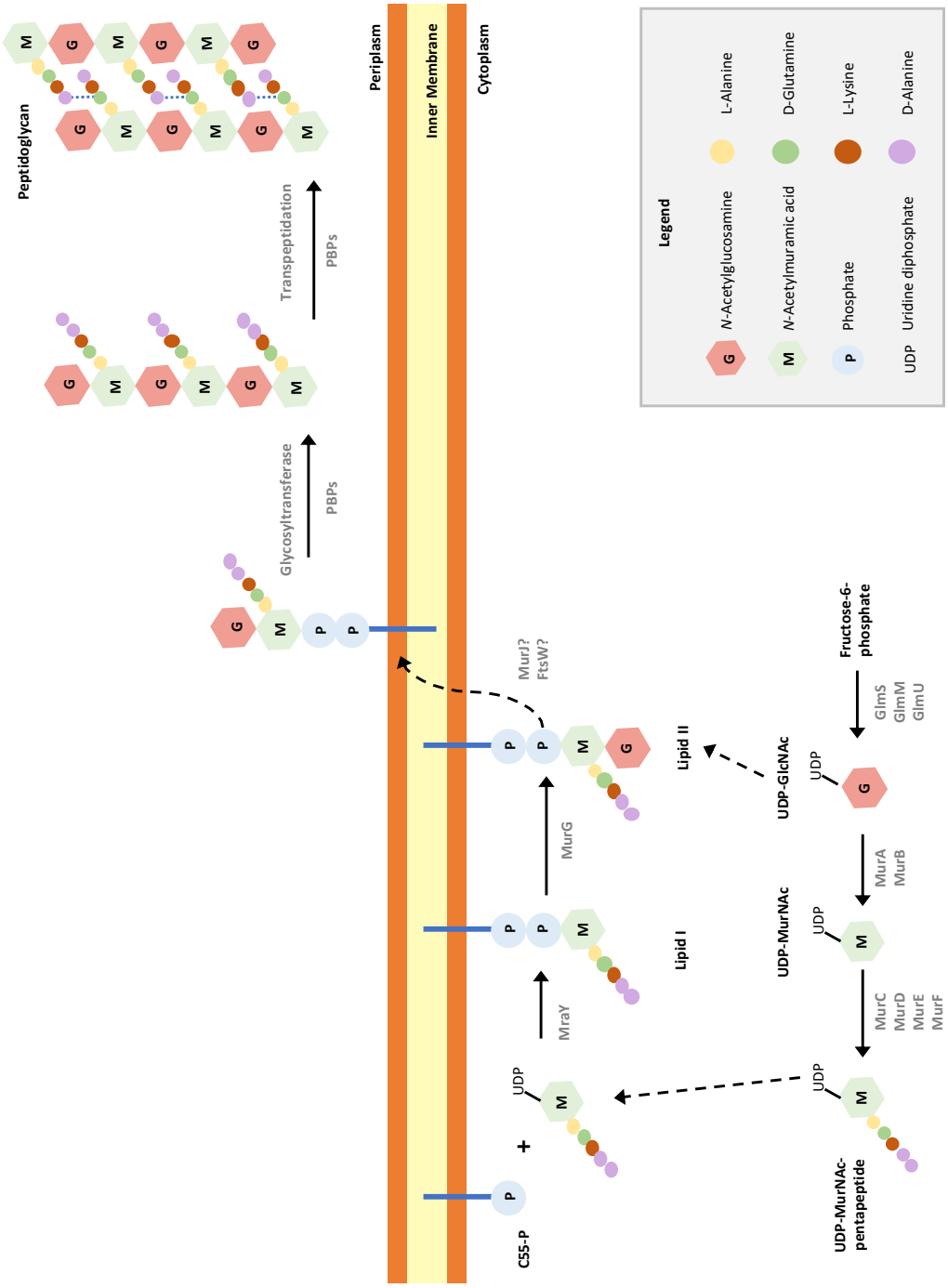

Figure 1.2. **Peptidoglycan synthesis in *E. coli*.** Fructose-6-phosphate is converted to UDP-GlcNAc by GlmS, GlmM and GlmU. MurA and MurB catalyse its conversion to UDP-MurNAc, and amino acid ligases MurC, MurD, MurE, MurF catalyse the addition of the pentapeptide sidechain. MraY catalyses the transfer of the UDP-MurNAc-pentapeptide to undecaprenyl phosphate (C55-P) to form lipid I. GlcNAc is transferred to lipid I by MurG to form Lipid II, which is then flipped across the periplasmic membrane by a flippase, debated to be either MurJ or FtsW. Lipid II monomers are polymerised into glycan strands and cross-linked through the pentapeptides by the activity of penicillin binding proteins (PBPs).

1.1.2 DNA replication

Once the bacterium has reached a particular cell size, called the initiation mass, replication of the chromosome can begin (Donachie, 1968). Replication begins at the *oriC (ori)* region and terminates in the *ter* region, which is also the site of chromosome segregation activities. In addition to *ori* and *ter*, the chromosome of *E. coli* is further organised into four macrodomains (MDs), Ori and Ter (containing *ori* and *ter*, respectively), Left, Right, plus two less-structured regions called the Non-structured (NS) regions, both left and right (figure 1.3).

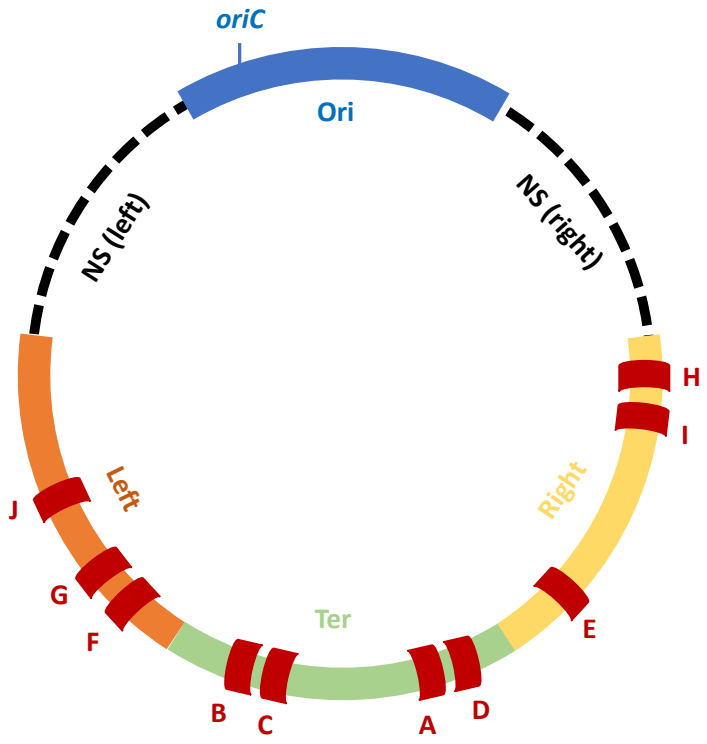

Figure 1.3. ***E. coli* chromosome organisation.** The chromosome can be divided into four macrodomains (Ori, Ter, Right, Left) and two non-structured (NS) regions (right, left). The ten Ter sites (A-J), oriC and dif are indicated in their approximate positions. Adapted from Esnault *et al.* (2007).

DNA replication is initiated at *ori* by DnaA-ATP. Initiation timing is thought to be linked to the initiation mass by the growth-dependent accumulation of DnaA-ATP (Hill *et al.*, 2012). DnaA-ATP binds 9-mer DnaA boxes at *ori* and opens the DNA helix at an A-T rich 13-mer called the DNA unwinding element (DUE), allowing DnaC to deliver DnaB helicase to form a pre-priming complex (Bramhill and Kornberg, 1988). The rest of replisome including Pol III polymerase is then formed at the replication fork, with one replisome on each strand, and the chromosome is replicated in both directions from *ori* (reviewed by Baker and Bell (1998)). The replisomes continue around the chromosome until they meet the terminus region *ter* roughly opposite *ori*. Within the *ter* are ten *Ter* sites (A-J) each bound to the Tus protein. Tus is bound to these *Ter* sites in a way that means each replication fork passes 5 *Ter* sites from a permissive direction and then meet a non-permissive *Ter* site stalling replication (Hill, Henson and Kuempel, 1987). This holds the first arriving replication fork at the terminus region until the other arrives and the final section of the chromosome is replicated.

1.1.3 DNA segregation

To ensure each daughter cell receives a copy of the chromosome, the newly replicated DNA must first be segregated. This process happens concurrently with replication, but the mechanisms involved are poorly understood.

Fluorescence *in situ* hybridisation (FISH) experiments have shed some light on the events during segregation. Firstly, segregation does not occur immediately; most sister loci are seen to separate around 7-10 mins after replication (Joshi *et al.*, 2011). However, some loci show much longer colocalisation, for example, *ori* loci within the Ori MD remain colocalised for

around 15 mins after replication (Bates and Kleckner, 2005). Additionally, four loci (*gln*, *psd*, *yftT* and *fecR*) in the first third of the right replichore segregate at the same time despite being separated by a distance of 0.5 Mb. These loci can be organised into two 'snap regions' that remain colocalised despite the surrounding DNA being segregated.

It is thought that precatenates, interwound replicating sister chromosomes, keep loci colocalised. TopoIV, a type II topoisomerase, usually removes these precatenates during replication. However, SeqA binds to newly replicated hemimethylated DNA and negatively regulates TopoIV until Dam methylation releases SeqA 5-10 mins after replication and allows TopoIV to decatenate and separate the sister chromatids (Joshi *et al.*, 2013). There is also a ten-fold enrichment of SeqA at *gln* over non-snap *dnaB*, and a 25 times enrichment at *ori,* suggesting that increased binding of SeqA keeps these regions colocalised for longer (Joshi *et al.*, 2013). Separation of these snap regions is concomitant with the appearance of bilobed nuclei and global reorganisation of the chromosome. It has been suggested that as in eukaryotic chromosome segregation, the build-up of tension at these regions is important for segregation (Joshi *et al.*, 2011).

During this global reorganisation, the two sister *ori* loci move into position at ¼ and ¾ of the cell length, which will become the midcell of each daughter cell, and the *ter* loci move to midcell (Bates and Kleckner, 2005). The Structural Maintenance of Chromosomes (SMC) complex MukBEF has been proposed as being important for *ori* localisation (Danilova *et al.*, 2007); however, how these proteins control the positioning of *ori* is yet to be described.

There is also still no conclusive model for how the chromosomes are physically reorganised. The first suggested model was that of a membrane tether pulling the chromosomes into place

as the cell elongated (Jacob, Brenner and Cuzin, 1963). However, this was later dismissed because chromosomes segregate faster than elongation can occur. Other models have proposed that segregation may be driven by the entropy of highly confined polymers (Jun and Mulder, 2006) or the polar gradient of the Min system (Di Ventura *et al.*, 2014), but none have been proven as majority source of segregation, suggesting there is still an as-yet-unknown mechanism at work.

After this global reorganisation, at which around 75% of the chromosome has been replicated, the rest of the chromosome segregates concomitantly with replication until only the *ter* region remains colocalised (Bates and Kleckner, 2005). Segregation of the Ter MD is reliant on the appearance of the mechanism for the final stage of the cell cycle, cell division.

1.1.4 Cell division

To complete the cell cycle, the cell must divide at the midpoint into two daughter cells. Division is achieved by a complex of proteins called the divisome, which assembles at mid-cell to execute cell envelope septation, a process discussed in detail in section 1.2. Divisome assembly is precipitated by the formation of the Z-ring, a ring structure of polymerised FtsZ monomers. The placement of the FtsZ ring must be tightly controlled to ensure that division happens at the midcell and not at the poles. This is achieved by two systems in *E. coli*: the Min system and nucleoid occlusion.

The Min system is composed of three proteins: MinC, MinD, MinE, all expressed from the minicell locus *minB* (de Boer, Crossley and Rothfield, 1989). MinC is the effector protein of the system; it inhibits assembly of FtsZ into filaments by sequestering FtsZ monomers, and when

activated by MinD it also destabilises existing interactions between filaments that form bundles (Park *et al.*, 2018). Without MinD and MinE, MinC would be found everywhere in the cell; it is the oscillation of MinD and MinE which controls the localisation of MinC and therefore the position of FtsZ filamentation (figure 1.4a-d). MinD bound to ATP dimerises and associates with the cytoplasmic membrane at one end of the cell, forming a cup at one pole (Raskin and de Boer, 1999). The polar localisation of MinD has been suggested to be as a result of the preference of MinD for anionic phospholipids, which are known to be enriched at cell poles (Mileykovskaya and Dowhan, 2000; Szeto *et al.*, 2003). MinE then localises to the rim of the cup and causes destabilisation by stimulating the ATPase activity of MinD, which induces MinD monomerisation (Hu, Gogol and Lutkenhaus, 2002). The released MinD monomers then diffuse through the cytoplasm to form a new cup at the opposite pole; this behaviour is thought to be driven by MinD localising to the furthest distance from MinE destabilisation (Raskin and de Boer, 1999; Corbin, 2002). MinC is recruited by dimerised MinD-ATP bound to the poles (Hu, Saez and Lutkenhaus, 2003); therefore MinC oscillates with MinD, and the time-averaged concentration of MinC is lowest at the midpoint (Meinhardt and de Boer, 2001), allowing FtsZ filamentation to proceed in this region.

While the Min system is usually sufficient for Z ring placement, the secondary system of nucleoid occlusion can be important for ensuring the septum does not form over nucleoids when segregation has been delayed (Bernhardt and de Boer, 2005).

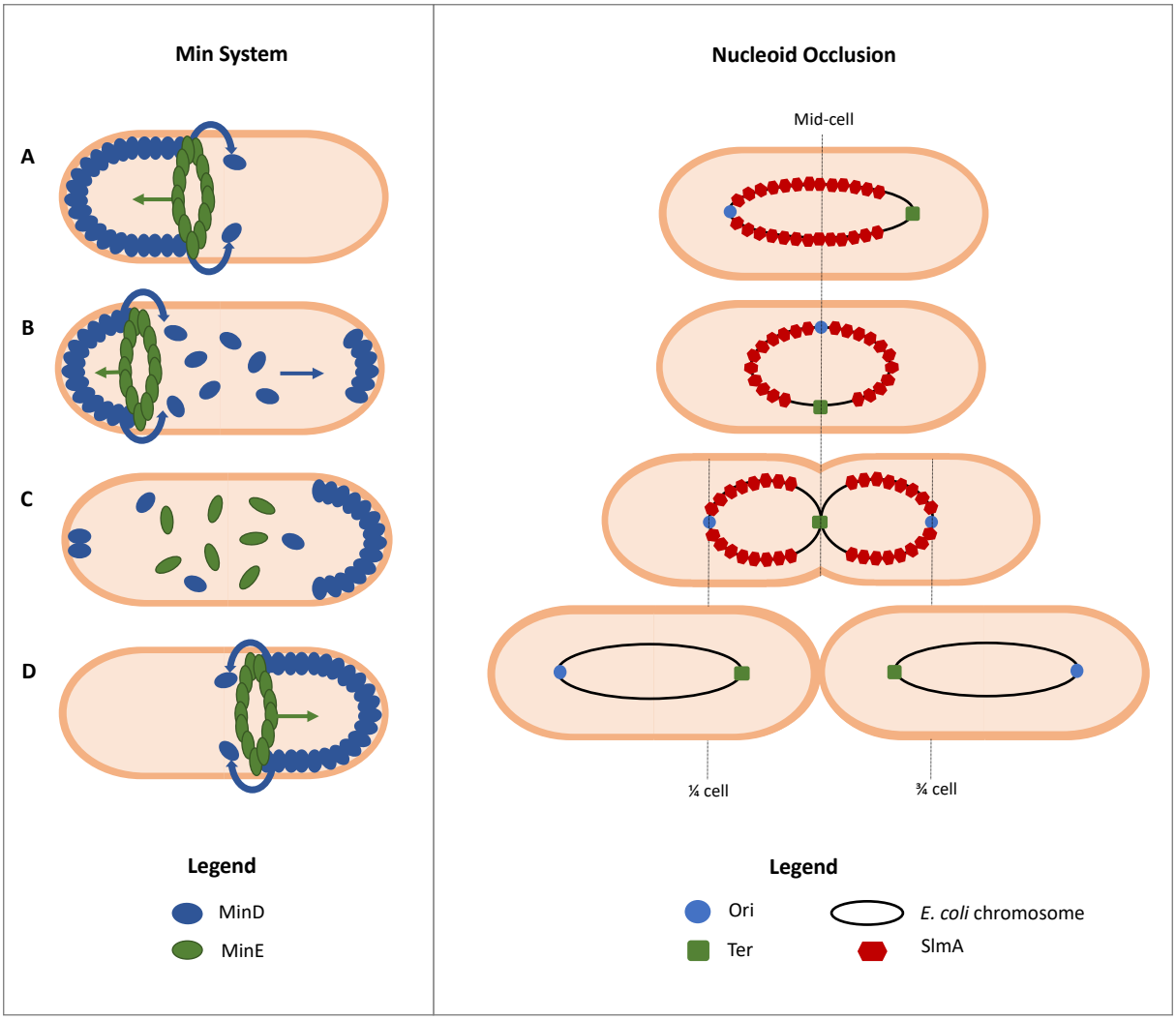

Figure 1.4. **Division site localisation.** In the Min system (left) MinC is the effector protein, inhibiting assembly of FtsZ into filaments. Localisation of MinC is controlled by the oscillation cycle of MinD (blue ovals) and MinE (green circles). MinD forms a cup at one pole, until MinE localises to rim of cup and begins to the destabilise the cup (A). MinD monomers then diffuse through the cytoplasm to form new cup at opposite pole (B). This pattern repeats as an oscillation of Min D and MinE between the poles (C+D). MinC is bound to MinD therefore oscillates with MinD, resulting in the time averaged concentration of MinC being lowest at the midpoint, permitting FtsZ filamentation to proceed in that region. In nuclei occlusion (right) SlmA (red hexagons) binds ZipA and causes depolymerisation of FtsZ polymers. SlmA-binding sequences are found throughout the chromosome except at Ter (green square). As replication progresses, Ter is reoriented to mid-cell while the SlmA bound MDs and Ori (blue circle) move towards ¼ and ¾ length positions, leaving the midcell devoid of SlmA and allowing FtsZ polymerisation to proceed. Adapted from Laloux and Jacobs-Wagner (2014).

Nucleoid occlusion is achieved in *E. coli* by the DNA-associated cell division inhibitor SlmA (Bernhardt and de Boer, 2005), which binds ZipA via the conserved C-terminal tail and causes depolymerisation of FtsZ polymers by an as yet unknown action (Du and Lutkenhaus, 2014). SlmA simultaneously binds DNA whilst bound to ZipA, and SlmA-binding sequences (SBSs) are found throughout the *E. coli* chromosome except at the Ter region (Tonthat *et al.*, 2011). As replication progresses, Ter is reoriented to mid-cell while the SlmA bound MDs and Ori move towards ¼ and ¾ length positions (figure 1.4e), leaving the midcell devoid of SlmA and allowing FtsZ polymerisation to proceed in this region.

Once formed at mid-cell, the proto-ring then recruits downstream proteins to the midpoint; these additional proteins are discussed in more detail in section 1.2. Once divisome assembly is complete, membrane invagination paired with peptidoglycan synthesis forms the septum. The source of the constriction force for invagination of the membrane has long been debated, but current evidence suggests that the force is generated by the transition of FtsZ protofilaments from straight to curved, reviewed in detail by Erickson and Osawa (2017). Peptidoglycan synthesis and remodelling then allow the membrane to follow the constriction of the midpoint, inserting new cell wall until the septum has been closed. Unlike Gram-positive bacteria, where a septum is formed and then cleaved to separate the daughter cells, *E. coli* septum cleavage happens concurrently with the insertion of new cell wall, resulting in a V-shaped constriction at the mid-point (Vollmer *et al.*, 2008). Septum cleavage in *E. coli* is mainly executed by the amidases AmiA, AmiB and AmiC, which cleave the amide bond between the pentapeptide side chain and the glycan backbone; their deletion results in 90-100% of cells growing in chains due to un-cleaved septa (Heidrich *et al.*, 2002).

1.2 The Divisome

As previously discussed, cell division is executed by a complex of proteins called the divisome. The divisome is composed of over 30 proteins, 12 of which are essential or conditionally essential in the process. Many of these are the filamentous-temperature sensitive or 'Fts' proteins, named as such due to the filamentous phenotype of temperature-sensitive mutations in the genes encoding these proteins. The 12 essential proteins are outlined in figure 1.5, and their roles will be further discussed below.

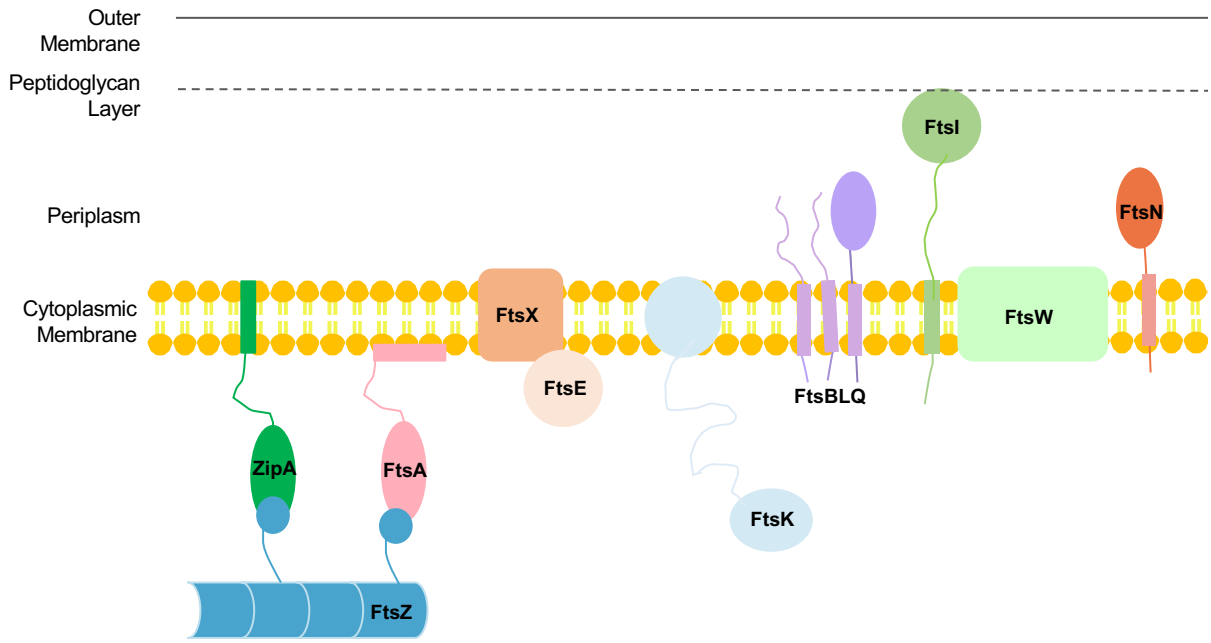

Figure 1.5. **Essential proteins of the *E. coli* Divisome.** 12 proteins have been found to be essential or conditionally essential for cell division in *E. coli*, outlined here with their approximate location and structure.

1.2.1 The Proto-ring: FtsZ, FtsA and ZipA

FtsZ is an ancestral homolog of the eukaryotic tubulin which in the presence of GTP polymerises to form dynamic filaments similar to the protofilaments found in microtubules (Mukherjee, 1998). These filaments form the Z-ring, a ring structure at midcell which recruits downstream proteins and later constricts to drive septum formation and cell separation. The persistence of the Z-ring structure is supported by ZapA, a non-essential cytoplasmic protein which cross-links FtsZ to stabilise longitudinal bonds (Dajkovic *et al.*, 2010).

The Z-ring is tethered to the cytoplasmic membrane by two essential proteins, ZipA and the actin homologue FtsA. While ZipA and FtsA are redundant in their role as membrane tethers, both are necessary for divisome maturation and the completion of cell division (Pichoff, 2002). Inactivating both anchors resulted in the disassembly of preformed Z rings and no formation of new rings, however, FtsZ was still able to localise to the midpoint, suggesting these anchors support the higher-order structuring of FtsZ into stable rings. The localisation of each protein to the septum is dependent on FtsZ, and independent of the other (Addinall and Lutkenhaus, 1996; Liu, Mukherjee and Lutkenhaus, 1999). ZipA is anchored to the membrane by a short transmembrane domain, while FtsA associates which the membrane via a conserved amphipathic helix (Pichoff and Lutkenhaus, 2005). Both proteins interact with FtsZ by binding its C terminal tail; however, mutations of this region affect ZipA and FtsA differently suggesting they bind this region differently (Haney *et al.*, 2001).

The specific role of ZipA and FtsA in cell division other than as anchors is still highly debated. It was thought that ZipA could play a role in the bundling of FtsZ filaments (Hale, Rhee and de Boer, 2000), however recent studies have found that at physiologically relevant

concentrations, ZipA does not promote bundling and may simply act as a passive anchor for FtsZ (Krupka *et al.*, 2018). It has also been shown that FtsA and ZipA can interact directly with each other, implying that these anchors may also regulate each other's behaviour (Vega and Margolin, 2019). Since mutants of FtsA that cannot self-interact bypass the need for ZipA (Pichoff *et al.*, 2012), it has been suggested that FtsA can only recruit downstream proteins when it is monomeric and that ZipA acts to keep FtsA unpolymerised in order to promote divisome assembly. More is known about the recruitment of downstream proteins by ZipA, FtsA and FtsZ. FtsK is the next divisome protein to be recruited to the mid-point, and this requires both FtsA and ZipA (Pichoff, 2002). The further recruitment of downstream proteins continues in a sequential pathway of dependency, outlined by Buddelmeijer and Beckwith (2002), as shown in figure 1.6.

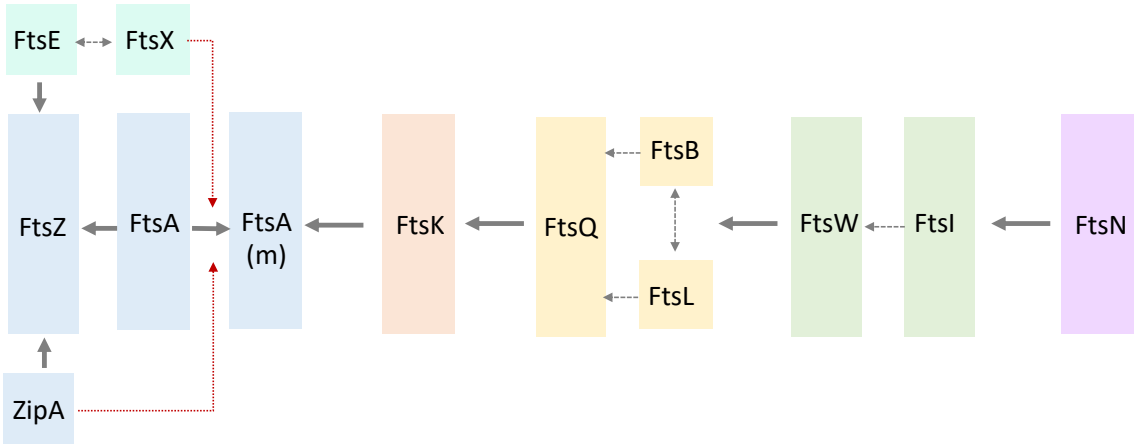

Figure 1.6. **Divisome recruitment pathway.** FtsZ recruits FtsA and ZipA, which act as membrane tethers for the Z ring. FtsZ also recruits the FtsEX complex via FtsE. FtsX and ZipA both keep FtsA in a monomeric state (FtsA(m)), that is permissive for recruitment of downstream proteins. Divisome proteins are then recruited in a step-wise manner. Solid grey arrows indicate upstream dependancy, double headed arrows indicate when localisation is codependant, and red arrows indicate regulation of protein states.

1.2.2 FtsE & FtsX

The ATP-binding cassette (ABC) transporter-like complex FtsEX is recruited to the septum by the proto-ring and is important in downstream recruitment. Recruitment of FtsE and FtsX to the septum is co-dependant and has been recently found to be directed by the interaction of FtsE with the conserved C-terminal peptide of FtsZ (Du *et al.*, 2019). In FtsEX null mutants the early divisome proteins FtsZ, FtsA and ZipA were recruited as normal to the mid-cell, but there were no late proteins recruited including FtsK, FtsQ, FtsL, FtsI and FtsN (Schmidt *et al.*, 2004). This resulted in filamentation and cell death. Interestingly, this defect was only seen when cells are grown in media deficient in NaCl; when the bacteria were grown in 1% NaCl LB they were viable, and late divisome proteins were recruited as in the wild type. As FtsEX is only conditionally essential, this suggests that it probably does not directly recruit downstream proteins but instead stabilises the proto-ring and regulates downstream assembly.

If FtsEX were to act as an ABC transporter as predicted, it would be assumed that the transmembrane regions of FtsX would act as the substrate channel. However, topological analysis of FtsX demonstrated that it contains only four transmembrane segments with no charged amino acids which would be unlikely to support function as a channel (Arends, Kustusch and Weiss, 2009), therefore it is presumed FtsEX does not behave like a typical ABC transporter. FtsX has instead been found to be important for interaction with the proto-ring. FtsX interacts with FtsA in a fashion that supports FtsA recruitment of downstream proteins, as mutations in the region of FtsA that disrupts its interaction with FtsX results in the same phenotype as the FtsEX null mutants in NaCl-free media (Du, Pichoff and Lutkenhaus, 2016). Additionally, FtsA mutants that bypass the need for ZipA also bypasses FtsEX, and these FtsA

mutants cannot self-interact (Du, Pichoff and Lutkenhaus, 2016). Therefore, it has been suggested that FtsEX modulates FtsA in a similar way to ZipA, by maintaining it in its monomeric state and allowing it to recruit downstream proteins.

The ATPase activity of FtsE is not necessary for this control of recruitment; however, it is necessary for the promotion of cell constriction (Arends, Kustusch and Weiss, 2009). FtsEX recruits EnvC to the septum via an FtsX periplasmic loop and activates it in an ATPase dependent manner (Yang *et al.*, 2011). EnvC can then activate the amidases AmiA and AmiB, which hydrolyse the existing cell wall at the septum to allow the separation of daughter cells (Uehara *et al.*, 2010). This dual functionality of activating cell constriction and cell wall hydrolysis places FtsEX as a possible checkpoint to ensure coordination between these two tasks.

1.2.3 FtsK

After the formation of the proto-ring, the first downstream protein to be recruited is FtsK. FtsK has three domains; the N-terminal domain $FtsK_N$, the only domain essential for cell division, a long linker region $FtsK_L$ and a C-terminal DNA translocase $FtsK_C$ (Draper *et al.*, 1998). Little is known about the $FtsK_N$ and $FtsK_L$ domains. $FtsK_N$ acts as a membrane anchor with four transmembrane helices and has been identified as the septum-localising portion of FtsK (Yu *et al.*, 1998). Both $FtsK_N$ and $FtsK_L$ have also been found to recruit downstream divisome components FtsZ, FtsQ, FtsL, and FtsI (Grenga *et al.*, 2008; Dubarry, Possoz and Barre, 2010). $FtsK_C$ is the best-characterised domain of FtsK, especially its role in the resolution of chromosome dimers, as outlined in figure 1.7. Chromosome dimers can occur during

replication of the circular chromosome by recombination between the sister chromatids, known as sister chromatid exchange (SCE). These dimers must be resolved to ensure that the closing septum does not 'guillotine' the dimer as it stretches across midcell. This is achieved by XerC and XerD, site-specific tyrosine recombinases that act at the *dif* site within the Ter domain. XerC and XerD bind cooperatively to both *dif* sites on the chromosome dimer and synapse the two sites via protein-protein interactions (Diagne *et al.*, 2014). XerD catalyses the first strand exchange to make a Holliday junction, which XerC then resolves, resulting in two monomer chromosomes (Grainge, Lesterlin and Sherratt, 2011). $FtsK_C$ loads onto short FtsK Orientating Polar Sequences (KOPS) which are orientated towards *dif*, and translocates the DNA towards the *dif* site until it reaches the XerC/XerD/*dif* complex (Graham *et al.*, 2010). $FtsK_C$ then activates XerD to generate the Holliday junction (Grainge, Lesterlin and Sherratt, 2011).

Because FtsK is localised to the septum, DNA translocation by $FtsK_C$ brings *dif* sites in close proximity at the midcell, allowing the proper formation of the XerC/XerD synapse, and ensures that dimer resolution results in sister chromosomes being segregated to either side of the septum. Interestingly, while only 15% of cells have chromosome dimers, $FtsK_C$ segregation activity has been shown in nearly all dividing cells, suggesting that the role of FtsK in *ter* segregation may extend further than just dimeric chromosomes (Stouf, Meile and Cornet, 2013).

The role of FtsK in both cell division and chromosome segregation led to the postulation that FtsK may act as a checkpoint connecting the clearing of chromosomes from the septum to the completion of septum closure (Dubarry, Possoz and Barre, 2010).

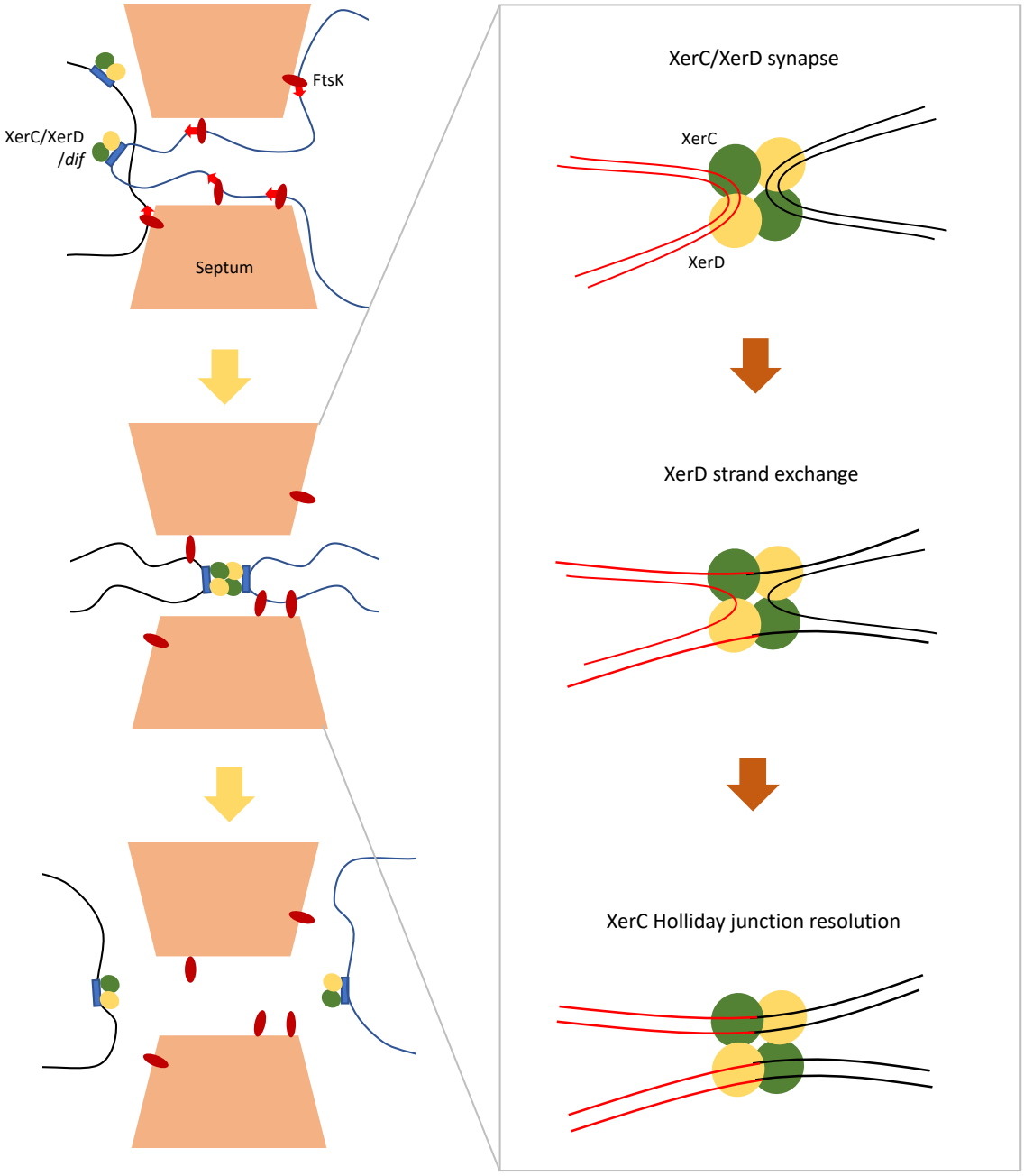

Figure 1.7. **FtsK Dimer Resolution.** Dimeric sister chromosomes are stretched across midcell, and septum closure without separation of the dimer would result in guillotining of the chromosome. FtsK binds to KOPS sequences on the chromosome and translocates (direction shown by red arrows) towards the *dif* sites located in the *ter* region. Inset: This translocation brings XerC/XerD complexes bound to each *dif* site in close contact, allowing synapsis of the two *dif* sites. XerD catalyses first strand exchange to make a Holliday junction, which XerC then resolves, resulting in two monomer chromosomes. Each sister chromosome is then segregated to either side of the septum.

In this model, FtsK stabilises the divisome by forming contacts with both the early divisome (FtsZ) and the late divisome (FtsQ/L/I). However, when $FtsK_C$ is engaging in chromosome dimer resolution, DNA translocation would extend the FtsK linker region and put a strain on $FtsK_N$, destabilising the interactions with the divisome. This could act to halt constriction of the septum until sister chromatids have been fully segregated, at which point FtsK can reform contacts with the divisome and permit constriction.

1.2.4 FtsB, FtsL & FtsQ

Recruited by FtsK, the FtsBLQ complex forms independently of the mid-cell and other divisome proteins and then migrates to the septum (Buddelmeijer and Beckwith, 2004). FtsB and FtsL, both small bitopic membrane proteins, complex with each other in the absence of FtsQ, and this association is postulated to stabilise both the proteins as both proteins are seen to become degraded when overexpressed in the absence of the other (Gonzalez and Beckwith, 2009). The FtsBL complex can then bind to FtsQ primarily via the interaction of the periplasmic domain of FtsQ and C-terminal fragment of FtsB (Choi *et al.*, 2018). FtsQ is recruited to the midcell by FtsK, localising the FtsBLQ complex to the division site (Chen and Beckwith, 2001). FtsQ is localised to the midcell in the absence of FtsB and FtsL; however, the reverse is not true. Similarly, FtsB and FtsL can recruit FtsI and FtsW to the mid-cell in the absence of FtsQ provided the FtsB/FtsL complex was targeted to midcell by fusion with the FtsZ-binding protein ZapA (Goehring, Gonzalez and Beckwith, 2006). As these proteins have no known enzymatic activity, they are therefore postulated to act as a structural 'bridge' between the early and late divisome components. However, recent work has also found that they may play

a more active role in sensing the completion of divisome assembly to initiate constriction (Liu *et al.*, 2015) (see section 1.2.6); therefore a better understanding of the structure and binding of these proteins is needed.

1.2.5 FtsW & FtsI

FtsW was first thought to be a Lipid II flippase (see section 1.1.1), but it is now known that FtsW has peptidoglycan glycosyltransferase (GTase) activity, by which Lipid II is polymerised into glycan strands to produce septal peptidoglycan during cell division (Taguchi *et al.*, 2019). For this GTase activity, FtsW must be in complex with its cognate peptidoglycan binding protein (PBP) FtsI (also called PBP3) (Taguchi *et al.*, 2019). FtsI has been demonstrated to possess transpeptidation activity but is not capable of transglycosylation (Adam *et al.*, 1997), thus is a Class B PBP. FtsI is exclusively involved in the synthesis of septal peptidoglycan (Botta and Park, 1981), reinforcing the similar but separate roles the RodA/PBP2 subcomplex of the elongasome and the FtsW/PBP3 subcomplex of the divisome have in the production of the lateral wall and septal peptidoglycan respectively. Recruitment of FtsW to the septum requires the early and late divisome proteins FtsZ, FtsA, FtsQ, and FtsL but does not require FtsI, while FtsI recruitment relies on FtsW (Mercer and Weiss, 2002). Little more is currently known about this complex, but recent studies determining the substrate preference of FtsW and RodA will open up the possibility of further biochemical and structural studies (Welsh *et al.*, 2019).

1.2.6 FtsN

FtsN is the last of the divisomal proteins to be recruited to mid-cell, requiring FtsA, FtsI and FtsQ for recruitment, and therefore represents the completion of divisome assembly (Addinall, Cao and Lutkenhaus, 1997). FtsN has a cytoplasmic N-terminal, a transmembrane region, and a larger periplasmic domain. The periplasmic region of FtsN has two important functions. Firstly, FtsN localisation to the mid-cell requires the C-terminal sporulation-related repeat (SPOR) domain within this region (Gerding *et al.*, 2009). SPOR domains target proteins to the septum by binding peptidoglycan without peptide sidechains, which are enriched at the septum as a product of amidase activity (reviewed by Yahashiri, Jorgenson and Weiss (2017)). Secondly, the essential function of FtsN is executed by a small 35 residue section of the periplasmic domain, and overexpression of this small peptide in *ΔftsN* cells rescues cell division and viability (Gerding *et al.*, 2009). The N-terminal domain of FtsN has been demonstrated to mediate the interaction of FtsN with FtsA, and this interaction has been postulated to be part of a feedback mechanism to translate the completion of divisome assembly back to the Z ring to initiate constriction (Busiek *et al.*, 2012).

1.2.7 Model for constriction control in *E. coli*

An insight into FtsN's role in cell division has been provided by recent work using bypass mutations. By substituting a single glutamic acid (E56) in FtsB, division in *ΔftsN* cells was restored (Liu *et al.*, 2015). Similarly, some mutant *ftsB and ftsL* alleles could work synergistically to recover Δ*ftsN*. From these results Liu *et al.* (2015) proposed a model for FtsN activation of cell constriction as outlined in figure 1.8. When FtsN levels are low the FtsBLQ

complex in some way suppresses the FtsW/FtsI subcomplex, blocking the production of septal PG. When FtsN levels rise, FtsN somehow switches "on" FtsBLQ, removing its suppression of FtsI/FtsW, allowing septal peptidoglycan to be synthesised. Processing of new PG by amidases leads to more substrate for FtsN and therefore, a positive feedback loop that initiates the formation of the septum and cell constriction.

This model is supported by the recent finding that *in vitro* FtsBLQ can inhibit the activity of PBP1b, a Class A PBP known to interact with FtsW/FtsI and that this inhibition is antagonised by the presence of FtsN (Boes *et al.*, 2019). However, how the on/off switching of FtsBLQ is achieved, and how FtsBLQ affects peptidoglycan synthesis machinery is still unknown; therefore, more in-depth studies are needed to elucidate the precise method of action.

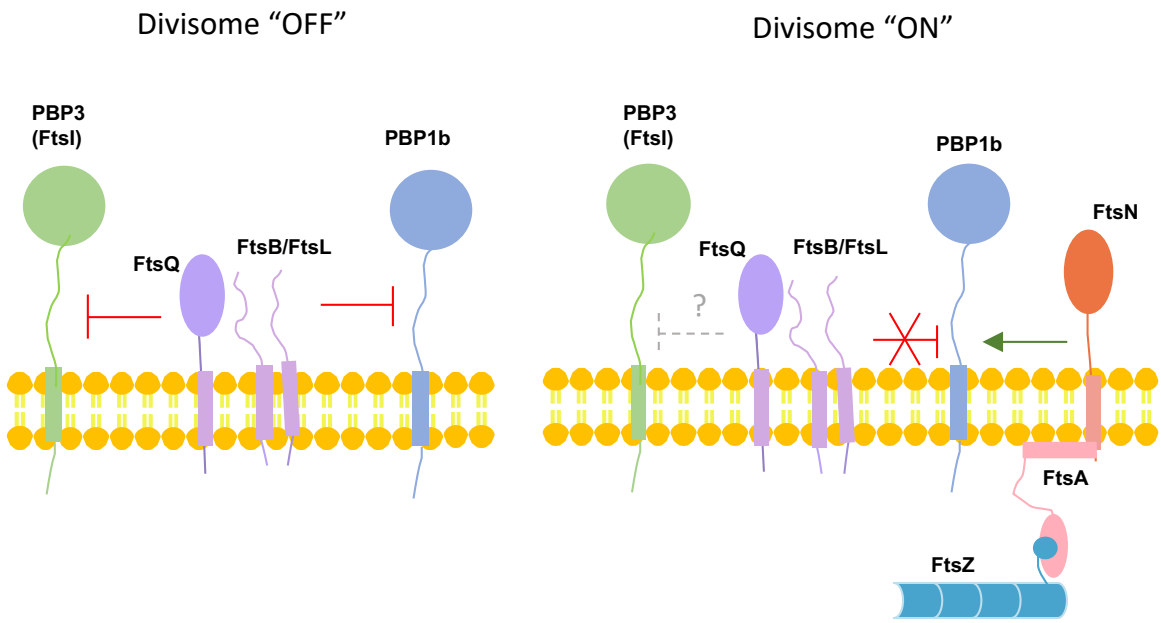

Figure 1.8. **Control of constriction by FtsN.** In the absence of FtsN, the FtsBLQ complex inhibits the activity of PBP3 via FtsQ and PBP1b via FtsL. The localisation of FtsN to midcell suppresses the inhibition of PBP1b, presumably by competing with FtsL, allowing the activation of the peptidoglycan synthesis machinery. The release of suppression by FtsQ is not yet understood. FtsN also interacts with FtsA, allowing the coordination of peptidoglycan synthesis and cell constriction.

1.3 The FtsBLQ Complex

The previous sections have demonstrated the integral role that divisome proteins play in the cell cycle of *E. coli*. In particular, the FtsBLQ complex has been placed at the centre of constriction control, whereby the complex senses the completion of divisome assembly and translates this into the initiation of peptidoglycan synthesis and septum formation (Liu *et al.*, 2015). It is therefore unsurprising that the FtsBLQ complex has been identified as a possible drug target. FtsQ in particular has been highlighted for several reasons: it is well conserved among bacteria, there have been no eukaryotic homologues found, it is present in low copy number, and it interacts with a wide range of downstream division proteins (Glas *et al.*, 2019). Additionally, cessation of cell division caused by the antibiotic mecillinam, which targets PBP2, can be restored by overexpressing FtsQ (Vinella, Cashel and D'Ari, 2000). Despite this, in comparison to many of the other divisome proteins, very little is known about the structure and *in vivo* function of this complex. This thesis aims to contribute additional insight into the FtsBLQ complex. To provide a background understanding, this section will focus on what is currently known about the FtsBLQ complex.

FtsB and FtsL are both small bitopic membrane proteins, with a short cytoplasmic domain, single transmembrane segment and periplasmic domain (figure 1.9). The periplasmic domains of FtsB and FtsL are both predicted to form coiled coils by the COILS program (Lupas, Van Dyke and Stock, 1991) and contain leucine zipper motifs whereby leucine is enriched at the 'd' position of the coiled-coil heptad repeat.

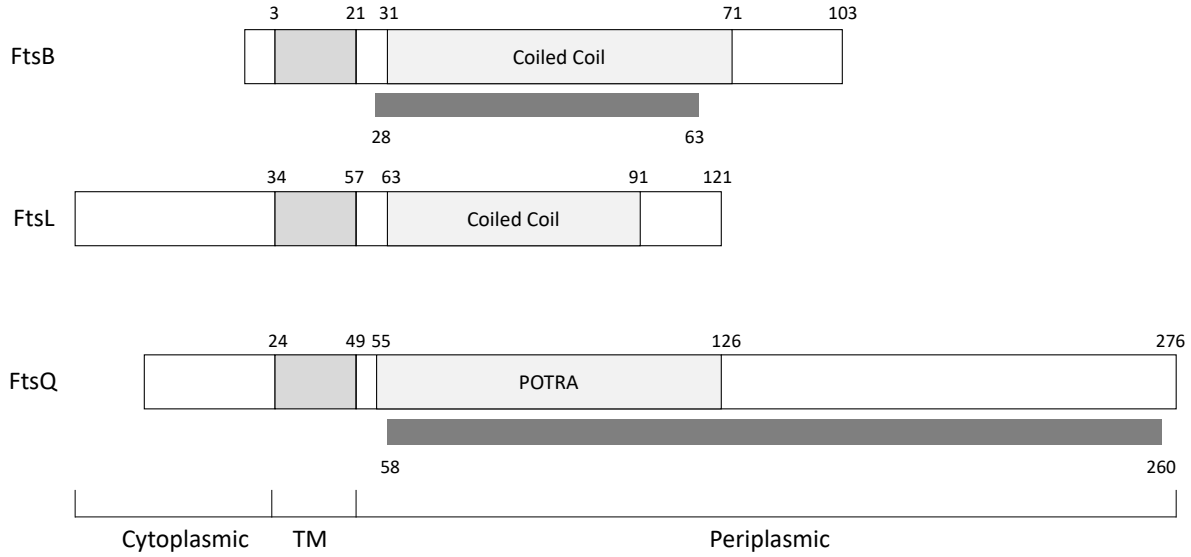

Figure 1.9. **Topology of FtsB, FtsL and FtsQ.** A schematic representation of the topology of FtsB, FtsL, and FtsQ, with structural domains indicated. Numbers represent the final residue position of each section. Transmembrane regions (TM) have been aligned for visual purposes. Dark grey bars represent regions that have crystal structures available. Not drawn to scale.

The predicted coiled-coil region of FtsB (amino acids 28-63) has been successfully crystallised by LaPointe *et al.* (2013), creating a fusion with the bacteriophage Gp7 proteins to support solubility and stabilise coiled coils. The crystal structure (figure 1.10) was solved for a dimeric molecule where the FtsB portion formed a canonical coiled-coil conformation, with hydrogen bonds forming between asparagine residues at the corresponding "a" position on each chain (LaPointe *et al.*, 2013). Although asparagine at the "a" position is destabilising, due to the cost of a polar inclusion into the hydrophobic interface, it has been found to give coiled-coil specificity for a parallel dimer oligomer state (Fletcher *et al.*, 2017), supporting the hypothesis that FtsB does form homodimers.

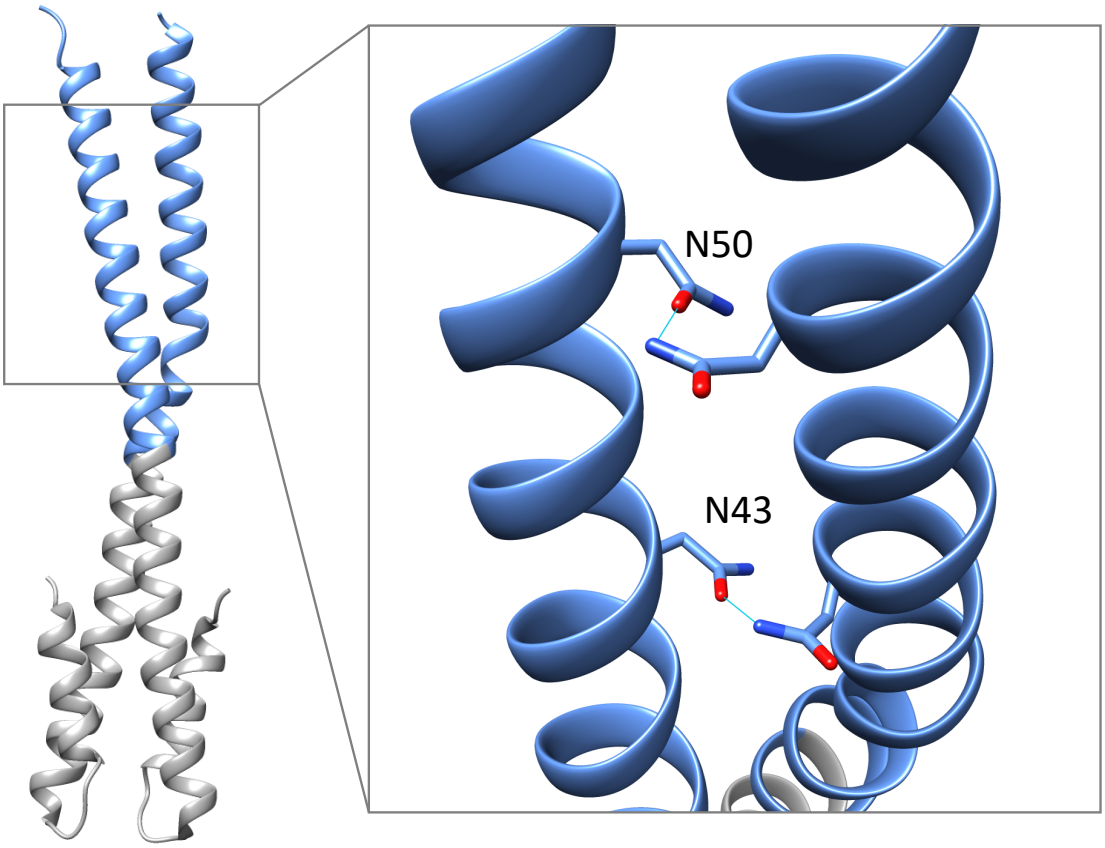

Figure 1.10. **Crystal structure of the *E. coli* FtsB coiled coil domain.** Crystal structure resolved to 2.3 Å of dimeric Gp7-FtsB$_{CC}$ fusion proteins. The bacteriophage Gp7 protein, highlighted in grey, was fused to the FtsB sequence from residue 28-63 representing the coiled coil domain, highlighted in blue. The inset displays the hydrogen bonds formed between corresponding asparagine residues at the "a" positions along the coiled coil. Image was prepared in Chimera with PDB accession number 4IFF (LaPointe et al., 2013).

FtsQ is similarly a bitopic protein, with a short cytoplasmic tail, a single transmembrane spanning region and a periplasmic domain. The periplasmic domain of FtsQ has been successfully crystallised, which revealed that this domain could be separated into two distinct regions (figure 1.11) (van den Ent *et al.*, 2008). The α domain is comprised of a three-stranded β sheet where the second and third strands are separated by two antiparallel α helices, a structure bearing high similarity to the polypeptide-transport-associated (POTRA) domain of YaeT (van den Ent *et al.*, 2008). POTRA domains are more commonly associated with transmembrane β barrels related to transport across the membrane and have been postulated to act in a chaperone-like manner (Sánchez-Pulido *et al.*, 2003).

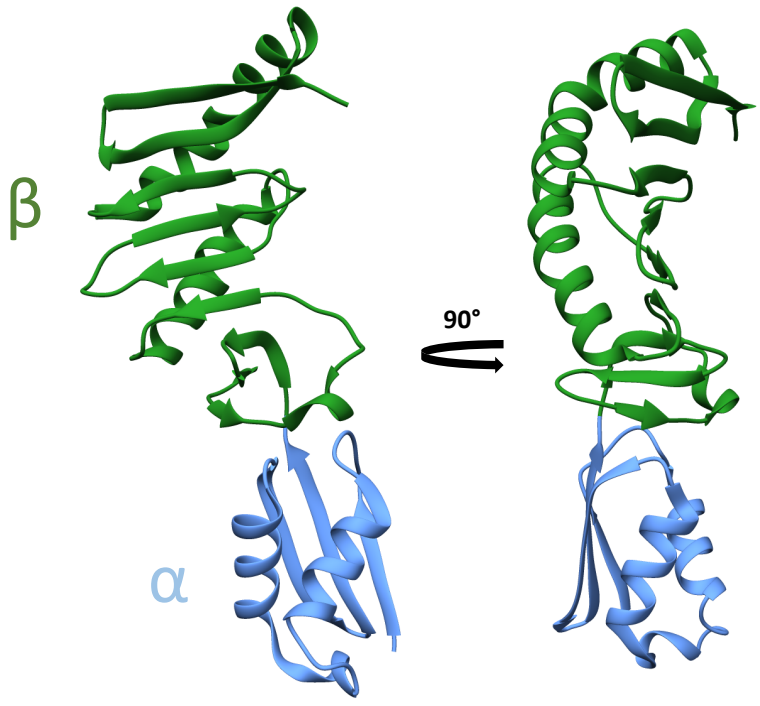

Figure 1.11. **Crystal structure of the *E. coli* FtsQ periplasmic domain.** Crystal structure resolved to 2.7 Å of FtsQ periplasmic domain from residue 58-260. The two structural domains α and β are highlighted in blue and green respectively. Image was prepared in Chimera with PDB accession number 2VH1 (van den Ent et al., 2008).

The POTRA domain of FtsQ was found to be necessary for FtsQ localisation, with mutations affecting localisation most commonly mapping to a solvent-exposed surface proximal to the membrane (van den Ent *et al.*, 2008) The crystal structure revealed a second domain, the β domain, which is composed of nine β strands forming a bent β sheet on top of which is two α helices. This domain was shown by mutagenesis to be involved in the localisation of FtsB and FtsL, with mutations that affected FtsB/FtsL localisation mapping to the surface formed by the two C-terminal β stands and the C-terminal tip of the α helix.

FtsB and FtsL first interact in a manner independent of FtsQ and the mid-cell (Goehring, Gonzalez and Beckwith, 2006). This interaction is predicted to stabilise FtsL as depletion of FtsB in *E. coli* results in a loss of FtsL detection, and in *Bacillus subtilis,* the FtsB homologue DivIC protects FtsL from cleavage by the protease RasP (Buddelmeijer *et al.*, 2002; Wadenpohl and Bramkamp, 2010). Similarly, FtsB is unstable in the absence of FtsL (Gonzalez and Beckwith, 2009). The C termini of FtsB and FtsL are dispensable for the FtsB/FtsL interaction, as interactions are localised to the membrane-proximal residues 4 to 55 of FtsB and residues 38 to 90 in FtsL (Gonzalez and Beckwith, 2009; Gonzalez *et al.*, 2010). The transmembrane (TM) regions of FtsB and FtsL have also been demonstrated to be important for their interaction, as when purified in isolation the TM regions hetero-oligomerise in a 1:1 ratio and purification of the proteins without the TM region has routinely resulted in the abolition of FtsB/FtsL association (Buddelmeijer and Beckwith, 2004; Khadria and Senes, 2013; Glas *et al.*, 2015). The C-terminal domain is instead required for the interaction of the FtsB/FtsL complex with FtsQ, and this interaction protects the C-terminus of FtsB from proteolysis (Gonzalez and Beckwith, 2009). In agreement with this, the *B. subtilis* homologue DivIB (FtsQ) has been

shown to interact with the C-terminal regions of FtsL and DivIC (FtsB) via its β domain (Masson *et al.*, 2009). The coiled coils of FtsB and FtsL are then free to interact with the downstream binding partners FtsI and FtsW.

The role of the FtsBLQ complex was long thought to be a structural bridging of the early and late divisome, as all three proteins have no known enzymatic activity. However, two recent publications have challenged this view. Firstly, specific residue mutations in FtsB and FtsL were found to allow the complete bypass of FtsN essentiality (Liu *et al.*, 2015). Secondly, *in vitro* the FtsBLQ complex can inhibit the glycosyltransferase activity of PBP1b, and that this inhibition was antagonised by FtsN (Boes *et al.*, 2019). Together these results suggest that FtsBLQ may perform a more active role in divisome activity, inhibiting the activity of PBPs and therefore delaying the onset of constriction until the rise in FtsN levels signals the completion of divisome assembly and releases the inhibition.

1.3.1 Solubilisation as a roadblock for the study of the FtsBLQ complex

Despite the possible role of FtsBLQ at the heart of septation initiation control, in comparison to many of the other divisome proteins very little is known about the structure and *in vivo* function of this complex. The detailed study of these proteins separately and in complex has been impeded by the difficulties faced expressing and purifying membrane proteins. To overcome these issues, one solution has been to study the membrane proteins in a soluble form by expressing only the periplasmic regions. However, the periplasmic coiled-coil interactions of FtsB and FtsL have routinely been found to be unstable in isolation. FtsB transmembrane regions were demonstrated to homo-oligomerise *in vivo* when expressed in

isolation, however, to successfully support a homo-dimer of the FtsB periplasmic region, it was necessary to the replace the deleted TM region with the bacteriophage Gp7 protein, a soluble globular protein which forms stable homodimers (Morais *et al.*, 2003; LaPointe *et al.*, 2013). Similarly, while the TM regions of FtsB and FtsL associate into a higher-order oligomer when expressed in isolation (Khadria and Senes, 2013), and FtsB and FtsL are known to interact via their periplasmic domains (Goehring, Gonzalez and Beckwith, 2006), when the periplasmic regions of FtsB and FtsL were expressed the proteins did not copurify or interact by SPR (Glas *et al.*, 2015; Kureisaite-Ciziene *et al.*, 2018). Therefore, many studies using the FtsB-FtsL dimer rely on fusing the proteins to coils of opposite charge, therefore artificially enforcing dimerisation (Masson *et al.*, 2009; Glas *et al.*, 2015; Choi *et al.*, 2018). While these fusion studies have allowed the crystallisation of the periplasmic portion of FtsB, and an insight into the binding domains important in FtsBLQ complex formation, the artificial enforcement of FtsB/FtsL dimerisation may not be an accurate model for the *in vivo* oligomerisation of the complex. A highly debated topic of the FtsBLQ complex has been whether the complex forms a 1:1:1 ternary complex as suggested by Masson *et al.* (2009) and Glas *et al.* (2015), or a 2:2:2 hexamer as per Villanelo *et al.* (2011) and Choi *et al.* (2018).

As discussed in section 1.3, the transmembrane regions of these proteins have been routinely demonstrated to be important for FtsBLQ protein association. Therefore, to further probe the structure and function of the FtsBLQ complex, the solubilisation of full-length protein may support a better understanding of the native oligomerisation states of this complex. However, this strategy presents its challenges as the proteins must then be solubilised from the lipid bilayer. Historically, detergents such as n-Dodecyl-β-D-Maltopyranoside (DDM) have been

used to solubilise membrane proteins from lipid bilayers, but a small number of generically applicable, detergent-free strategies have also been developed. The next section will discuss the current landscape of techniques for membrane protein preparation.

1.4 Techniques for Membrane Protein Solubilisation

Historically, membrane proteins have been solubilised with detergents. Detergents are amphipathic molecules, consisting of a polar hydrophilic head group and a non-polar hydrophobic tail. In the process of membrane protein solubilisation, the hydrophobic tails partition into the lipid bilayer to cause destabilisation and eventual dissolution of the bilayer. This results in the extraction of membrane proteins into soluble micelles with the detergent tails shielding the hydrophobic portion of extracted membrane proteins by forming a torus around the transmembrane region (Le Maire, Champeil and Møller, 2000), and the head groups facing outwards to provide water solubility (figure 1.12).

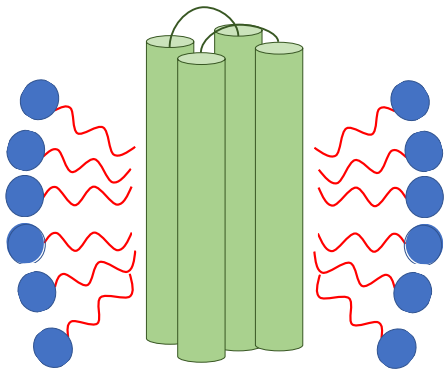

Figure 1.12. **Schematic of a detergent solubilised protein.** Membrane proteins (green) are surrounded by a torus of detergent with the hydrophobic tails (red) interacting with the hydrophobic region of the transmembrane domain and hydrophilic head groups (blue) facing the aqueous environment.

Detergents can be classified into three major groups according to their charge: ionic, non-ionic, and zwitterionic (figure 1.13a-c). Ionic detergents have a charged head group with either a positive (cationic) or negative (anionic) charge. Due to this charge, ionic detergents are relatively harsh and can interfere with protein-protein interactions, causing protein denaturation (Schlager, Straessle and Hafen, 2012). An example of an ionic detergent is sodium dodecyl sulfate (SDS). The denaturing effect of SDS is commonly exploited in SDS-based electrophoresis techniques to ensure proteins migrate efficiently through the gel by shielding the protein's intrinsic charge.

Non-ionic detergents have uncharged head groups and are typically considered to be milder than ionic detergents. Common head groups found in non-ionic detergents are glyosidic groups, such as those found in n-Octyl-β-d-Glucopyranoside (OG), n-Decyl-β-d-Maltopyranoside (DM), and n-Dodecyl-β-D-Maltopyranoside (DDM), polyoxythylene moieties such as that found in TRITON, or PEG-sorbitan units as found in TWEEN. Non-ionic detergents tend to disrupt protein-lipid and lipid-lipid interactions, but leave protein-protein interactions intact, and are therefore commonly the detergent of choice for the solubilisation of membrane proteins; analysis of the 'Membrane Proteins of Known 3D Structure' demonstrated that DDM, DM and OG were collectively used in 66% of membrane protein purifications within the database (Stetsenko and Guskov, 2017).

Zwitterionic detergents such as 3-[(3-Cholamidopropyl)dimethylammonio]-1-propanesulfonate (CHAPS) carry both a positively and negatively charged groups in their head group, rendering them electro-neutral. Because of this, zwitterionic detergents are typically

milder than ionic detergents, but harsher than non-ionic detergents, and may still interfere with protein-protein interactions (Seddon, Curnow and Booth, 2004).

In addition to head-group charge, the length of the detergent alkyl tails can also affect protein stability during solubilisation. Detergents with longer alkyl tails are less likely to cause protein denaturation (Privé, 2007), however, these detergents often produce large micelles, which can make techniques such as crystallisation and NMR difficult (Hitscherich *et al.*, 2000). Shorter chain detergents form smaller micelles and are therefore more suited to crystallisation, but these detergents are often more destabilisating (Privé, 2007). Destabilisation by short chain detergents can be as a result of the disruption of protein-protein or lipid-protein interactions which are important for protein stability (Breyton *et al.*, 1997; Zhou, 2001).

Another major drawback of detergents is that to prevent the aggregation of extracted proteins, the detergent concentration must always be kept above its critical micelle concentration (CMC). Free micelles in solution can act as “hydrophobic sinks” into which stabilising lipids and proteins co-purified with the membrane protein of study can partition (Popot, 2010). Other factors to take into consideration when considering protein instability in detergent micelles include the release of the lateral pressure usually applied by the membrane environment during solubilisation (Rosenbusch, 2001) and the effect of hydrophobic mismatch, where the mismatch between the dimensions of the hydrophobic surface and micelle can cause perturbation in protein structure (Columbus *et al.*, 2009).

To combat the issues associated with the use of conventional detergents, there has been a wide range of techniques developed using novel agents for protein solubilisation, including

novel small amphipathic agents, lipoproteins, peptides and the use of nano-assemblies. The following sections will discuss these techniques and the strengths and weaknesses of their use in the solubilisation of membrane proteins.

A. Ionic Detergent

Sodium Dodecyl Sulfate (SDS)

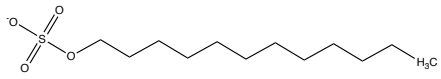

B. Non-ionic Detergent

n-Dodecyl-β-D-Maltopyranoside (DDM)

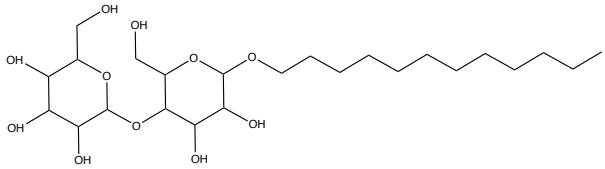

C. Zwitterionic Detergent

CHAPS

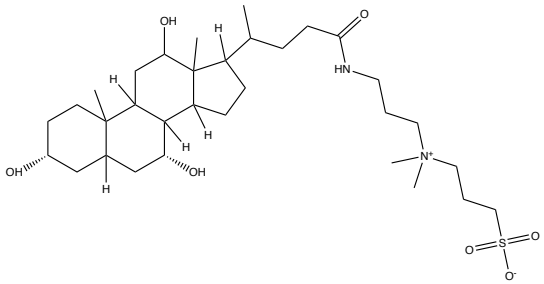

D. Tripod Amphiphile

Tripod Amphiphile 2 (TPA-2)

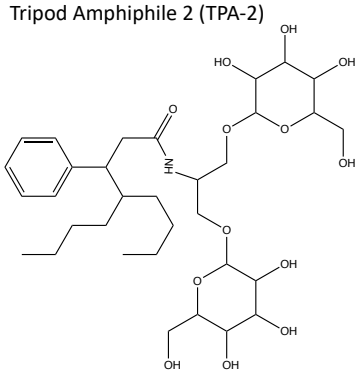

E. Neopentyl Glycol Amphiphile

Maltose Neopentyl Glycol (MNG)

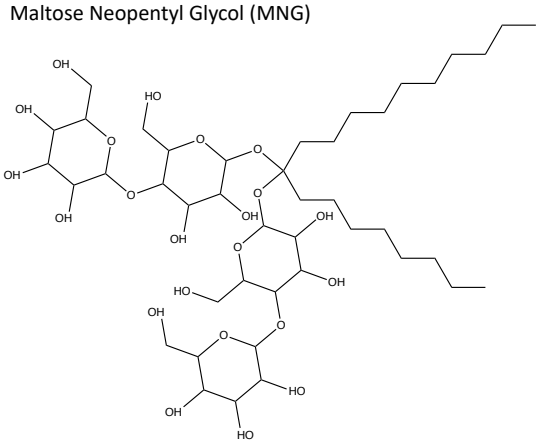

Figure 1.13. **Examples of common detergents and novel amphipathic agents.**

1.4.1 Novel Small Amphipathic Agents

Owing to the difficulties of membrane solubilisation with conventional detergents, a range of small amphipathic compounds have been developed with structures distinct from typical detergents. An example of these novel architectures is tripod amphiphiles (TPAs), amphiphiles with a single hydrophilic appendage and three hydrophobic appendages (figure 1.13d). TPAs were designed to be more conformationally rigid than conventional detergents to promote crystallisation, as conventional detergents typically contain flexible linear alkyl chains which remain disordered during crystallisation (McQuade *et al.*, 2000). Since their introduction, TPAs have been developed extensively to investigate variations of both the hydrophilic and hydrophobic portions (Chae *et al.*, 2008, 2014). TPAs have been demonstrated to extract integral membrane proteins in a functional state with improved stability compared to DDM, and have been successfully used in electron microscopy (Ehsan *et al.*, 2017).

Another class of note is the neopentyl glycol (NG) amphiphiles. Maltose-neopentyl glycol (MNG) amphiphiles were first reported by Chae *et al.* (2010), and are built around a central quaternary carbon atom allowing the incorporation of two hydrophilic and two hydrophobic subunits (figure 1.13e). Glucose-neopentyl glycol (GNG) amphiphiles were later introduced, and although were found to be inferior to MNGs for membrane protein stabilisation, they also resulted in smaller protein-detergent complexes making them more suitable for certain types of crystallisation (Chae *et al.*, 2013). Since their introduction, NG class agents have contributed to the crystal structure determinations of more than 30 new membrane proteins (Ehsan *et al.*, 2017), highlighting the value of small amphipathic agents in the structural studies of membrane proteins.

1.4.2 Amphipols

Detergents can cause particular problems when attempting to study membrane proteins by solution state nuclear magnetic resonance (NMR), as this technique requires the macromolecule to be smaller than about 30 kDa and uses high temperatures to achieve better sensitivity (Kielec, Valentine and Wand, 2010). Detergent-protein complexes on the other hand have a much increased molecular weight and are sensitive to temperature changes (Privé, 2007). To combat this issue, amphipathic polymers, or amphipols were designed. The most commonly studied amphipol, A8-35, is comprised of a short polyacrylate chain where some of the carboxylates are grafted with octylamine or isopropylamine (Tribet, Audebert and Popot, 1996) (figure 1.14a). The polymer associates with the transmembrane region of the protein with a high affinity (figure 1.14b), stabilising the complex in comparison to protein-detergent complexes (Popot, 2010). There is now a wide variety of amphipol and amphipol-like compounds, including modifications such as isotopic labelling, fluorescent labelling and the addition of immobilisation tags (see review by Zoonens and Popot (2014)).

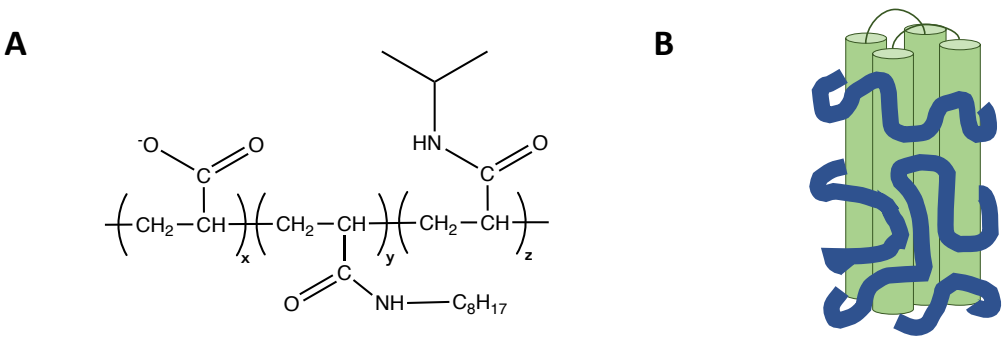

Figure 1.14. **Amphipols** (A) Chemical structure of the A8-35 amphipol, x ≈ 0.35, y ≈ 0.25, and z ≈ 0.4 (Tribet, Audebert and Popot, 1996). (B) Schematic of an amphipol stabilised membrane protein**.**

However, amphipols typically cannot directly solubilise the membrane, therefore a detergent step is still required before transferring to the amphipol system (Popot *et al.*, 2003). Additionally, as the amphipol interacts directly with the protein surface, surrounding lipids are not maintained by the complex.

1.4.3 Nanodiscs

The apolipoprotein apoA-I is the major protein component of human serum high-density lipoproteins (HDLs), emulsion particles comprising lipids and proteins important in the transport of cholesterol to the liver (reviewed by Lund-Katz and Phillips (2010)). When incubated with dimyristoyl phosphatidyl-choline (DMPC) multilamellar vesicles, ApoA-I solubilised the vesicles into 10 nm discoidal structures, whereby ApoA-1 forms a "belt" around the lipid bilayer (Koppaka *et al.*, 1999). Bayburt, Grinkova and Sligar (2002) exploited this behaviour for membrane protein preparation by designing a synthetic gene that expressed proteins based on the amphipathic α-helical segment of the ApoA-I sequence.

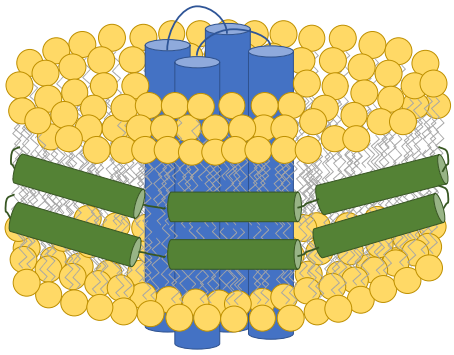

Figure 1.15. **Schematic of a Nanodisc encorporated protein.** Membrane proteins (blue) are embedded into a discoidal structure of lipids (yellow) encircled by membrane scaffold proteins (green).

The proteins were termed membrane scaffold proteins (MSPs) and when detergent was removed from a lipid/cholate/MSP mixture, 10 nm Nanodiscs of lipid surrounded by an MSP belt were demonstrated to self-assemble (Bayburt, Grinkova and Sligar, 2002).

This method was extended to incorporate detergent solubilised cytochrome P450 into the Nanodisc system (Baas, Denisov and Sligar, 2004), and has since been applied to a range of membrane proteins including bacteriorhodopsin (Bayburt, Grinkova and Sligar, 2006), a GPCR (Leitz *et al.*, 2006) and an amino acid transporter (Nasr and Singh, 2014). Compared to the use of detergents alone, this method allows for the solubilisation of membrane proteins into a lipid bilayer, which better recreates the lateral pressure and lipid environment of the native membrane.

However, one drawback of the method is that MSPs cannot directly solubilise membranes, therefore detergent solubilisation of the membrane protein is still required before integration into a Nanodisc. To trigger Nanodisc formation detergents must then be removed by incubation with Bio-beads or a similar alternative, adding an extra cost and time-consuming step to protein preparation. Preparation of proteins with detergent often removes the native lipids surrounding the protein, and although lipids are reintroduced within the Nanodiscs, it can be difficult to fully recreate the native lipid environment surrounding membrane proteins. The effect of lipid composition on the activities of membrane proteins is well documented (see Lee (2004) for a review) and correspondingly Proverbio *et al.* (2013) demonstrated that the choice of lipids within Nanodiscs had a significant effect on the ligand-binding activity of Nanodisc complexed receptors. To circumvent the need for detergents, Nanodiscs have also been used to support the cell-free expression of membrane proteins. Cell-free expression

avoids the issues of toxicity and poor growth caused by overexpression of membrane proteins in *E. coli* by expressing the proteins in an artificial system of translation machinery (Klammt *et al.*, 2004). To avoid precipitation of the newly translated membrane proteins, which must then be solubilised in detergent, the cell-free expression technique has been combined with the provision of detergent micelles (Ishihara *et al.*, 2005) or liposomes (Kalmbach *et al.*, 2007), into which the membrane protein can insert for soluble expression. This approach has also been applied to Nanodiscs, demonstrating that cell-free expression in the presence of Nanodiscs produced soluble Nanodisc-protein complexes (Malhotra and Alder, 2014). This process eliminates the need for detergents in Nanodisc preparation, simplifying the purification process, and allows for high-level expression of membrane proteins into a soluble environment.

Therefore, Nanodiscs offer an alternative to detergents whereby proteins are solubilised into a well-defined lipid bilayer, which can be finely tuned towards optimal solubilisation and activity, however some aspects of the native membrane will not be completely recreated. Additionally, the use of a protein-based scaffold can complicate estimation of target protein concentration and excludes Nanodiscs from some downstream techniques such as nuclear magnetic resonance and circular dichroism.

1.4.4 Styrene Maleic Acid

While each of these methods offers significant improvements over detergent solubilisation, the focus of our lab has been the use of styrene maleic acid (SMA). SMA is the hydrolysed form of styrene maleic anhydride (SMAnh), a copolymer used heavily in the automotive

industry for interior components (Gauthier, 1995), but which can also be found in a range of other products such as carpet shampoos and paper manufacturing (Moutinho, Ferreira and Figueiredo, 2007; Williams, 2007). There is a wide range of SMAnh variants available, each with variations in monomer ratios and molecular weights, but for simplicity, this thesis will only cover SMA2000 (Cray Valley), a 2:1 (styrene/maleic anhydride) variant, and will simply be referenced as SMA hereafter. For a review of SMA polymer variations please see Stroud, Hall and Dafforn (2018).

The behaviour of SMA is largely defined by the pH of its environment. When SMAnh is hydrolysed to SMA, this produces two carboxyl groups which depending on pH can be protonated or deprotonated (figure 1.16). Due to the short distance between the acid groups, there is a large difference between their pKa values, the first being around pH 5.5, and second at pH 8.6 (Scheidelaar *et al.*, 2016). At low pH, the polymer will be completely protonated and will hypercoil as a result of hydrophobic interactions between styrene groups.

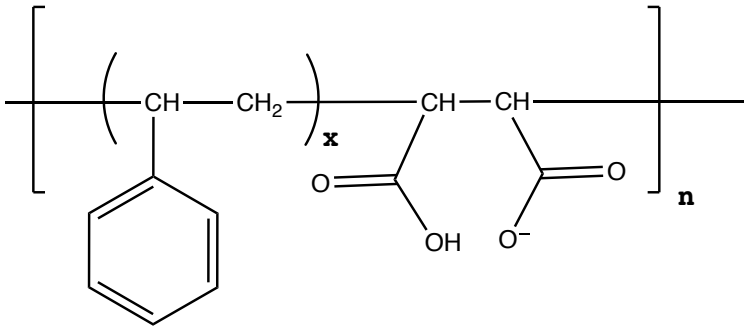

Figure 1.16. **Structure of styrene maleic acid (SMA) copolymer.** SMA is comprised of repeating units of styrene and maleic acid. The ratio of styrene to maleic acid can be altered to change polymer behaviour, and chain length can vary. For SMA produced by the manufacturers Cray Valley, as used in this thesis, x=1-4,6,8 and n=8-12.

When the pH is increased to neutral or high pH, the carboxyl groups are deprotonated and ionic repulsion becomes the predominant factor, leading to an extended chain conformation (Tonge and Tighe, 2001). When mixed with polar lipids, it was found that SMA interacted with the lipid in a pH-dependant manner to form discoidal assemblies with a lipid core surrounded by polymer (Tonge and Tighe, 2003). The effectiveness of SMA for solubilisation of hydrophobic substances was subsequently commercialised by Malvern Cosmeceutical as Lipodisq, a delivery platform for cosmetics and pharmaceuticals capable of penetrating the skin and releasing target compounds (Tonge, 2006).

The application of SMA as a method of membrane protein solubilisation was first reported by Knowles *et al.* (2009). Upon incubation of SMA with phosatidylcholine (PC) liposomes containing transmembrane proteins, roughly 10nm SMA lipid particles (SMALPs) containing said proteins were produced (figure 1.17). The proteins within the discs were confirmed to be folded, active and thermostable, and more amenable to biophysical studies than traditional membrane protein preparation techniques.

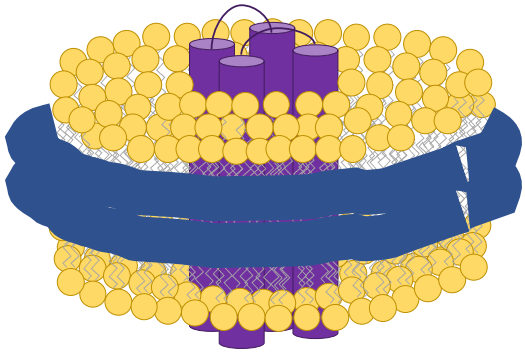

Figure 1.17. **Schematic of a SMALP encorporated protein.** Membrane proteins (purple) are embedded into a discoidal structure of lipids (yellow) encircled by styrene maleic acid (SMA) (blue).

Since this original publication, SMALPs have been used to study proteins from insect, mammalian, bacterial and fungal membranes (Gulati *et al.*, 2014; Jamshad, Charlton, *et al.*, 2015; Logez *et al.*, 2016) using a range of techniques such as cryo- electron microscopy (Parmar *et al.*, 2018; Sun *et al.*, 2018), X-ray crystallography (Broecker, Eger and Ernst, 2017), circular dichroism (Dörr *et al.*, 2014) and hydrogen-deuterium mass spectroscopy (Reading *et al.*, 2017).

A major advantage of using SMA is that it is capable of solubilising membrane proteins without the addition of detergents (Lee *et al.*, 2016). While the exact process of membrane solubilisation by SMA is unknown, work by (Scheidelaar *et al.*, 2015) proposed that SMALP formation is driven by the insertion of SMA copolymers into the hydrophobic core of the membrane due to the hydrophobic interaction between the styrene moieties on the polymer and lipid acyl chains. Much like the action of detergents, this insertion causes membrane destabilisation and solubilisation into discrete lipid particles. These roughly 10 nm lipid particles are stabilised by a "bracelet" of SMA encircling the lipid bilayer (figure 1.16), whereby the styrene ring intercalates between the lipid chains, and the maleic acid group face out into the solvent (Jamshad, Grimard, *et al.*, 2015).

Compared to the requirements of detergent preparations, membrane protein solubilisation using SMA is relatively simplistic. Firstly, hydrolysation of SMA from SMAnh is inexpensive and can be scaled up to requirement, compared to the high cost of purchasing detergents. Secondly, due to the increased stability of SMALP-protein complexes, membrane solubilisation can be carried out at room temperature, unlike many detergents that require solubilisation to take place on ice. After solubilisation, there is no need to supplement buffers

with additional SMA, and excess SMA after solubilisation can be removed by dialysis or other techniques. This simplifies downstream applications once the protein is solubilised as SMALPs can be dialysed into a range of simple buffers compatible with spectroscopic techniques such as CD.

SMALPs have been demonstrated to increase the stability of membrane proteins in comparison to detergent preparations (Knowles *et al.*, 2009; Dörr *et al.*, 2014), and have allowed the identification of distinct lipid profiles across different classes of membrane proteins (Teo *et al.*, 2019). SMALP encapsulated proteins are well documented to retain activity (Knowles *et al.*, 2009; Postis *et al.*, 2015) and are compatible with small molecule binding studies (Gulati *et al.*, 2014; Jamshad, Charlton, *et al.*, 2015). Additionally, compared to the protein scaffold of Nanodiscs, SMA has different optical properties from proteins and therefore does not interfere with spectroscopic techniques such as CD.

1.5 Aims of this study

The previous sections have introduced the FtsBLQ complex and its importance in the *E. coli* cell cycle, and have also discussed the problems faced in its solubilisation and characterisation of the complex. Styrene maleic acid is a polymer that has been successful in the solubilisation of many difficult to study proteins, such as a range of GPCRs (Jamshad, Charlton, *et al.*, 2015). Therefore, the aim of chapter 3 was to establish whether SMA can efficiently solubilise the individual FtsBLQ proteins from the *E. coli* membrane. This “bottom-up” approach to studying each protein in isolation was chosen to simplify data analysis and it allowed for the complex to be pieced together in a well-defined manner.

Membrane proteins solubilised in SMALPs have been successfully characterised using a range of techniques such as circular dichroism (Dörr *et al.*, 2014) and native-PAGE (Pollock *et al.*, 2019). There is limited structural information available for the full-length FtsBLQ proteins in the current literature, therefore the aim of chapter 4 was to investigate whether these techniques could be used to characterise the individual FtsBLQ proteins solubilised into SMALPs.

FtsB and FtsL have been demonstrated to associate in the absence of FtsQ, and before their localisation to the mid-cell (Goehring, Gonzalez and Beckwith, 2006). The aim of chapter 5 was to establish whether SMA can efficiently solubilise the FtsBL subcomplex, and to characterise these complexes using techniques such as native-PAGE and small angle x-ray scattering.

Finally, analytical ultracentrifugation (AUC) is a well-established method for measuring the size distribution of particles within a sample. This method is particularly attractive for the characterisation of membrane proteins within SMALPS as it requires a small amount of protein compared to other biophysical methods. However, the increased complexity of the presence of lipids and polymer within the SMALP samples requires additional characterisation for the accurate measurement of sample size by AUC. Therefore, the aim of chapter 6 was to establish a method for accurately measuring protein complex molecular weight within SMALPs using AUC.

CHAPTER 2: MATERIALS AND METHODS

2.1 Suppliers

Unless stated otherwise, all chemicals and reagents were purchased from Sigma Aldrich.

2.2 General Buffers

Phosphate Buffered Saline (PBS) was prepared by dissolving one Dulbecco 'A' PBS tablet (Oxoid) into 100 mL and autoclaving at 121°C, 1.4 bar for 20 minutes.

2.3 Strains

Table 2.1. ***E. coli*** **strains used in this study.**

Strain	**Supplier**	**Genotype**	**Application**
BL21 (DE3)	New England Biolabs	*fhuA2 [lon] ompT gal (λ DE3) [dcm] ΔhsdS* *λ DE3 = λ sBamHIo ΔEcoRI-B int::(lacI::PlacUV5::T7 gene1) i21 Δnin5*	Protein expression
Subcloning efficiency™ DH5α	Invitrogen™, ThermoFisher Scientific	*F⁻ Φ80lacZΔM15 Δ(lacZYA-argF) U169 recA1 endA1 hsdR17(r_k^-, m_k^+) phoA supE44 thi-1 gyrA96 relA1 λ⁻*	Subcloning
One Shot™ Top10F'	Invitrogen™, ThermoFisher Scientific	F′{*lac*I^q Tn*10* (Tet^R)} *mcr*A Δ(*mrr-hsd*RMS-*mcr*BC) Φ80*lac*ZΔM15 Δ*lac*X74 *rec*A1 *ara*D139 Δ(*ara-leu*)7697 *gal*U *gal*K *rps*L *end*A1 *nup*G	Subcloning
NEB® 5-alpha	New England Biolabs	*fhuA2 Δ(argF-lacZ)U169 phoA glnV44 Φ80 Δ(lacZ)M15 gyrA96 recA1 relA1 endA1 thi-1 hsdR17*	Site-directed mutagenesis

2.4 Plasmids

Figure 2.1. **pET52b(+) plasmid map.** pET52b(+) is an expression vector for the expression of proteins fused with a HRV 3C protease cleavable N-terminal Strep-Tag II and a thrombin cleavable C-terminal His-Tag. The plasmid also contains the *bla* gene for ampicillin resistance, a T7lac promoter, an optimized RBS, and multiple unique restriction enzyme sites (XmaI and SacI shown) in the multiple cloning region (MCR) to facilitate insert transfer.

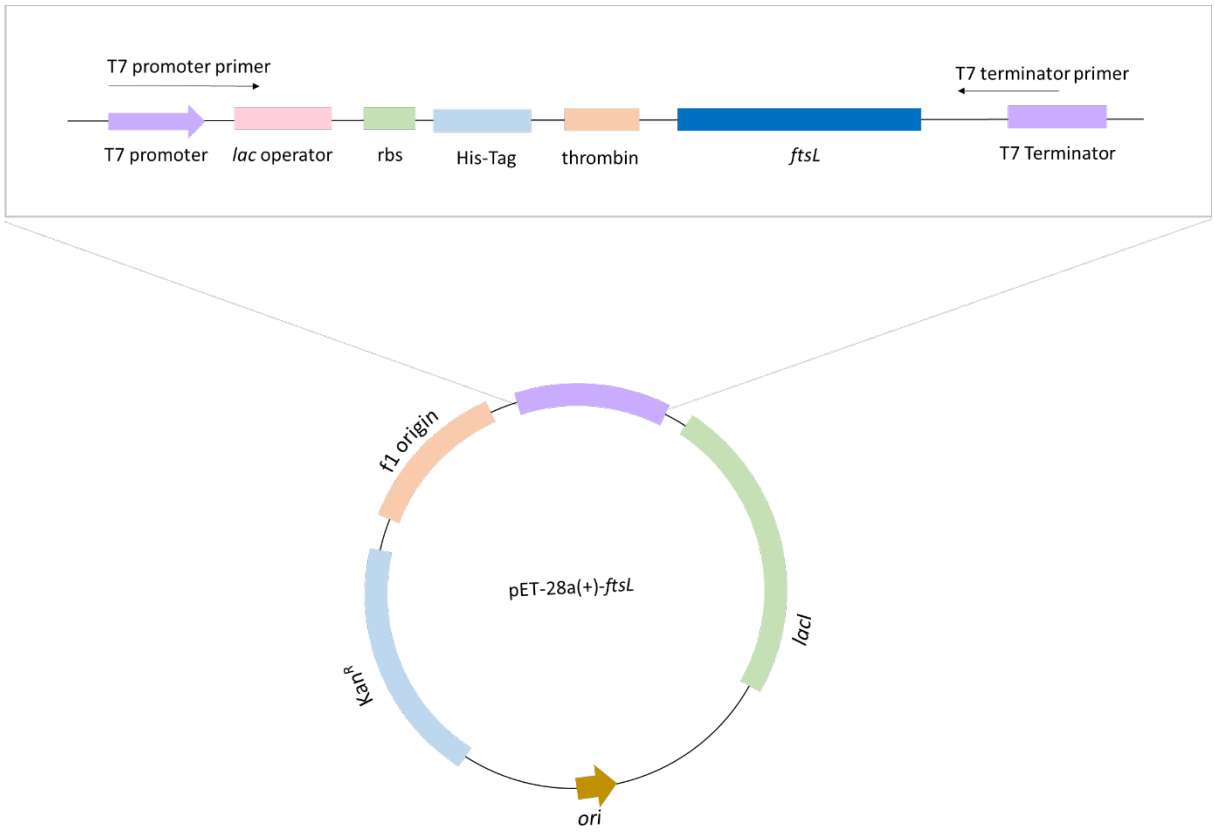

Figure 2.2. **pET28a(+)-*ftsL* plasmid map. pET28a(+)-*ftsL* plasmid map.** pET28a(+)-*ftsL* is an expression vector for the expression of FtsL fused with a thrombin cleavable N-terminal His-Tag. The plasmid also contains the *KanR2* gene marker for kanamycin resistance, a T7lac promoter, and an optimized RBS.

Table 2.2. **Plasmids used in this study.**

Plasmid	Supplier	Description	Plasmid Map
pET-52b(+)	Novagen	Protein expression vector carrying a HRV 3C protease cleavable N-terminal Strep-Tag II and, thrombin cleavable C-terminal His-Tag and ampicillin resistance	Figure 2.1
pET-28a(+)-*ftsL*	Dr Ian Cadby, University of Birmingham	Protein expression vector carrying a His-Tag/thrombin/T7-Tag configuration, kanamycin resistance and the *E. coli* K12 *ftsL* gene	Figure 2.2
pACYCDuet-1	Novagen	Protein expression vector carrying an N-terminal His-Tag in multiple cloning site (MCS) 1, a C-terminal S-Tag in MCS 2, and chloramphicol resistance	Figure 2.3
pET101/DTOPO-*zipA*	Dr Yu-Pin Lin, University of Birmingham	Protein expression vector carrying the *zipA* gene and a C terminal V5 epitope and 6xHis-Tag	See Lin (2011)

2.5 Oligonucleotides

All oligonucleotides were purchased from Sigma, and supplied freeze dried. On receipt, all oligos were diluted to 100 μM stock concentration in sterile deionised water and stored at -20°C. Before use, stock solutions were further diluted to a working concentration of 10 μM in sterile deionised water. Working stocks were also stored at -20°C.

Table 2.3. **Oligonucleotides used in this study.**

Oligo name	Sequence (5' to 3')	Application
Oligonucleotides for sequencing and diagnostic PCR		
T7promoter	TAATACGACTCACTATAGGG	Forward primer for confirming insertions into pET plasmids, annealing site shown in figures

T7terminator	GCTAGTTATTGCTCAGCGG	Reverse primer for confirming insertions into pET plasmids, annealing site shown in figures
ACYCDuetUP1	GGATCTCGACGCTCTCCCT	Forward primer for confirming insertions into pACYC plasmid, annealing site shown in figures
DuetDOWN1	GATTATGCGGCCGTGTACAA	Reverse primer for confirming insertions into pACYC plasmid, annealing site shown in figures
Oligonucleotides for PCR amplification		
Bforward	TTTGCG**CCCGGG**CCCATGGGTAA ACTAACGCTGCTGTTGCTG	Upstream primer for amplification of *ftsB*, incorporating an XmaI restriction site (bold)
Breverse	TTTGCG**GAGCTC**TCGATTGTTTTG CCCCGCAGACTG	Downstream primer for amplification of *ftsB*, incorporating a SacI restriction site (bold)
Lforward	TTTGCG**CCCGGG**CCCATGGTCAG CAGAGTGACAGAAGCTCTAAGC	Upstream primer for amplification of *ftsL*, incorporating an XmaI restriction site (bold)
Lreverse	TTTGCG**GAGCTC**TTTTTGCACTAC GATATTTTCTTGTGACGG	Downstream primer for amplification of *ftsL*, incorporating a SacI restriction site (bold)
Qforward	TTTGCG**CCCGGG**CCCATGGCGCA GGCTGCTCTGAACACGCG	Upstream primer for amplification of *ftsQ,* incorporating an XmaI restriction site (bold)
Qreverse	TTTGCG**GAGCTC**TTGTTGTTCTGC CTGTGCCTGATTTTGTTG	Downstream primer for amplification of *ftsQ*, incorporating a SacI restriction site (bold)
pETduetfront	GTGGTGATGATGGTGATGGCTGC TGCCCATGG	Forward primer for amplification of the pACYCDuet-1 vector for HiFi DNA assembly into MCS 1
pETduetend	TAATGCTTAAGTCGAACAGAAAGT AATCG	Reverse primer for amplification of the pACYCDuet-1 vector for HiFi DNA assembly into MCS 1
HiFiQForward	CATCACCATCATCACCACGAAAAC CTGTATTTTCAGGGCATGTCGCAG GCTGCTCTGAAC	Upstream primer for amplification of *ftsQ* for HiFi DNA assembly
HiFiQReverse	CGATTACTTTCTGTTCGACTTAAGC ATTATTGTTGTTCTGCCTGTGCCTG	Downstream primer for amplification of *ftsQ* for HiFi DNA assembly

2.6 Liquid Growth Media

Luria Bertani (LB) broth powder (Lennox) was prepared to manufacturer's instructions in deionised water and sterilised by autoclaving at 121°C, 1.4 bar for 20 minutes. Media was allowed to cool to room temperature before supplementation with antibiotics and inoculation.

2.7 Solid Growth Media

LB agar was prepared by dissolving LB broth powder as above with the addition of 15 g/L of agar. LB agar was sterilised by autoclaving at 121°C, 1.4 bar for 20 minutes, and allowed to cool to 50°C before supplementation with appropriate antibiotics. LB agar plates were poured and allowed to set under aseptic conditions and stored at 4°C. Plates were pre-warmed at 37°C before use.

2.8 Antibiotics and Supplements

Unless otherwise stated, all stock solutions were made up deionised water. Solutions were filter sterilised with a 0.2 µm syringe filter and stored at -20 °C.

Table 2.4. **Antibiotics and supplements used in this study.**

Antibiotic	**Stock Concentration**	**Working Concentration**
Ampicillin	100 mg/mL	100 µg/mL
Kanamycin	50 mg/mL	50 µg/mL
Chloramphenicol	25 mg/mL (dissolve in EtOH)	25 µg/mL
IPTG	500 mM	0.5 mM

2.9 General cloning techniques

2.9.1 Polymerase Chain Reaction (PCR)

All primers used in PCR amplification are outlined in table 2.5. PCR reactions were assembled on ice with Phusion® High-Fidelity PCR Master Mix with HF Buffer (NEB) to the recipe outlined in table 2.5. Phusion® Master Mix was always added last to avoid the degradation of oligonucleotides by the polymerases' 3´→ 5´ exonuclease activity. Thermocycling conditions are outlined in table 2.6.

Table 2.5. **Phusion® High-Fidelity PCR recipe.**

Component	**Volume for 50 μL reaction**	**Final Concentration**
Forward primer at 10 μM	2.5 μL	0.5 μM
Reverse primer at 10 μM	2.5 μL	0.5 μM
2X Phusion Master Mix	25 μL	1X
E. coli chromosomal DNA (or vector for HiFi)	Appropriate volume for 100 ng	100 ng
Sterile deionised water	Make up to 50 μL final volume	

Table 2.6. **PCR thermocycling conditions**

Stage	**Temperature**	**Time**
Hot Start	98°C	30 seconds
30 X denaturing, annealing and extension	98°C Variable 72°C	10 seconds Variable 10 seconds
Final extension	72°C	10 minutes
Hold	4°C	Indefinite

Prior to downstream use, any successful PCR products were purified from residual primers, nucleotides, and enzymes using QIAquick® PCR purification kit (Qiagen) as per manufacturer's instructions.

2.9.2 Agarose Gel Electrophoresis

A 0.8% (w/v) agarose gel was prepared by adding 0.8 g agarose powder to 100 mL 1X Tris-acetate-EDTA (TAE) buffer (40mM Tris, 20mM acetic acid, 1mM EDTA) and heating until the agarose was fully dissolved. GelRed® Nucleic Acid Gel Stain (Biotium) was added at a 1:10,000 dilution to allow later DNA visualisation. The agarose solution was then cast and allowed to set before use. Samples were prepared by combining 5 μL of sample with 1 μL 6X Purple Gel Loading Dye (New England Biolabs). 1 kb DNA Ladder (New England Biolabs) also was prepared as above. Samples were loaded alongside prepared DNA ladder and gels run at 140V, 400 mA in 1X TAE for 20-30 minutes until the dye front had travelled sufficiently far into the gel. DNA fragments were visualised with a UV light box with an ethidium bromide filter.

2.9.3 Nucleic Acid Quantification

DNA concentration was quantified by measuring the absorbance of the sample at 260 nm and converting to concentration using the modified Beer-Lambert equation:

$$\text{Nucleic Acid Concentration} = \frac{\text{OD}_{260}\ (\text{AU})}{\text{Pathlength (cm)}} \times \text{Standard Coefficient (μg/mL)}$$

Where the standard coefficient for double stranded DNA is 50 μg/mL.

2.9.4 Transformation of Top10F' Chemically Competent Cells

One Shot® TOP10F' Competent Cells (Invitrogen) were transformed with the pET52b-*ftsB*, pET52b-*ftsL* or pET52b-*ftsQ* ligation products, ligation control products, or HiFi assembly products by thawing one 50 μL of cells for each ligation on ice, adding 5 μL of the corresponding ligation reaction and incubating on ice for 30 minutes. Cells were then heat

shocked in a 42°C water bath for exactly 30 seconds, and then quickly placed on ice for 2 minutes. 250 μL prewarmed Super Optimal Broth (SOC) medium (Invitrogen, provided with competent cells) was added to each vial and the vials incubated at 37°C for 1 hour in a shaking incubator shaking at 180 rpm. 100 μL of the transformed cells were plated onto a LB agar plate with the appropriate antibiotic and the plates incubated at 37°C overnight. If the vector control and vector ligation control plates were free from colonies, colonies from the 'Vector+Insert' plate could then be screened for the correct insert by plasmid isolation and sequencing.

2.9.5 Plasmid Isolation

To isolate the plasmid from the freshly transformed cells, single colonies were used to inoculate 5 mL of LB broth containing the appropriate antibiotic, and the culture incubated at 37°C overnight with shaking at 180 rpm. The overnight culture was harvested by centrifugation at 13,000 rpm in a desktop microcentrifuge for 5 minutes at room temperature. Plasmid DNA was then purified using a QIAprep® Spin Miniprep Kit (Qiagen) to the manufacturer's instructions, eluting from the column with 50 μL water.

2.9.6 Diagnostic PCR

To confirm the presence and length of insertions into the plasmid, a diagnostic PCR was carried out. PCRs were performed as in section 2.9.1, except using isolated plasmid instead of chromosomal DNA. The PCR products were then analysed by agarose gel electrophoresis (section 2.9.2).

2.9.7 Plasmid Sequencing

To confirm the sequence of the insertion, isolated plasmids were sequenced with the sequencing primers outlined in table 2.3. Primers were diluted to 3.2 mM in sterile deionised water before use. Samples for sequencing were prepared to the recipe in table 2.7 and then were sequenced by the Functional Genomics Laboratory, University of Birmingham. All inserts were sequenced with both forward and reverse primers to ensure full coverage of the insert.

Table 2.7. **Plasmid sequencing recipe.**

Component	**Volume/Amount**
Template DNA	200-500 ng
Primer	1 μL
Sterile deionised water	Make up to 10 μL

2.10 Cloning by Restriction Digestion

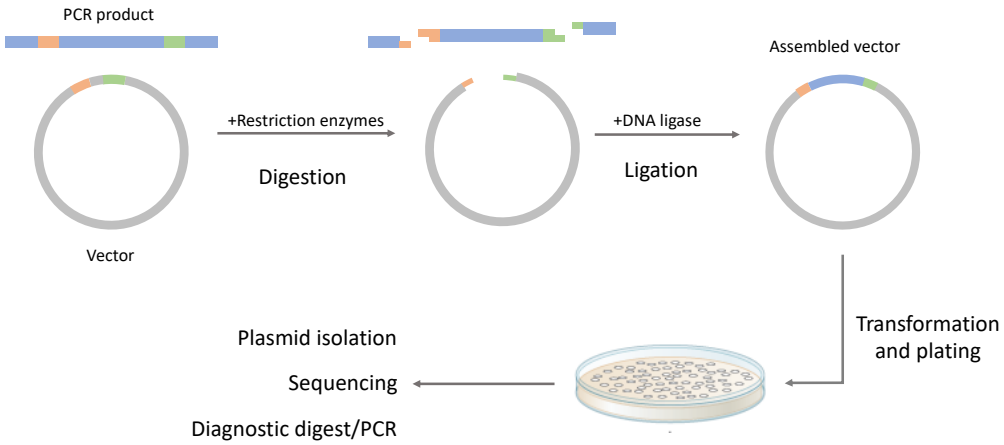

Figure 2.4. **Restriction enzyme digestion cloning.** The gene to be cloned into the vector is amplified by PCR using primers which introduce restriction sites (orange and green) to each end of the gene. The PCR product and vector are digested with the appropriate restriction enzymes, and then ligated together to produce the assembled vector. This vector can then be transformed into *E. coli* and assessed by techniques such as sequencing.

Each gene for cloning was amplified from *E. coli* genomic DNA by PCR as outlined by section 2.9.1, using the primers given in table 2.3. The upstream incorporated an XmaI restriction site onto one end of the gene, and the downstream primer incorporated a SacI restriction site at the other end. These sites could then be used to assemble the genes into the vector by restriction enzyme digest, as outlined in figure 2.4.

2.10.1 Digestion

Amplified gene products and pET52b(+) plasmid were digested with XmaI and SacI in CutSmart® Buffer (NEB) using the recipe in table 2.7. The reactions were incubated at 37°C for 3 hours. The digested plasmid was then further treated with the addition of shrimp alkaline phosphatase (rSAP, NEB) to catalyse the dephosphorylation of the 5' and 3' ends of the newly linearised vector to prevent re-ligation. 1 μL of rSAP was added to the plasmid digestion reaction and incubated for a further 30 minutes at 37°C. rSAP was then inactivated by incubation at 65°C for 5 minutes.

Table 2.8. **Restriction digest recipe.**

Component	**Volume for 50 μL reaction**
DNA	1 μg
10 X Cutsmart® Buffer	5 μL
XmaI	1 μL
SacI	1 μL
Sterile deionised water	Make up to 50 μL

Prior to downstream use, all digestion products were purified from residual primers, nucleotides, and enzymes using QIAquick® PCR purification kit (Qiagen) as per manufacturer's instructions.

2.10.2 Ligation

To ligate the digested PCR product into the linearised vector, ligation reactions using T4 DNA Ligase (NEB) were set up to the recipe in table 2.9 and incubated for 3 hours at room temperature. For efficient ligation, a minimum 1:3 molar ratio of vector to insert is necessary. To ensure that apparent ligation wasn't a result of undigested vector, a vector control with only vector and no ligase was carried out. To ensure that apparent ligation wasn't a result of the vector religating without insert, a vector ligation control with only vector and T4 ligase was carried out.

Table 2.9. **Restriction ligation recipe.**

Component	**Vector+Insert**	**Vector Control**	**Vector Ligation Control**
T4 DNA Ligase Buffer (10X)	2 μL	2 μL	2 μL
Vector DNA	0.020 pmol	0.020 pmol	0.020 pmol
Insert DNA	0.060 pmol	-	-
T4 DNA Ligase	1 μL	-	1 μL
Autoclaved deionised water	Make up to 20 μL	Make up to 20 μL	Make up to 20 μL

2.11 Cloning by Restriction-free Methods

FtsQ was cloned into pACYCDuet-1 (for triple transformation of *ftsB/ftsL/ftsQ*) using restriction free cloning, as outlined in figure 2.5. The *ftsQ* gene was amplified from *E. coli* genomic DNA by PCR as outlined by section 2.9.1, using the primers given in table 2.3. Similarly, the pACYCDuet-1 vector was amplified by PCR, using primers that would linearise the vector in the first cloning site, designing primers in a way which removes the His-Tag (figure 2.3). The primers were also designed to introduce overlapping ends, which could then be used to assemble the genes into the vector.

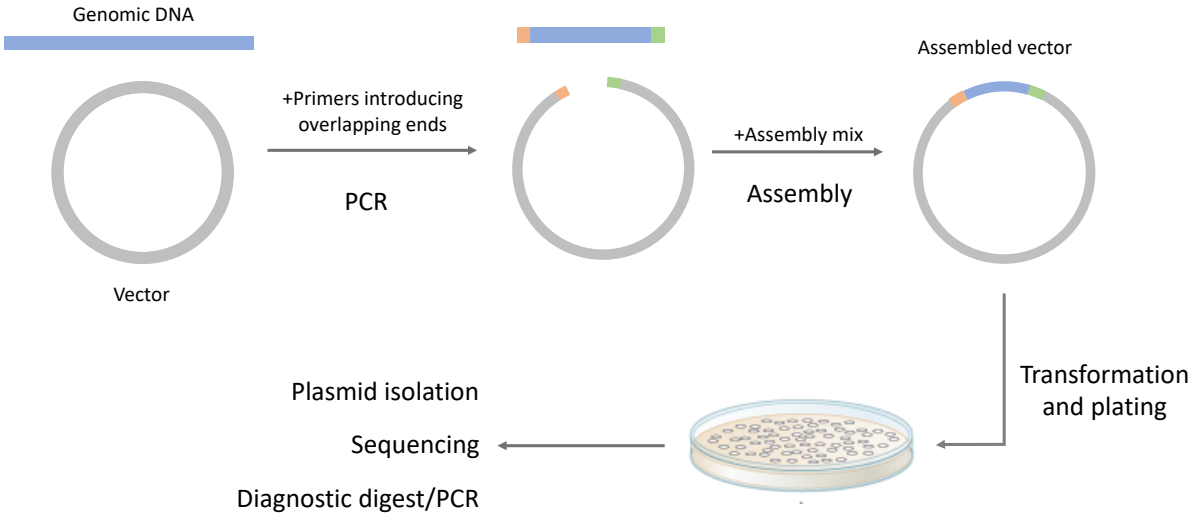

Figure 2.5. **Restriction-free cloning.** The gene and the vector are amplified by PCR using primers which introduce overlapping ends (orange and green) to each end. The PCR product and vector are then incubated with exonucleases, DNA polymerase and DNA ligase to produce the assembled vector. This vector can then be transformed into *E. coli* and assessed by techniques such as sequencing.

Table 2.10. **HiFi DNA Assembly Protocol.**

Component	**Volume for 20 μL reaction**
Vector	50 ng
Insert	100 ng
NEBuilder HiFi DNA Assembly Master Mix	10 μL
Sterile deionised water	Make up to 50 μL

The amplified vector and insert were assembled with NEBuilder® HiFi DNA assembly cloning kit (New England Biolabs) using the recipe in table 2.10. The reaction was set up on ice, and then incubated at 50°C for 15 minutes. Samples were stored at -20°C until needed for subsequent transformation of competent cells.

2.12 Site Directed Mutagenesis

Mutagenesis was carried out using the Q5® site-directed mutagenesis kit (New England Biolabs). Primers for mutagenesis were designed using the online NEBaseChanger tool (New England Biolabs), to introduce the desired mutation. Primers used are given in table 2.3. Reagents were assembled for PCR amplification was as given in the recipe in table 2.11, and PCR was performed using the thermocycling conditions given in table 2.12.

Table 2.11. **Q5® site-directed mutagenesis PCR recipe.**

Component	**Volume for 25 μL reaction**	**Final Concentration**
Forward primer at 10 μM	1.25 μL	0.5 μM
Reverse primer at 10 μM	1.25 μL	0.5 μM
Q5® hot start high-fidelity 2X master mix	12.5 μL	1X
Template DNA (1-25 ng/μL)	1 μL	1-25 ng
Sterile deionised water	9 μL	

Table 2.12. **Q5® site-directed mutagenesis PCR thermocycling conditions**

Stage	Temperature	Time
Hot Start	98°C	30 seconds
30 X denaturing, annealing and extension	98°C Variable 72°C	10 seconds Variable 3 minutes
Final extension	72°C	2 minutes
Hold	4°C	Indefinite

The PCR products were then assembled for kinase, ligase and DpnI (KLD) treatment using the recipe in table 2.13. The sample was thoroughly mixed by pipetting and incubated at room temperature for 5 minutes. Samples were stored at -20°C until needed for subsequent transformation of competent cells.

Table 2.13. **Q5 site-directed mutagenesis kinase, ligase and DpnI (KLD) treatment recipe.**

Component	Volume
PCR product	1 μL
2X KLD reaction buffer	5 μL
10X KLD enzyme mix	1 μL
Sterile deionised water	3 μL

2.13 Preparation of Styrene Maleic Acid

Styrene maleic acid was prepared using the method given in Lee *et al.* (2016). In short, styrene maleic anhydride co-polymer was refluxed in 1 M NaOH for 2 hours, and allowed to cool. The polymer was then precipitated by the addition of concentrated HCl, until the pH of the solution was <5. To wash the precipitate, the polymer suspension was centrifuged at 11,000

x g at room temperature for 15 minutes, and the supernatant discarded. The pelleted polymer was re-suspended in distilled water and again centrifuged at 11,000 xg at room temperature for 15 minutes. These washing steps were repeated twice, and then the polymer was dissolved in 0.6 M NaOH at 37°C overnight in an orbital shaker. Once re-dissolved, the polymer was again precipitated with HCl, washed three times in water and re-dissolved in 0.6 M NaOH. The pH of the solution was then adjusted to 8.0 using concentrated HCl or NaOH, and then the solution was frozen at -20°C. Once frozen, the polymer was freeze dried to a fine powder and stored at room temperature.

2.14 Protein Overexpression in *E. coli*

2.14.1 Transformation of BL21(DE3) Competent Cells

For high level protein expression, plasmids containing the gene for the protein in question were transformed into BL21(DE3) Competent *E. coli* (New England Biolabs). Vials of competent cells were thawed on ice, 1–5 μL containing 1 pg–100 ng of plasmid DNA was added to the cells and the cells were left on ice for 30 minutes. Cells were then heat shocked in a 42°C water bath for exactly 10 seconds, and then quickly placed on ice for 5 minutes. 950 μL pre-warmed Super Optimal Broth (SOC) medium (New England Biolabs, provided with competent cells) was added to each vial and the vials incubated at 37°C for 1 hour in a shaking incubator shaking at 180 rpm. 100 μL of the transformed cells were plated onto a LB agar plate with the appropriate antibiotic and the plates incubated at 37°C overnight.

2.14.2 Preparation of Glycerol Stocks

For long term storage of transformed cells, glycerol stocks were prepared. A single colony from a LB agar plate was used to inoculate 5 mL of LB broth containing the appropriate antibiotic, and the culture incubated at 37°C overnight with shaking at 180 rpm. 500 μL of this overnight culture was added to 500 μL of sterile 50% glycerol in a 2 mL cryovial and frozen at -80°C. When colonies were needed, glycerol stocks were streaked onto LB agar plates containing the correct antibiotics, which were incubated at 37°C overnight.

2.14.3 Large Scale Protein Expression

A single colony from a LB agar plate was used to inoculate 100 mL of LB broth containing the appropriate antibiotic in a 250 mL flask, and the culture incubated at 37°C overnight with shaking at 180 rpm. 10 mL of this overnight culture was then used to inoculate 1 L of LB broth containing the correct antibiotic in 2.5 L conical flasks, and incubated at 37°C with shaking at 180 rpm. Cell growth was followed by measuring the absorbance of the cultures at 600 nm; once cultures reached an OD_{600} of 0.4, the incubator was cooled to 18°C. Once cultures reached an OD_{600} of 0.6, they were induced with IPTG at a final concentration of 0.5 mM IPTG and incubated for 3 hours at 18°C with shaking at 180 rpm. Cells were harvested by centrifugation at 4,000 x g for 15 minutes at 4°C, resuspended in PBS, and transferred to 50 mL conical centrifuge tubes. Cells were pelleted by centrifugation at 3220 x g in an Eppendorf Multi-purpose centrifuge for 30 minutes at 4°C, PBS poured off and cell pellet frozen at -20°C until use.

2.14.4 Measurement of *E. coli* Growth Rate

To assess cell growth during induction, OD_{600} readings were taken at 0, 3, 9, and 18 hours post induction. If the OD_{600} was greater than 1, samples were diluted with deionised water as the relationship between OD_{600} and cell density becomes non-linear after 1.

2.14.5 Analysis of Protein Expression Levels

To assess protein expression levels during induction, 500 µL of culture from was transferred to a 1.5 mL microcentrifuge tube. Cells were pelleted by centrifugation at 13,000 rpm in a desktop microcentrifuge for 5 minutes at room temperature and supernatant was removed. B-PER Bacterial Protein Extraction Reagent (Thermo Scientific) was prepared by adding 2 µL of TURBO™ DNase (2 U/µL, Invitrogen) per 1 mL of reagent needed, and then each pellet resuspended in 100 µL reagent. Samples were incubated at room temperature for 15 minutes and then stored at -20°C until analysis by SDS-PAGE and western blotting (see section 2.16).

2.14.6 Phase Contrast Microscopy

To assess cell morphology during induction, 500 µL of culture from each flask was transferred to a 1.5 mL microcentrifuge tube. Cells were pelleted by centrifugation at 13,000 rpm in a desktop microcentrifuge for 5 minutes at room temperature and supernatant was removed. Cells were then fixed by resuspending the pellets in 500 µL 4% paraformaldehyde in PBS (Thermo Scientific) and incubating for 20 minutes at room temperature. Cells were pelleted again by centrifugation and resuspended in 500 µL PBS. Samples were stored at 4°C until use. 5 µL of sample was spotted onto a glass microscope slide and covered with a plastic cover slip.

Phase contrast images were taken on an A1R Confocal System equipped with a Ti inverted microscope (Nikon) by Dr Alessandro Di Maio at the Birmingham Advanced Light Microscopy Facility. Images were captured using NIS-Elements 4.13 Microscope Imaging Software (Nikon) and processed using Fiji.

2.15 Membrane Protein Solubilisation and Purification

Table 2.14. **Buffers used in membrane protein solubilisation and purification.**

Disruption buffer	50 mM TrisHCl pH 7.5 (r.t) 5 mM $MgCl_2$ 5 mM $CaCl_2$ 5% (v/v) glycerol Just before use, dissolve one Pierce™ EDTA-free Protease Inhibitor Tablet (Thermo Scientific) and 10 μL TURBO™ DNase (Invitrogen) per 50 mL buffer
Solubilisation buffer	50 mM TrisHCl pH 8.0 (r.t) 500 mM NaCl 10% (v/v) glycerol
DDM solubilisation buffer	Solubilisation buffer + 2% (w/v) n-Dodecyl-β-D-Maltopyranoside (DDM)
SMA solubilisation buffer	Solubilisation buffer + 5% (w/v) SMA
Ni-NTA wash buffer	Solubilisation buffer + 20 mM imidazole *(+0.2% (w/v) DDM for detergent preparations*
Ni-NTA elution buffer	Solubilisation buffer + 500 mM imidazole *(+0.2% (w/v) DDM for detergent preparations*
Streptavidin elution buffer	Solubilisation buffer + 2.5 mM desthiobiotin *(+0.2% (w/v) DDM for detergent preparations*

2.15.1 *E. coli* Membrane Preparation

All stages of membrane preparation were carried out on ice to preserve protein integrity. If the cell pellets being used for membrane preparation were previously frozen, they were allowed to defrost on ice before use. Cell pellets were then re-suspended by hand homogenisation using a borosilicate glass mortar and pestle with at least 2 mL disruption

buffer per gram of pellet. Cells were then disrupted using an Emulsiflex C3 Homogeniser (Avestin), passing the cell suspension through at least 3 times under pressure of around 17,000 psi. Cell debris was pelleted by centrifugation at 12,000 x g for 30 minutes at 4°C. The supernatant from this step was collected and centrifuged at 120,000 x g for 1 hour to collect the membrane fraction. The membranes were then weighed and re-suspended by hand homogenisation to a final concentration of 60 mg/mL in solubilisation buffer. For long term storage, the re-suspended membrane solution was stored at -20°C, and thawed on ice immediately before use.

2.15.2 n-Dodecyl-β-D-Maltopyranoside (DDM) Solubilisation

If overexpressed proteins were to be solubilised with detergent, the re-suspended membranes were combined with DDM solubilisation buffer at a 1:1 ratio, and left to solubilise overnight at 4°C with mild agitation. Any material not solubilised at the end of the incubation was removed by centrifugation at 120,000 x g for 1 hour, and the supernatant collected.

2.15.3 SMA Solubilisation

If overexpressed proteins were to be solubilised with SMA, the re-suspended membranes were combined with SMA solubilisation buffer at a 1:1 ratio, and left to solubilise for 3 hours at room temperature with mild agitation. Any material not solubilised at the end of the incubation was removed by centrifugation at 120,000 x g for 1 hour, and the supernatant collected.

2.15.4 Ni-NTA Affinity Purification

To purify overexpressed His-tagged proteins from other solubilised membrane proteins, immobilized metal affinity chromatography (IMAC) was used. SMA solubilised proteins were purified as below, DDM solubilised proteins were purified as below with the exception that all buffers hereafter were supplemented with 0.2% (w/v) DDM. Super Ni-NTA Agarose Resin (Generon) was prepared by transferring the required volume of the suspension to a 15 mL conical centrifuge tube, and making up to 15 mL with deionised water. After centrifugation at 3220 x g in an Eppendorf Multi-purpose centrifuge for 15 minutes at room temperature, the supernatant was removed and the preparation steps repeated twice more. After the final centrifugation step, the supernatant was removed and resin re-suspended as a 50% (v/v) suspension in solubilisation buffer. This resin suspension was then added to the supernatant from section 2.15.2/3 at a ratio of 1:50, i.e. 1 mL 50% resin suspension to 50 mL supernatant. The supernatant was incubated with the resin overnight at 4°C with gentle agitation.

After incubation, the resin/supernatant solution was transferred to a gravity flow column and the flow through collected. To remove non-specifically bound proteins, the resin was then washed with 10 column volumes (CV) Ni-NTA wash buffer 4 times, collecting each wash fraction separately. To elute his-tagged proteins bound to the column, the resin was then incubated with 1 CV of Ni-NTA elution buffer for 5 minutes, and then eluent collected; this was repeated at least 6 times. All collected fractions were analysed by Polyacrylamide Gel Electrophoresis (PAGE) (section 2.16) to confirm the presence of the target protein and to assess the purity of the sample. To quickly remove imidazole from the elution fractions, the fractions were pooled and dialysed in 500 mL solubilisation buffer using GeBAflex-Maxi

Dialysis Tubes (max. sample vol. 3000ul, 3.5kDa MWCO) (Generon) as per manufacturer's instructions.

2.15.5 Strep-Tactin Affinity Purification

To purify overexpressed Strep-tag II tagged proteins from other solubilised membrane proteins, an alternative IMAC technique was used. Strep-Tactin® Superflow® 50% suspension (IBA) was prepared by transferring the required volume of resin (1:10 ratio resin to sample being applied) into a gravity flow column and equilibrating with 10 CV solubilisation buffer. The dialysed elution fractions from section 2.15.4 were then applied to the resin and the flow through collected. To remove non-specifically bound proteins, the resin was then washed with 1 CV solubilisation buffer 5 times, collecting each wash fraction separately. To elute Strep-Tag II tagged proteins bound to the column, the resin was then incubated with 1 CV of streptavidin elution buffer for 5 minutes, and then eluent collected; this was repeated at least 6 times. All collected fractions were analysed by Polyacrylamide Gel Electrophoresis (PAGE) (section 2.16) to confirm the presence of the target protein and to assess the purity of the sample.

2.15.6 Size Exclusion Chromatography (SEC)

To improve the purity of protein samples and separate components on the basis of hydrodynamic radius, SEC of protein samples was performed on a Superdex® 200 Increase 10/300 GL gel filtration column attached to an ÄKTAexplorer 10 chromatography system (Amersham) controlled by UNICORN 4.0 chromatography software (Amersham). Before use the column was equilibrated in 2 CV SEC Running Buffer (50 mM Tris, 150 mM NaCl, pH 8 r.t.).

Samples to be purified by SEC were pooled and concentrated to a volume of 250 μL in an Amicon® Ultra Centrifugal Filter (Merck Milipore) with a 3,000 Da molecular weight cut off (MWCO) by centrifugation at 4,000 rpm, 4°C in an Eppendorf Multi-purpose centrifuge. Samples were then loaded into a 500 μL sample loop and injected onto the column. The column was run for 1 CV at 0.5 mL/min in SEC Running Buffer, collecting 0.5 mL fractions. Elution absorbance was monitored at 280 nm and 254 nm to identify the elution of protein and SMA respectively.

2.15.7 Superdex® 200 Increase 10/300 Calibration Curve

A commercial protein standard mix (15-600 kDa, Merck) was used to determine the relationship between molecular weight and elution volume from the Superdex® 200 Increase 10/300 GL column. The lyophilised protein mix was re-suspended in 1 mL 50 mM TrisHCl, 150 mM NaCl (pH8). 250 μL of this sample was then injected onto the column and analysed as in section 2.15.6. 1 mg/mL bovine serum albumin and 1 mg/mL green fluorescent protein (GFP, gifted by Dr Timothy Knowles, University of Birmingham) were similarly analysed. Each sample was individually prepared and analysed three times, and the results were plotted on a scatter graph using Microsoft Excel. An exponential trend line was fitted to the data and the equation of this line was used for estimation of molecular weight from the elution volume.

2.16 Polyacrylamide Gel Electrophoresis (PAGE)

2.16.1 Sodium Dodecyl Sulfate-PAGE (SDS-PAGE)

Dependant on protein size, 12% or 18% SDS-PAGE gels were prepared using the recipe shown in table 2.15. SDS-PAGE gels were then assembled into a vertical electrophoresis tank and submerged in 1X Running Buffer made up from 10X Tris-Glycine-SDS Buffer Concentrate (Sigma). Samples to be analysed by SDS-PAGE were prepared by transferring 15 μL of each sample into a micro-centrifuge tube with 5 μL of 4X NuPAGE® LDS sample buffer (Novex®, ThermoFisher Scientific) and 2 μL of 10X NuPAGE® sample reducing agent (Novex®, ThermoFisher Scientific). 15 μL of each sample was then loaded into the wells of the gel along with 5 μL of Broad Range Blue Pre-Stained Protein Standard (New England Biolabs) (figure 2.6). Gels were run at 100 V until samples were beyond the resolving gel and thereafter run at 200 V until sample dye reached the bottom of the gel.

Table 2.15. **SDS-PAGE gel recipe.**

	Stacking Gel	**Resolving Gel**	
	4%	*12%*	*18%*
30% Acrylamide/bis	1.33 mL	6 mL	9 mL
0.5M Tris-HCl, 0.4% SDS pH 6.8	2.5 mL	-	-
1.5M Tris HCl, 0.4% SDS pH 8.8	-	3.75 mL	3.75 mL
dH_2O	6 mL	5 mL	2 mL
Tetramethylethylenediamine (TEMED)	10 μL	15 μL	15 μL
10% Ammonium persulfate (APS)	100 μL	150 μL	150 μL
Total Volume	10 mL	15 mL	15 mL

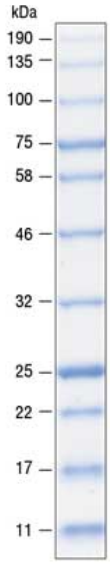

Figure 2.6. **NEB Broad Range Blue Pre-Stained Protein Standard.**

2.16.2 Coomassie Staining

If protein bands were to be visualised by Coomassie staining, gels were removed from their glass plates and stained with SimplyBlue™ SafeStain buffer (Novex®, ThermoFisher Scientific) as per manufacturer's instructions. All staining and washing steps were carried out on a rocker at room temperature. In short, gels were washed in deionised water 3 times for 5 minutes, and then incubated with SafeStain for 1 hour. After 1 hour the stain was removed and replaced with deionised water, and washed for 1 hour. For increased sensitivity, after I hour of washing 20 mL of 20% NaCl was added to the water and the gel was left washing overnight.

2.16.3 Western Blotting

If protein bands were to be visualised by western blotting, gels were removed from their glass plates and placed into deionised water. Proteins were then transferred from the gel onto a

nitrocellulose membrane using the Trans-Blot Turbo Transfer System (Bio-Rad) with Trans-Blot® Turbo™ Mini Nitrocellulose Transfer Packs (Bio-Rad). Transfer was carried out using the preprogramed 'Mixed MW' protocol, applying 1.3 V up to 25 V for 7 minutes. After transfer, the membrane was blocked for 45 minutes on a rocker at room temperature with 25 mL of 5% Skim Milk Powder in PBS. 2.5 μL of 6xHis monoclonal antibody (Clontech) was then added to the milk solution and incubated on a rocker overnight at 4°C. After incubation the membrane was twice washed in PBS with 0.05% Tween 20 for 5 minutes on a rocker at room temperature. The membrane was then incubated with 25 mL of 5% Skim Milk Powder in PBS with the addition of 2.5 μL of Goat Anti-Mouse IgG Antibody [HRP] (2BScientific), and incubated on a rocker at room temperature for at least 3 hours. The membrane was again washed twice with PBS with 0.05% Tween 20 for 5 minutes. His-tag proteins were then visualised by the addition of EZ-ECL Enhanced Chemiluminescence Detection Kit for HRP (Biological Industries). The detection solution was prepared by combining 2 mL of each supplied solution, and allowed to equilibrate for 10 minutes before use. The solution was then added directly on top of the membrane and incubated for exactly 1 minute, before visualisation of the bands using chemiluminescence imaging on a Uvitec Gel Imaging System.

2.16.4 Protein Identification

To identify a protein in a particular SDS-PAGE gel band, the gel was run and stained as per sections 2.16.1 and 2.16.2, and then washed thoroughly in deionised water and placed in a clean container. The band of interest was then cut out using a clean razor blade, and the gel

plug was placed into a microcentrifuge tube. The sample was then submitted to the University of Birmingham Advanced Mass Spectrometry Facility for tandem mass spectrometry analysis.

2.16.5 Blue Native-PAGE

For electrophoresis of samples in a non-denaturing, non-reducing environment, Native-PAGE was used. Samples were prepared by transferring 15 μL of each sample into a microcentrifuge tube with 5 μL of 4X tris-glycine native sample buffer pH 8.6 (Alfa Aesar). Native-PAGE was performed with NativePAGE™ 4-16% Bis-Tris protein gels (Novex) using XCell SureLock™ Mini-Cell Electrophoresis System (ThermoFisher). For non-detergent samples the inner chamber was filled with 1X Light Cathode Buffer while the outer chamber was filled with 1X Anode Buffer (see table). For detergent samples the inner chamber was instead filled with 1X Dark Blue Cathode Buffer until the dye front had migrated one third of the way into the gel, at which point it was removed and replaced with 1X Light Cathode Buffer for the remainder of the run. 15 μL of each sample was loaded into the wells along with 5 μL of NativeMark™ Unstained Protein Standard (Invitrogen). The gel was then run for 100 minutes at 150 V.

Table 2.16. **Running Buffers for Blue Native-PAGE.**

	NativePAGE Running Buffer (20X)	**NativePAGE Cathode Additive (20X)**	**Deionised Water**
1X Anode Buffer (1000 mL)	50 mL	-	950 mL
1X Light Cathode Buffer (200 mL)	10 mL	1 mL	189 mL
1X Dark Cathode Buffer (200 mL)	10 mL	10 mL	180 mL

If the Native-PAGE was to be assessed by Coomassie staining, then the gel was stained by the manufacturer's instructions. In short, the gel was fixed in 100 mL 40% methanol, 10% acetic acid by microwaving for 45 seconds and then rocking at room temperature for 30 minutes. The fix step was repeated, and then the gel was stained with 100 mL 30% methanol, 10% acetic acid, 0.02% Brilliant Blue R by microwaving for 45 seconds and then rocking at room temperature for 30 minutes. The gel was finally de-stained in 8% acetic acid by microwaving for 45 seconds and then rocking at room temperature overnight.

If the Native-PAGE was to be assessed by western blotting, the proteins were transferred to a nitrocellulose membrane as per section 2.16.3. After transfer, proteins were fixed to the membrane by incubating the membrane with 8% acetic acid for 15 minutes, before rinsing in deionised water and allowing the membrane to air dry. Once dry, the residual Coomassie dye was lifted from the membrane with methanol, the membrane was washed briefly with deionised water and then the membrane was blocked, incubated and visualised as per section 2.16.3.

2.17 Biophysical Analysis

2.17.1 Circular Dichroism (CD)

All CD measurements were made on a JASCO J-1500 Circular Dichroism Spectrophotometer controlled by Spectra Manager software. All measurements were taken in a quartz cuvette, with a pathlength of 1 mm for standard spectra measurements. Before use the instrument was calibrated with d-10-Camphorsulfonic Acid, comparing to published spectra (Chen and Yang, 1977).

Due to the high absorbance of chloride ions in the far-UV region, samples were prepared for CD by dialysing into 10 mM potassium phosphate pH 8. Sample concentrations were approximately 0.1 mg/mL. A single spectrum was taken to assess the appropriate wavelength range for the sample. For most samples, the high tension voltage exceeded 600 V below 200 nm, indicating a loss of reliable CD signal, therefore wavelength scans were only taken down to this wavelength. Spectra were then measured using the parameters in table 2.17. Each spectrum is an average of 5 scans.

Table 2.17. **Parameters for circular dichroism (CD) analysis**

Channel 1	CD
Channel 2	HT
Channel 3	Abs
Start	275 nm
End	200 nm
Data pitch	0.5 nm
Scanning mode	Continuous
Scanning speed	50 nm/min
D.I.T	2 seconds
Bandwidth	1 nm
Number of accumulations	5

Baseline spectra were taken with the buffer in which the sample had been prepared and similarly averaged. Baseline spectra were then subtracted from the sample spectra and the resulting spectrum smoothed using the Savitzky-Golay method within the Spectra Manager software.

2.17.2 Thermal Melt Analysis

All thermal melt experiments were performed on a JASCO J-1500 Circular Dichroism Spectrophotometer, fitted with the PTC-517 single-position Peltier thermostatted cell holder accessory (Jasco) and MCB-100 Mini Water Circulation Bath. The spectrophotometer was controlled by Spectra Manager software. All measurements were taken in a quartz cuvette, with a pathlength of 10 mm. Before use the instrument was calibrated with d-10-Camphorsulfonic Acid, comparing to published spectra (Chen and Yang, 1977).

Table 2.18. **Parameters for thermal melt analysis.**

General parameters	
Channel 1	CD
Channel 2	HT
Channel 3	Abs
Start	275 nm
End	200 nm
Data pitch	0.5 nm
Scanning mode	Continuous
Scanning speed	50 nm/min
D.I.T	2 seconds
Bandwidth	1 nm
Number of accumulations	5
Temperature parameters	
Start temperature	15°C
End temperature	95°C
Data interval	5°C
Temperature Gradient	1°C/minute
Wait time	20 seconds
Start condition	Keep within +/- 0.1°C of the target temp. for 5 seconds
Stirrer	100 rpm

Due to the high absorbance of chloride ions in the far-UV region, samples were prepared for CD by dialysing into 10 mM potassium phosphate pH 8. Sample concentrations were approximately 0.1 mg/mL. A single spectrum was taken to assess the appropriate wavelength range for the sample. For most samples, the high tension voltage exceeded 600 V below 200 nm, indicating a loss of reliable CD signal, therefore wavelength sans were only taken down to this wavelength. Thermal melt experiments were then conducted using the parameters in table 2.18. Each spectrum is an average of 5 scans.

2.17.3 Analytical Ultracentrifugation (AUC)

Unless otherwise stated, samples to be analysed by AUC were prepared to a concentration of 0.1-0.5 mg/mL in 50 mM Tris, 150 mM NaCl, pH 8.0. Sedimentation velocity experiments were performed by Pooja Sridhar at the Birmingham Biophysical Characterisation Facility, University of Birmingham. Experiments were performed in a Beckman Coulter ProteomeLab XL-I Analytical Ultracentrifuge with a Ti50 rotor at 20°C, 30,000-40,000 rpm depending on predicted sample molecular weight. Samples were monitored by absorbance at 245 nm, 260 nm and/or 280 nm. Data was analysed in SEDFIT (Schuck, 2000) applying the continuous c(s) distribution model. Buffer density and viscosity were calculated with SEDNTERP (Laue *et al.*, 1992). The frictional ratio parameter was allowed to float. For SMA, the partial specific volume was calculated from the inverse of the published density of 1.18. For SMALP samples the partial specific volume was calculated with density contrast sedimentation experiments (section 2.17.4).

2.17.4 Density Contrast Sedimentation

For samples with no published density or partial specific volume, it was measured experimentally by density contrast sedimentation. 250 μL of sample in 50 mM Tris, 150 mM NaCl, pH 8.0 was mixed with 250 μL of either filter sterilised water or deuterium oxide and allowed to equilibrate at 4°C overnight. For each sample, this was done 3 times in H_2O and 3 times in D_2O. Samples were then analysed by AUC as above, allowing the partial specific volume to remain on the pre-set value, as it does not affect sedimentation coefficients.

The sedimentation coefficients from the H_2O experiments were averaged, and similarly with the D_2O experiments. The equation from Martin, Winkler and Cook (1959) was then used to calculate the partial specific volume:

$$\bar{\upsilon} = \left(\frac{\eta_D}{\eta_H} - \kappa\frac{S_D}{S_H}\right)\left(\frac{\rho_H\eta_D}{\eta_H} - \frac{\rho_D S_H}{S_D}\right)^{-1}$$

Where $\bar{\upsilon}$, η, S, and ρ represent partial specific volume, buffer viscosity, sedimentation coefficient, and buffer density respectively. Subscript $_D$ denotes D_2O samples and subscript $_H$ denotes H_2O samples. κ represents the molar mass ratio of the sample in deuterated compared to non-deuterated solvent. κ was calculated in protein samples by identifying the number of labile hydrogens in the sample protein sequence and assuming 100% hydrogen-deuterium exchange.

2.17.5 Small Angle X-ray Scattering (SAXS)

Size-exclusion chromatography SAXS (SEC-SAXS) data was collected at Diamond Light Source, Didcot on beamline B21 (proposal SM19905). Inline SEC-SAXS was performed on an Agilent 1200 high-performance liquid chromatography (HPLC) system, using a Superdex 200 Increase 3.2/300 SEC column (GE Healthcare). Before use the column was equilibrated in 2 CV SEC Running Buffer (50 mM Tris, 150 mM NaCl, pH 8 r.t.). Samples were pooled and concentrated to a volume of 60 μL in an Amicon Ultra Centrifugal Filter (Merck Milipore) with a 3,000 Da molecular weight cut off (MWCO) by centrifugation at 4,000 rpm, 4°C in an Eppendorf Multi-purpose centrifuge. Samples were then injected onto the column using the EMBL Arinax sample handling robot, and the column was run for 1 CV at 0.075 mL/min in SEC Running Buffer. Eluent passed into the data collection chamber where SAXS data was collected at 3 second intervals using 1 second exposure times. Data was recorded on a Pilatus 2M detector at a fixed camera length configuration of 4.014 m at 12.4 keV, allowing the collection of data in a resolution range of 0.0031 to 0.38 $Å^{-1}$. Data reduction was automatically performed at Diamond Light Source using DAWN, and further data analysis was carried out in ScÅtter, a JAVA-based application developed by Robert Rambo at the Diamond Light Source (Didcot, UK). Low resolution *ab initio* models were produced from the P(r) distribution using DAMMIF (Franke and Svergun, 2009), performing 13 independent runs, which were then averaged using DAMAVER (Volkov and Svergun, 2003).

2.17.6 Dynamic Light Scattering (DLS)

Dynamic light scattering experiments were performed at the Molecular Analytical Science Centre (University of Warwick) on a Zetasizer Nano S (Malvern Instruments). Samples were loaded into a standard disposable polystyrene cuvette and equilibrated at 25°C for 60 seconds. DLS measurements were then taken using a HeNe gas laser at 633 nm, with the detector at a 175° angle to the incident beam. Each measurement is an average of 11 scans taken over 10 seconds.

2.18 Thin Layer Chromatography (TLC)

Samples to be analysed by TLC were concentrated to achieve a target concentration of 0.5 mg/mL in an Amicon Ultra Centrifugal Filter (Merck Milipore) with a 3,000 Da molecular weight cut off (MWCO) by centrifugation at 4,000 rpm, 4°C in an Eppendorf Multi-purpose centrifuge. Samples were then analysed as outlined in the methods of Hughes *et al.* (2019). 2 mL of this sample was added to 2 mL methanol and 1 mL chloroform. Samples were vortexed continuously for 5 minutes, and then incubated at 50°C for 30 minutes. The samples were then vortexed again for 5 minutes, and centrifuged at 2,000 x g for 10 minutes. After centrifugation, the lower phase was extracted and evaporated. The dried lipids were resuspended in 100 μL chloroform, and 5 μL was loaded onto a Silica TLC plate (Sigma). The TLC plate was run with a 6.5:2.5:1 (chloroform:methanol:acetic acid) solvent, and then dried for 30 minutes. The plate was stained with 10% (w/v) phosphomolybic acid in ethanol and heated until staining occurred.

CHAPTER 3: SOLUBILISATION OF THE COMPONENTS OF THE FTSBLQ SUBCOMPLEX USING STYRENE MALEIC ACID

3.1 Introduction

The FtsBLQ complex has been proposed to be the "on/off" switch of the divisome, preventing septum formation and subsequent division until the divisome has been correctly assembled, signalled by the accumulation of FtsN, the final protein in the divisomal assembly pathway (Liu *et al.*, 2015). However, there is still very little known about this complex, as many studies have reported low expression levels, and difficulties in purifying the complex in a stable and folded state have slowed progress (Bramkamp *et al.*, 2006; Masson *et al.*, 2009; van den Berg van Saparoea *et al.*, 2013). Previous studies have often relied on expressing just the periplasmic domain of these proteins to enable their purification as a soluble protein. However, coiled coils such as that in FtsB and FtsL are known to be unstable when isolated, and therefore require fusion to globular proteins such as bacteriophage Gp7 (LaPointe *et al.*, 2013) or soluble coiled coils (Glas *et al.*, 2015; Choi *et al.*, 2018) to remain stable. Since the transmembrane (TM) region of FtsB has been found to homo-oligomerise when purified in isolation (LaPointe *et al.*, 2013), it seems likely that the transmembrane region of FtsB may play a role in the oligomerisation of FtsB *in vivo*. Similarly, Khadria and Senes (2013) demonstrated by Förster resonance energy transfer (FRET) that the purified TM regions of FtsB and FtsL associated and formed a higher-order oligomer in a 1:1 ratio, suggesting these regions play a role in FtsB-FtsL association.

These results suggest that isolating full-length proteins with an intact transmembrane region may help elucidate their structure and function; however, the purification of full-length membrane proteins presents new difficulties due to the need for solubilisation from the lipid environment. Historically, this has been achieved with detergents such as n-Dodecyl-β-D-

Maltopyranoside (DDM), which are made up of a hydrophilic head group and a hydrophobic tail. The hydrophobic tail partitions into the lipid bilayer and masks the hydrophobic portion of the membrane protein, while the hydrophilic head group provides water solubility, allowing solubilisation of the membrane protein from the membrane. However, detergents can have a destabilising effect on proteins and often ignore the complexity found within membranes (Privé, 2007). Additionally, detergent solubilisation can remove the lipids surrounding membrane proteins. For many proteins, their activity is directly modulated by the local lipid environment; this includes a range of cell signalling proteins which associate with lipid rafts, regions of higher than average cholesterol and glycosphingolipid thought to play a role in signal transduction (Staubach and Hanisch, 2011). Detergents can also be unreliable when working with protein-protein interactions. When attempting to solubilise membrane complexes, Lee *et al.* (2018) demonstrated that only select detergents could preserve protein interactions and that the detergent capable of this varied between the different complexes. The unpredictability of detergent-protein compatibility can result in lengthy processes of investigating multiple combinations of detergents, which is expensive and time-consuming.

The advent of the use of styrene-maleic acid (SMA) copolymer as a tool for solubilisation offered a novel solution to the membrane purification problem. The styrene-maleic acid-lipid particles (SMALPs) formed by the interaction of SMA with lipid bilayers results in roughly 10 nm discs, which can contain membrane proteins within them. This technique allows the solubilisation of full-length membrane proteins while still surrounded by their native lipid environment, which may also help support protein-protein interactions.

The aim of this chapter was to firstly clone the full-length *ftsB*, *ftsL* and *ftsQ* genes from the *E. coli* genome into an appropriate expression vector, and to overexpress these proteins in an *E. coli* expression strain. Previous studies had reported difficulties with expressing the full-length proteins without the other proteins of the sub-complex (Buddelmeijer *et al.*, 2002); therefore, steps were taken to improve expression levels. Secondly, this chapter aimed to establish whether SMA can efficiently solubilise the over-expressed proteins from the membrane and whether these proteins can then be adequately purified using IMAC and SEC methods.

3.2 Cloning of Full-length *ftsB/ftsL/ftsQ* for High Level Expression

In order to express the full-length proteins, the *ftsB*, *ftsL* and *ftsQ* genes first had to be cloned into a suitable expression vector. pET52b was chosen as the vector as it is designed for high-level expression and fuses the proteins with two cleavable tags: an HRV cleavable Strep-Tag and a thrombin cleavable 10xHis-Tag. To clone the genes into the vector, the genes first had to be amplified from *E. coli* K12 genomic DNA by PCR amplification. PCR primers were designed to include two specific restriction sites, one at the start and one at the end of each gene, for downstream digestion and insertion into a linearised vector. In order to find the optimal annealing temperature for the primer pairs, a gradient PCR was run, varying the annealing temperature between 50-60°C. Figure 3.1 shows the resulting PCR products run on an agarose gel. The *ftsL* products appeared as a strong band at the correct weight for the predicted 366 bp sequence. There were some higher weight bands, but these were reduced upon higher annealing temperature with limited loss of product; therefore, an annealing temperature of 60°C was chosen for *ftsL* annealing.

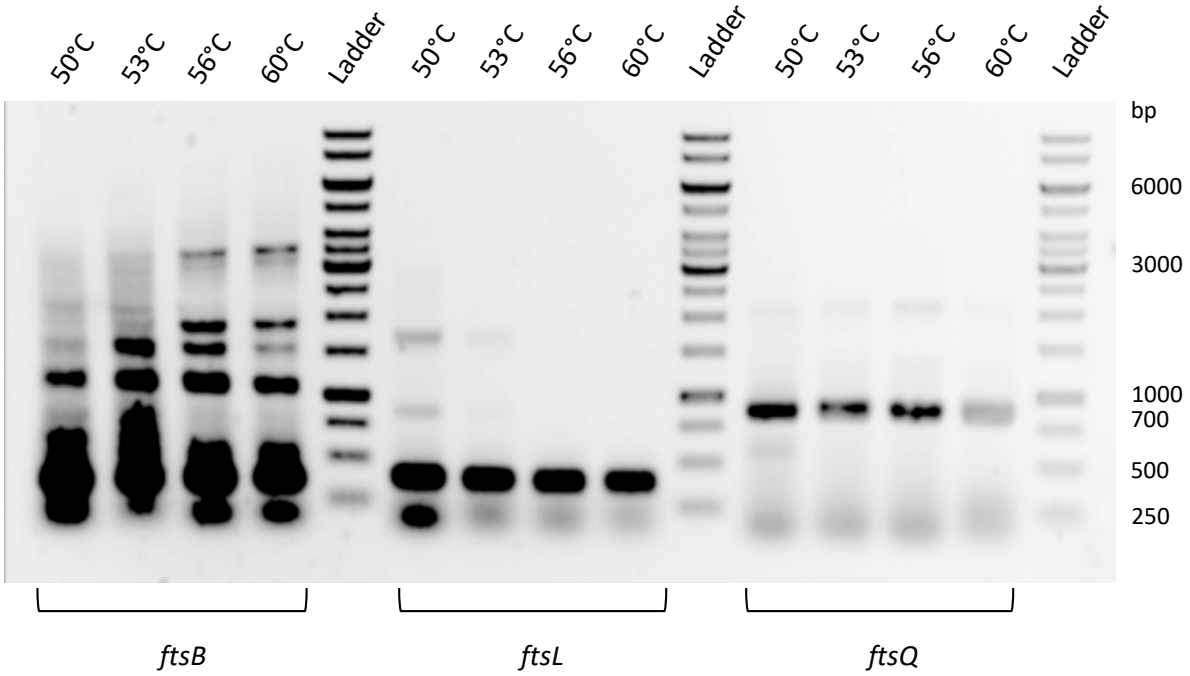

Figure 3.1. **PCR products of gene amplification.** The *ftsB*, *ftsL* and *ftsQ* genes were amplified from *E. coli* genomic DNA by PCR, varying the primer annealing temperature between 50°C to 60°C. The resulting PCR products and DNA ladder were run on a 1% agarose gel containing Gelred for 45 minutes and DNA bands visualised using UV light.

The *ftsQ* gene product was also successfully amplified at the correct weight for an 831 bp product between 50-56°C, with a reduction in product seen at 60°C. As a higher annealing temperature is associated with higher specificity, an annealing temperature of 56°C was chosen for *ftsQ*. However, *ftsB* was not successfully amplified, as the PCR products showed a large amount of laddering and smearing, suggesting that there was a large amount of unspecific product. As *ftsB* was the shortest gene to be amplified (306 bp), one possibility was that the extension time used was too long.

The PCR was repeated for *ftsB*, reducing the extension time from 30 seconds to 10 seconds, as the polymerase manufacturer's recommendation for the extension time step is 10-30 seconds per kb of template. Additives were also included to test whether this improved results, as DMSO is known to improve specificity during PCR. Figure 3.2 demonstrates that the shorter extension time greatly improved the amplification of *ftsB*, with a good yield at the expected weight and very faint banding at a larger molecular weight. Additives appeared to have little to no effect on the yield or specificity of *ftsB* amplification, therefore they were not used in future PCR methods.

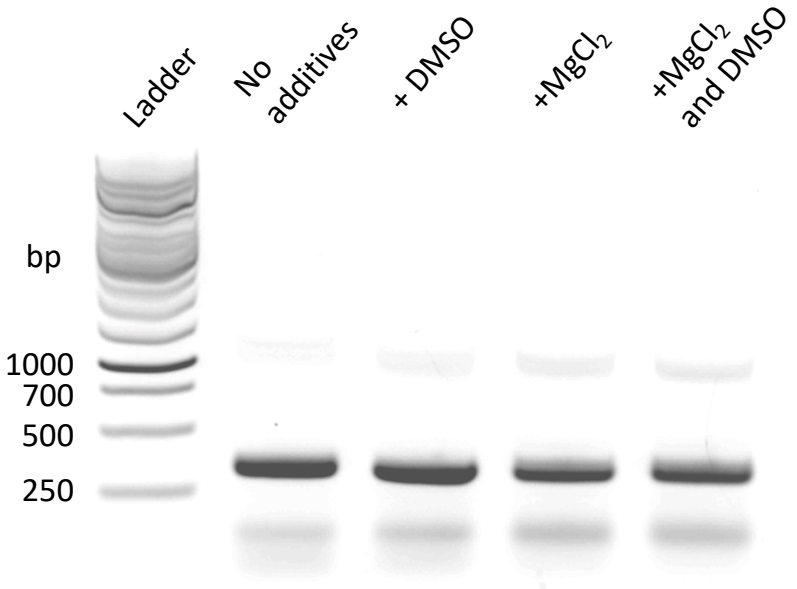

Figure 3.2. **PCR products of *ftsB* amplification with reduced extension time.** *ftsB* was amplified from *E. coli* genomic DNA by PCR at a single annealing temperature of 55°C and a reduced annealing time of 10 seconds, varying the use of PCR additives. The resulting PCR products and DNA ladder were run on a 1% agarose gel containing GelRed for 45 minutes and DNA bands visualised using UV light.

The amplified genes were then ligated into the expression vector. This was achieved by restriction digest, whereby the plasmid was linearised by digestion with two restriction enzymes whose restriction sites were found only in the vectors cloning site. The PCR product was then digested with the same enzymes to produce sticky ends, as the restriction sites has previously been inserted at each end of the DNA sequence by insertion into the PCR primers. The PCR product and vector were ligated to produce a circular vector containing the gene in question. To screen for vectors with the correct insert, *E. coli* DH5α competent cells were transformed with the ligation product, and the plasmid DNA prepared from these cells. Plasmid DNA size was assessed by agarose gel electrophoresis and candidates that appeared at the correct weight underwent diagnostic PCR and restriction digest to confirm the presence of the correct insert (Figure 3.3).

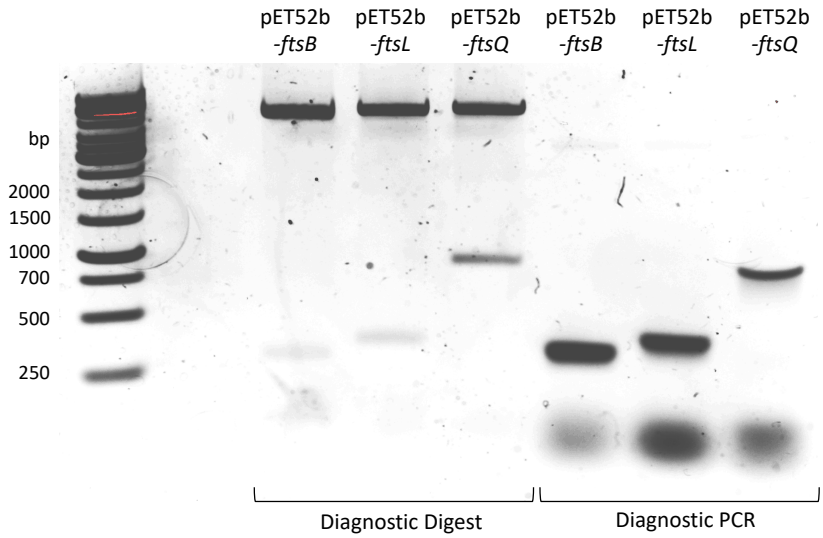

Figure 3.3. **Confirmation of insertion of gene inserts into pET52b.** The pET52b-*ftsB*, pET52b-*ftsL* and pET52b-*ftsQ* plasmids were confirmed to contain the correct inserts by diagnostic digest and PCR. The resulting PCR products and DNA ladder were run on a 1% agarose gel containing Gelred for 45 minutes and DNA bands visualised using UV light.

When digested with the restriction enzymes used in the previous cloning steps, each plasmid migrated as two components: the plasmid at the correct weight of ~5.2 kb and the inserts, also at the correct weights. Diagnostic PCR similarly showed that when the cloning region of the plasmid was amplified, PCR products at the correct size for each gene were produced. These results showed that plasmids containing each gene had been successfully constructed. To ensure that each gene had also been amplified and ligated with no errors, the cloning region of each plasmid was sequenced. Sequencing results confirmed that the inserted genes had the same nucleotide sequence as the published gene sequence proving that full-length, wild-type *ftsB*, *ftsL* and *ftsQ* had been successfully cloned into expression vectors.

3.3 Expression of Full-length FtsB/FtsL/FtsQ

To overexpress the three proteins, each plasmid was individually transformed into the *E. coli* BL21(DE3) expression strain. A single colony from each transformation was used to prepare overnight cultures of cells expressing each protein. This overnight culture was used to inoculate 1 L of LB broth and grown at 37°C until the cells were in the exponential growth phase, indicated by an OD_{600} of 0.4-0.6. The cultures were then cooled to 18°C and induced with IPTG. Time points were taken just before induction, and then at 1, 3, 9 and 20 hours post induction. These samples were then analysed by SDS-PAGE and western blotting with a His-Tag specific antibody to detect expression of His-Tagged protein. The growth of the cultures was sampled at the same time points, taking 1 mL aliquots and measuring the OD_{600}.

Western blot analysis demonstrated that each protein had been successfully expressed at the molecular weight predicted for the protein and additional tags.

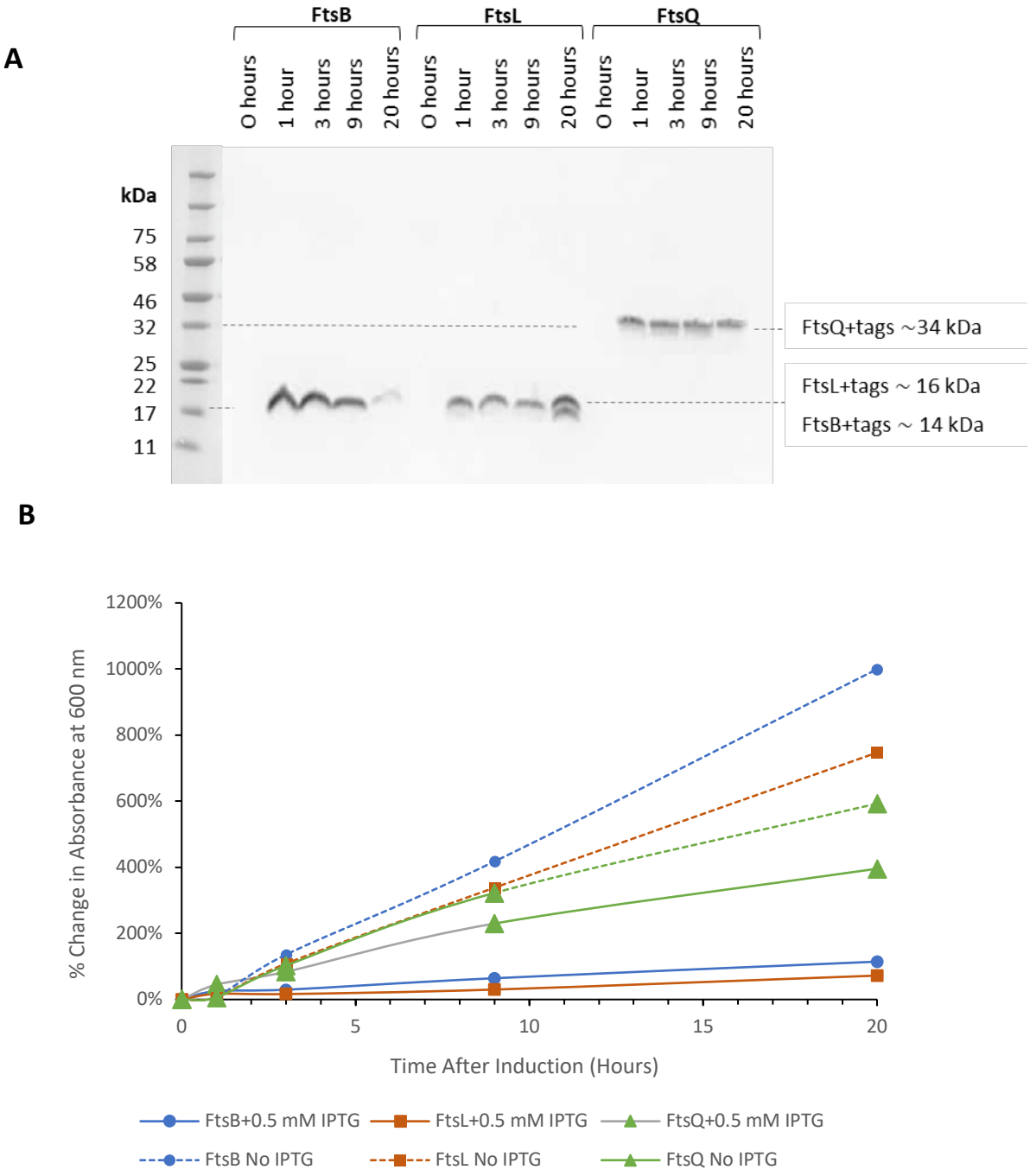

Figure 3.4. **Expression of FtsBLQ proteins.** BL21(DE3) *E. coli* containing the expression plasmid for FtsB, FtsL or FtsQ were grown to an OD_{600} of 0.6 and then either induced with 0.5 mM IPTG or left uninduced. **(A)** The expression levels of the three proteins were assessed at 0,1,3,9 and 20 hours after expression by SDS-PAGE and western blotting with an anti-His-Tag antibody**. (B)** Growth rates of induced and uninduced cultures were followed by measuring the change in OD_{600} across the time points.

Additionally, no protein bands were seen in any of the uninduced samples, suggesting there was no detectable expression of the His-Tagged proteins before IPTG induction. Upon IPTG induction, FtsB expressed to a similar level between 1 and 9 hours, while at the 20 hours post-induction the expression levels were significantly reduced. FtsL also expressed to a similar level between 1 and 9 hours post-induction, while at 20 hours post-induction a second lower molecular weight band beneath that of FtsL was visible, possibly suggesting the degradation of FtsL. The expression of both FtsB and FtsL significantly slowed the growth rate of the *E. coli* in comparison to the uninduced cultures, reaching only a third of the cell density of the uninduced cells after a 20 hour incubation. In comparison, FtsQ appeared to express uniformly across all the time points taken, and induction of FtsQ had a less marked impact on the growth rate of the *E. coli*.

To understand why cell growth is particularly poor in the FtsB and FtsL cultures, aliquots of the cultures from the expression trial were visualised by phase contrast microscopy. As shown in figure 3.5, *E. coli* BL21(DE3) cultures grown for 20 hours have cells that are uniform in shape. However, in cultures when FtsB, FtsL or FtsQ had been overexpressed for 20 hours, the cells are much less uniform and hair-like filamentous structures are common. This is particularly seen in the pET52b-*ftsL* sample, where filamentous structures reach a length of up to 60 µm compared to the average length of 2.5 µm for the BL21(DE3) sample. This demonstrates that the regulation of FtsB, FtsL and FtsQ levels is important for the division of *E. coli* and the maintance of cell morphology.

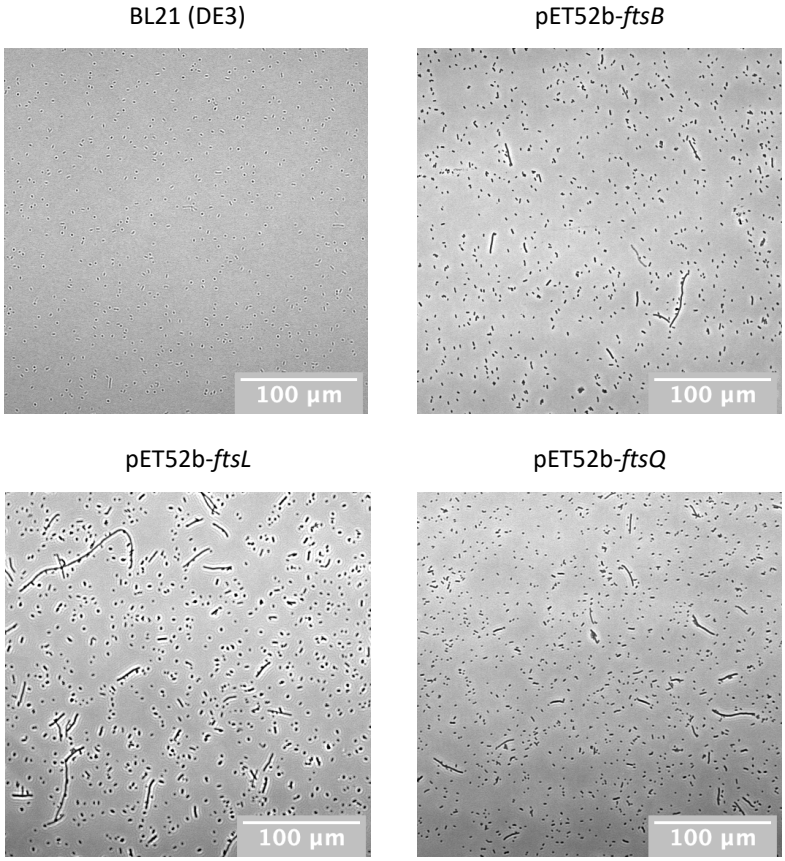

Figure 3.5. **Microscopy of cell morphology.** *E. coli* BL21(DE3) transformed with the expression vectors pET52b-*ftsB*, pET52b-*ftsL* or pET52b-*ftsQ* were grown to an OD_{600} of 0.6 and then induced with 0.5 mM IPTG. Samples of the cultures were taken after 20 hours. Samples were fixed with paraformaldehyde and then washed in PBS. Samples were placed onto a glass microscope slide, coverslip applied, and cells were then visualised by phase contrast microscopy. For comparison, non-transformed BL21(DE3) *E. coli* cells were grown for 20 hours and prepared in the same manner.

To investigate whether expression could be improved by altered growth conditions, an expression trial was carried out for FtsB. Reduction of IPTG concentration and increased induction temperatures have previously been reported to increase expression of proteins under the control of T7 promoters (Larentis *et al.*, 2014; Mühlmann *et al.*, 2017), therefore these variables were chosen.

As in previous experiments, 1 L flasks were inoculated with overnight culture and grown at 37°C to an OD_{600} of 0.6. At the point of induction, flasks were then cooled to either 18°C or 25°C and induced with a range of IPTG concentrations between 0.1-1 mM. Time points were taken at 3 and 20 hours and expression assessed by SDS-PAGE and western blotting (Figure 3.6). At the 3 hour time point, expression was highest in the 18°C culture, and at this temperature the culture induced with 0.5 mM IPTG expressed the most FtsB. Throughout the trial, cultures induced with 1 mM IPTG had the lowest level of expression. Additionally, as seen previously the 20 hour induction resulted in a lower expression level in all conditions.

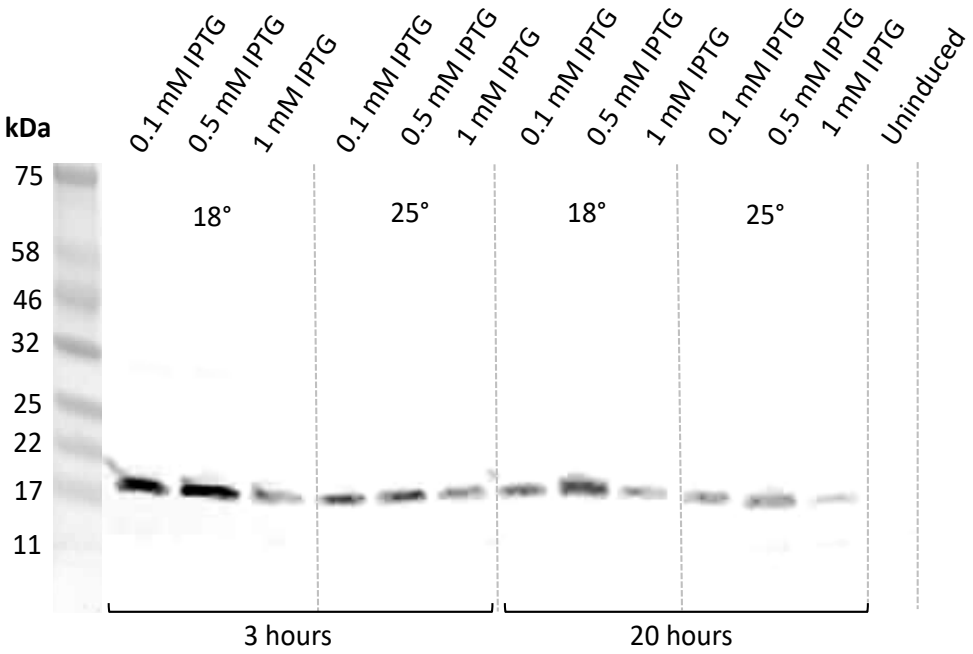

Figure 3.6. **Growth condition trial for improved FtsB expression.** BL21(DE3) *E. coli* containing the expression plasmid for FtsB were grown to an OD_{600} of 0.6 and then either induced with 0.1, 0.5 or 1 mM IPTG and incubated for 20 hours at either 18°C or 25°C. The expression levels of the different conditions were assessed by SDS-PAGE and western blotting with an anti-His-Tag antibody**.** (B) Growth rates of induced and uninduced cultures were followed by measuring the change in OD_{600} across the time points. Experiments were repeated three times and representative data is shown.

Therefore, the conditions chosen for the expression of FtsB was induction with 0.5 mM IPTG, followed by incubation at 18°C for 3 hours. As co-expression of the proteins was a future aim of these experiments, these growth conditions were used for the expression of all proteins and co-expressions hereafter.

3.4 Solubilisation of FtsB using Styrene Maleic Acid

Using the conditions chosen in section 3.3, FtsB was overexpressed in the *E. coli* BL21(DE3) expression strain and induced for 3 hours before the cells were collected by centrifugation, and the membrane fraction was prepared. To isolate *E. coli* membranes, cells must be disrupted with high pressure homogenisation, and then the membrane fraction is separated from cell debris and soluble proteins through a series of high speed and ultra-centrifugation steps (Fotiadis, Harder and Fotiadis, 2012). The pressure used to disrupt cells, and the number of passes a sample is subjected to has been shown to significantly affect protein yield (Tam *et al.*, 2012). Additionally, the method of Fotiadis, Harder and Fotiadis (2012) does not include the addition of DNase, but DNase is often added during cell disruption to reduce sample viscosity, allowing easier passage through the Emulsiflex. With this in mind, a range of cell disruption conditions were trialled to identify the optimum condition. After disruption the samples were centrifuged at 12000 x g for 30 minutes, the supernatant was collected and the insoluble pellet was weighed (table 3.1).

	3 passes	3 passes with DNase	5 passes	5 passes with DNase
Weight of insoluble pellet (mg)	700	600	500	460

Table 3.1. **Insoluble yield from different cell disruption conditions.** *E. coli* cells were disrupted using a C3 Emulsiflex under a range of conditions. After disruption the samples were centrifuged at 12000 x g for 30 minutes and the insoluble pellet was weighed.

From these results, the condition using a higher number of passes through the Emulsiflex and DNase in the disruption buffer appeared to result in the most effective cell disruption as there was the least insoluble material after disruption. To identify whether this also improved FtsB yield, the insoluble pellet was resuspended in an equal volume to the supernatant, and the amount of FtsB in the soluble fraction and pellet of each condition was detected by western blotting after separation by SDS-PAGE (figure 3.7a). In all conditions, a large amount of FtsB was detected in the insoluble pellet. This could be due to incomplete cell disruption but may also be indicative of the aggregation of FtsB into inclusion bodies. As FtsB was to be solubilised from a bilayer environment, the recovery of FtsB from inclusion bodies was not investigated. There was not an easily detectable difference in FtsB yield between the conditions in the western blot, therefore the condition chosen was to use 5 passes through the Emulsiflex with DNase included in the buffer as this resulted in the lowest insoluble pellet weight. After cell disruption and high-speed centrifugation, the soluble fraction was then centrifuged at 120,000 x g for 1 hour to collect the membrane fraction, which was subsequently solubilised with SMA. Time of SMA solubilisation has been reported to have a significant effect on membrane protein yield (Charlton, 2016), therefore solubilisation was measured at two time points.

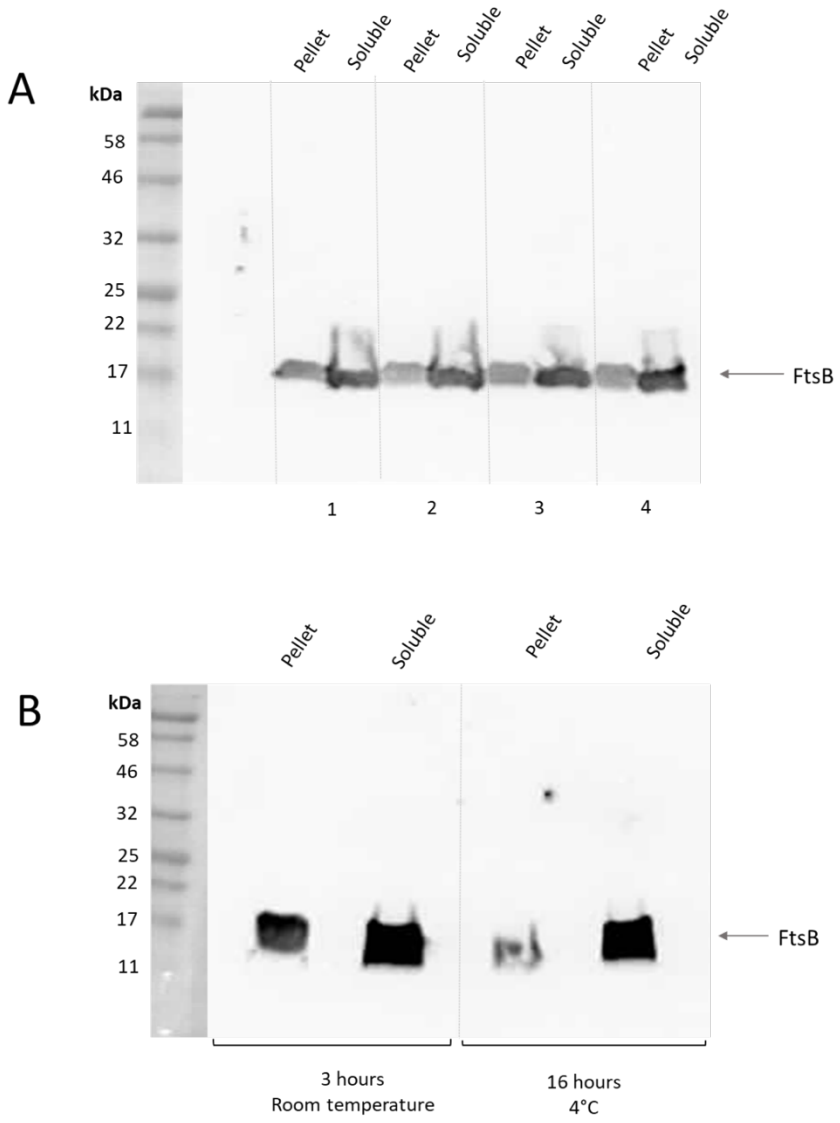

Figure 3.7. **Improving membrane yield and solubilsation.** (A) Cell pellets were lysed in a C3 emulsiflex under four different conditions. 1=three passes through the emulsiflex, 2=three passes through the emulsiflex with DNase added to buffer, 3=five passes through the emulsiflex, 4=five passes through the emulsiflex with DNase added to buffer. After lysis, the samples were centrifuged at 12000 x g for 30 minutes, supernatant collected and pellet resuspended in an equal volume to the supernatant. (B) *E. coli* membranes were solubilised with SMA either for 3 hours at room temperature or overnight at 4°C. Any material not solubilised at the end of the incubation was removed by centrifugation at 120,000 x g for 1 hour, supernatant collected and pellet resuspended in an equal volume to the supernatant. Samples were separated by SDS-PAGE on an Any kD™ Mini-PROTEAN® TGX™ Precast Protein Gel, transferred to a nitrocellulose membrane and probed with an anti-HisTag antibody.

The membrane fraction was resuspended and combined with SMA at a final concentration of 2.5%. After incubation for 3 hours at room temperature or overnight at 4°C, the insoluble fraction was removed by ultracentrifugation. The soluble fraction was collected, and the insoluble pellet resuspended in an equal volume to the soluble fraction. The amount of FtsB in each sample was detected by western blotting after separation by SDS-PAGE (figure 3.7b). Under visual inspection, the overnight solubilisation had less FtsB in the insoluble fraction therefore this time point appears to be more successful in solubilising FtsB.

After identifying the conditions for membrane collection and SMA solubilisation, the SMA solubilised membranes were combined with prepared Ni-NTA resin to purify solubilised FtsB from other solubilised membrane proteins. After incubation for 1 hour on a rotating platform, the resin was transferred to a gravity flow column and the flow-through collected. The resin was washed with a low imidazole concentration buffer to remove any non-specifically bound contaminants. His-tagged proteins were eluted with increasing imidazole concentrations. All wash and elution fractions were collected and analysed by SDS-PAGE (figure 3.8).

The flow through fraction (FT) demonstrated that a large percentage of solubilised material did not bind the resin. The low imidazole washes (W1-6) removed any un-tagged proteins until no detectable protein was removed from the column. The elution fractions using imidazole concentrations between 100 mM and 250 mM (E1-4) did not elute any protein. The elution fractions using imidazole concentrations above 250 mM (E4-8) showed the elution of a protein around at a molecular weight of ~18 kDa.

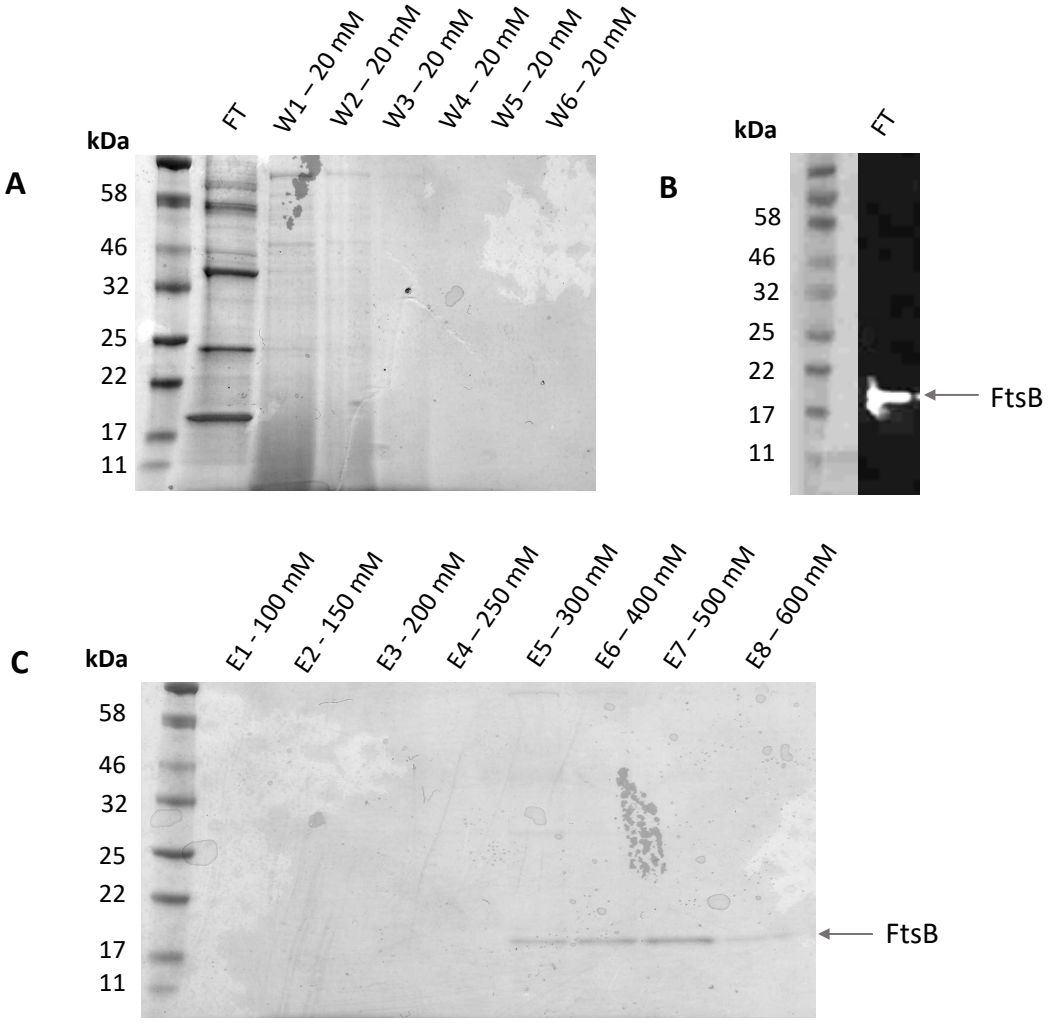

Figure 3.8. **Trial FtsB Ni-NTA purification.** SMA solubilised membranes were incubated with Ni-NTA resin overnight and then transferred to a gravity flow column and flow through (FT) collected. The resin was washed 4 times with 10 CV 20 mM imidazole buffer (W1-4) and then His-Tagged proteins were then eluted 8 times with 1 CV 100-600 mM imidazole buffer (E1-8). (A) and (C) Fractions were analysed by electrophoresis on a 12% SDS-PAGE gel and protein bands visualised by Coomassie staining. (B) SDS-PAGE separated FT was transferred to a nitrocellulose membrane and probed with an anti-HisTag antibody.

The predicted molecular weight of FtsB with the weight of the purification tags included is 14 kDa, however gel shifting of membrane proteins in SDS-PAGE is well documented. Some proteins can migrate up to 30% more slowly than predicted from their formula weights due to SDS-loading by α-helical structures (Rath *et al.*, 2009). The band at 18 kDa was confirmed to be FtsB by excising the E7 band from the SDS-PAGE and submitting it for mass spectrometric analysis. A darkly stained band at 18 kDa was also seen in the flow-through, which indicated that most of the FtsB in the sample had not bound to the column. To confirm that the FtsB in the flow through had retained the His-Tag, the SDS-PAGE separated FT was transferred to a nitrocellulose membrane and probed with an anti-HisTag antibody. This showed that the FtsB band in the flow-through was His-tagged FtsB, therefore much of the FtsB in the sample did not bind to the column despite the His-Tag being present.

To improve the yield from affinity purification of FtsB, a range of binding conditions were investigated (figure 3.9). In the trial purification a binding time of 1 hour was used as suggested by the resin manufacturer, but the presence of the SMALP disc could interfere with the binding process, so an overnight incubation with this resin was also trialled. To investigate the possibility that the resin used was incompatible with SMA, a second Ni-NTA resin (Super NI-NTA, Generon) was trialled with overnight incubation for comparison. Finally, when expressed in pET52b FtsB is tagged with both a C-terminal His-Tag and an N-terminal Strep-Tag II, therefore the binding of FtsB to streptactin resin was also attempted. The solubilised membranes were passed over a streptactin resin, which was washed with Tris-HCl buffer before elution of strep-tagged proteins with d-Desthiobiotin. From these investigations it appeared that FtsB-SMALP binding was improved by overnight incubation with the Ni-NTA

resin, and that the Super Ni-NTA resin offered a slight improvement over the HisPur resin. The streptactin resin had a smaller amount of FtsB in the flow through than the 1-hour Ni-NTA incubation, but no elution from the resin could be detected, therefore the use of streptactin resin required further investigation before it could be used to purify FtsB.

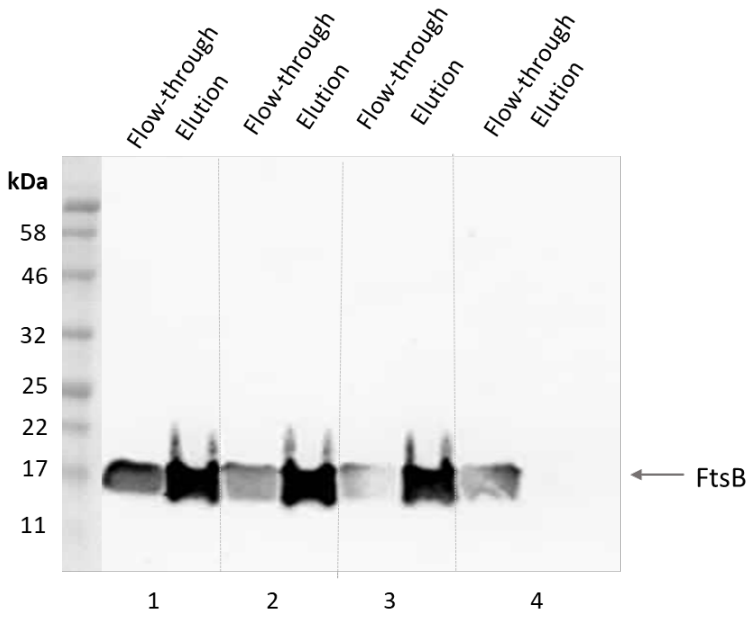

Figure 3.9. **Improving affinity resin binding of FtsB.** SMA solubilised membranes were incubated with affinity resin under different conditions to improve binding and FtsB yield. 1 = 1 hour incubation with HisPur resin, 2= overnight incubation with HisPur resin, 3= overnight incubation with Super Ni-NTA, 4= gravity flow binding to streptactin resin. After incubation, the flow through from the resin was collected. Ni-NTA resins were washed extensively with a 20 mM imidazole concentration buffer and then His-Tagged proteins were eluted with 500 mM imidazole. The steptactin resin was washed with TrisHCl buffer and then strep-tagged protein was eluted with 5 mM d-Desthiobiotin. Flow through and elution fractions were seperated by SDS-PAGE, transferred to a nitrocellulose membrane and probed with an anti-HisTag antibody.

Using the improved binding conditions of an overnight incubation with Super Ni-NTA resin, SMA-solubilised FtsB was purified and the results were assessed by SDS-PAGE. For comparison, the same dry weight of membranes was used as in the initial purification. These conditions resulted in a much higher yield of FtsB in the elution fractions (E1-E4) compared to the trial purification (Figure 3.10). However, a protein band at 18 kDa representing FtsB was still visible in the flow through from the resin, which suggests that the binding of FtsB to the resin is not optimal despite the improvement.

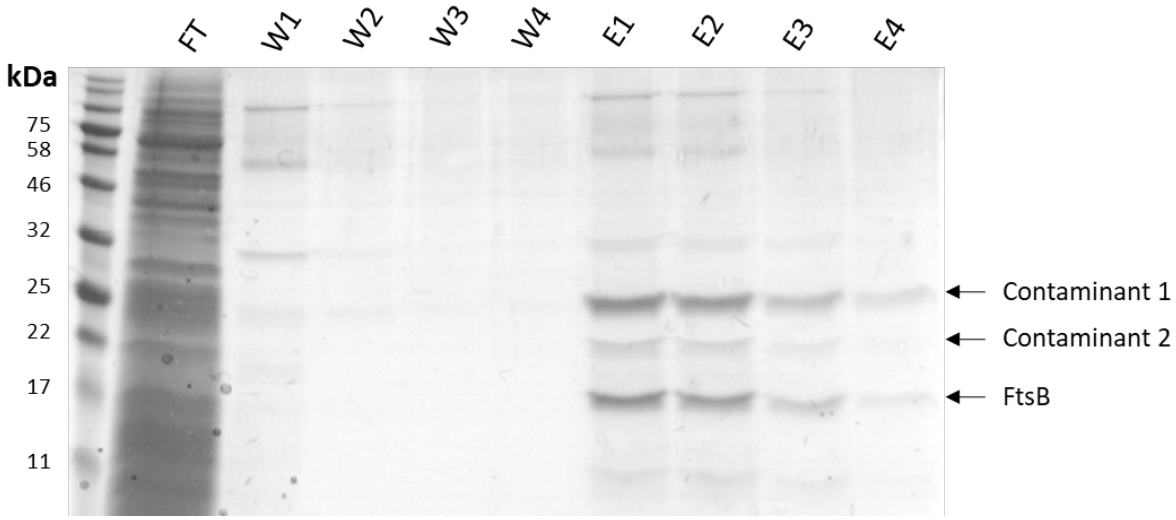

Figure 3.10. **FtsB Ni-NTA purification.** SMA solubilised membranes were incubated with Ni-NTA resin overnight and then transferred to a gravity flow column and flow through (FT) collected. The resin was washed 4 times with 10 CV 20 mM imidazole buffer (W1-4) and then His-Tagged proteins were then eluted 4 times with 1 CV 500 mM imidazole buffer (E1-4). Fractions were analysed by electrophoresis on an 18% SDS-PAGE gel and protein bands visualised by Coomassie staining.

The improved yield of FtsB also resulted in the co-elution of a range of contaminants, the most prominent being at 25 kDa. During this purification, 20 mM imidazole was used to wash the resin and 500 mM imidazole was used for the elution of FtsB from the resin to achieve optimal elution. While the contaminants were not washed off with 20 mM imidazole, they may be eluted at a lower concentration of imidazole than FtsB, allowing elution of the contaminants without losing the protein of interest. To address this, once binding had taken place, an imidazole gradient was performed to identify at which concentration each of the contaminants elute.

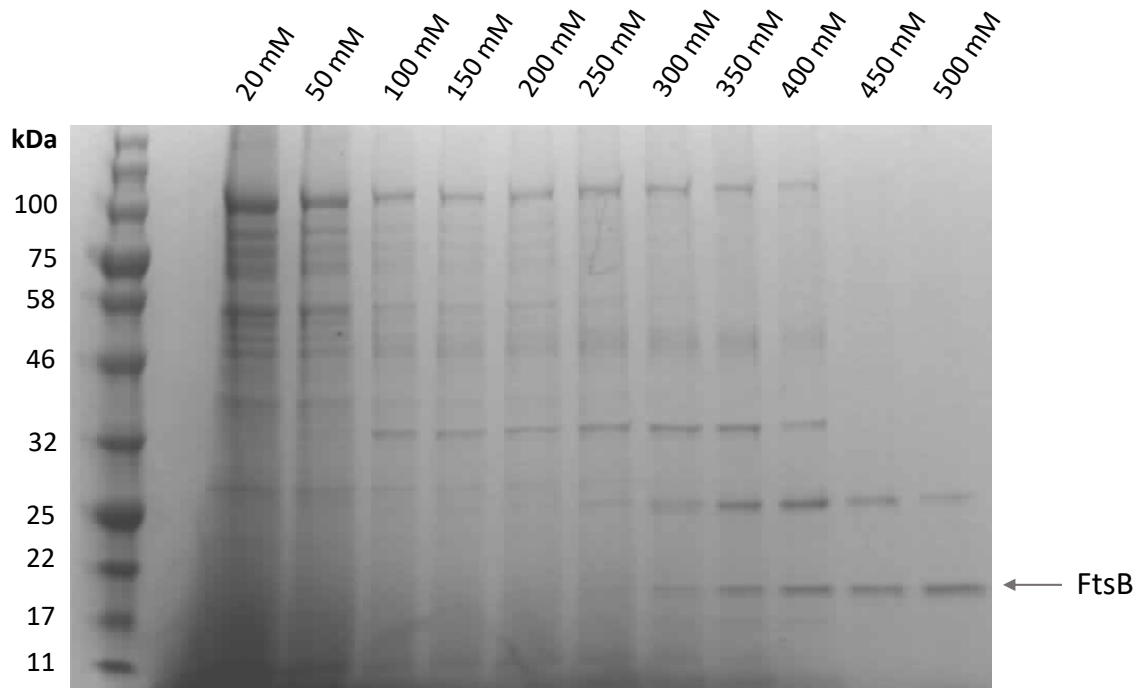

Figure 3.11. **FtsB Ni-NTA imidazole gradient.** SMA solubilised membranes were incubated with Ni-NTA resin overnight and then transferred to a gravity flow column and flow through (FT) collected. The resin was washed once with 10 CV 20 mM imidazole buffer and then the resin was then washed 10 times with 1 CV of imidazole buffer, with the concentration of imidazole increasing from 50 mM to 500 mM. Fractions were analysed by electrophoresis on an 18% SDS-PAGE gel and protein bands visualised by Coomassie staining.

At lower imidazole concentrations (20-100 mM), the major contaminants at 100 kDa, 46 kDa, and 32 kDa eluted from the column, with no visible elution of FtsB. However, the contaminant at 25 kDa did not begin to elute from the column until the imidazole concentration was increased to 300 mM, at which point FtsB also began to elute from the column. Therefore, more stringent washing with 100 mM imidazole removed most of the contaminants from the column but the contaminant at 25 kDa could not be purified separately to FtsB using specific imidazole concentrations.

As shown previously in figure 3.9, FtsB successfully binds streptactin resin, and use of this second purification tag was investigated to improve the purity of FtsB. The elutions from the Ni-NTA resin were passed over a streptactin resin, which was washed with Tris-HCl buffer before elution of strep-tagged proteins with d-Desthiobiotin. No elution of FtsB could be detected, despite a range of d-Desthiobiotin concentrations and incubation times with the d-Desthiobiotin being trialled (data not shown). This suggested that FtsB-SMALPs were incompatible with streptactin purification, and the Strep-Tag was not used for further purification.

As attempts to further purify FtsB using affinity purification had failed, the pooled elutions from the Ni-NTA purification were concentrated and proteins were separated on the basis of hydrodynamic radius using size exclusion chromatography (SEC). Elution of protein and SMA was monitored by absorbance at 280 nm and 254 nm respectively (figure 3.12a). Multiple peaks were detected between 8 mL and 18 mL. Aliquots of the 0.5 mL elution fractions collected were analysed by SDS-PAGE (figure 3.12b) and western blotting with an anti-HisTag antibody (figure 3.12c).

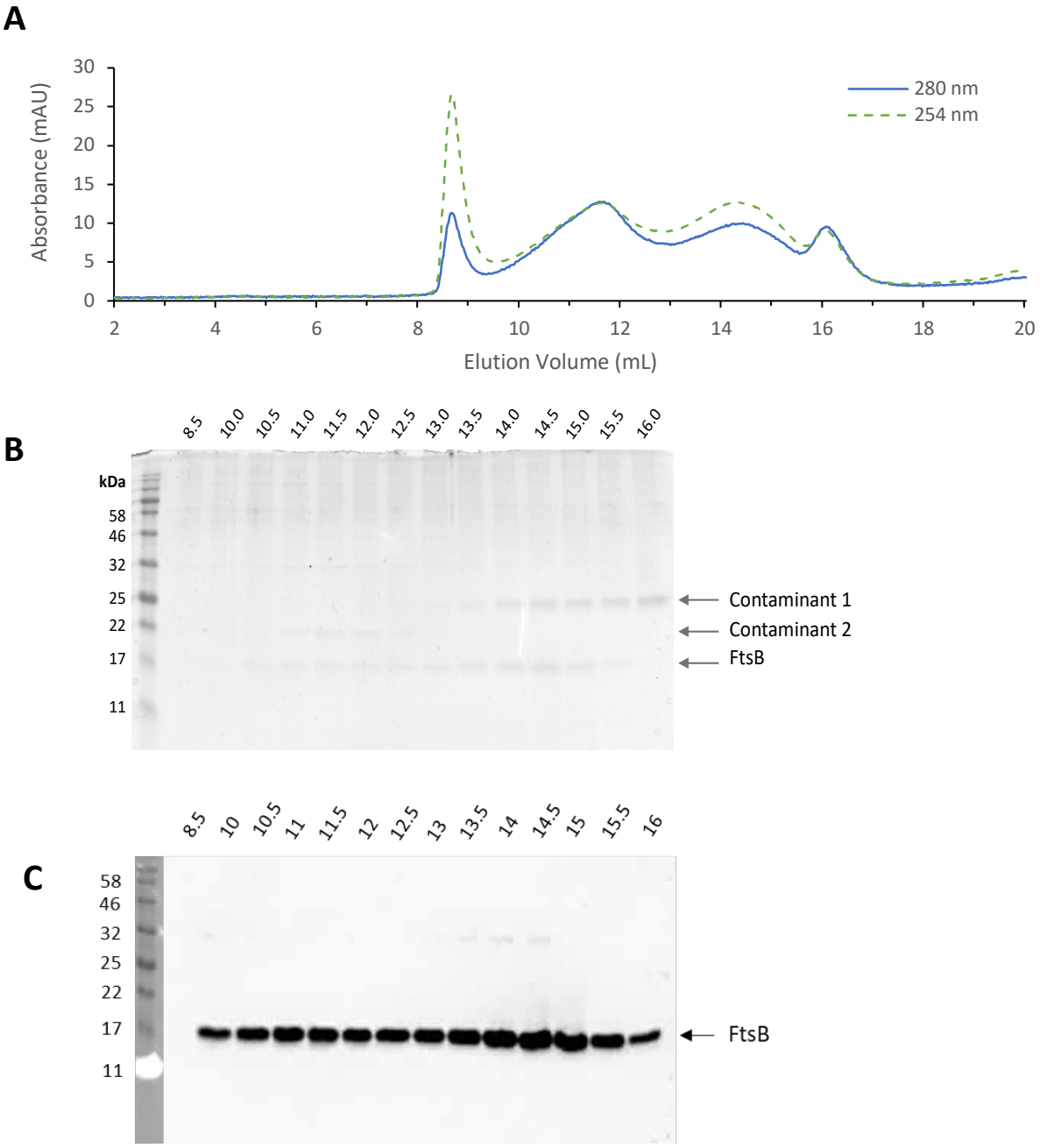

Figure 3.12. **SEC purification of FtsB.** Elution fraction fractions from Ni-NTA purification were pooled and injected onto a Superdex 200 Increase 10/300 GL column. The column was run at 0.5 mL/min for 25 mL, collecting 0.5 mL fractions. **(A)** SEC elution profile. Elution of protein and SMA from the column was monitored by absorbance at 280nm and 254 nm respectively. **(B)** SDS-PAGE of elution profile. Elution fractions at the given volumes were analysed by electrophoresis on an 18% SDS-PAGE gel and protein bands visualised by Coomassie staining. **(C)** The SDS-PAGE was also transferred to a nitrocellulose membrane and probed with an anti-HisTag antibody**.**

Despite having the highest absorbance at both 280 nm and 254 nm, the first sharp peak appeared not to contain a large amount of protein. This peak may contain aggregated polymer or SMALPs. From the results of the western blot of the elution fractions, FtsB appeared to elute broadly between 10-16 mL, with three distinctive peaks at 12 mL, 14 mL and 16 mL. Using the trendline equation from the calibration curve of the Superdex 200 Increase 10/300 GL column (supplementary figure 8.1), these volumes represent molecular weights of approximately 300 kDa, 110 kDa and 40 kDa respectively.

Contaminant 2 co-eluted with FtsB early in the elution profile, until ~ 12.5 mL, while contaminant 1 began to elute later at ~13 mL, and the band intensity appeared to be strongest at 16 mL, which represents the elution of the fourth peak. Contaminant 1 is the larger of the two proteins at 25 kDa, compared to FtsB at 14 kDa, however it eluted later from the column. This would suggest it is smaller than the FtsB-SMALP and therefore, it may be a soluble protein, as the added molecular weight of the SMALP makes FtsB-SMALPs run 'larger' on the SEC column than protein weight alone. To identify this contaminant, this higher molecular weight band was excised and submitted for protein identification by tandem mass spectrometry (MS/MS). The band was identified to be 7-carboxy-7-deazaguanine (CDG) synthase, a 25 kDa cytosolic protein. Contaminant 2 was also sent for MS/MS analysis, but due to the low concentration of eluted protein, this was repeatedly unsuccessful.

3.4 Solubilisation of FtsL using Styrene Maleic Acid

Using the framework provided by the previous experiments with FtsB, FtsL was similarly expressed and solubilised, and then purified on Ni-NTA resin. Figure 3.13 demonstrates that FtsL was successfully solubilised on treatment with SMA, and that it could be purified using Ni-NTA. As seen with FtsB, a large amount of FtsL did not bind to the resin during incubation, as it was detected both in the flow through and wash fractions. However, FtsL can also be visibly seen to elute in the higher imidazole fractions, indicating that some FtsL had successfully bound to the column. As seen with the FtsB purification, a band around 25 kDa co-purified with FtsL in the elution steps. This was predicted to be CDG synthase, as it later purified in the same manner during SEC purification and ran to the same molecular weight on SDS-PAGE. Another contaminant (contaminant 3) was found during FtsL purification that migrated to ~28 kDa.

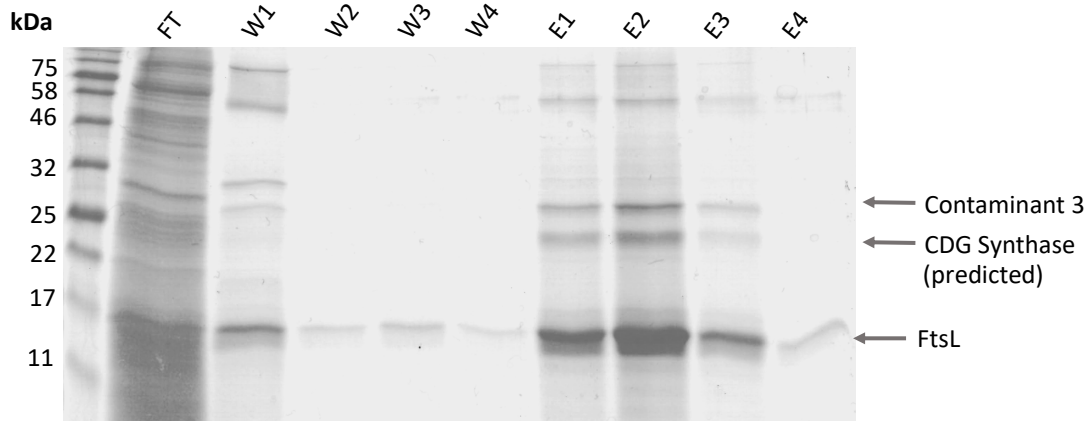

Figure 3.13. **FtsL Ni-NTA purification.** SMA solubilised membranes were incubated with Ni-NTA resin overnight and then transferred to a gravity flow column and flow through (FT) collected. The resin was washed 4 times with 10 CV 20 mM imidazole buffer (W1-4) and then His-Tagged proteins were then eluted 4 times with 1 CV 500 mM imidazole buffer (E1-4). Fractions were analysed by electrophoresis on an 18% SDS-PAGE gel and protein bands visualised by Coomassie staining.

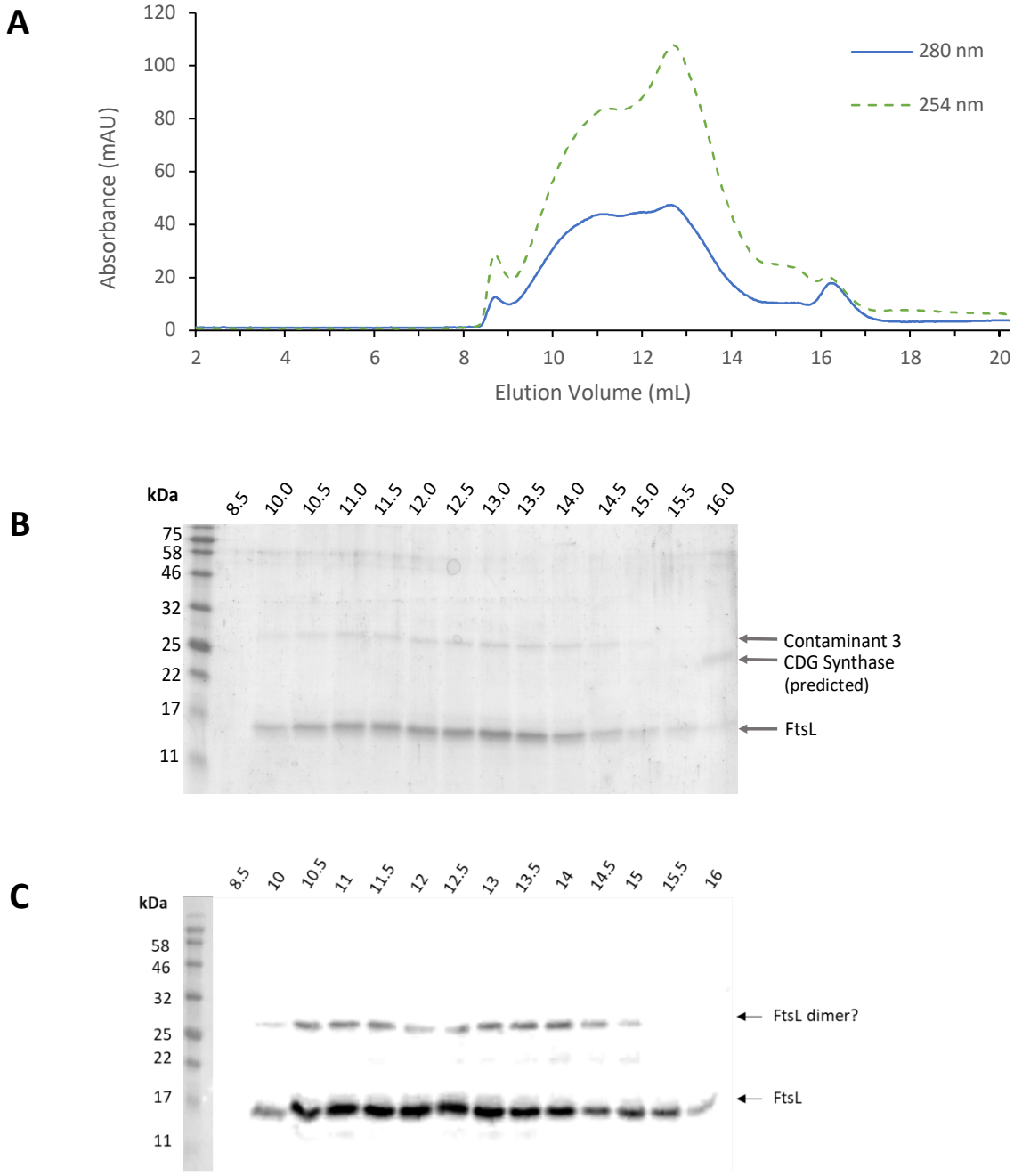

Figure 3.14. **SEC purification of FtsL.** Elution fraction fractions from Ni-NTA purification were pooled and injected onto a Superdex 200 Increase 10/300 GL column. The column was run at 0.5 mL/min for 25 mL, collecting 0.5 mL fractions. **(A)** SEC elution profile. Elution of protein and SMA from the column was monitored by absorbance at 280nm and 254 nm respectively. **(B)** SDS-PAGE of elution profile. Elution fractions at the given volumes were analysed by electrophoresis on an 18% SDS-PAGE gel and protein bands visualised by Coomassie staining**. (C)** The SDS-PAGE was also transferred to a nitrocellulose membrane and probed with an anti-HisTag antibody**.**

To further purify FtsL, the elution fractions were pooled, concentrated and then separated on a Superdex 200 Increase 10/3000 size exclusion column. Figure 3.14a presents the elution profile of the sample at both 280 nm and 254 nm, indicating the elution of protein and SMA respectively. The profile shows that both protein and SMA eluted across a large range of elution volumes, with distinct peaks at 11 mL, 13 mL and 16 mL. Fractions across this profile were then analysed by SDS-PAGE and western blotting, as shown in figure 3.14 b&c. FtsL eluted between 10 mL and 16 mL, as confirmed by the western blot which detected the HisTag of FtsL. As seen with FtsB, CDG synthase eluted at the far end of the profile but eluted with less overlap of FtsL compared to FtsB, which is probably due to the higher molecular weight of FtsL compared to FtsB.

Contaminant 3 co-eluted across the profile with FtsL. As the contaminant appeared to be around double the molecular weight of FtsL, and these higher molecular weight bands contained a His-Tag as confirmed by western blotting (figure 3.14c), it was predicted that these bands may be FtsL that had formed SDS-resistant oligomers. To test this hypothesis, aliquots of the elution samples were treated with 2-mercaptoethanol to reduce disulfide bonds, and then the samples were re-analysed (figure 3.15). After treatment with 2-mercaptoethanol, the higher molecular weight bands were no longer visible, and their absence from the samples was confirmed with western blotting with an anti-His-Tag antibody to ensure low levels of the contaminant were no longer present. This confirmed that contaminant 3 was in fact FtsL that had formed intermolecular disulfide bonds that were resistant to previous reduction treatment. FtsL had previously been reported to form dimers which are artefacts of preparation (Gonzalez *et al.*, 2010). To further investigate this, an

undergraduate project carried out mutagenesis of the cysteine residues in FtsL to eliminate the formation of disulfide bridges. The results of this work demonstrated that the mutation of the cysteine residues to alanine had no major effect on FtsL oligomerisation in SMALPs (Khalil Adasenya, unpublished data). On reduction, light bands also appeared below the FtsL protein, which suggested these dimers may be formed by degraded FtsL that has retained its His-Tag, rather than full-length FtsL.

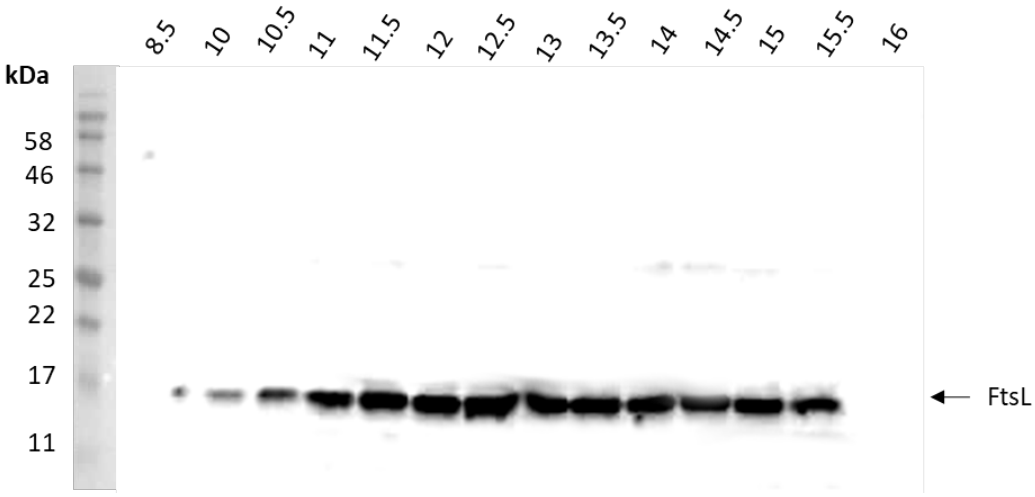

Figure 3.15. **2-Mercaptoethanol treatment of FtsL samples.** FtsL SEC elution fractions at the given volumes were treated with 2-Mercaptoethanol and analysed by electrophoresis on an 18% SDS-PAGE gel and transferred to a nitrocellulose membrane and probed with an anti-HisTag antibody**.**

3.5 Solubilisation of FtsQ using Styrene Maleic Acid

Finally, FtsQ was purified using the same methods applied to FtsB and FtsL. FtsQ was expressed in *E. coli* BL21(DE3) for 3 hours before collection of cells, preparation of membranes and solubilisation with SMA. After incubation with Ni-NTA resin, the resin was washed and His-Tagged proteins eluted with imidazole. As shown in figure 3.16, FtsQ was successfully solubilised with SMA, and eluted from the Ni-NTA resin on incubation with 500 mM imidazole. Little FtsQ was detected in the wash fractions, however a band at the molecular weight of FtsQ was seen in the flow through suggesting that not all of the FtsQ had bound to the resin. A protein band co-eluting with FtsQ was seen at the same molecular weight as in the FtsB and FtsL purifications, therefore it was again predicted to be CDG synthase as per the mass spectrometry analysis of the band found in FtsB.

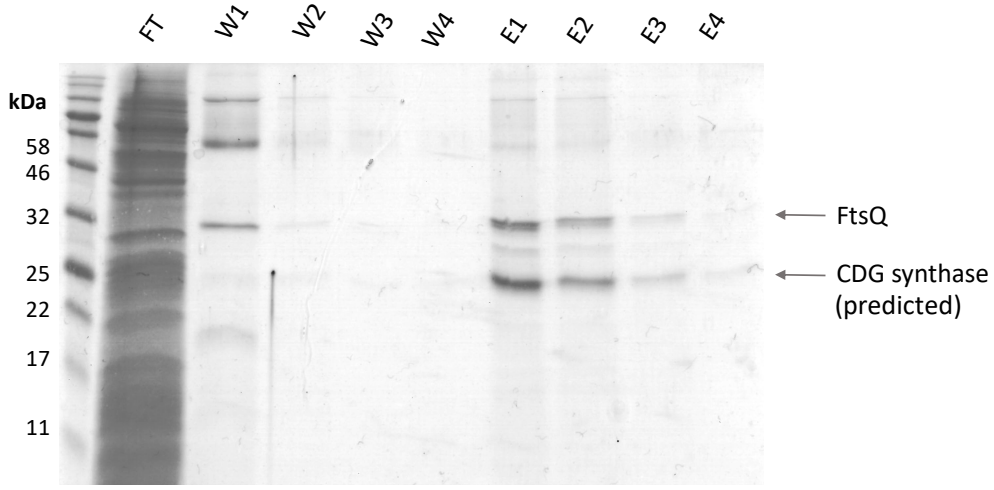

Figure 3.16. **FtsQ Ni-NTA purification.** SMA solubilised membranes were incubated with Ni-NTA resin overnight and then transferred to a gravity flow column and flow through (FT) collected. The resin was washed 4 times with 10 CV 20 mM imidazole buffer (W1-4) and then His-Tagged proteins were then eluted 4 times with 1 CV 500 mM imidazole buffer (E1-4). Fractions were analysed by electrophoresis on an 18% SDS-PAGE gel and protein bands visualised by Coomassie staining.

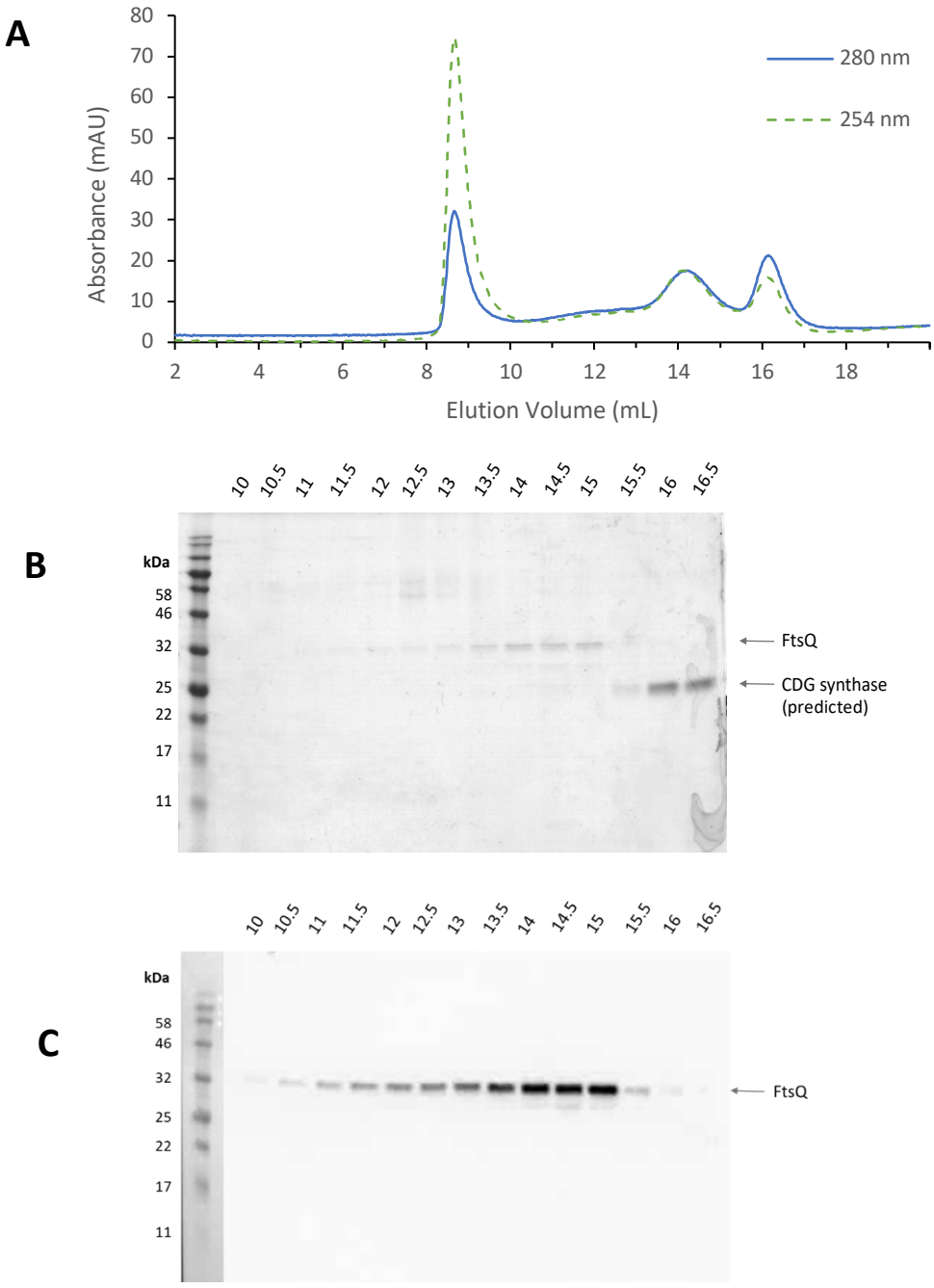

Figure 3.17. **SEC purification of FtsQ.** Elution fraction from the Ni-NTA purification were pooled and injected onto a Superdex 200 Increase 10/300 GL column, which was run at 0.5 mL/min for 25 mL, collecting 0.5 mL fractions. **(A)** SEC elution profile. Elution of protein and SMA from the column was monitored by absorbance at 280nm and 254 nm respectively. **(B)** SDS-PAGE of elution profile. Elution fractions at the given volumes were analysed by electrophoresis on an 18% SDS-PAGE gel and protein bands visualised by Coomassie staining**. (C)** The SDS-PAGE was also transferred to a nitrocellulose membrane and probed with an anti-HisTag antibody**.**

FtsQ eluted from the Ni-NTA resin was further purified by size exclusion chromatography on a Superdex 200 Increase 10/300 column, collecting 0.5 mL fractions and following the elution of protein and SMA at 280 nm and 254 nm respectively (figure 3.17a). Compared to FtsB and FtsL an unusually large peak at 8.5 mL, which represents aggregated material, was seen when purifying FtsQ. Subsequently, three distinct peaks eluted from the column, the first at 12 mL, then 14 mL and 16 mL. These elution fractions were then analysed by SDS-PAGE and western blotting (figure 3.17b&c). The elution of FtsQ from the column could be seen with faint bands between 11 mL and 15 mL, the volumes attributed to peak 1 and peak 2. This was confirmed with western blotting, which highlighted the elution of FtsQ between 10 mL and 16 mL, but at concentration undetectable by Coomassie staining. As predicted from the purification of FtsB and FtsL, the 25 kDa contaminant presumed to be CDG synthase eluted later from the elution profile at 16 mL, and due to the combined molecular weight of FtsQ and the SMALP disc, there was little overlap between the contaminant and FtsQ elution fractions.

3.6 Discussion

The first aim of this chapter was to clone the full-length *ftsB*, *ftsL* and *ftsQ* genes from the *E. coli* genome into an appropriate expression vector, and to overexpress these proteins in *E. coli*. Using traditional restriction digest methods, the full-length genes were successfully cloned into an expression vector, and the proteins were then each expressed in *E. coli*. Expression of all three proteins was successfully detected across a 20-hour induction time course; however, expression of FtsB and FtsL was greatly reduced in induced cultures grown

overnight, therefore limiting the growth of induced cells to only 3 hours. Compared to cells expressing FtsQ, cells expressing FtsB and FtsL also demonstrated a reduced growth rate upon induction. Previous studies have found that that the interaction of FtsB and FtsL protects both proteins from degradation (Buddelmeijer *et al.*, 2002; Gonzalez and Beckwith, 2009; Wadenpohl and Bramkamp, 2010). Therefore, increasing the expression levels of FtsB without increasing FtsL levels may result in insufficient FtsL for FtsB to associate with, leaving FtsB vulnerable to degradation, and vice versa in the case of FtsL overexpression. In comparison, FtsQ is stable in absence of its association with FtsB and FtsL, which may explain why expression of FtsQ was stable across all time points. By trialling multiple growth conditions, expression levels of each protein were improved sufficiently to proceed to large scale expression and protein preparation.

The second aim of this chapter was to establish whether SMA can efficiently solubilise the over-expressed proteins from the membrane and whether these proteins can then be adequately purified using IMAC and SEC methods. The results shown in this chapter demonstrate that SMA can successfully solubilise all three proteins from the membrane, however, there were significant challenges to purification, such as inefficient binding to Ni-NTA resin. SMALPs are around 10 nm wide, and this additional structure around the membrane protein may partially occlude purification tags on the protein. One solution to this problem would be to investigate using a tag at the opposite terminus of the protein, however, for FtsB use of the StrepTag II at the N-terminus was also unsuccessful as no protein could be successfully eluted from the column. Another solution that could be investigated is the use of

flexible linkers to increase the distance between the protein and the purification tag and therefore improve the accessibility of the tag (Chen, Zaro and Shen, 2013).

Another common issue in the purification of all three proteins was the co-purification of contaminants at concentrations similar to the protein of interest. One common contaminant migrated to a molecular weight of 25 kDa. Using mass spectrometry, this contaminant was found to be 7-carboxy-7-deazaguanine (CDG) synthase, a 25 kDa cytosolic protein encoded by the *queE* gene. CDG synthase is one of the four enzymes that syntheses GTP into $preQ_{0,}$ a precursor of the hypermodified base queuosine found in tRNA (McCarty *et al.*, 2009). Co-purification of the cytosolic protein due to an innate affinity for Ni-NTA resin appeared unlikely, as *E. coli* membranes were separated from soluble proteins before being solubilised and therefore high levels of free cytosolic proteins were not expected to be in the preparation that was loaded onto the Ni-NTA resin. Additionally, inspection of the protein sequence of CDG-synthase revealed no histidine clusters that may interact with the resin. Therefore, it was postulated that CDG synthase may be interacting with FtsB.

Recently, a study by Yadavalli *et al.* (2016) discovered a surprising link between CDG synthase and cell division. When *E. coli* were grown in sub-lethal concentrations of the antimicrobial peptide C18G, it caused the cells to filament. These filamentous cells had a continuous cytoplasm, which suggested filamentation was due to septation being blocked. Additionally, the cells displayed intact Z rings uniformly along their length, which would suggest that division had been blocked sometime after the assembly of the early divisome. In the search for genes involved in this morphology, deletion screening found that filamentation was supressed by the deletion of *queE,* the gene coding for CDG synthase. Similarly, increased *queE*

expression caused filamentous growth in wild type cells. How CDG synthase causes this filamentation was investigated and it was discovered that spontaneous mutations in *ftsA* or *ftsZ* suppress *queE* induced filamentation. Considering these findings, and that CDG synthase was seen to colocalise with Z rings during filamentation, it was predicted that CDG synthase blocks cell division by binding directly to a component of the divisome. Further experiments would be needed to confirm to interaction of the FtsBLQ complex with CDG-synthase, however, this presents an interesting avenue for further work.

CHAPTER 4: CHARACTERISATION OF THE COMPONENTS OF THE FTSBLQ COMPLEX IN STYRENE MALEIC ACID LIPID PARTICLES

4.1 Introduction

Due to the difficulties in expressing and purifying the components of the FtsBLQ complex, very little is known about how these proteins self-associate and associate with one another. Much of what is known about the binding of the components has been discovered through mutagenesis and co-immunoprecipitation, which provides information about the presence and absence of binding and the regions important for this, but cannot indicate the oligomerisation states of these complexes. In order to gain further information on the homo-oligomerisation states of the components, each protein must first be solubilised. As the solubilisation of full-length proteins was not successful in many studies, focus moved to the periplasmic domain, which could be purified as a soluble domain. However, as coiled coils tend to be unstable in isolation, therefore requiring fusion to stabilising coils such as the bacteriophage GP7 protein in order to be studied (LaPointe *et al.*, 2013). Therefore, the first aim of this chapter was to investigate whether SMALP solubilisation supports the preparation of full-length folded proteins in the native environment.

The aforementioned studies using the periplasmic domains of the FtsBLQ proteins have been hugely beneficial in producing structural information. However, it has been shown that the transmembrane region of FtsB homo-oligomerises in isolation (Khadria and Senes, 2013; LaPointe *et al.*, 2013), and that the absence of a transmembrane region can affect the interaction of FtsBLQ components (Glas *et al.*, 2015; Choi *et al.*, 2018). Consequently, including the transmembrane region in the characterisation of these proteins may further elucidative its native oligomerisation state within the membrane. The second aim of this chapter was

therefore to investigate whether SMALP solubilisation can aid the elucidation of the homo-oligomerisation states of the full-length components of the FtsBLQ complex.

4.2 Circular Dichroism of SMA solubilised FtsB and FtsL

Circular dichroism is a spectroscopy technique that measures the differential absorption of left and right circularly polarised light by a molecule. This can be particularly useful in the estimation of protein structure, as these structures display well-defined motifs due to the chiral arrangement of $\eta \rightarrow \pi^*$ and $\pi \rightarrow \pi^*$ transitions in the peptide backbone. An α-helical CD spectrum has two negative peaks at 208 nm and 222 nm, and a positive peak at 195 nm. The β-sheet CD is less well-defined as they are structurally more variable, but is generally found to have a negative band around 215-219 nm and a positive band at 195-202 nm.

To determine whether SMA solubilised FtsB/L/Q proteins were properly folded, purified samples were pooled and analysed by circular dichroism (CD). FtsB and FtsL are predicted to form coiled-coil structures, and the periplasmic region of FtsB has been successfully crystallised and shown to have an alpha-helical structure (LaPointe *et al.*, 2013). In the CD analysis, FtsB and FtsL both demonstrated two clear negative peaks, with one minimum at 208 nm and the other at 226 nm (figure 4.1). Small shifts in the CD spectra of membrane proteins is a known phenomenon due to the dielectric constant of the phospholipid bilayer being largely different from that of water (Miles and Wallace, 2016). Therefore, the peak minimum at 226 nm was assigned as a shifted peak from 222 nm and the spectra were both confirmed to be that of a folded α-helical protein within SMALPS. Due to the low concentrations of FtsQ that were purified, reliable CD spectra could not be collected. These

results demonstrate that SMA-solubilised FtsB and FtsL were folded into the predicted α-helical structure within the disc, therefore this method of solubilisation does not significantly disrupt native structure.

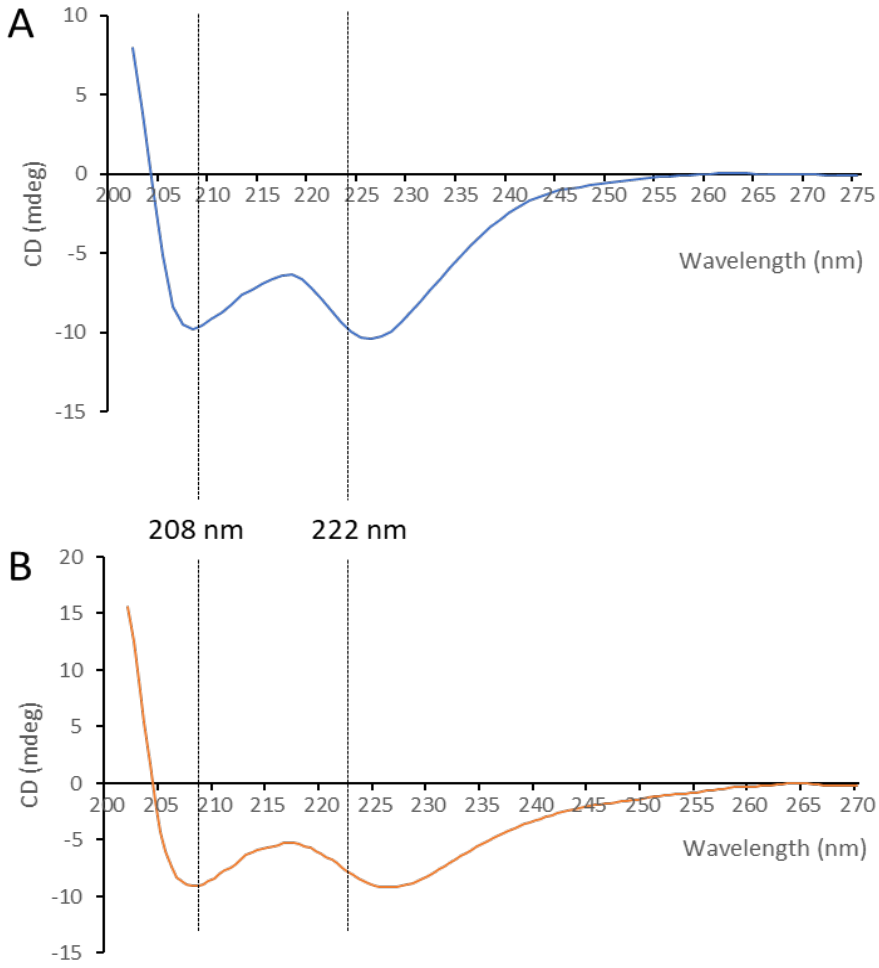

Figure 4.1. **CD analysis of SMALPs.** Elution fractions from the SEC purification of **(A)** FtsB-SMALPs and **(B)** FtsL SMALPs that were found to be free of contaminant were analysed by CD spectroscopy to assess secondary structure. Measurements were made on a JASCO J-1500 Circular Dichroism Spectrophotometer controlled by Spectra Manager software. Measurements were taken in a quartz glass cuvette, with a pathlength of 1 mm, and a protein concentration ~0.1 mg/mL. Each spectrum is an average of 5 scans. Baseline spectra taken with the buffer in which the sample had been prepared were subtracted from the sample spectra and the resulting spectrum smoothed using the Savitzky-Golay method within the Spectra Manager software.

4.3 Thermal stability comparison of FtsB in SMA and detergent

When the periplasmic domain of FtsB was purified by fusion to the globular Gp7 protein, CD thermal melts demonstrated that the protein became nearly completely unfolded when the temperature was increased from 5°C to 40°C, with a greater than 50% loss of CD signal at 222 nm (LaPointe *et al.*, 2013). SMA solubilisation has previously been reported to offer increased thermal stability of proteins compared to traditional detergents (Knowles *et al.*, 2009), therefore, thermal melt studies were conducted with FtsB solubilised in both SMA and n-Dodecyl-β-D-Maltopyranoside (DDM) in order to assess whether SMA offers improved thermal stability over periplasmic and detergent preparations. FtsB was overexpressed in *E. coli*, and then FtsB-SMALPs were purified from one half of the prepared membranes. The other half of the membranes were solubilised with DDM, and FtsB was purified using Ni-NTA resin (figure 4.2). FtsB was successfully solubilised by DDM, and appeared to purify to a higher purity than SMA solubilsed FtsB, with no visible contaminants detected by Coomassie staining.

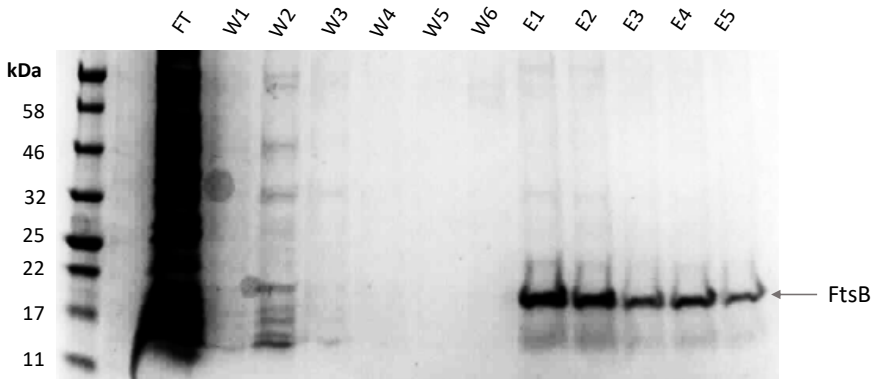

Figure 4.2. **DDM-FtsB Ni-NTA purification.** DDM solubilised membranes were incubated with Ni-NTA resin overnight and then transferred to a gravity flow column and flow through (FT) collected. The resin was washed 6 times with 10 CV 20 mM imidazole buffer (W1-6) and then His-Tagged proteins were then eluted 5 times with 1 CV 500 mM imidazole buffer (E1-5). Fractions were analysed by electrophoresis on an 18% SDS-PAGE gel and protein bands visualised by Coomassie staining.

Very little FtsB was lost during the wash steps, indicating FtsB was tightly bound to the resin. DDM-purified FtsB also yielded a higher concentration across the elutions compared to SMA-FtsB, at an average of 100 μg/ml compared to 25 μg/ml, and required a higher volume of elution to remove all bound protein. This suggested that more FtsB had bound to the resin in the DDM sample. The elution samples were further purified by SEC purification and elution fractions containing FtsB were pooled for CD analysis.

FtsB-SMALPs and DDM-FtsB samples were diluted to 0.1 mg/mL and thermal melt studies were conducted. CD spectra were taken at 5°C intervals between 15°C and 95°C, allowing the sample to equilibrate to the measurement temperature before each spectrum was taken. As seen in figure 4.3a and b, both the FtsB-SMALP and DDM sample displayed a degree of unfolding as a result of increased temperature, demonstrated by gradual reduction of CD signal across the spectra. Measurements below 205 nm for SMA samples and below 210 nm for DDM samples were found to exceed the high tension (HT) voltage cut limit at increased temperatures and therefore are not accurate representations of secondary structure changes. This behaviour is common during thermal melt experiments, and the HT cut-off is commonly increased by around 6 nm during temperature increases from 20°C to 85°C (Miles and Wallace, 2016). Therefore, to accurately assess secondary structure changes, the CD of each sample was assessed at a single wavelength of 222 nm, which translates to one of the peaks for α helical structure. This wavelength was unaffected by HT changes during temperature ramping. Changes were expressed in percentage change in relation to the sample at 15°C, in order to normalise against small differences in concentration (figure 4.3c).

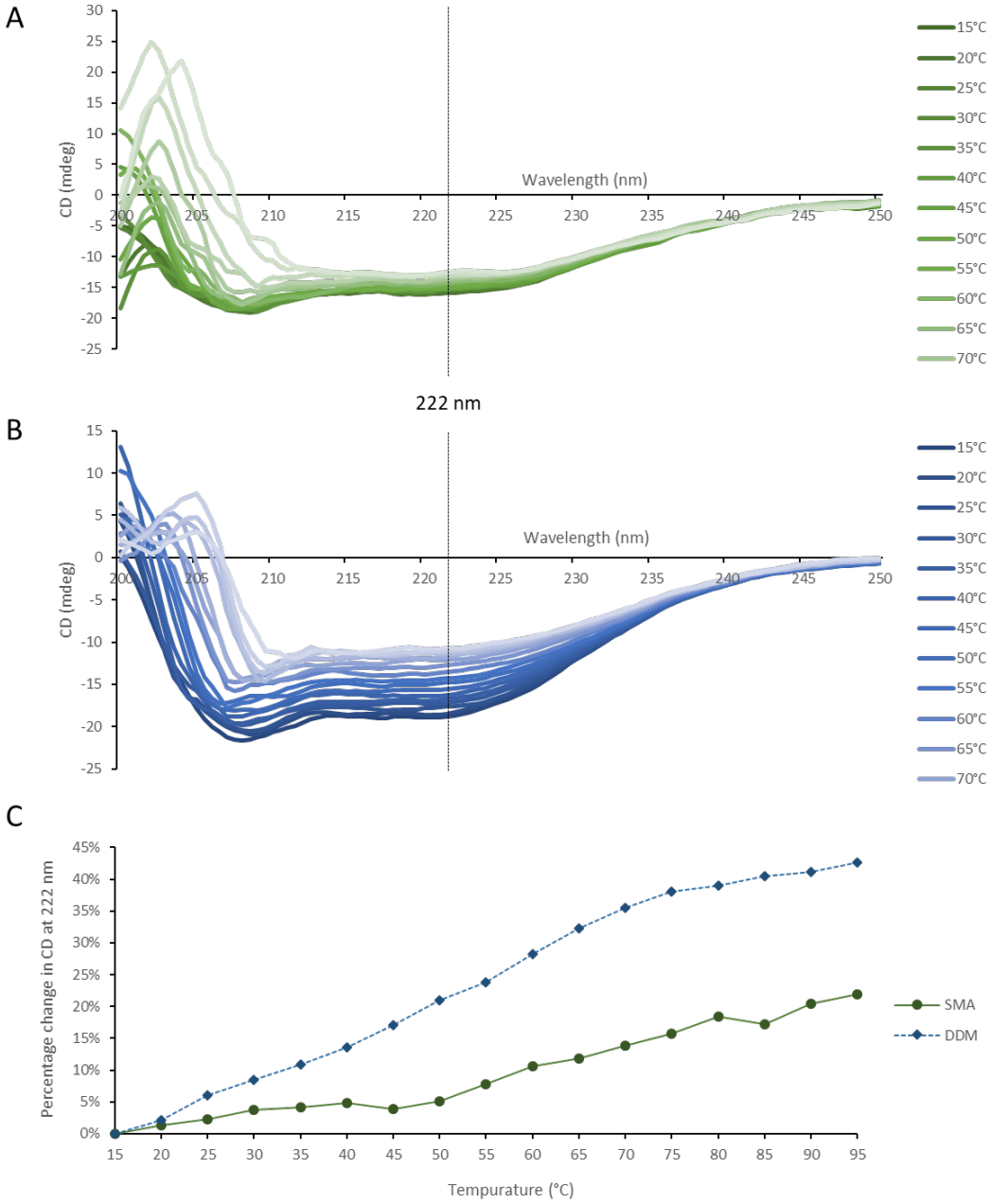

Figure 4.3. **Thermal Melt CD analysis of FtsB. (A)** SMALP-FtsB and **(B)** DDM-solubilised FtsB were analysed by thermal melt CD. Measurements were made on a JASCO J-1500 Circular Dichroism Spectrophotometer. Measurements were taken in a quartz glass cuvette, with a pathlength of 10 mm, and a protein concentration ~0.1 mg/mL. Samples were heated from 15°C to 95°C at 5°C intervals, allowing the sample to equilibrate to the measurement temperature before sprectra were measured. Each spectrum is an average of 5 scans and the resulting spectrum was smoothed using the Savitzky-Golay method within the Spectra Manager software. **(C)** Comparison of the percentage change in CD value at 222 nm for SMA FtsB and DDM FtsB samples during melting**.**

Compared to DDM-solubilised FtsB, FtsB-SMALPs were subject to smaller changes in CD signal as the temperature increased, suggesting that they are more thermally stable. Both DDM- and SMA-solubilised FtsB samples demonstrated improved stability over published thermal melt data for the FtsB periplasmic domain purified in isolation (LaPointe *et al.*, 2013). These results demonstrate that expression of full-length FtsB can improve stability of the protein compared to truncates, and that SMA solubilisation of this protein offers improved stability over the traditional detergent solubilisation, although this was only tested using DDM.

4.4 Lipid analysis of DDM- and SMA-solubilised FtsB

The lipid cardiolipin (CL) has been demonstrated to preferentially localise to the septum and poles in living *E. coli* cells (Mileykovskaya and Dowhan, 2000). This localisation pattern is predicted to arise as a consequence of membrane curvature sensing by CL (Renner and Weibel, 2011), and has been found to play an important role in the targeting of membrane proteins to the polar region (Romantsov *et al.*, 2007). Additionally, MinD, which is part of a complex that enforces the formation of the Z ring at mid-cell (see section 1.1.4), has been shown to display a preference towards anionic phospholipids (Szeto *et al.*, 2003), dictated by its membrane targeting sequence (MTS). As the MTS of MinD has been shown to be functionally interchangeable with the MTS of FtsA, successfully targeting FtsA to the Z ring (Pichoff and Lutkenhaus, 2005), this anionic preference may also extend to proteins of the divisome.

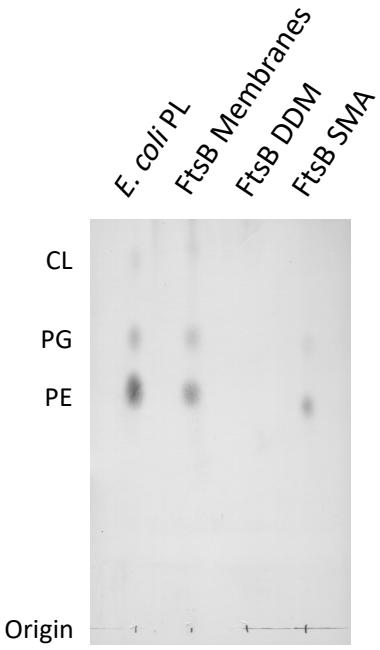

Figure 4.4. **Thin-layer chromatography.** Thin-layer chromatography of the lipid content of *E. coli* membranes overexpressing FtsB, DDM-solubilised FtsB and FtsB-SMALPs. *E. coli* polar lipids (PL) were included for reference. The positions of phosphatidylglycerol (PG), phosphatidylethanolamine (PE) and cardiolipin (CL) are shown. Transfer studies were performed three times independently, with representative data shown.

These studies demonstrate the importance of the lipid composition of membranes for protein localisation and function, however most membrane protein solubilisation methods strip the surrounding lipids, making analysis of a protein's native lipid environment difficult. In comparison, SMALPs have been reported to preserve the native lipid environment around membrane proteins, and recent work has demonstrated that lipids extracted from SMA solubilised membrane proteins show distinct lipid profiles between proteins (Teo *et al.*, 2019). To confirm whether SMA solubilisation of Fts- proteins can similarly capture the native lipid environment of the membrane proteins, thin-layer chromatography (TLC) analysis was performed (figure 4.4). Samples were prepared from *E. coli* membranes overexpressing FtsB, purified FtsB solubilised with DDM and purified FtsB solubilised with SMA. These samples

were analysed alongside commercial *E. coli* polar lipids as a control. As expected, the DDM sample had no visible lipids, confirming that detergent preparation removes native lipids surrounding the protein during solubilisation. In comparison, the SMA sample had copurified with both phosphatidylglycerol (PG) and phosphatidylethanolamine (PE), the predominant lipids of the membrane as shown in the FtsB membrane sample. Cardiolipin was not detected, however SMA samples were loaded at a lower than optimal concentration due to purification constraints therefore cardiolipin may be present but at a concentration below the detection limit for this method. These results show that SMA solubilisation of membrane proteins can provide additional information about the native environment compared to traditional preparation methods, and this may be useful in piecing together how the divisome is localised and controlled.

4.4 Native-PAGE for studying homo-oligomerisation

The homo-oligomerisation state of FtsQ has been highly debated in the literature. FtsQ self-interaction has been detected *in vivo* by D'Ulisse *et al.* (2007) and crystallised by van den Ent *et al.* (2008), while subsequent studies using analytical ultracentrifugation (AUC) and photocrosslinking have found FtsQ to be monomeric (van den Ent *et al.*, 2008; van den Berg van Saparoea *et al.*, 2013). However, these results were found when only the periplasmic portion of FtsQ was expressed, therefore, as predicted by (D'Ulisse *et al.*, 2007) the transmembrane region may be necessary for FtsQ self-association. SMA-solubilised FtsQ is full

length, and is supported by the native lipid environment, therefore this technique may be useful in elucidating the homo-oligomerisation state of FtsQ.

Native-PAGE is an electrophoresis technique which allows the analysis of proteins in a non-denaturing, non-reducing environment, therefore keeping the protein in its native, folded state. In blue native-PAGE (BN-PAGE) Coomassie dye is introduced into the cathode buffer to provide charge to the sample for separation which is usually contributed by sodium dodecyl sulfate (SDS) in SDS-PAGE. BN-PAGE has been used to successfully separate intact membrane protein complexes (Peng *et al.*, 2011), and membrane protein complexes extracted from BN-PAGE have been demonstrated to remain enzymatically active (Schägger and von Jagow, 1991). Recently, native-PAGE has been successfully used to study the oligomerisation of proteins within SMALPS, and was shown to be a robust method for the evaluation of quaternary structure within the disc (Pollock *et al.*, 2019). SMALPs extracted from the gel were intact and able to be visualised by negative stain electron microscopy. Additionally, the lipid within the SMALP was amenable to extraction and characterisation by mass spectrometry. Therefore, native-PAGE of SMALPs offers a methodology for the identification of membrane complexes in a manner which requires very little sample, as large sample demands are often a roadblock in the characterisation of membrane proteins.

To determine whether BN-PAGE can predict the oligomeric state of FtsQ in SMALPs, affinity purified FtsQ was separated on a Superdex 200 Increase 10/300 GL SEC column, and the elution fractions were analysed by both SDS-PAGE and BN-PAGE (figure 4.5). When separated by SDS-PAGE, FtsQ is seen as a single band at its monomeric molecular weight of 32 kDa.

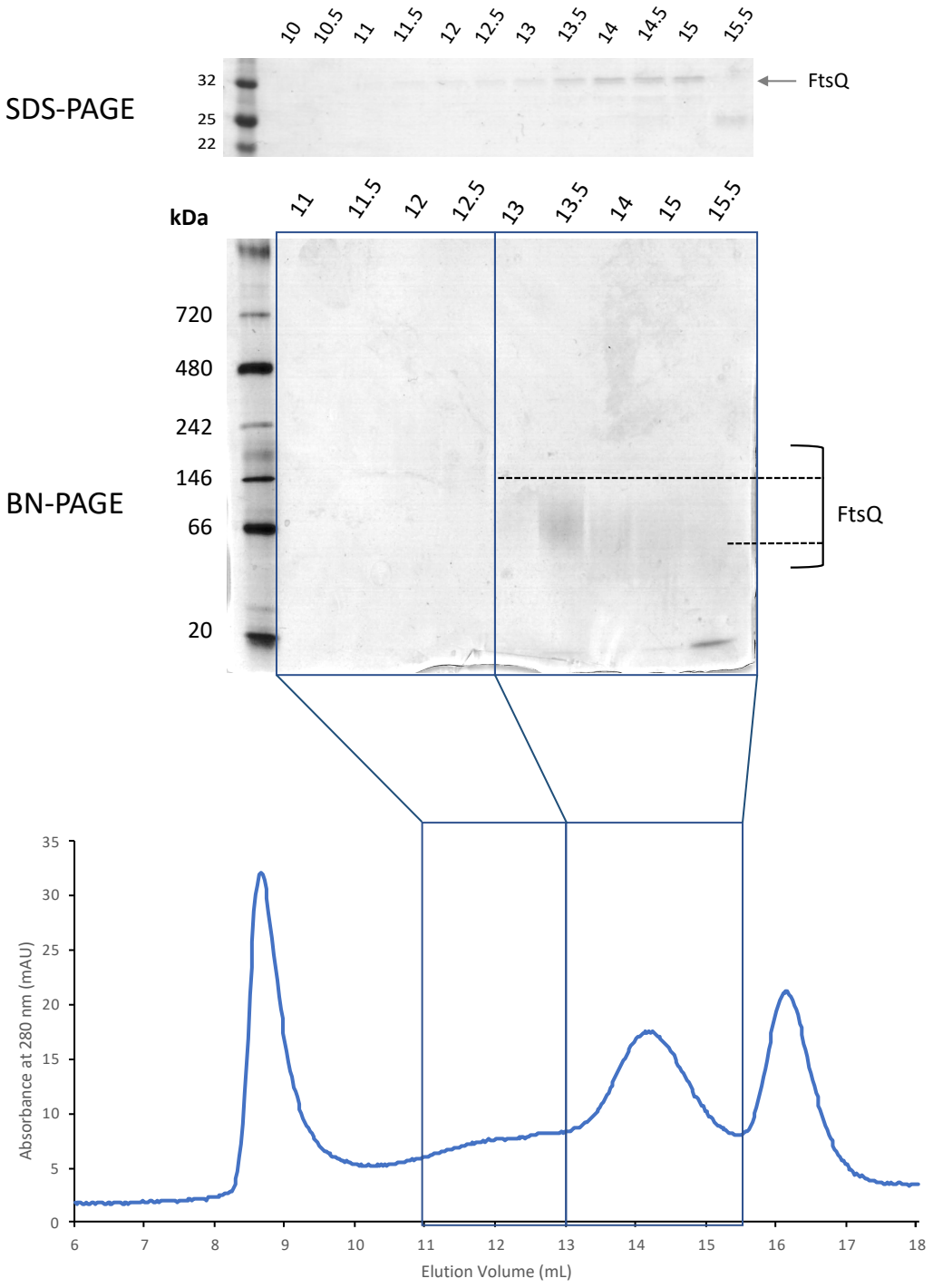

Figure 4.5. **BN-PAGE of FtsQ.** Elution fractions from Ni-NTA purification were pooled and injected onto a Superdex 200 Increase 10/300 GL column. The column was run at 0.5 mL/min for 25 mL, collecting 0.5 mL fractions. Elution was followed at 280 nm for detection of protein, as shown in the trace (bottom). Elution fractions at the given volumes were analysed by SDS-Page (top) and BN-PAGE (middle) electrophoresis on an 4-16% Bis-Tris gel and protein bands visualised by Coomassie staining.

When these elutions fractions are separated by BN-PAGE, two populations of diffuse bands are seen at ~150 kDa and ~70 kDa, eluting between 12 mL and 15.5 mL, and a sharp band at 20 kDa was seen only in the 15.5 mL elution sample. To confirm which bands could be assigned to FtsQ, the BN-PAGE was transferred to a nitrocellulose membrane and probed with an anti-6XHis antibody (figure 4.6).

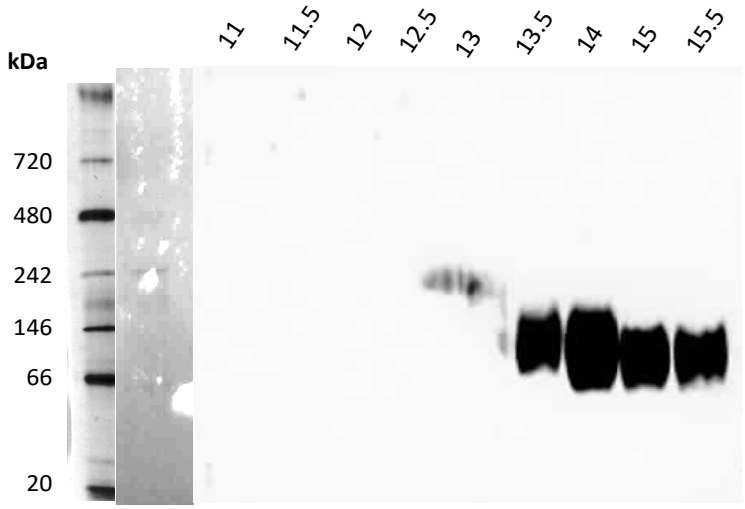

Figure 4.6. **Western blot of FtsQ BN-PAGE.** Elution fractions from Ni-NTA purification were pooled and injected onto a Superdex 200 Increase 10/300 GL column. The column was run at 0.5 mL/min for 25 mL, collecting 0.5 mL fractions. Elution fractions at the given volumes were analysed by BN-PAGE electrophoresis on an 4-16% Bis-Tris gel and transferred to a nitrocellulose membrane before western blotting with an anti-6xHis antibody.

The western blot of the BN-PAGE demonstrated that the protein band at 70 kDa can be attributed to His-Tagged FtsQ. As BN-PAGE separated SMALPs have been demonstrated to migrate to a molecular weight consistent with the weight of the contained protein (Pollock *et al.*, 2019), the migration of FtsQ-SMALPs to 70 kDa would suggest that these SMALPs contain dimeric FtsQ. The 140 kDa band found in the Coomassie stained BN-PAGE was partially detected in the western blot, however the quality of the blotting for this band was not ideal.

This molecular weight would represent tetrameric FtsQ or the presence of two dimers of FtsQ in the same disc. There is currently no evidence for tetrameric FtsQ, therefore it would be likely that a small amount of dimeric FtsQ can be solubilised into the same SMALP. The protein band at 20 kDa in the Coomassie-stained BN-PAGE was not detected in the western blot, therefore this represents the 25 kDa contaminant which is not His-tagged. No bands were detected in the Coomassie stained BN-PAGE or the western blot at 30 kDa therefore there was no evidence of monomeric FtsQ in this sample.

As BN-PAGE had successfully identified the molecular weights of oligomeric states in FtsQ-SMALPs, this technique was then applied to FtsB and FtsL in SMALPs. FtsB and FtsL are both predicted to form homodimers (Villanelo *et al.*, 2011), and *in vivo* the transmembrane domains of these protein can dimerise (LaPointe *et al.*, 2013); however, efforts to reconstruct their association *in vitro* been unsuccessful without the use of fusions to coiled-coils that enforce dimeric associations (Glas *et al.*, 2015; Choi *et al.*, 2018).

After separation by SEC on a Superdex 200 Increase 10/300 GL column, the elution fractions of FtsB SMALPs were separated by SDS-PAGE and BN-PAGE. As seen in FtsQ samples, FtsB-SMALPs migrate as a single band at 16 kDa. Two major contaminants are present which migrate to 21 kDa and 25 kDa. When these elution fractions were separated by BN-PAGE, diffuse bands were seen between 11.5 mL and 15.5 mL. These bands migrated to approximately 380 kDa, 120 kDa 60 kDa and 30 kDa. Sharp bands migrating to around 20 kDa were also seen as in the FtsQ samples, therefore these bands were assigned as the 25 kDa contaminant.

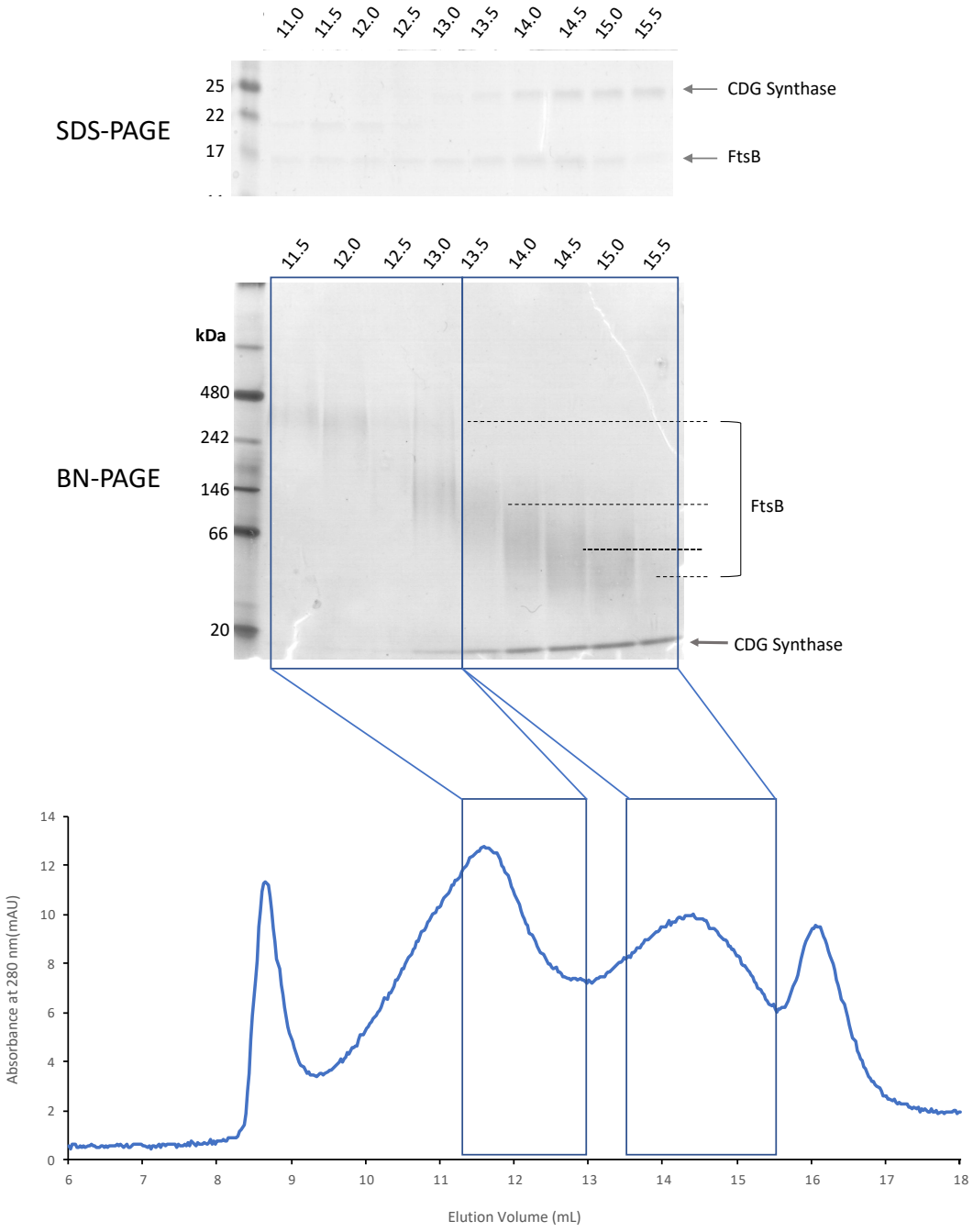

Figure 4.7. **BN-PAGE of FtsB.** Elution fractions from Ni-NTA purification were pooled and injected onto a Superdex 200 Increase 10/300 GL column. The column was run at 0.5 mL/min for 25 mL, collecting 0.5 mL fractions. Elution was followed at 280 nm for detection of protein, as shown in the trace (bottom). Elution fractions at the given volumes were analysed by SDS-Page (top) and BN-PAGE (middle) electrophoresis on an 4-16% Bis-Tris gel and protein bands visualised by Coomassie staining.

As both the 20 kDa and the 25kDa contaminant had previously been confirmed not to contain a His-tag (figure 3.12c), the BN-PAGE was transferred to a nitrocellulose membrane and western blotting was performed with an anti-6xHis antibody to identify the bands containing His-tagged FtsB (figure 4.8). The western blot showed that all diffuse bands between 380 kDa and 30 kDa contained His-tagged FtsB.

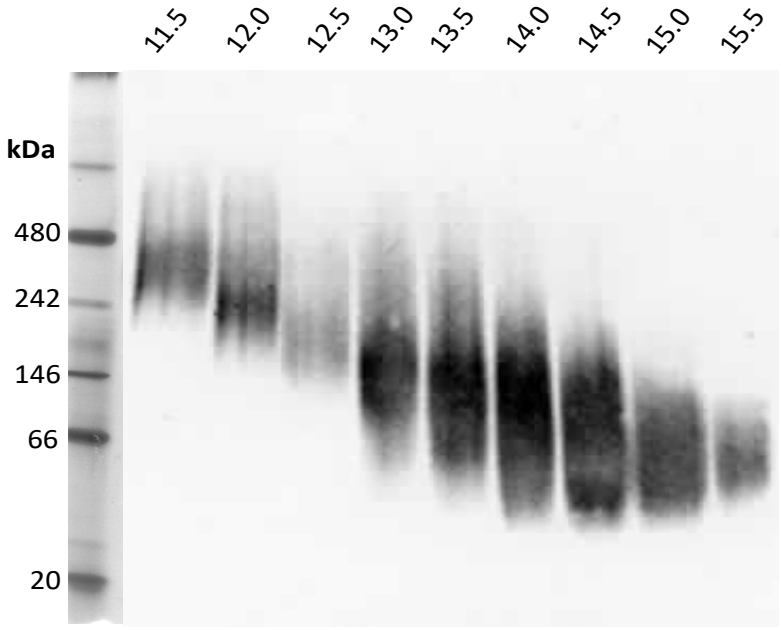

Figure 4.8. **Western blot of FtsB BN-PAGE.** Elution fractions from Ni-NTA purification were pooled and injected onto a Superdex 200 Increase 10/300 GL column. The column was run at 0.5 mL/min for 25 mL, collecting 0.5 mL fractions. Elution fractions at the given volumes were analysed by BN-PAGE electrophoresis on an 4-16% Bis-Tris gel and transferred to a nitrocellulose membrane before western blotting with an anti-6xHis antibody.

The migration of FtsB-SMALPs to 30 kDa would suggest that these SMALPs contain dimeric FtsB. The higher molecular weight bands at 60 kDa, 120 kDa and 380 kDa may be higher-order structures of these dimers, however it is not clear whether these dimers are associating within the disc or whether the SMALPs simply capture multiple dimers. In comparison to FtsQ, which is a larger and more globular protein, FtsB dimers appear to achieve a higher number of dimers within one SMALP, therefore it may be that the extended a helical structure of FtsB allows for multiple dimers to be captured inside the same SMALP. Monomers of FtsB would migrate to 15 kDa, which cannot be resolved on 4-16% native-PAGE gels, therefore the presence of monomers in these samples cannot be ruled out. For future experiments on low molecular weight proteins within SMALPs, native-PAGE gels that allow better resolution of the 1-100 kDa molecular weight range would be useful.

Finally, the above methodology was applied to FtsL-SMALPs (figure 4.9). FtsL-SMALPs elute between 10 mL and 16 mL and when separated by SDS-PAGE migrate to a single band at 16 kDa. A 25 kDa contaminant appears in only the 16 mL elution volume. When separated by BN-PAGE, FtsL-SMALPs instead migrate to a range of molecular weights between 700 kDa and 30 kDa.

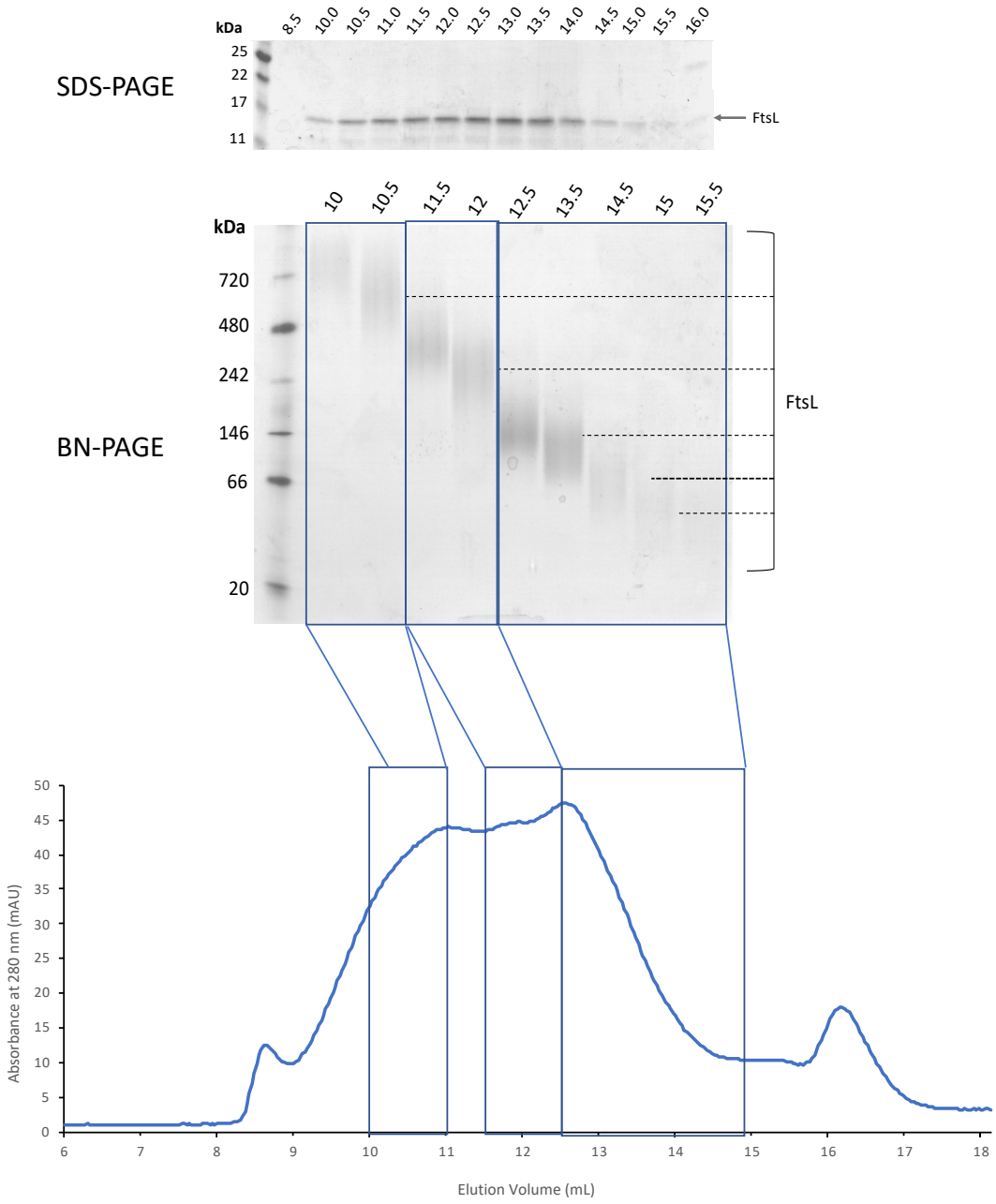

Figure 4.9. **BN-PAGE of FtsL.** Elution fractions from Ni-NTA purification were pooled and injected onto a Superdex 200 Increase 10/300 GL column. The column was run at 0.5 mL/min for 25 mL, collecting 0.5 mL fractions. Elution was followed at 280 nm for detection of protein, as shown in the trace (bottom). Elution fractions at the given volumes were analysed by SDS-Page (top) and BN-PAGE (middle) electrophoresis on an 4-16% Bis-Tris gel and protein bands visualised by Coomassie staining.

A western blot of the BN-PAGE confirmed that these bands all contain His-tagged FtsL (figure 4.10). As seen in the FtsB-SMALPs, the smallest molecular weight band at 30 kDa indicates that FtsL within these discs is in a dimeric state. Higher molecular weight bands are then representative of higher order structures of these dimers, or multiple non-interacting dimers within each SMALP.

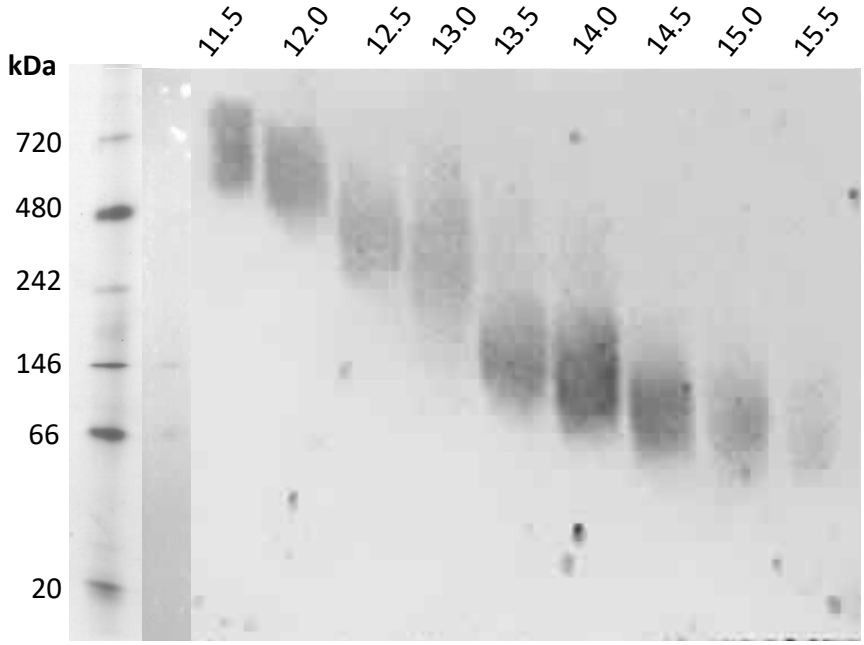

Figure 4.10. **Western blot of FtsL BN-PAGE.** Elution fractions from Ni-NTA purification were pooled and injected onto a Superdex 200 Increase 10/300 GL column. The column was run at 0.5 mL/min for 25 mL, collecting 0.5 mL fractions. Elution fractions at the given volumes were analysed by BN-PAGE electrophoresis on an 4-16% Bis-Tris gel and transferred to a nitrocellulose membrane before western blotting with an anti-6xHis antibody

4.5 Investigating the effect of the Gln16 mutation on FtsB oligomerisation with BN-PAGE

Using the TOXCAT assay for transmembrane association, LaPointe *et al.* (2013) demonstrated that the self-association of FtsB transmembrane helices is mediated by an evolutionarily conserved glutamine at position 16. Substitution of this polar amino acid with hydrophobic amino acids reduced oligomerisation by up to 90%, and substitution of this amino was found to be the most disruptive in comparison to other amino acids in the transmembrane region. Polar amino acids within transmembrane regions are often found to be important for interhelical hydrogen bonding (Bowie, 2011), therefore Gln16 may support FtsB self-association in this manner. However, this study was carried out with only the transmembrane region of FtsB, therefore to understand the contribution of Gln16 to the homodimerisation of FtsB, it would be useful to consider these mutations in the context of the full length protein. In section 4.4, it was demonstrated how BN-PAGE provides a method for defining protein oligomerisation within SMALPs. The aim of the following experiment was to use BN-PAGE to define the oligomeric state of FtsB with a Gln16 mutation in the transmembrane region, to determine whether this mutation continues to be disruptive in the full length protein.

To determine the effect of a Gln16 mutation on the self-association of full length FtsB, a glutamine to alanine substitution was chosen. This was because in the LaPointe *et al.* (2013) TOXCAT assay, alanine had the largest negative effect on transmembrane association. The mutation was introduced to the *ftsB* gene in the pET52b-*ftsB* plasmid by Q5 site-directed mutagenesis, using non-overlapping primers containing the mutation (figure 4.11).

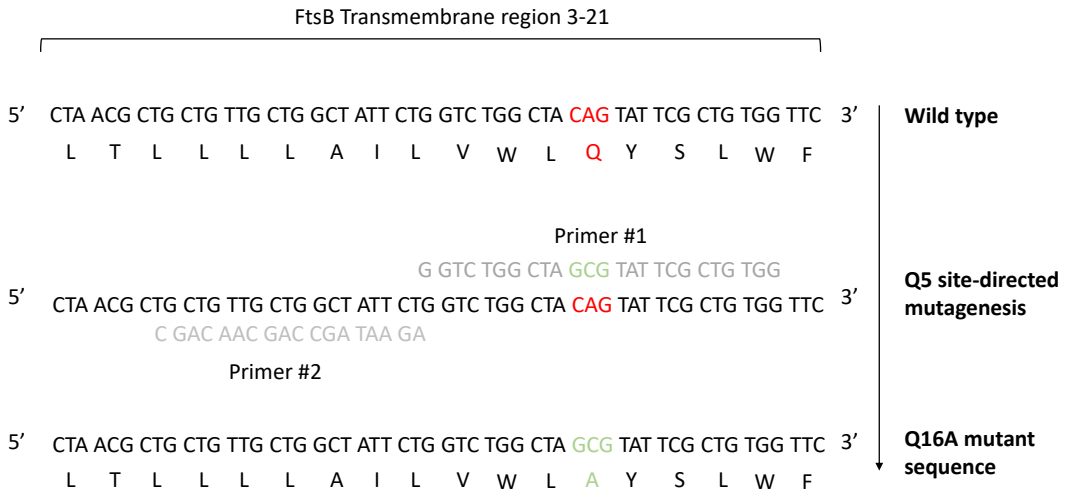

Figure 4.11. **Site directed mutagenesis of FtsB.** Glutamine 16 (red) in the FtsB transmembrane domain was mutated to alanine (green) using Q5 site directed mutagenesis. Non-overlapping primers were designed to introduce the mutation into pET52b-*ftsb*

The FtsB Q16A mutant was expressed, solubilised and purified as per the wild-type protein, and showed no changes in expression level, solubilisation yield or purity to wild-type FtsB (data not shown). Ni-NTA purified FtsB Q16A was then separated by SEC on a Superdex 200 Increase 10/300 GL column. Figure 4.12a compares the elution profile of wild type FtsB and the Q16A mutant; no obvious differences in the profile were seen between the two proteins. The elution fractions of Q16A were collected for analysis by BN-PAGE and compared to the BN-PAGE of wild-type FtsB (figure 4.12b). In the wild-type, as discussed in section 4.4, FtsB-SMALPs migrated to 30, 60, 120, and 380 kDa under BN-PAGE. In the Q16A mutant, the SMALPs migrating to each of these molecular weights could be identified. This suggests that the Q16A mutation has not affected FtsB oligomerisation within SMALPs in a manner that can be detected by BN-PAGE.

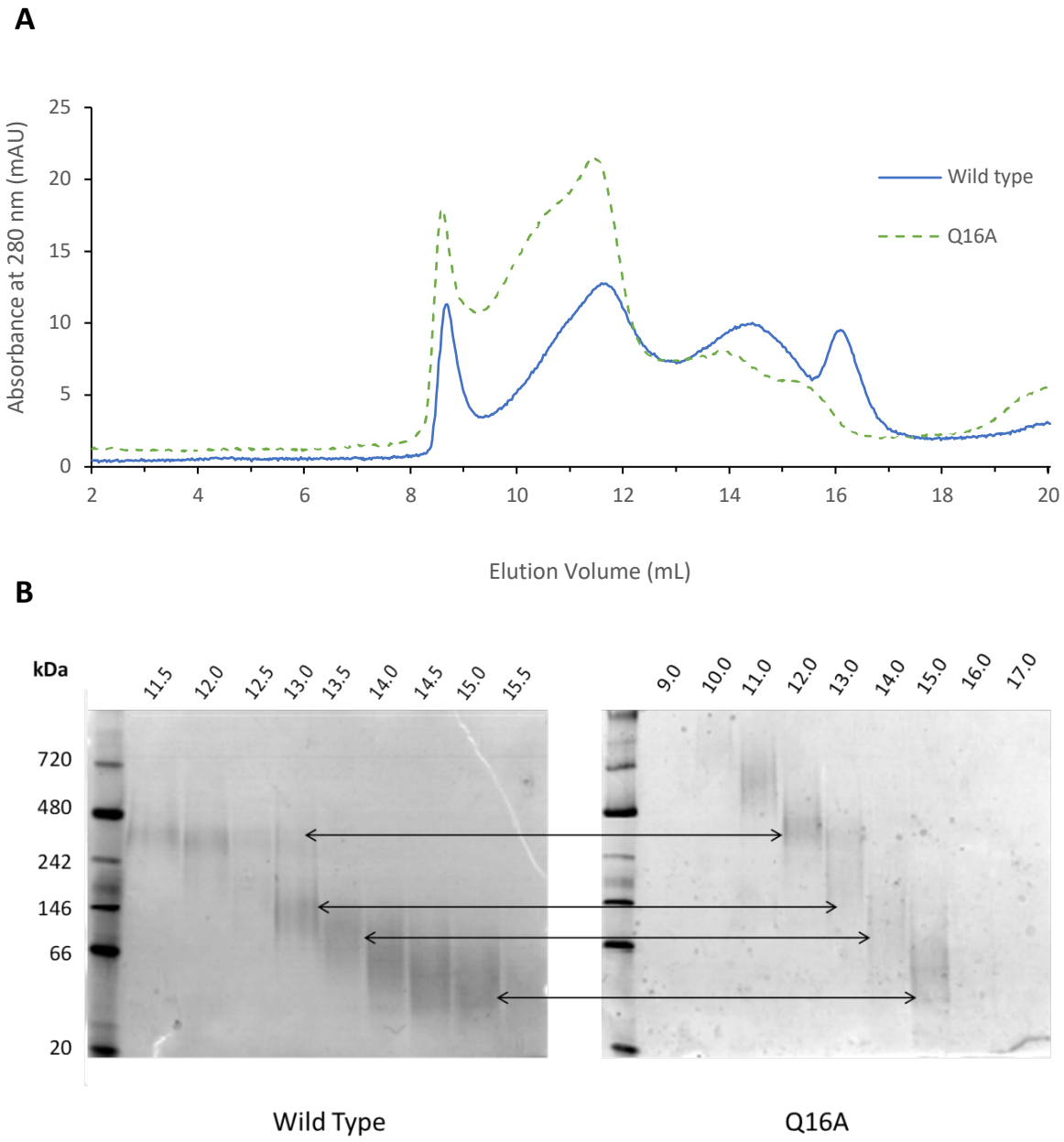

Figure 4.12. **Effect of Q16A mutation on FtsB oligomerisation.** Wild type and Q16A FtsB were individually injected onto a Superdex 200 Increase 10/300 GL column. The column was run at 0.5 mL/min for 25 mL, collecting 0.5 mL fractions. (A) Elution was followed at 280 nm for detection of protein. (B) Elution fractions at the given volumes were analysed by BN-PAGE electrophoresis on an 4-16% Bis-Tris gel and protein bands detected by Coomassie staining.

4.6 Discussion

The first aim of this chapter was to investigate the stability of the FtsBLQ components within SMALPs. Circular dichroism studies of FtsB and FtsL confirmed that these proteins retained their predicted structure within the SMALP. Additionally, comparisons between DDM and SMA-solubilised FtsB demonstrated the improved thermal stability of the protein when contained within a SMALP. Due to the low protein yield of FtsQ, structural characterisation of this protein could not be completed. Low yield of all three proteins, typically <0.2 mg per preparation using 6 L of media, also prevented further characterisation by higher resolution methods such as small angle X-ray scattering and electron microscopy. To achieve higher resolution data of these proteins within SMALPs in future experiments, protein yield would need to be increased. The data shown in this chapter presents protein preparations from 6 litres of bacterial culture, therefore scaling up the culture volume is possible, but it would be labour intensive, and many laboratories cannot support very large culture volumes. As discussed in chapter 3, a large proportion of the SMA-solubilised target protein is lost during resin binding in purification, therefore further investigation into improving binding would likely increase the yield from SMALP preparations. An alternative to these changes is to use a different method of protein expression. Cell-free expression offers increased yields of proteins that are typically toxic to *E. coli* when overexpressed. The overexpression of FtsB and FtsL was determined to be detrimental to E. coli growth in chapter 3, therefore cell-free expression could allow for higher-level expression of these proteins. Additionally, cell-free expression has been used in conjunction with Nanodiscs, a system similar to SMALPs which instead utilises a protein scaffold to support the bilayer. Proteins expressed in the cell-free system were

assembled directly into Nanodiscs without the use of detergents (Malhotra and Alder, 2014). However, Nanodiscs complicate downstream studies due to the presence of a protein scaffold that, for example, would contribute to CD spectra. Therefore, an interesting avenue would be to investigate whether SMALPs can similarly be used as a platform for cell-free expression of membrane proteins.

The second aim of this chapter was to investigate the oligomerisation of each of the FtsBLQ proteins within SMALPs. Due to the difficulties of protein yield, common techniques for studying oligomerisation states such as analytical ultracentrifugation were not possible. However, recently it was shown that Native-PAGE, which requires less than 100 ng of protein per sample, can be used to measure the quaternary structure of proteins within SMALPs (Pollock *et al.*, 2019). Therefore, this technique was applied to SMA solubilised FtsB, FtsL and FtsQ in order to analyse each of their oligomeric states and was found to successfully identify multiple states within each protein. All three proteins were found to migrate to a molecular weight in agreement with the presence of dimers within the SMALP. The dimerisation of FtsB, FtsL and FtsQ has been widely debated (Masson *et al.*, 2009; Villanelo *et al.*, 2011; Glas *et al.*, 2015; Choi *et al.*, 2018), therefore this technique presents a simple method of confirming predicted oligomerisation, using proteins contained in the native lipid environment.

One drawback of the BN-PAGE method is that it is not possible to distinguish between larger oligomers and multiple smaller oligomers, for example, a tetramer or two dimers. As the target proteins have been overexpressed into the membrane, it would not be unlikely for protein density to be high enough to capture multiple non-interacting dimers within the same SMALP. One possible solution to this problem is the use of short spacer arm crosslinkers such

as 1,5-difluoro-2,4-dinitrobenzene (DFDNB). These linkers will only crosslink proteins in very close contact, therefore would likely capture dimers/tetramers but not unbound proteins in the same disc. The use of crosslinkers was trialled during this study, however this approach was challenging due to samples appearing excessively smeared when analysed by SDS-PAGE (data not shown). It is possible that proteins in different discs were cross-linked, therefore causing large-scale aggregation within the sample. Future experiments would benefit from trialling a range of available crosslinkers that target different functional groups.

Finally, the Native-PAGE technique was used to investigate the effect of mutating Gln16 in the FtsB transmembrane region that has been predicted to be critical in FtsB transmembrane self-association (LaPointe *et al.*, 2013). When this mutant was compared to wild-type FtsB, no change in quaternary structure was seen in the Native-PAGE analysis. This suggests that while this amino acid may be critical in the context of the isolated transmembrane region, in full-length FtsB inter-helical interactions in the periplasmic region may support FtsB self-association therefore counteracting the effect of the mutation. Future experiments may therefore consider a larger panel of mutations for screening, combining multiple mutations to study the additive effect of the targeted residues.

CHAPTER 5: PURIFICATION AND CHARACTERISATION OF THE FTSB/FTSL SUBCOMPLEX

5.1 Introduction

The work of the previous chapters has demonstrated that SMA can successfully solubilise the individual proteins of the FtsBLQ complex, and that these proteins can be studied by a range of techniques such as circular dichroism and native-PAGE. These experiments also demonstrated that SMALPs can capture each protein in multiple homo-oligomeric states. The next aim of this thesis was to determine whether SMALPs can similarly be used to purify the proteins in complex with one another. FtsB and FtsL have been demonstrated to associate with one another in the absence of FtsQ and before their localisation to the mid-cell (Goehring, Gonzalez and Beckwith, 2006), therefore the FtsB/FtsL subcomplex was chosen to investigate the use of SMA in the purification of membrane protein complexes.

Previous attempts to co-purify the periplasmic regions of FtsB and FtsL found that these domains do not interact when purified in isolation (Masson *et al.*, 2009; Glas *et al.*, 2015). Therefore, most studies of FtsB and FtsL in complex have been carried out with an artificially constrained dimer of the periplasmic regions, which is enforced by fusing the periplasmic regions to artificial coils of opposite charge (Masson *et al.*, 2009; Glas *et al.*, 2015; Choi *et al.*, 2018). Other studies have focused on only the transmembrane regions, which have been demonstrated to associate as a 1:1 ratio higher order oligomer *in vitro*, and this was hypothesised to be indicative of an FtsB/FtsL tetramer (Khadria and Senes, 2013). Purifying the full-length FtsB/FtsL subcomplex in SMALPs offers the opportunity to determine the interaction of these proteins in the native lipid environment, therefore once the subcomplex had been purified, the second aim of this chapter was to characterise the oligomeric state of the FtsB/FtsL subcomplex within SMALPs.

5.2 Co-expression of FtsB and FtsL

Previous attempts to overexpress both FtsB or FtsL overnight had resulted in a marked decrease in expression levels compared to expression for only 3 hours (see section 3.3). The interaction between FtsB and FtsL has previously been shown to stabilise the proteins, therefore it was hypothesised that the overexpression of only one of the proteins may leave the protein unprotected and therefore prone to degradation. Cells overexpressing only one of the components of the FtsBLQ complex were also shown to filament, suggesting that uncoupling the expression of these proteins leads to dysfunctional cell division. Co-expression of FtsB and FtsL was therefore predicted to restore normal growth and support higher level protein expression.

FtsB and FtsL had previously been expressed from the same expression vector, therefore for co-expression it was necessary to express FtsL into a vector with a different resistance marker to allow selection for both vectors. FtsL was therefore expressed from a pET28a-*ftsL* vector, a kind gift from Dr Ian Cadby, University of Birmingham. To ensure that this vector did not differ in FtsL expression levels compared to the pET52b vector, all expression trials were repeated with pET28a-*ftsL* (figure 5.1). *E. coli* BL21(DE3) competent cells were transformed with pET52b-*ftsB*, pET28a-*ftsL* or co-transformed with both plasmids. Overnight cultures of these transformants were used to inoculate 1 L of LB broth and grown at 37°C until the cells were in the exponential growth phase, indicated by an OD_{600} of 0.4-0.6. The cultures were then cooled to 18°C and induced with IPTG. Time-points were taken before induction, and then at 1, 3, and 20 hours post induction. These samples were then analysed by SDS-PAGE and western blotting with an His-Tag specific antibody to detect expression of His-Tagged protein (figure 5.1).

As demonstrated in chapter 3, upon IPTG induction FtsB expressed to a similar level between 1 and 9 hours, however at the 20 hours post-induction the expression levels were significantly reduced. FtsL also expressed to a similar level across all three time points, however a second lower molecular weight band beneath that of FtsL was visible, possibly suggesting the degradation of FtsL, and at 20 hours post induction higher molecular weight products were seen. This may be as a result of interactions between degradation products or of aberrant protein expression. When FtsB and FtsL are co-expressed, the expression level of His-tagged protein increased with time, including at the 20-hour time point; however, the resolution of FtsB and FtsL expression levels was not possible, even with the use of 18% SDS-PAGE gels. Additionally, degradation products were not detected at any of the time points.

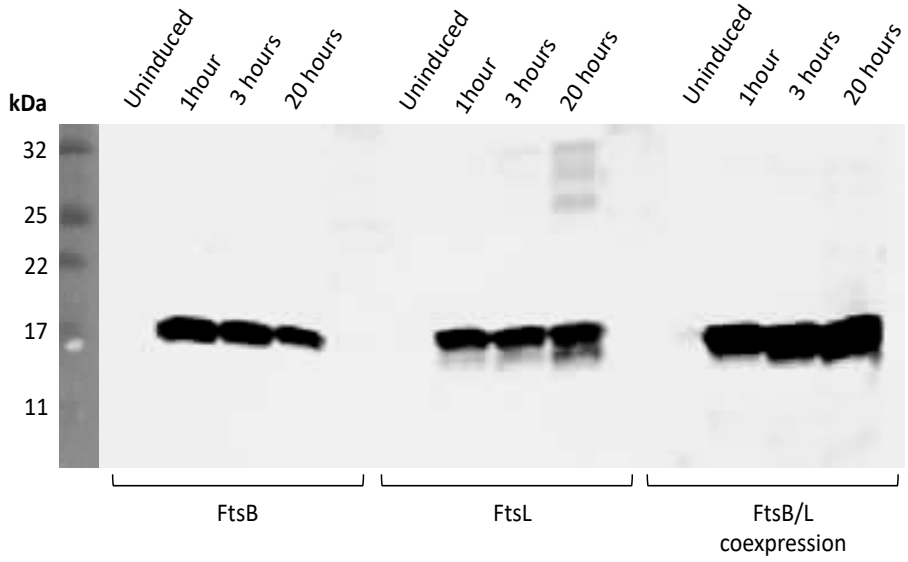

Figure 5.1. **Co-expression of FtsB and FtsL.** *E. coli* BL21(DE3) transformed with the expression vector pET52b-*ftsB*, pET28a-*ftsL* or co-transformed with both vectors were grown to an OD_{600} of 0.6 and then either induced with 0.5 mM IPTG or left uninduced. **(A)** The expression levels of the three proteins were assessed at 0, 1, 3 and 20 hours after expression by SDS-PAGE and western blotting with an anti-His-Tag antibody**.**

As co-expression of FtsB and FtsL appeared to support the expression of these protein for longer time periods, it was also investigated whether co-expression also reduced the filamentation morphology seen previously. Aliquots of the samples shown in the expression trial were fixed with paraformaldehyde to prevents further growth and were visualised by phase contrast microscopy (figure 5.2).

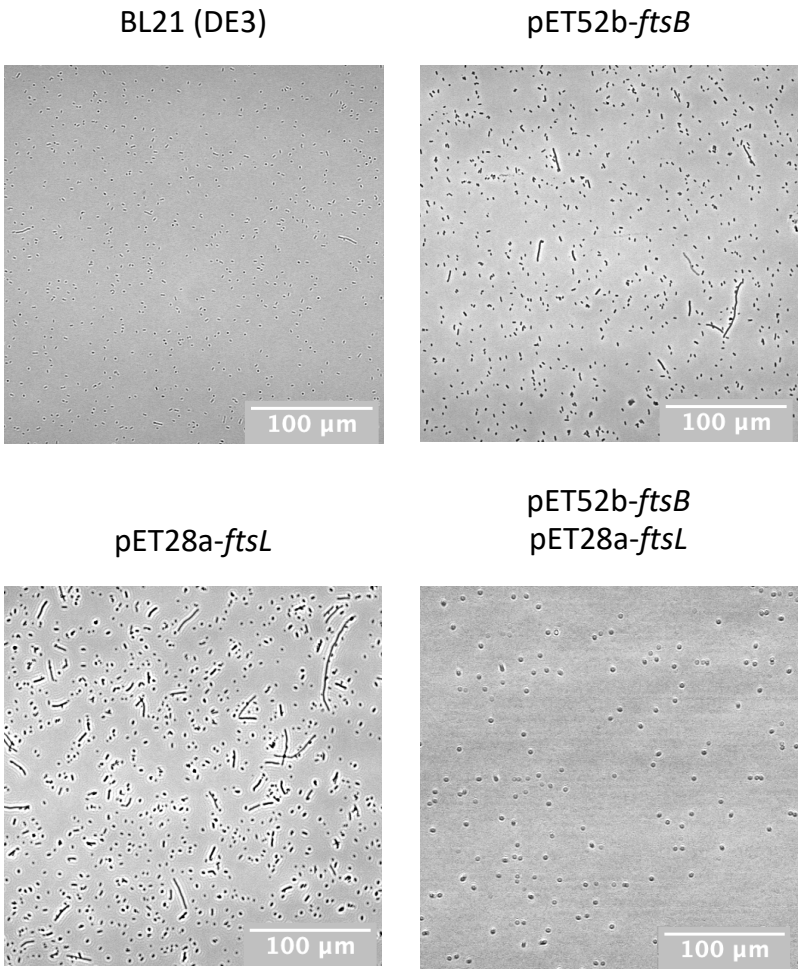

Figure 5.2. **Microscopy of cell morphology.** *E. coli* BL21(DE3) either untransformed or transformed with the expression vector pET52b-*ftsB*, pET25a-*ftsL* or co-transformed with both vectors were grown to an OD_{600} of 0.6 and then induced with 0.5 mM IPTG. Samples of the cultures were taken after 20 hours and were fixed with paraformaldehyde and then washed in PBS. Samples were then placed onto a glass microscope slide and a coverslip was applied and the cells were then visualised by phase contrast microscopy.

As previously demonstrated, protein overexpression of FtsB or FtsL individually resulted in filamentation of cells after 20 hours of induction. However, when FtsB and FtsL were co-expressed the filamentation morphology was no longer apparent. Cell shape in these cells was similar to the *E. coli* BL21(DE3) control cells, therefore it appears that co-expression of FtsB and FtsL rescues the morphological defects seen when proteins are individually expressed.

5.3 SMA solubilisation of the FtsBL subcomplex

After successful co-expression of FtsB and FtsL, the next aim of this chapter was to solubilise and purify the FtsB/FtsL subcomplex. Purification of SMALPs containing both FtsB and FtsL would require that each protein be fused a different affinity tag (figure 5.3).

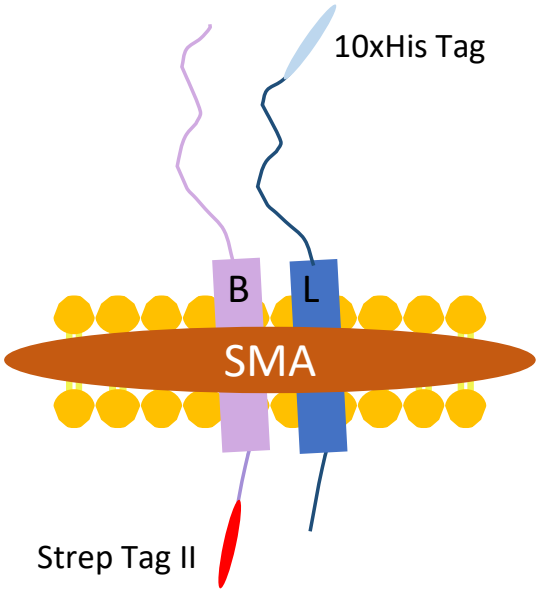

Figure 5.3. **Affinity tagging approach for purification of FtsBL subcomplex.** To allow for the purification SMALPs containing both FtsB and FtsL, the His Tag of FtsB was removed to leave only the N terminal Strep Tag II. FtsL was tagged with a C terminal 10 x His Tag.

To achieve this in the expression vectors available, the His-Tag of FtsB was removed from the expression vector by Q5 site directed mutagenesis. This resulted in FtsB being expressed with an N-terminal Strep-Tag II and FtsL with a C-terminal 6xHis-Tag. By sequential purification with Ni-NTA and streptactin resins, this would yield only the SMALPs containing both proteins.

FtsB-Strep II and His-FtsL were overexpressed in *E. coli* BL21 (DE3) for 3 hours, and the cells were collected by centrifugation. The membrane fraction was prepared by cell disruption, and fractionated from cell debris and soluble proteins through a series of high speed and ultra-centrifugation. As previous experiments found that overnight solubilisation yielded the highest amount of protein, the membrane fraction was solubilised by incubation with 2.5 % SMA for overnight at 4°C.

The insoluble fraction was pelleted by ultracentrifugation and the supernatant was incubated with Ni-NTA resin overnight. The resin mix was then transferred to a gravity flow column, washed with low imidazole buffer and then His-tagged proteins were eluted with a high imidazole buffer (figure 5.4). A large percentage of solubilised material did not bind the resin and was collected in the flow though. As expected, more FtsB was seen to be removed from the resin during the low imidazole washing steps than FtsL, as FtsB is not His-tagged therefore relies on co-purification with FtsL. Despite this, both proteins were seen to elute from the resin on incubation with high imidazole buffer, demonstrating that had FtsB been successfully co-purified with FtsL during SMALP solubilisation. As seen previously with the purification of the individual FtsBL components, multiple contaminants are co-eluted from the resin with the target proteins.

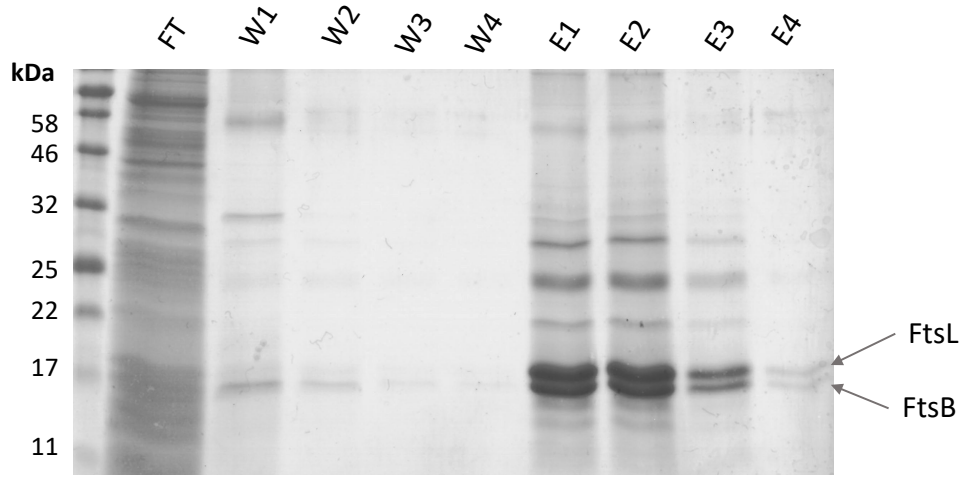

Figure 5.4. **FtsBL Ni-NTA purification.** SMA solubilised membranes were incubated with Ni-NTA resin overnight and then transferred to a gravity flow column and flow through (FT) collected. The resin was washed 4 times with 10 CV 20 mM imidazole buffer (W1-4) and then His-Tagged proteins were then eluted 4 times with 1 CV 500 mM imidazole buffer (E1-4). Fractions were analysed by electrophoresis on an 18% SDS-PAGE gel and protein bands visualised by Coomassie staining.

The eluted complexes from the Ni-NTA purification were concentrated and analysed by using size exclusion chromatography (SEC). Elution of protein and SMA was monitored by absorbance at 280 nm and 254 nm respectively (figure 5.5a). Multiple peaks were seen to elute between 9 mL and 18 mL. Aliquots of the 0.5 mL elution fractions collected were analysed by SDS-PAGE (figure 5.5b). The first sharp peak at 9 mL contained a large amount of protein at various molecular weights, therefore may represent aggregated SMALPs. FtsB and FtsL co-eluted broadly between 11.5-17 mL, and the major contaminant eluted at the later end of the elution volume at 17 mL.

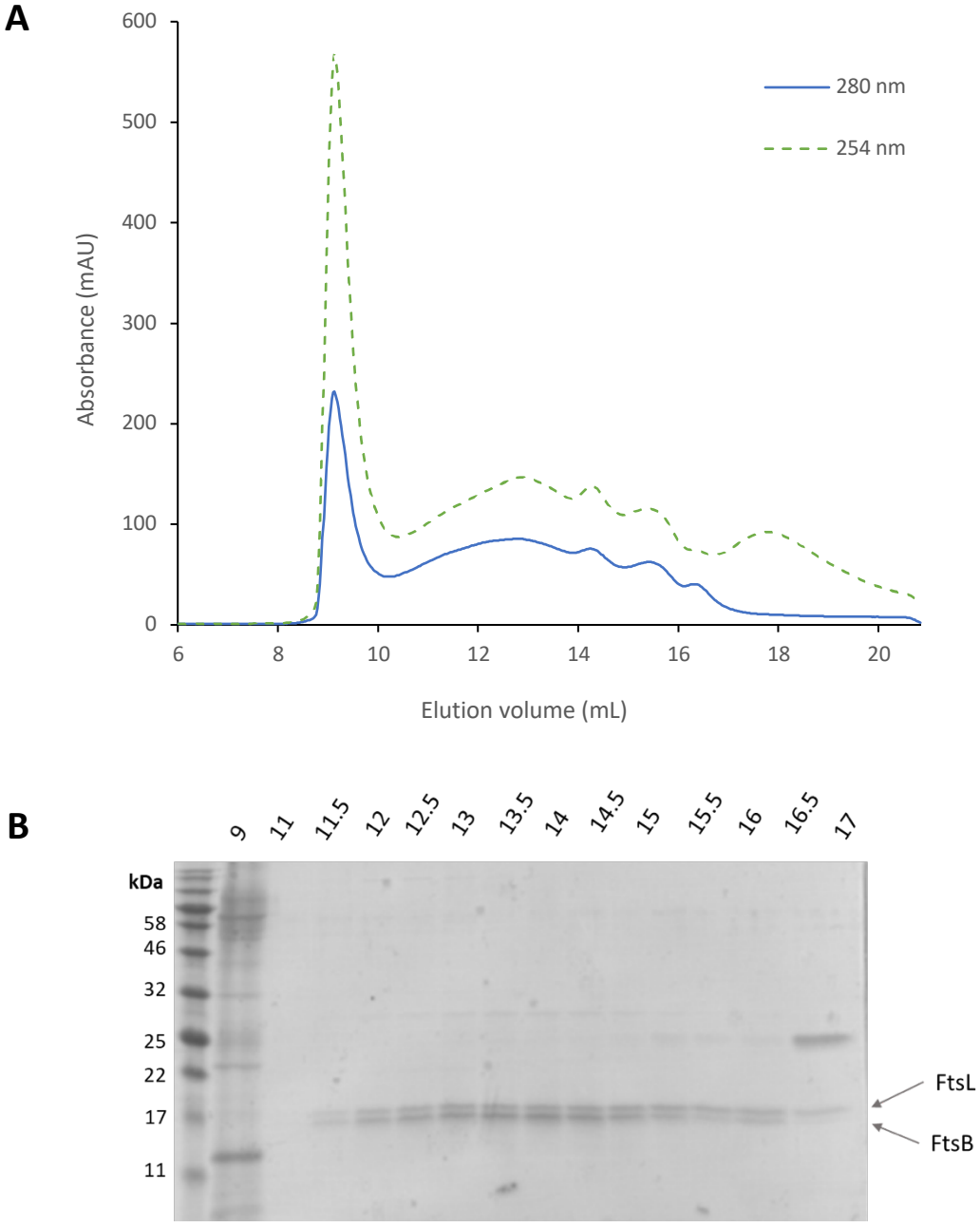

Figure 5.5. **SEC purification of the FtsB/FtsL complex.** Elution fraction fractions from Ni-NTA purification were pooled and injected onto a Superdex 200 Increase 10/300 GL column. The column was run at 0.5 mL/min for 25 mL, collecting 0.5 mL fractions. **(A)** SEC elution profile. Elution of protein and SMA from the column was monitored by absorbance at 280nm and 254 nm respectively. **(B)** SDS-PAGE of elution profile. Elution fractions at the given volumes were analysed by electrophoresis on an 18% SDS-PAGE gel and protein bands visualised by Coomassie staining.

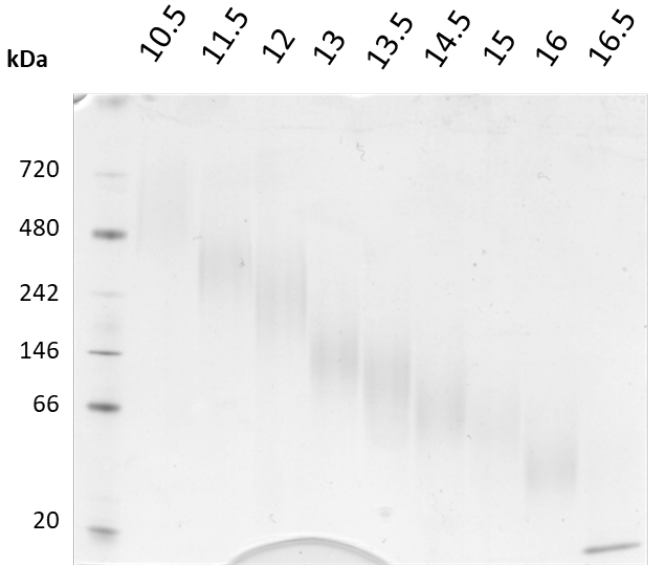

Figure 5.6. **BN-PAGE of the FtsB/FtsL subcomplex.** Elution fractions from Ni-NTA purification were pooled and injected onto a Superdex 200 Increase 10/300 GL column. The column was run at 0.5 mL/min for 25 mL, collecting 0.5 mL fractions. Elution fractions at the given volumes were analysed by BN-PAGE electrophoresis on an 4-16% Bis-Tris gel and protein bands visualised by Coomassie staining.

To assess the oligomeric state of FtsB/FtsL complexes in SMALPs, the elution fractions from the SEC analysis were also separated by BN-PAGE (figure 5.6). Diffuse bands migrated to molecular weights between 30 kDa and 480 kDa. The soluble contaminant migrated as a sharp band at 20 kDa. BN-PAGE of individually purified FtsB and FtsL indicated that the migration of bands to the 30 kDa position was due to the purification of FtsB or FtsL homodimers. As the FtsB/FtsL subcomplex had only been purified using one affinity tag, it is possible that some of the sample contains discs with only FtsL. It is therefore is not possible to distinguish the 30 kDa band in the BN-PAGE of the subcomplex as either a FtsB/FtsL heterodimer or an FtsL homodimer.

To remove any FtsL that was not bound to FtsB, FtsB/FtsL complexes eluted from the Ni-NTA were additionally passed through streptactin gravity flow resin to bind strep-tagged FtsB. The resin was washed with 50 mM Tris-HCl, 500 mM NaCl (pH 8) buffer to remove any contaminants. Strep-tagged protein were then eluted with d-Desthiobiotin, which competes for the Strep-Tactin binding sites (figure 5.7).

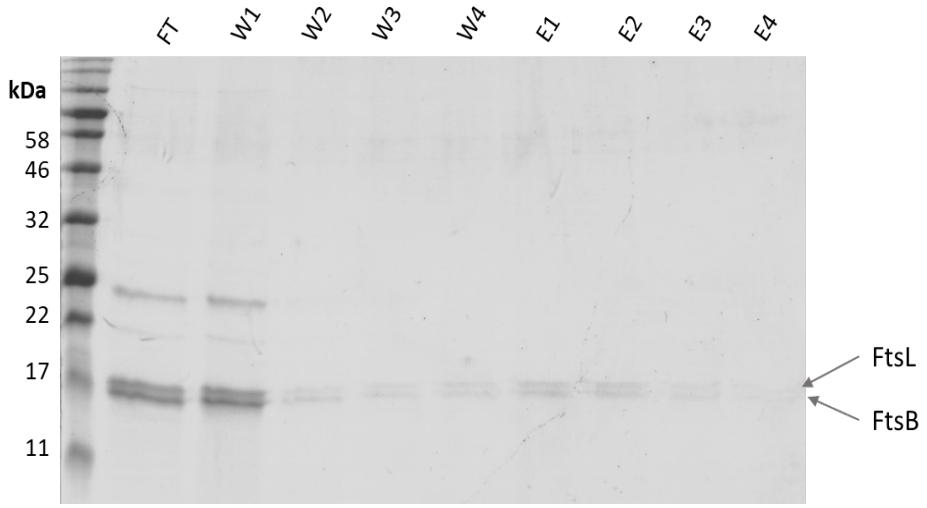

Figure 5.7. **FtsB/FtsL streptactin purification.** Ni-NTA elution fractions were passed through the streptactin resin under gravity flow. The resin was washed 4 times with 1 CV buffer (W1-4) and then Strep-Tagged proteins were eluted 4 times with 1 CV buffer + 2.5 mM d-Desthiobiotin (E1-4). Fractions were analysed by electrophoresis on an 18% SDS-PAGE gel and protein bands visualised by Coomassie staining.

The flow through (FT) and wash fractions show that very little of the sample bound to streptactin resin, which was surprising as all FtsB in the sample should be capable of binding the resin. As discussed in chapter 3, inefficient binding of SMA solubilised protein to affinity resin is a major roadblock in the purification of membrane proteins by this technique, and further work on improving binding efficiency is much needed. However, a very small fraction

of the sample was found to elute on incubation with D-desthiobiotin, indicating the partly successful co-purification of FtsB and FtsL using dual purification methods.

The limited protein yield from the streptactin resin presented a challenge for the characterisation of copurified FtsB/FtsL, as many techniques require a substantial amount of protein for analysis. However, as Native-PAGE is compatible with western blotting this technique allows the analysis of quaternary structure in samples containing less than 1 ng of protein. The streptactin purified samples were concentrated and separated by SEC purification. Absorbance readings were taken at 280 nm and 254 nm to identify the elution of proteins and SMA respectively, and a trace amount of SMA and protein could be seen to elute from the column. This elution trace was similar to that of the FtsB/L proteins when purified independently, therefore although the trace was of poor quality (data not shown), it was assumed to be representative of FtsBL elution from the column. The elution fractions containing protein were then separated by BN-PAGE and transferred to a nitrocellulose membrane for western blotting with an anti-his tag antibody. Western blotting would be predicted to only detect FtsL, however as FtsB and FtsL had been co-purified, any FtsL detected by the antibody would be in complex with FtsB.

As shown in figure 5.8, the elution fractions could be successfully visualised on BN-PAGE by western blotting. The bands were seen at multiple molecular weights, suggesting the possibility of multiple complexes within any one disc. To assist in the assessment of which the oligomeric states these bands represent, the BN-PAGE of the dual purification samples was compared to that of samples only purified by Ni-NTA.

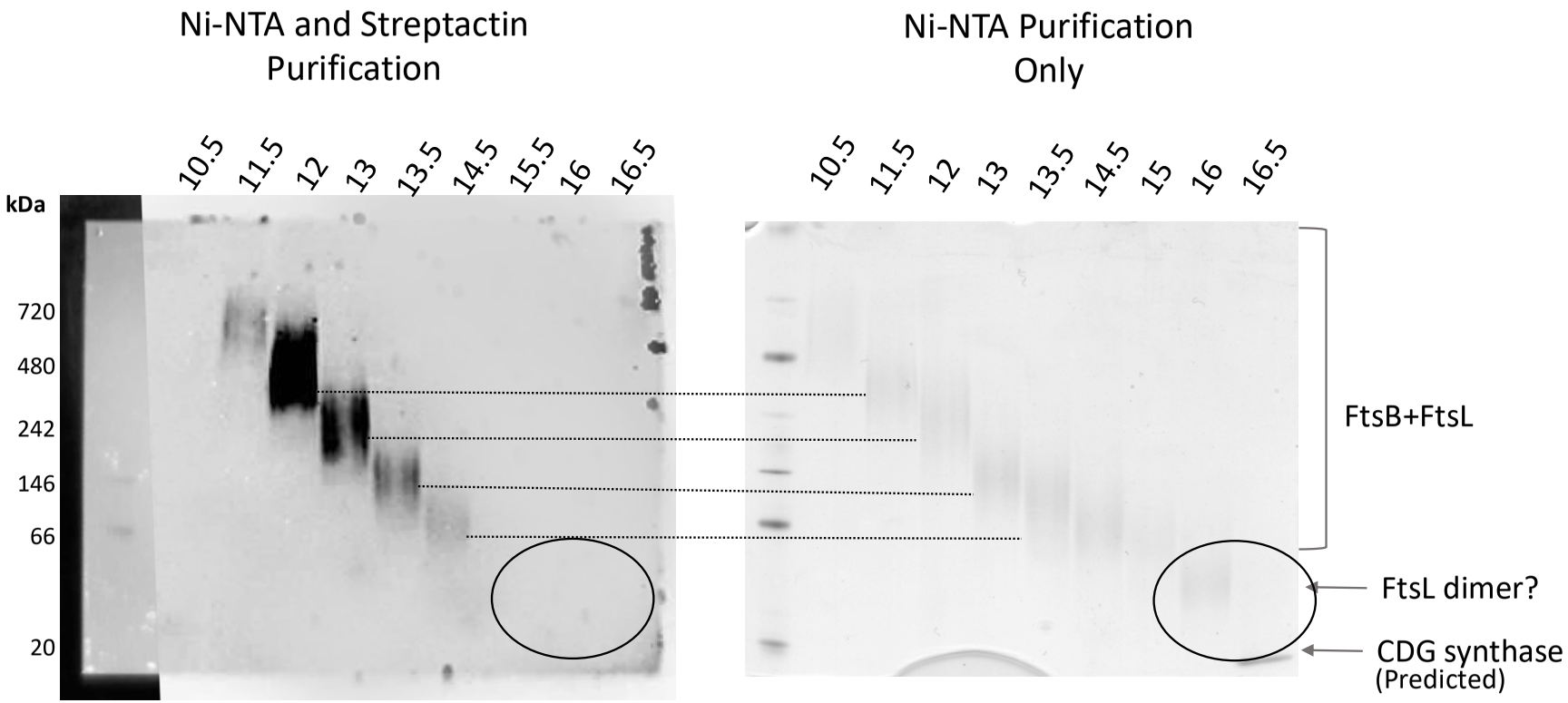

Figure 5.8. **BN- PAGE of FtsBL purification steps.** Elution fractions from either the Ni-NTA purification or the Ni-NTA/Strep-Tactin dual purification were pooled and injected onto a Superdex 200 Increase 10/300 GL column. The column was run at 0.5 mL/min for 25 mL, collecting 0.5 mL fractions. Elution fractions at the given volumes were analysed by BN-PAGE electrophoresis on an 4-16% Bis-Tris gel and protein bands visualised by (A) western blotting with anti-his antibody or (B) Coomassie staining.

By comparing these two purifications, it is clear that for the higher molecular weight bands, the elution profile of both samples is comparable. However, the Ni-NTA only purification contains a protein band at ~30 kDa that is not found in the dual purification. As the Ni-NTA purification will also purify FtsL that has homo-dimerised, rather than hetero-dimerised with FtsB, this band likely represents dimeric FtsL. Therefore, the band at ~60 kDa represents a tetrameric structure of FtsB and FtsL. As this band is seen in the dual purification, it can be assumed that it is a hetero-tetramer of FtsBL and not a form of homo-oligomerisation on just one of the proteins. Further bands could represent higher order oligomers of this structure, or may just be the inclusion of multiple tetramers within the same disc.

While this data is low resolution, it demonstrates that inclusion of membrane proteins within SMALPs allows the purification of membrane protein complexes, and rudimentary analysis of their quaternary structure. To acquire more accurate estimations of the molecular weights of the complexes within the purified SMALPs, analytical ultracentrifugation (AUC) was performed. The analysis of the resultant AUC data required further experimentation for the measurement of experimental parameters, therefore for clarity these experiments are instead discussed in detail in chapter 6.

5.4 Small Angle X-Ray Scattering of FtsBL-SMALPs

While BN-PAGE offers a simple method for the analysis of protein complex molecular weights, obtaining higher resolution structural data on the complex requires alternative techniques such as small angle X-ray scattering (SAXS) and X-ray crystallography. However, these techniques require sample concentrations of around 0.5-10 mg/mL. As previously mentioned

in this chapter, the yield of FtsB/FtsL-SMALPs was limited by inefficient resin binding, therefore, large scale culture volumes were increased to 18 L compared to 6 L used previously. This yielded enough protein to perform small angle X-ray scattering (SAXS), a technique that can provide structural information on proteins in solution by measuring the scattering of X-ray photons by electrons. SAXS data analysis is highly sensitive to sample monodispersity, however, as shown by the BN-PAGE analysis, SMA preparations of FtsBL are polydisperse, with multiple species of varying molecular weights. Therefore, to allow for accurate data analysis size exclusion chromatography-SAXS was performed, whereby size exclusion chromatography is placed in-line with SAXS data collection, and samples are taken across the elution profile.

SEC-SAXS data was collected on the B21 beamline at Diamond Light Source. Ni-NTA purified FtsBL-SMALPs were concentrated and separated on a Superdex 200 Increase 3.2/300 column at 0.075 mL/min in-line with the flow cell for SAXS data collection. Images were recorded every 3 seconds, with 1 second of exposure per image, resulting in a total collection of 600 images. Data reduction was performed at Diamond Light Source using DAWN, and further data analysis was carried out in ScÅtter, a JAVA-based application developed by Robert Rambo at the Diamond Light Source (Didcot, UK). Figure 5.9 shows the resultant signal plot for the SEC-SAXS analysis of FtsBL-SMALPS.

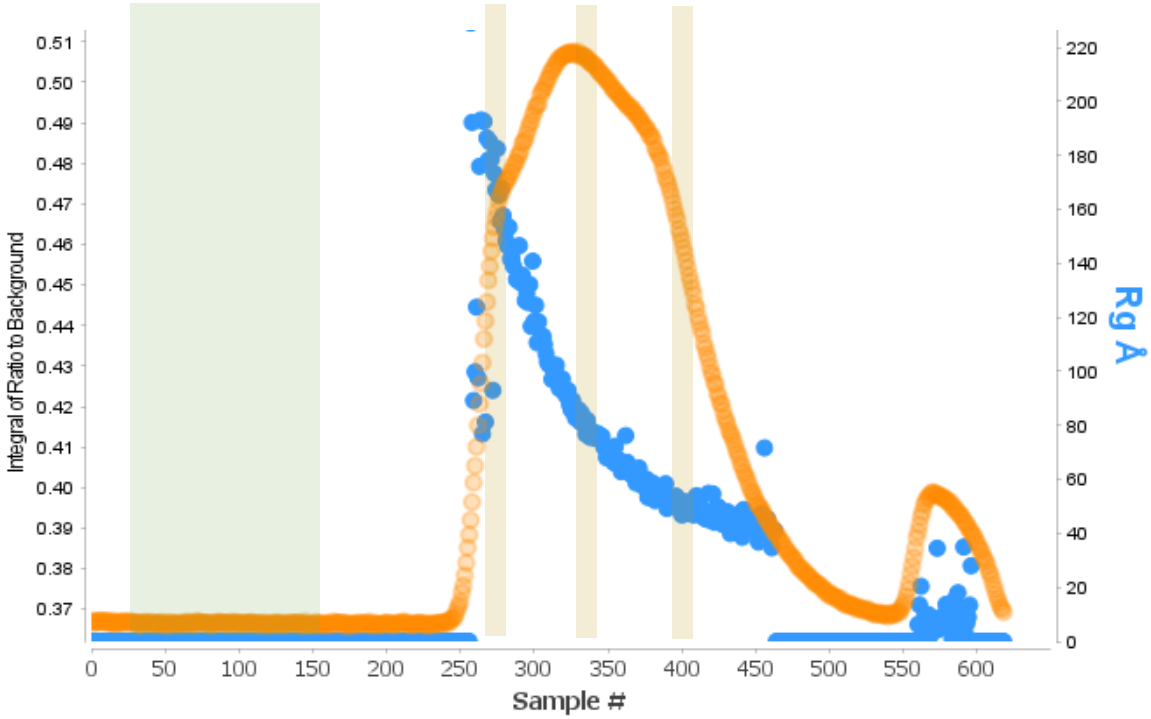

Figure 5.9. **Signal plot for the size- exclusion chromatography-small angle X-ray scattering (SEC-SAXS) of FtsBL-SMALPs.** The change in Rg (blue dots) is given across the elution profile (orange dots). The green bar represents samples used as the buffer region for subtraction, and the yellow bars are the sample regions for analysis. Plot generated in ScÅtter.

Two elution peaks were detected across the collection window. Using the published calibration curve for the SEC column (GE Healthcare, 2018), the first peak which elutes between 1-1.6 mL (samples 250-450) was assigned as SMALPs, whilst the small peak eluting after 2 mL (samples 550 onward) was assigned as the elution of soluble proteins and contaminants. Across the SMALP elution peak, the R_g can be seen to gradually decrease from a maximum of 200 Å to a minimum of 40 Å.

Because there were no regions where the R_g value stabilised, no distinct populations could be identified from the signal plot. This prevented the merging of multiple frames for increased exposure times and therefore individual frames were chosen to further processing. Sample numbers 275, 325, and 375 were chosen as highlighted on figure 5.9. Each sample was subtracted from the selected buffer region, and the resultant scattering curves are shown in figure 5.10. Each sample exhibited a distinct scattering profile; the profile of sample 275 appeared to be similar to the profile of a predicted unfolded protein whereas the profile of sample 375 matched more closely to that of a globular protein (Kikhney and Svergun, 2015).

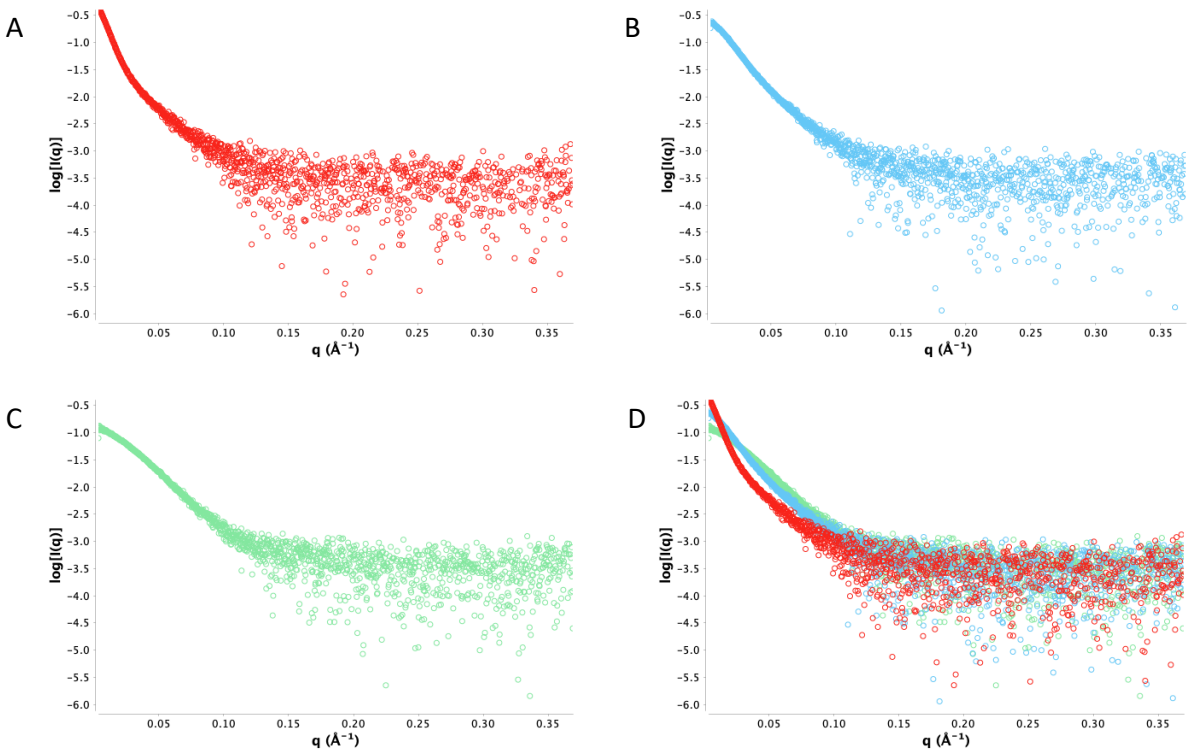

Figure 5.10. **Scattering intensity of FtsBL-SMALPs.** Logarithmic intensity plot of (A) sample 275, (B) sample 325, (C) sample 375 and (D) all three samples overlaid.

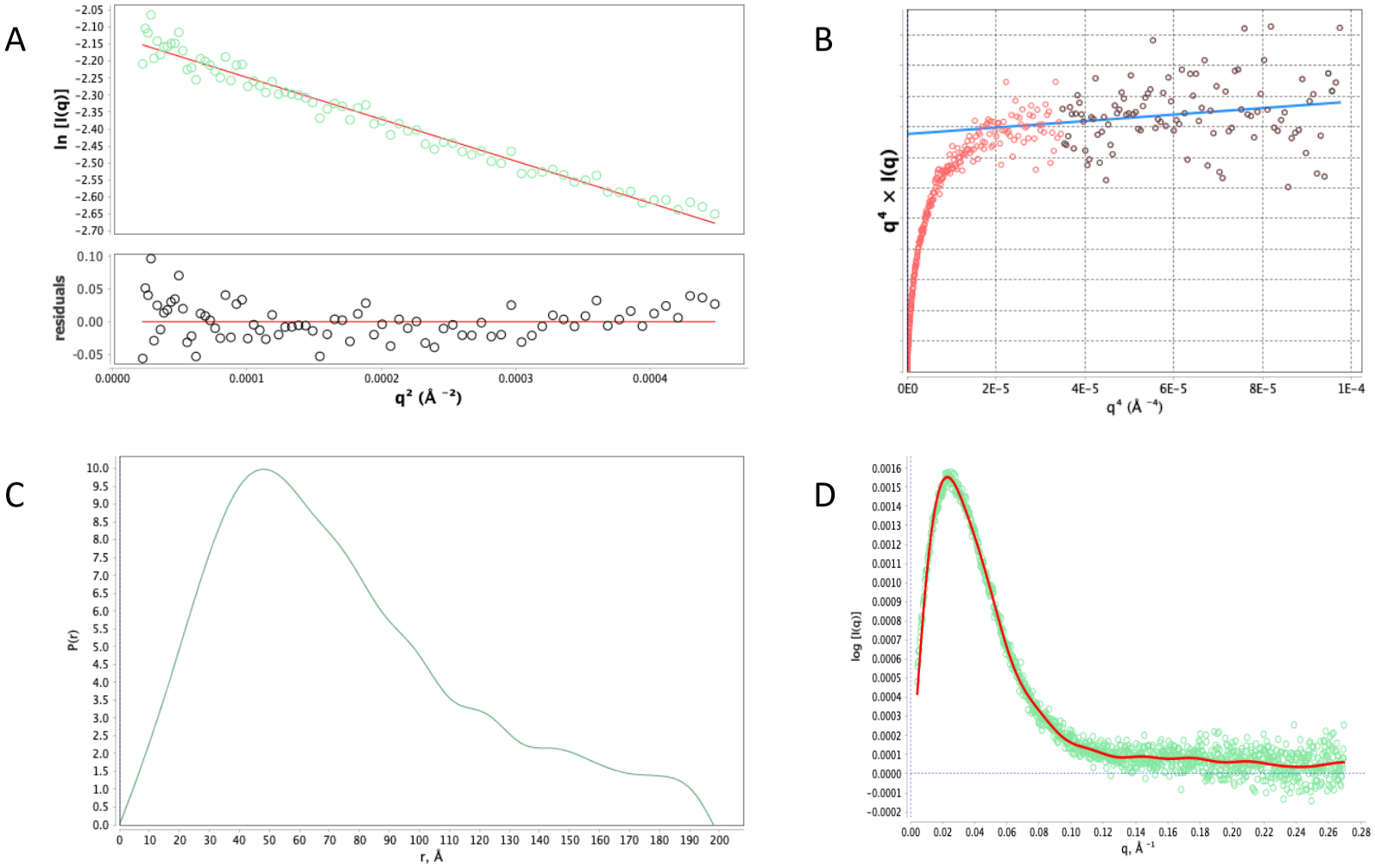

Figure 5.11. **SAXS analysis of FtsBL-SMALPs.** (A) Guinier fitting of the low-q region (q x R_g < 1.3) for the estimate of the radius of gyration (R_g). (B) Linear fitting of the Porod-Debye plot to determine the Porod volume (V_p) and exponent (P_x) (C) P(r) distribution to determine the particles maximum dimension (D_{max}) (D) Plot of P(r) fit to the q vs q*I(q) scattering intensity

For each curve, a Guinier plot (ln I(q) vs q^2) was obtained to predict the radius of gyration (R_g). Additionally, a Porod volume (V_p) and exponent (P_x) were determined, and a P(r) distribution function was produced to calculate the maximum dimension (D_{max}) of each particle. Representative analysis is shown for sample 375 in figure 5.11 and these results for all three samples are summarised in table 5.1.

Sample no.	Elution volume (mL)	I(0)	R_g	d_{max}	P_x	V_p (Å^3)
275	1.0	0.438	161.5	523	3.8	3,900,000
325	1.2	0.235	89.4	284	3.3	1,360,000
375	1.4	0.118	59.2	190	3.6	500,000

Table 5.1. **SAXS analysis of FtsBL-SMALPs.**

The linear fit of the Guinier plot demonstrates that there is no aggregation in the sample. The Porod exponent calculated for each sample was >3.3, suggesting all samples are fairly compact. As expected, the predicted volume of the sample decreased between the earliest and latest eluted samples. The volume is commonly converted from Å^3 to daltons by dividing by the density of protein (~1.35 g/cm^3, (Andersson and Hovmöller, 1998)), however, as these samples are a complex mix of SMA, lipid and protein, these calculations cannot be made accurately. The R_g similarly decreases with along the elution profile.

Due to the incomplete separation of multiple FtsB/FtsL-SMALP populations, and the lack of a region of stable R_g values, this data was not used for *ab initio* modelling. Higher sample concentrations would allow for samples to be separated on a SEC column with a larger bed volume, thereby providing better resolution. However, these results have provided initial data for SAXS analysis of FtsB/FtsL-SMALP complexes by SAXS.

5.4 Detergent solubilisation of the FtsB/FtsL Subcomplex

Further structural analysis of FtsB/FtsL-SMALPs was limited by the yield that could be achieved during purification. Therefore, it was considered whether the traditional approach of detergent purification may be more suitable for the preparation of FtsB/FtsL complexes for structural characterisation. Membranes overexpressing FtsB and FtsL were therefore incubated overnight with DDM and the insoluble fraction removed by ultracentrifugation. The supernatant was incubated with Ni-NTA resin overnight and then transferred to a gravity flow column. The resin was washed with low imidazole buffer and then His-tagged proteins were eluted with high imidazole buffer. As shown in figure 5.12, FtsB and FtsL were successfully solubilised by DDM and co-eluted from the column at high concentrations.

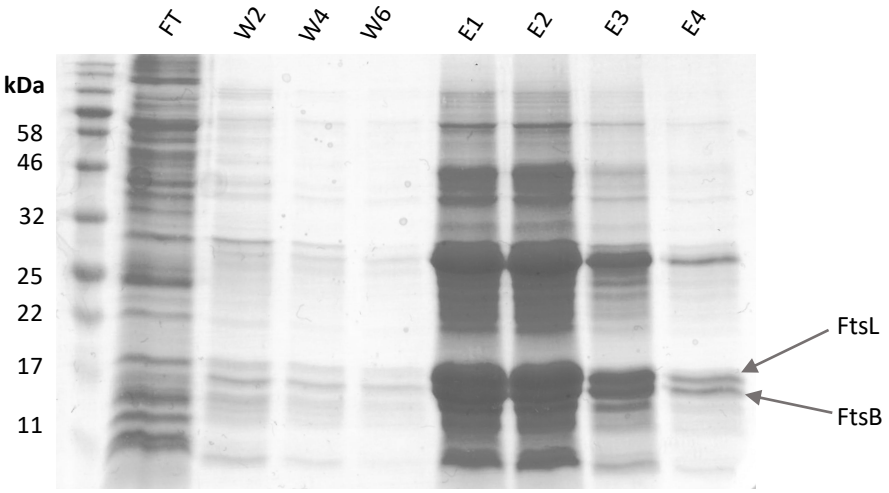

Figure 5.12. **FtsBL DDM purification.** DDM solubilised membranes were incubated with Ni-NTA resin overnight and then transferred to a gravity flow column and flow through (FT) collected. The resin was washed 6 times with 10 CV 20 mM imidazole buffer (W2,4,6) and then His-Tagged proteins were then eluted 4 times with 1 CV 500 mM imidazole buffer (E1-4). Fractions were analysed by electrophoresis on an 18% SDS-PAGE gel and protein bands visualised by Coomassie staining.

The Ni-NTA elutions fractions had a significant amount of contaminants which co-eluted with FtsB and FtsL, therefore these elutions were purified by separation by SEC (figure 5.13a).

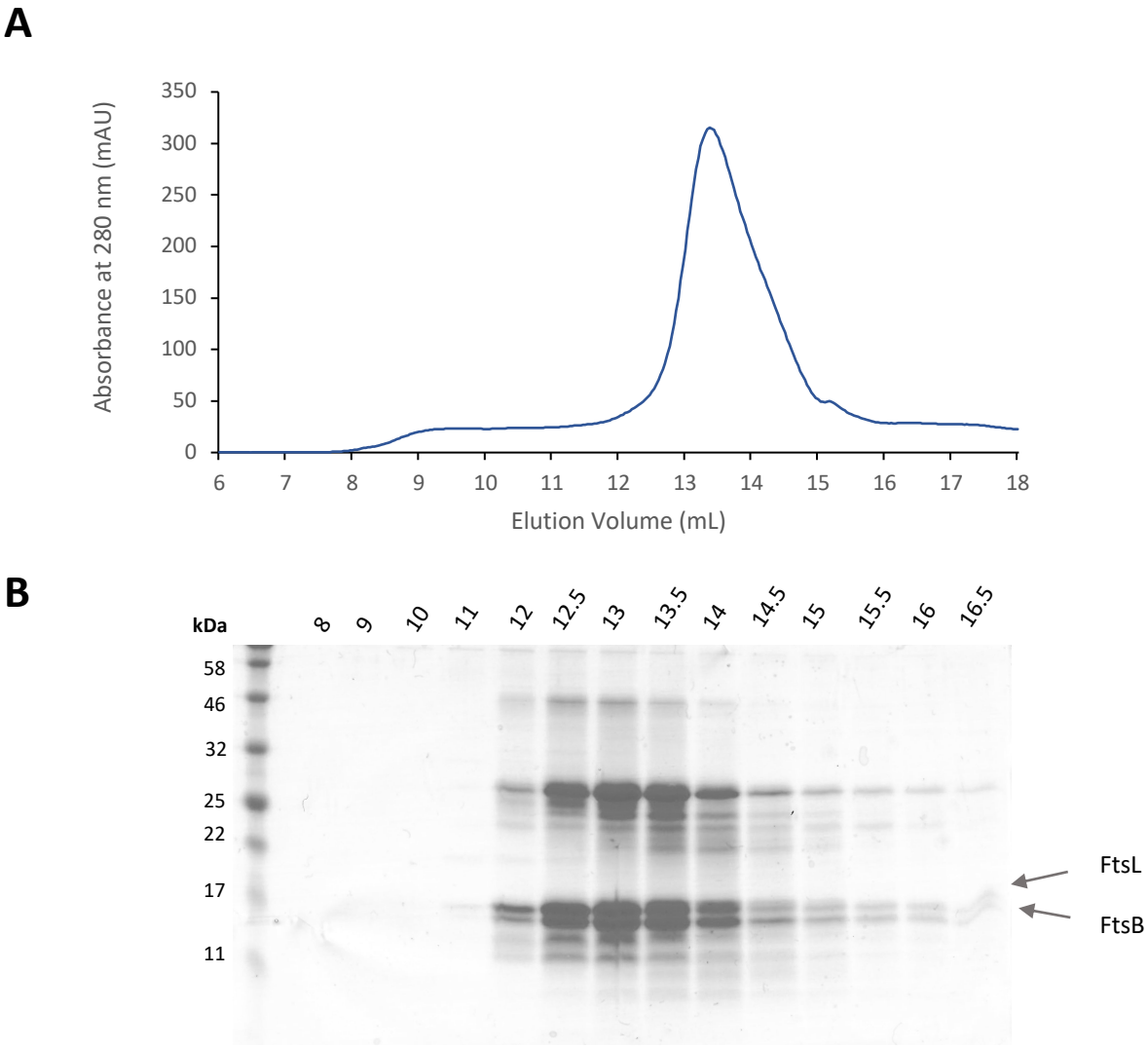

Figure 5.13. **SEC purification of DDM solubilised FtsB/FtsL.** Elution fractions from streptavidin purification were pooled and injected onto a Superdex 200 Increase 10/300 GL column. The column was run at 0.5 mL/min for 25 mL, collecting 0.5 mL fractions. **(A)** SEC elution profile. Elution of protein from the column was monitored by absorbance at 280nm **(B)** SDS-PAGE of elution profile. Elution fractions at the given volumes were analysed by electrophoresis on an 18% SDS-PAGE gel and protein bands visualised by Coomassie staining**.**

Compared to the multi-peak elution profile of the SMA purifications, the DDM-solubilised FtsB/FtsL eluted as a single, narrow elution peak around 13.5 mL. This elution peak of the SEC purification was analysed by SDS-PAGE as shown in figure 5.13b. FtsB and FtsL were co-eluted across the elution profile, however significant contamination remained. Some contamination appeared as laddering of lower molecular weight products beneath the full-length protein band, which could be products of degradation.

To assess whether the quaternary structure of the solubilised proteins could be identified, the elution fractions from the SEC column were also analysed by BN-PAGE (figure 5.14).

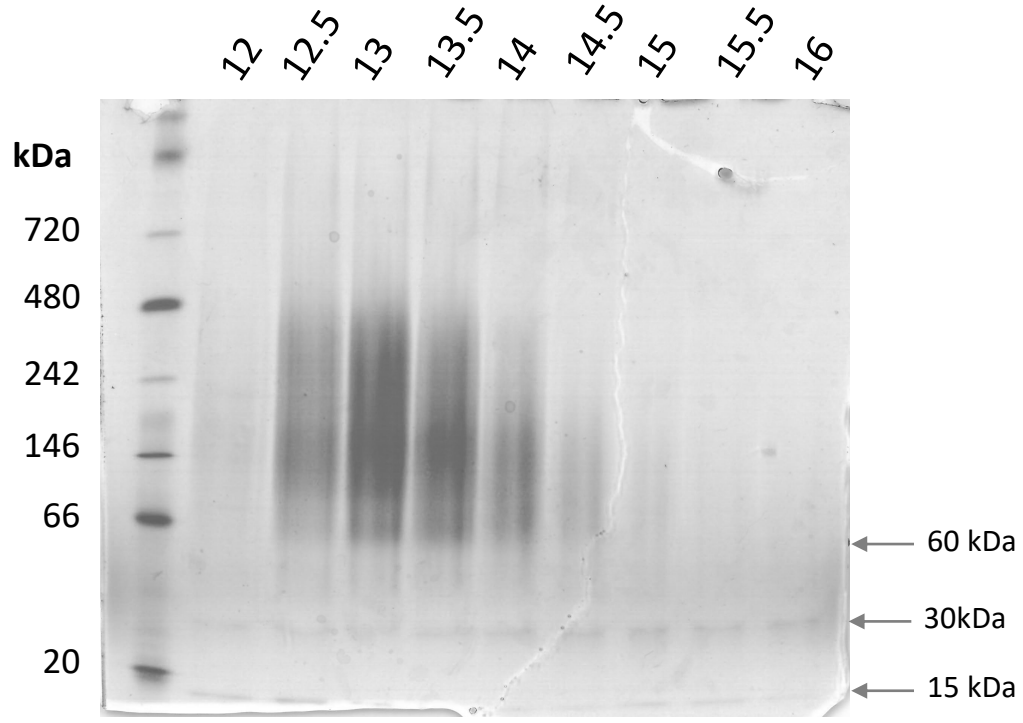

Figure 5.14. **BN-PAGE of DDM solubilised FtsB/FtsL.** Elution fraction fractions from Ni-NTA purification were pooled and injected onto a Superdex 200 Increase 10/300 GL column. The column was run at 0.5 mL/min for 25 mL, collecting 0.5 mL fractions. Elution fractions at the given volumes were analysed by BN-PAGE on an 4-16% Bis-Tris gel and protein bands visualised by Coomassie staining**.**

As indicted on the gel, bands migrating to 15, 30 and 60 kDa could be detected on the BN-PAGE at multiple elution volumes. This result was indicative of the purification of oligomers of FtsB, FtsL or the proteins in complex. However, the high concentration of contaminating proteins prevented the definitive identification of these complexes. Western blotting of the BN-PAGE was repeatedly unsuccessful due to the poor resolution of DDM-solubilised proteins by BN-PAGE (data not shown).

To further purify the FtsB/FtsL proteins from co-eluting contaminants, the fractions eluted from the SEC analysis between 12-17 mL were then bound to streptactin resin (figure 5.15).

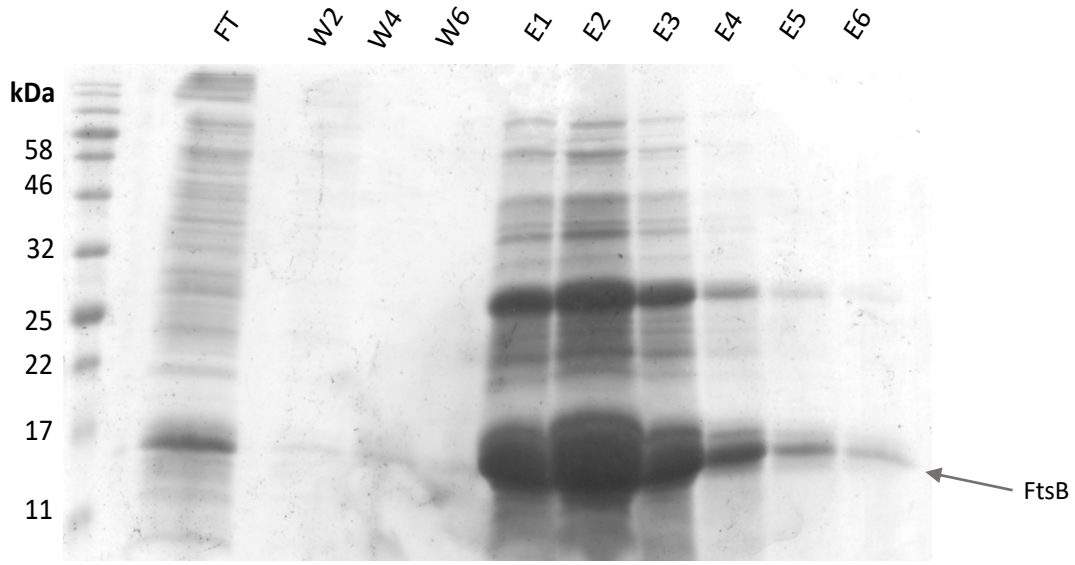

Figure 5.15. **FtsBL DDM streptactin purification.** FtsB/FtsL SEC elutions were passed through the streptactin resin under gravity flow. The resin was washed 6 times with 1 CV buffer (W2,4,6) and then Strep-Tagged proteins were eluted 6 times with 1 CV buffer + 2.5 mM desthiobiotin (E1-6). Fractions were analysed by electrophoresis on an 18% SDS-PAGE gel and protein bands visualised by Coomassie staining.

As expected, a large band migrating to the molecular weight of FtsL was seen in the flow-through, as it is not His-tagged and therefore will only bind the streptactin resin in complex with FtsB. On incubation with D-desbiothiotin, a large amount of protein was eluted from the resin. The successful elution from streptactin resin when using DDM, compared to the difficulties of elution when using SMA, suggests that the incompatibility of FtsB/FtsL-SMALPs with streptactin resin is due to the presence of the SMALP. Despite the wash fractions appearing clear of contaminants, the elution steps have very poor purity compared to SMA purifications. Unlike in figure 5.13b, where on visual inspection FtsB and FtsL purified at similar concentrations, FtsB eluted at a much higher concentration from the streptactin resin than FtsL. This suggested that during the purification, the interaction between FtsB and FtsL may have been disrupted. In order to preserve the protein-protein interactions in the sample, a range of alternative detergents and detergent concentration could be trialled, however due to time constraints this was not considered further in this study.

5.5 Discussion

The first aim of this section was to determine whether SMALPs can be used to purify the FtsB/FtsL proteins in complex with one another. To achieve this, FtsB and FtsL were co-expressed in *E. coli*. In comparison to the morphological defects of *E. coli* over-expressing just one of these proteins, co-expression of FtsB and FtsL did not cause any major morphological changes and resulted in an increase in protein expression level. These results demonstrate that overexpression of these proteins is supported in *E. coli,* however, maintaining the FtsB/FtsL ratio within the membrane may be important. In *B. subtilis* FtsL levels have been

proposed as a rate-limiting step in division (Bramkamp *et al.*, 2006). FtsL in *B. subtilis* is degraded by a zinc metalloprotease YluC, and when this protease is inactivated by mutation cells have a short cell phenotype as a consequence of early division (Bramkamp *et al.*, 2006). FtsB stabilises FtsL against proteolytic cleavage (Wadenpohl and Bramkamp, 2010), therefore it could be that without the presence of enough FtsB to stabilise FtsL, FtsL is degraded at a faster rate and therefore does not trigger cell constriction, causing the filamentous phenotype.

The co-expressed proteins were then solubilised with SMA, and purified using Ni-NTA resin. As the His-tag on FtsB was removed by site-directed mutagenesis, only FtsL would bind the resin. Both FtsB and FtsL eluted from the resin, demonstrating that SMA successfully solubilised FtsB/FtsL complexes. To further purify the complex and remove any SMALPs in which there was only FtsL, the solubilised proteins were then passed over streptactin resin, which only FtsB should bind to. However, as found in chapter 3 for FtsB-SMALPs, a large proportion of the FtsB/FtsL-SMALPs did not successfully bind to the streptactin resin and only a small fraction of the sample was eluted from the resin. In comparison, when FtsB/FtsL complexes were purified in detergent, FtsB was eluted from the streptactin resin at much higher concentrations. The Strep-Tag of FtsB is at the end of the short cytoplasmic domain, which is only 3 residues long, compared to the placement of the His-Tag of FtsL which is at the end of the 63 residue periplasmic domain. Therefore, one possible explanation for the poor binding was that the large volume of the SMALP disc hindered the binding of the Strep-Tag to the resin. In comparison, detergent micelles are much smaller and therefore likely do not interfere with the binding of the Strep-Tag. Therefore, in future studies the placement of

purification tags only at the C-terminal of the proteins may assist with improved binding of SMA-solubilised proteins to streptactin resins.

Despite these complications, the successful elution of FtsB and FtsL from the streptactin resin demonstrated that SMA-solubilisation had successfully captured FtsB and FtsL within the same SMALP. The second aim of this chapter was to characterise the oligomeric state of these complexes. Purified FtsB/FtsL-SMALPs were separated by SEC, and the elution fraction were analysed by BN-PAGE. By comparing the BN-PAGE from Ni-NTA and Ni-NTA/streptactin double purifications, the oligomerisation states of the complexes within the discs were successfully identified. The oligomerisation state of the FtsB/FtsL subcomplex has been widely studied (Villanelo *et al.*, 2011; Khadria and Senes, 2013; Condon *et al.*, 2018) but has not been demonstrated for full-length proteins. Therefore, these results demonstrate that the use of BN-PAGE in conjunction with SMA solubilisation offers a simple method for studying the quaternary structure of full-length FtsB/FtsL complexes. From these results, a 2:2 oligomerisation model of FtsB/FtsL association appears to be most likely.

In order to achieve higher resolution structural data for these complexes, SEC-SAXS data was collected. However, the complexity of SMALPs complicated data analysis. While FtsB/FtsL-SMALPs can be grouped into discrete populations based on molecular weight when analysed by BN-PAGE, this was not possible on the basis of R_g when analysing the SAXS data. The R_g instead gradually decreased across the SEC elution profile, preventing the identification of different oligomeric states. This is unsurprising as SMALPs have been demonstrated to rapidly exchange lipids with their environment (Hazell *et al.*, 2016), therefore it is likely that the SMALP discs constantly grow and shrink and have largely variable sizes, as opposed to the ‘10

nm disc' ideal often presented. From the SAXS data, some rudimentary analysis was possible, but *ab initio* modelling was not conducted. To improve future SEC-SAXS experiments, separation of the sample on a longer SEC column would improve the resolution of different SMALP populations. However, as mentioned across this study, this requires more sample, and the limitations of SMA-solubilisation prevented the purification of protein concentrations high enough to achieve this.

In chapter 3, DDM solubilisation of FtsB produced significantly higher yields of FtsB than SMA solubilisation. With this in mind, it was considered whether detergent preparation could similarly purify FtsB/FtsL complexes with a higher yield than SMA. While DDM solubilisation did result in a higher yield of FtsB and FtsL, the solubilisation method was also demonstrated to interfere with FtsB/FtsL association, and the co-elution of a range of contaminants was also much higher. Compared to the FtsB/FtsL SMALPs, when the SEC elution fractions of DDM solubilised proteins were analysed by BN-PAGE, the multiple populations within the sample were shown to be poorly separated. This data shows that SMA and DDM solubilisation techniques both have significant strengths and weaknesses, and while SMA is a useful tool for studying full-length proteins in their native lipid environment, it is not a "one-size-fits-all" solution.

CHAPTER 6: ANALYTICAL ULTRACENTRIFUGATION OF SMALPS

6.1 Introduction

As demonstrated in the previous chapters, native-PAGE is a useful technique for the estimation of the molecular weight of protein complexes within SMALPs. However, the resolution of native-PAGE is limited as proteins bands are diffuse and migrate across a wide range of molecular weights. This can prove difficult when working with low molecular weight proteins such as FtsB and FtsL where the difference between monomeric and dimeric states is less than 15 kDa. To accurately measure the molecular weight of these samples, an alternative technique is analytical ultracentrifugation (AUC). AUC measures the sedimentation of particles under strong gravitational forces (commonly >100,000 x g), producing a size-distribution profile of the particles within the sample. AUC is a particularly attractive method for the study of membrane proteins as it does not require a large amount of sample; a typical sedimentation velocity run requires 500 µL of sample at a concentration of around 0.1-0.5 mg/mL. Additionally, samples can be analysed in their native state, in free solution, in a wide range of buffers, and samples can be rescued post-experiment.

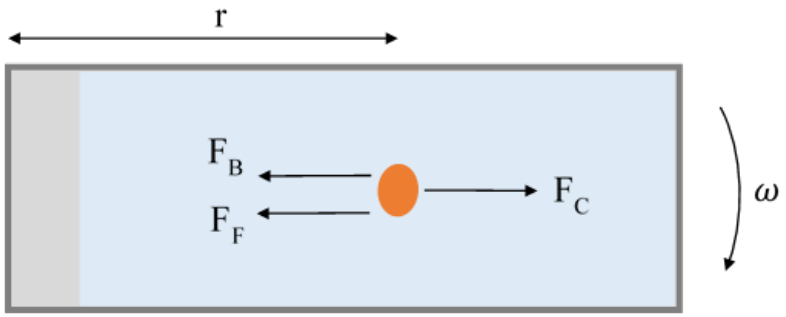

Figure 6.1. **The forces acting on a solute particle during analytical ultracentrifugation.** F_c is the centrifugal force, which is the mass of the particle m_p multiplied by the centrifugal acceleration given by $\omega^2 r$, where ω is the rotor speed, and r is the distance from the centre of the rotor. F_F is the frictional force, equal to the mass of the fluid displaced by the particle and F_B is the buoyant force.

The sedimentation behaviour of a particle during AUC is characterised by its sedimentation coefficient s, which is the ratio between the sedimentation velocity of the particle and the centrifugal acceleration applied. The sedimentation coefficient can be defined by the balance of three forces: F_C, F_B, and F_F, as shown in figure 6.1. F_c is the centrifugal force, which is the mass of the particle m_p multiplied by the centrifugal acceleration given by ω^2r, where ω is the rotor speed and r is the distance from the centre of the rotor. F_F is the frictional force, equal to the mass of the fluid displaced by the particle. F_F is therefore $m_p(1-\bar{v}\rho)$, where $\bar{v}$ is the partial specific volume of the particle and ρ is the buffer density. F_B is the buoyant force, given by fv, the frictional coefficient f multiplied by the velocity v. By balancing these forces, the Svedburg equation to determine the sedimentation coefficient of a particle can be obtained:

$$s = \frac{v}{\omega^2 \mathrm{r}} = \frac{m_p(1-\bar{v}\rho)}{f} \qquad \textit{Equation 6.1}$$

In order to obtain the molar mass of the particle M_p, Avogadro's constant N_A can be added to the equation to produce:

$$s = \frac{v}{\omega 2\mathrm{r}} = \frac{M_p(1-\bar{v}\rho)}{N_A f} \qquad \textit{Equation 6.2}$$

The frictional coefficient f is calculated using Stokes' law, where the frictional coefficient of a spherical particle f_0 is denoted as:

$$f_0 = 6\pi\eta R_0 \qquad \textit{Equation 6.3}$$

Where η is the buffer viscosity and R_0 is the radius of the sphere as given by:

$$R_0 = (\frac{3M_p\bar{v}}{4\pi N_A})^{\frac{1}{3}} \qquad \textit{Equation 6.4}$$

The frictional coefficient can then be manipulated with multiplication by the frictional ratio f/f_0 in order to reflect non-spherical samples. The frictional ratio is commonly found experimentally by sedimentation analysis software such as SEDFIT (Schuck, 2000).

As is clear from these calculations, the input of an accurate value for partial specific volume $\bar{v}$ is highly important for the determination of sedimentation and therefore particle size. For samples with known density, this can be quickly calculated, however for biological samples this is rarely known. Partial specific volume can be measured experimentally by pycnometry or magnetic float apparatus, however these methods require large volumes of protein and extra apparatus. Partial specific volumes for proteins can also be calculated using their amino acid composition, a function integrated into sedimentation analysis programs such as SEDNTERP (Laue *et al.*, 1992). However, for the analysis of FtsBL-SMALPs which contain a mixture of polymer, lipids and protein, this may not accurately predict the partial specific volume of the discs. To date, there has been no in depth study of the sedimentation of SMALPs in AUC or their partial specific volume.

An alternative method of partial specific volume determination is using differential sedimentation. First described by Martin, Cook and Winkler (1956), differential sedimentation involves centrifuging samples in both water and deuterium and using the change in sedimentation coefficient to estimate $\bar{v}$.

The sedimentation of samples in water and deuterium can be described accordingly by rearranging the Svedburg equation:

$$s_H f p_H = M(1 - \bar{\upsilon}\rho_H) \qquad \textit{Equation 6.5}$$

$$s_D f p_D = M\kappa(1 - \bar{\upsilon}\rho_D/\kappa) \qquad \textit{Equation 6.6}$$

Where $\bar{\upsilon}$, η, S, and ρ represent partial specific volume, buffer viscosity, sedimentation coefficient, and buffer density respectively. Subscript $_D$ denotes D_2O samples and subscript $_H$ denotes H_2O samples. κ represents the molar mass ratio of the sample in deuterated compared to non-deuterated solvent. Buffer viscosity differences are corrected for by replacing the f coefficient with fp.

These equations can then be rearranged to give an equation to calculate partial specific volume:

$$\bar{\upsilon} = \left(\frac{\eta_D}{\eta_H} - \kappa\frac{s_H}{s_D}\right)\left(\frac{\rho_H\eta_D}{\eta_H} - \frac{\rho_D s_H}{s_D}\right)^{-1} \qquad \textit{Equation 6.7}$$

This method was successfully used to calculate partial specific volumes for a range of proteins within 1% of published values found by conventional methods (Martin, Cook and Winkler, 1956). While the method is prone to some degree of error due to estimations of sedimentation coefficients, unlike more classical methods it is much less sensitive to errors in concentration calculations and the presence of impurities. This method also requires a much smaller sample size, which for the analysis of membrane proteins is often a huge benefit.

The aim of this chapter was to:

1. Characterise a soluble protein by differential sedimentation to confirm the methods compatibility with modern instrumentation and analysis software.
2. Characterise DMPC-SMALPs by differential sedimentation to model the sedimentation of lipid only discs.
3. Characterise ZipA-SMALPs by differential sedimentation to confirm the molecular weight estimation gained from differential sedimentation against a well-characterised protein.
4. Characterise FtsBL-SMALPs by differential sedimentation and use these parameters to calculate the molecular weight of each oligomeric state as identified in BN-PAGE.

6.2 Application of Differential Sedimentation to Bovine Serum Albumin

Since the publication of the differential sedimentation method in 1959, the instrumentation and analysis methods used in AUC have changed significantly, therefore to ensure that differential sedimentation is compatible with the use of analysis software such as SEDFIT, the technique was applied to the well-defined soluble protein bovine serum albumin (BSA). Commercial BSA was dissolved in distilled water at a range of concentrations, and then diluted at a 1:1 ratio with either water or deuterium. These samples were then analysed by AUC at 40,000 rpm, following the sedimentation of the samples at an absorbance of 280 nm. Resulting data was analysed in SEDFIT to produce a continuous sedimentation c(s) distribution. A representative distribution of 0.5 mg/mL BSA in non-deuterated solvent is shown in figure 6.2. Two peaks are seen in the distribution, the first peak at s = 4.3 represents

the majority of the sample and monomeric BSA, with a smaller second peak at s = 6.4 corresponding to dimeric BSA.

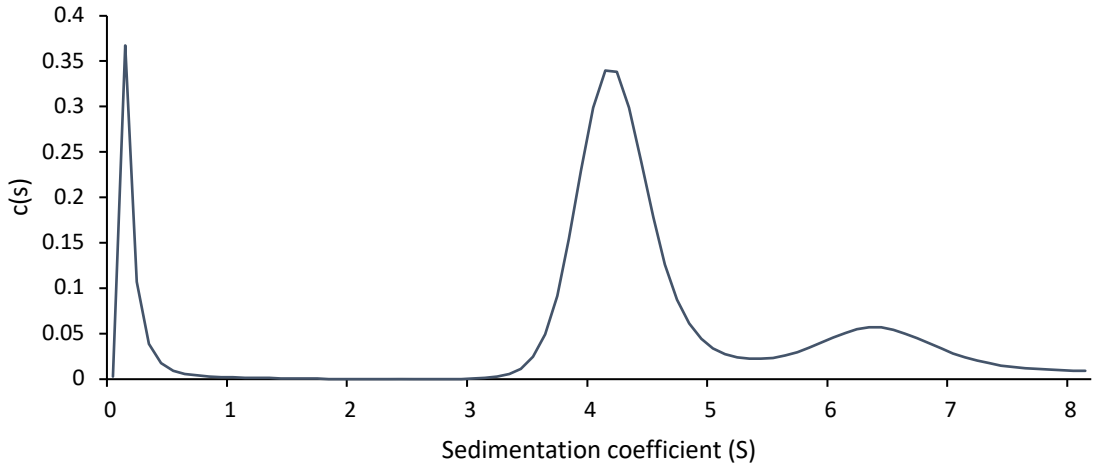

Figure 6.2 **Sedimentation distribution of bovine serum albumin (BSA).** 0.5 mg/mL BSA was prepared in distilled water. A sedimentation velocity experiment was performed at 20°C, 40,000 rpm, monitoring the sample by absorbance at 280 nm. Data was analysed in SEDFIT (Schuck, 2000) applying the continuous c(s) distribution model.

Figure 6.3a shows the sedimentation distribution of BSA samples in deuterated and non-deuterated solvent. BSA diluted in water has an average sedimentation coefficient of 4.33 S for the monomer peak, while in deuterated buffer the monomer peak shifted to a lower average of 2.80 S. Similarly, the dimer peak of BSA in water has an average sedimentation coefficient of 6.45 S, while the deuterated dimer peak averaged to 4.44 S.

To ensure the protein concentration of the analysed samples did not affect the sedimentation coefficient value in later calculations, the s values were plotted in respect to BSA concentration and a linear trend line fitted (figure 6.3b).

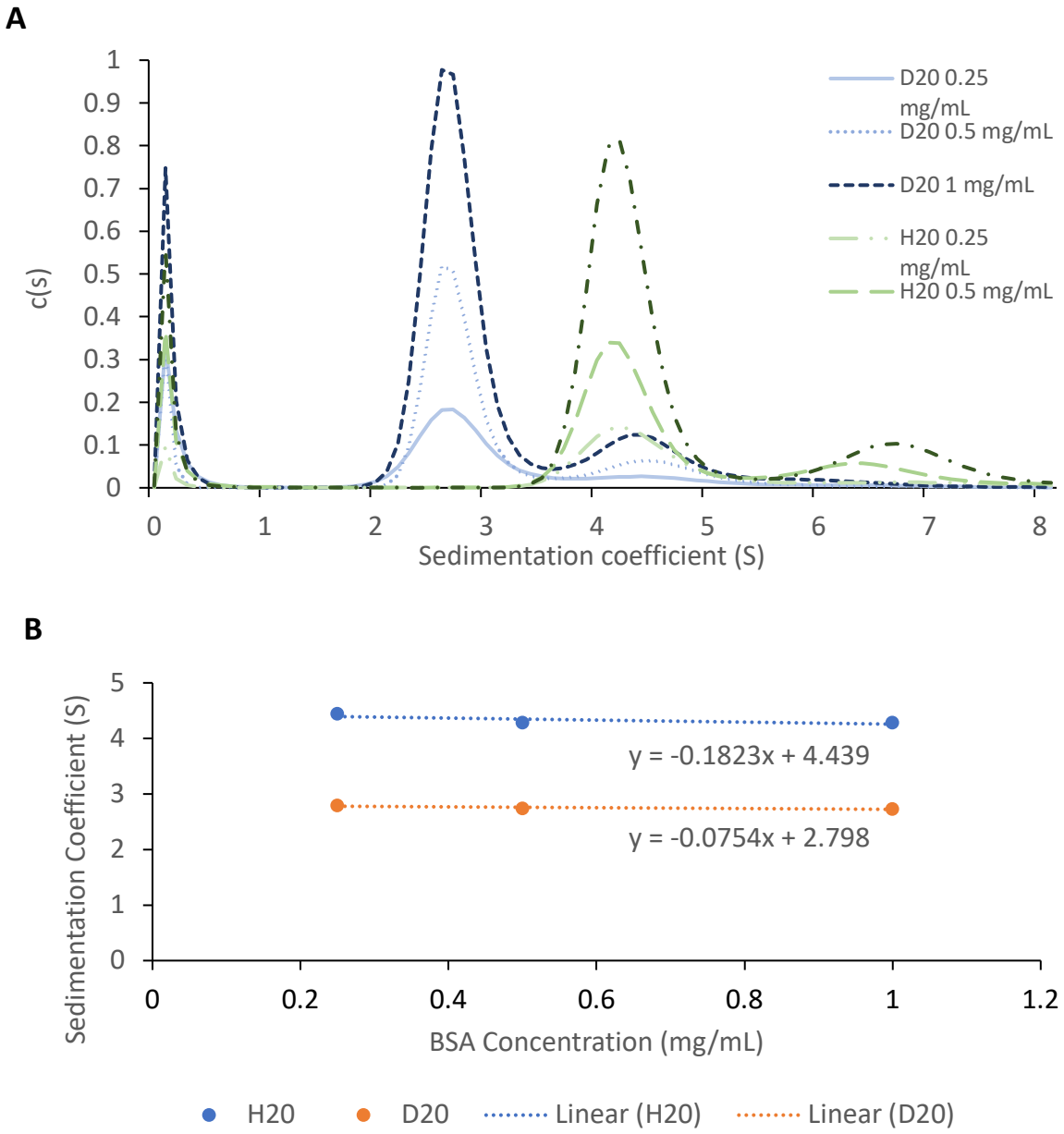

Figure 6.3 **Differential sedimentation of bovine serum albumin (BSA).** 0.25, 0.5 mg/mL and 1 mg/mL BSA was prepared in either 50% deuterated solvent (D_20) or non-deuterated solvent (H_2O). A sedimentation velocity experiment was performed at 20°C, 40,000 rpm, monitoring the samples by absorbance at 280 nm. (A) Data was analysed in SEDFIT (Schuck, 2000) applying the continuous c(s) distribution model. (B) The sedimentation coefficient value of the major peak of each distribution was plotted in respect to BSA concentration and a linear trend line fitted. The equation of each line is shown.

Both H_2O and D_2O samples did show a slight decrease of s with increased concentration, therefore, the x intercept of this line was then used as a concentration independent value of s.

The calculated s values were then used to calculate the partial specific volume using equation 6.7. The κ value for BSA was calculated by determining the number of labile hydrogens in the protein sequence and, assuming 100% hydrogen-deuterium exchange, predicting the molar mass ratio of the sample in deuterated compared to non-deuterated solvent. The values for ρ and η were found using SEDNTERP, correcting for the increase of density and viscosity by the addition of deuterium. The frictional ratio f/f_0 was calculated by SEDFIT during data analysis, by allowing the program to fit the most likely f/f_0. The calculated values are outlined in table 6.1.

κ	ρ_H	ρ_D	η_H	η_D	s_H	s_D	f/f_0
1.017	0.997614	1.1048	0.9149	1.1242	4.439	2.798	1.493

Table 6.1 **Parameters for the estimation of bovine serum albumin (BSA) partial specific volume.** $\bar{\upsilon}$, η, S, and ρ represent partial specific volume, buffer viscosity, sedimentation coefficient, and buffer density respectively. Subscript $_D$ denotes D_2O samples and subscript $_H$ denotes H_2O samples. κ represents the molar mass ratio of the sample in deuterated compared to non-deuterated solvent.

From these parameters, the partial specific volume of BSA was calculated to be 0.73. The parameters for the H_2O samples in table 6.1 and the calculated partial specific volume could then be used to calculate the mass of the particle by rearranging equation 6.6 to give equation 6.8:

$$M_p = \frac{sN_A f}{(1 - \bar{v}\rho)}$$ *Equation 6.8*

The mass of the monomer peak was calculated to be 65,000 Da. The mass of the second peak at a sedimentation value of 6.45 was similarly calculated, and was determined to be 120,000 Da. The published molecular weight of a BSA monomer is 66.5 kDa, therefore differential sedimentation had allowed the accurate prediction of the molecular weight of a soluble protein from sedimentation velocity data with no prior knowledge of the partial specific volume or density of the protein.

6.3 Application of Differential Sedimentation to DMPC SMALPs

In order to accurately define the lipid, SMA and protein components during AUC analysis of SMA solubilised proteins, lipid only SMALPs were first characterised. DMPC liposomes were solubilised with SMA and purified by size exclusion chromatography (SEC). The SEC trace of a DMPC-SMALP preparation is shown in figure 6.4. DMPC-SMALP preparations have multiple elution peaks between 12 mL and 24 mL. The first peak at 14 mL was assigned to be SMALPs in line with previous characterisation of lipid disc elution profiles (Hall *et al.*, 2018). To confirm the presence of SMALPs at the predicted 10 nm diameter, dynamic light scattering (DLS) measurements were taken across the peak. Measured diameters ranged from 21 nm at the front end of the peak elution, to a minimum value of 9.4 nm at the lagging end of the peak. As the second elution peak begins there is an increase in diameter, due to elution of aggregated polymer with a lower molecular weight but larger hydrodynamic radius (Hall *et al.*, 2018).

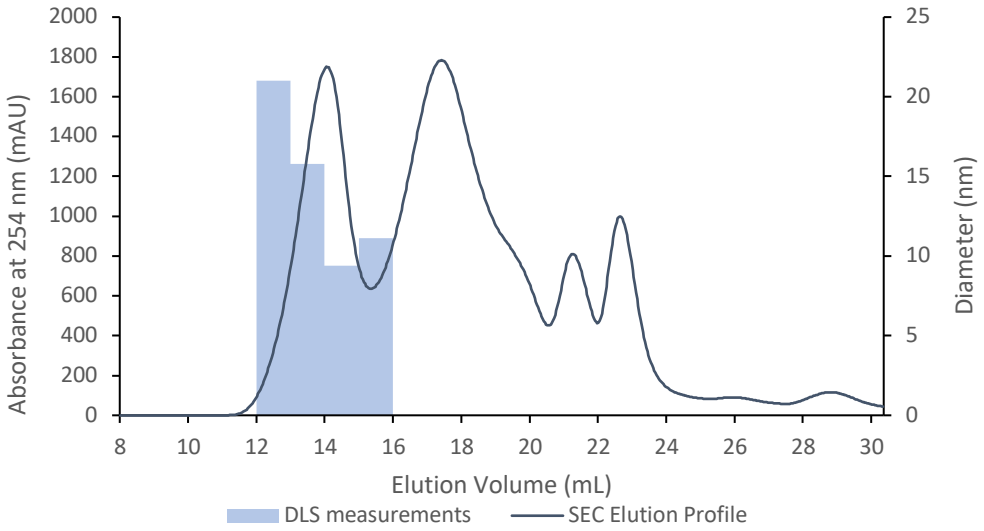

Figure 6.4 **Size exclusion chromatography (SEC) of SMA solubilised DMPC liposomes.** DMPC liposomes were solubilized with 2.5 % SMA for 3 hours and then separated by SEC on a Superdex 200 Increase 10/300 column. Elution from the column was measured by absorbance at 254 nm. Blue bars represent the dynamic light scattering of the elution fractions, measured on a Malvern Nano-series DLS.

Elution fractions between 13-14 mL were pooled and diluted at a 1:1 ratio with either H_2O or D_2O. The DMPC-SMALP samples were then analysed by AUC, slowing the rotor to 30,000 rpm compared to 40,000 rpm for BSA due to the higher predicted molecular weight of DMPC-SMALPs. The sedimentation distribution for deuterated and non-deuterated DMPC-SMALPs are shown in figure 6.5. Non-deuterated discs primarily sedimented at an s value of 2.78 S, while deuterated sample sedimented at 1.89 S. A smaller sedimentation peak in the non-deuterated sample is seen at around 1.5 S. This most likely represents a small amount of aggregated polymer co-purified with the DMPC SMALPs. As seen in figure 6.4, the elution peaks of the DMPC-SMALPs (peak 1) and aggregated polymer (peak 2) overlap and therefore some aggregated polymer will likely be in the SMALP samples. This peak is not seen in the

deuterated samples, presumably because the polymer sediments at an S value too low to be resolved in this analysis.

As described for BSA, the calculated s values were then used to calculate the partial specific volume of DMPC-SMALPs using the values outlined in table 6.2. The κ value for the SMALPs was calculated by determining the number of labile hydrogens in DMPC and SMA and assuming 100% hydrogen-deuterium exchange, predicting the molar mass ratio of the sample in deuterated compared to non-deuterated solvent. The κ value for SMA is 1.003 while the κ value for DMPC is 1 therefore 1 was used as it is likely DMPC makes up the majority of the mass of the disc.

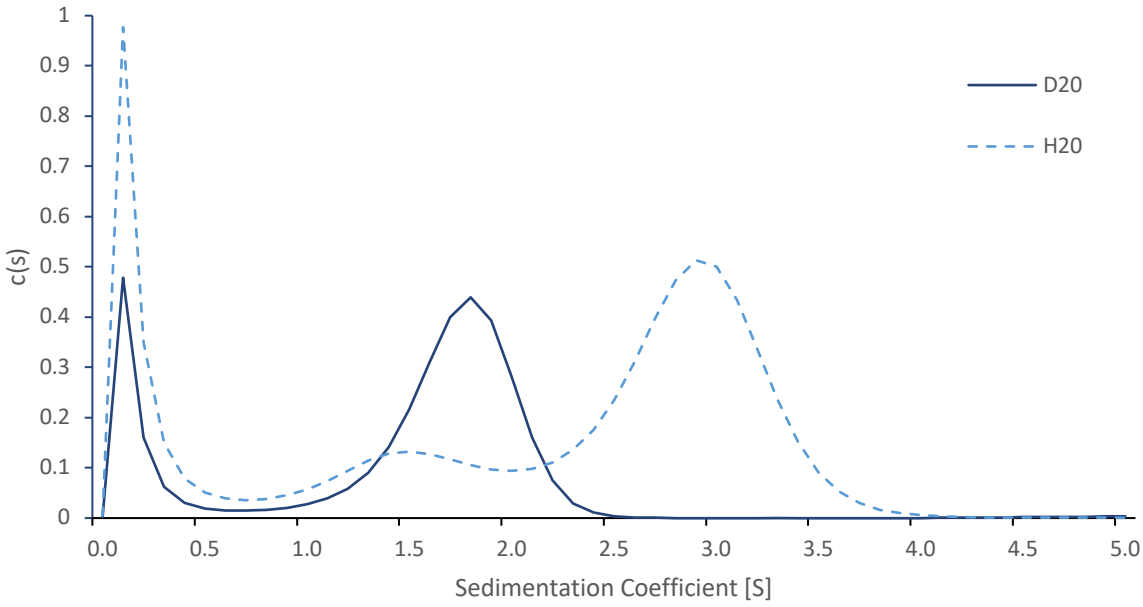

Figure 6.5 **Differential sedimentation of DMPC-SMALPs.** DMPC-SMALPs were prepared in either 50% deuterated solvent (D_2O) or non-deuterated solvent (H_2O). A sedimentation velocity experiment was performed at 20°C, 40,000 rpm, monitoring the samples by absorbance at 280 nm. Data was analysed in SEDFIT (Schuck, 2000) applying the continuous c(s) distribution model.

κ	ρ_H	ρ_D	η_H	η_D	s_H	s_D	f/f_0
1	1.000814	1.0535	0.9243	1.0096	2.78	1.74	1.85

Table 6.2 **Parameters for the estimation of DMPC-SMALP partial specific volume.** $\bar{\upsilon}$, η, S, and ρ represent partial specific volume, buffer viscosity, sedimentation coefficient, and buffer density respectively. Subscript $_D$ denotes D_2O samples and subscript $_H$ denotes H_2O samples. κ represents the molar mass ratio of the sample in deuterated compared to non-deuterated solvent.

From these variables, the partial specific volume of DMPC-SMALPs was calculated to be 0.857. The variables for the H_2O samples in table 6.2 and the partial specific volume could then be used to calculate the mass of the particle. The particle was calculated to be 135,000 Da. Using a calculated calibration curve for the Superdex 200 Increase 10/300 column (supplementary figure 8.1), elution between 13-14 mL corresponds to a molecular weight of 180 kDa to 110 kDa, in agreement with the molecular weight calculations from the AUC data. Therefore, differential sedimentation was successfully applied to DMPC-SMALPs to accurately measure the partial specific volume and molecular weight.

6.4 Application of Differential Sedimentation to ZipA-SMALPs

To investigate the analysis of SMA solubilised proteins using AUC, the divisome protein ZipA was chosen as a model, as its oligomerisation state is well defined (Skoog and Daley, 2012) and the protein has been previously solubilised using SMALP and investigated by AUC (Lee *et al.*, 2016). A glycerol stock of *E. coli* BL21(DE3) containing the plasmid for overexpression of His-tagged ZipA was a kind gift from Dr Sarah Lee at the University of Birmingham. ZipA was

overexpressed in *E. coli* with 0.5 mM IPTG induction overnight, before pelleting the cell mass and preparing the membrane fraction. The membranes were then solubilised with SMA at room temperature for 3 hours before any material not solubilised was pelleted by ultracentrifugation. The supernatant was incubated with Ni-NTA resin overnight at 4°C to bind any His-Tagged proteins to the resin. The resin was washed with a low imidazole concentration to remove any un-specifically bound protein, and then His-Tagged proteins were eluted with a high concentration of imidazole (figure 6.6).

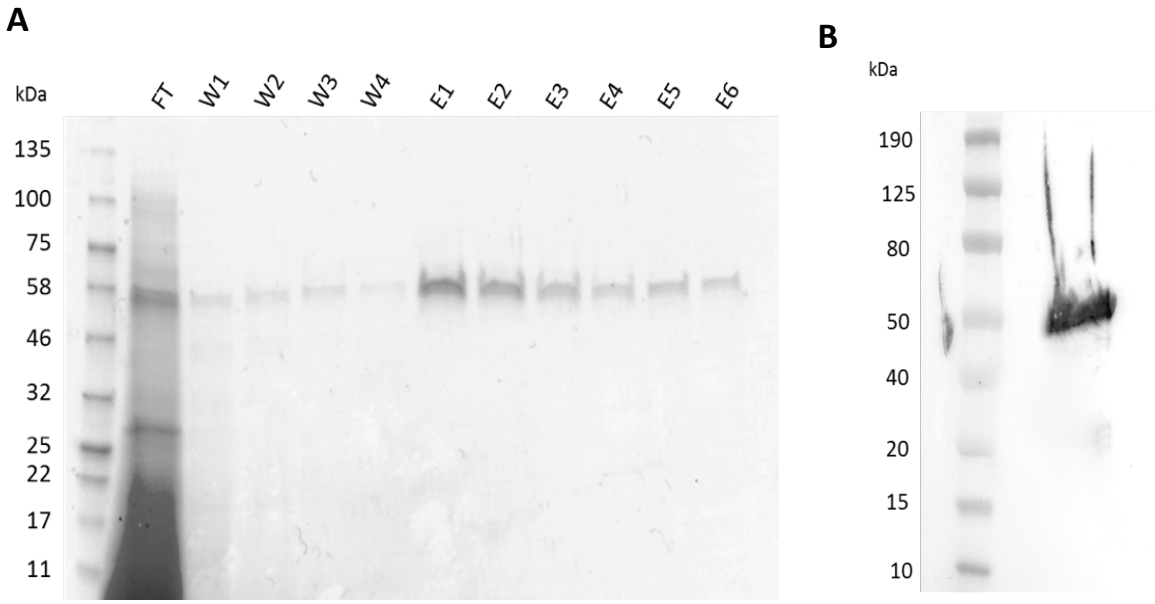

Figure 6.6. **ZipA Ni-NTA purification.** SMA solubilised membranes were incubated with Ni-NTA resin overnight and then transferred to a gravity flow column and flow through (FT) collected. The resin was washed 4 times with 10 CV 20 mM imidazole buffer (W1-4) and then His-Tagged proteins were then eluted 4 times with 1 CV 500 mM imidazole buffer (E1-4). (A) Fractions were analysed by electrophoresis on a 12% SDS-PAGE gel and protein bands visualised by Coomassie staining. (B) A whole cell sample of cells *E. coli* overexpressing ZipA was analysed by electrophoresis on a 12% SDS-PAGE gel and His-tagged protein bands visualised by western blotting with anti-his antibody.

ZipA eluted off the column as a single band with no visible contaminants. With the additional of the 6XHis-Tag and V5 epitope tag, ZipA is expected to have a molecular weight of 39.5 kDa, however the purified ZipA ran at ~54 kDa.

ZipA has been previously reported to migrate to a higher molecular weight than expected when solubilised in Triton-X100 (Hale, Rhee and de Boer, 2000), and ZipA in whole cell samples runs at the same size (figure 6.6), therefore this aberration in SDS-PAGE predicted molecular weight is presumably due to the protein itself and unrelated to its purification in SMALPs.

The eluted ZipA from the Ni-NTA purification was concentrated and analysed by using size exclusion chromatography (SEC). Elution of protein was monitored by absorbance at 280 nm (figure 6.7a), and aliquots of the 0.5 mL elution fractions collected were analysed by SDS-PAGE (figure 6.7b). ZipA-SMALPs eluted between 7.5 and 12.5 mL, corresponding to molecular weights between 1000 to 230 kDa using the column calibration curve (supplementary figure 8.1).

When the elution profile of ZipA-SMALPs is overlaid with the elution profile of DMPC-SMALPs (figure 6.7a), it shows that ZipA-SMALPs elute earlier from the column than DMPC-SMALPs, and that these two profiles do not overlap by more than 2 mL. This suggests than in ZipA-SMALPs the SMA/lipid component is likely to have a molecular weight close to that of DMPC SMALPs, and the increased molecular weight is due to additional ZipA protein within the disc.

To investigate the quaternary structure of ZipA within the SMALPs, the elution fractions were analysed by BN-PAGE. When analysed by SDS-PAGE (figure 6.7b), single bands at ~54 kDa representing ZipA were seen along the elution profile.

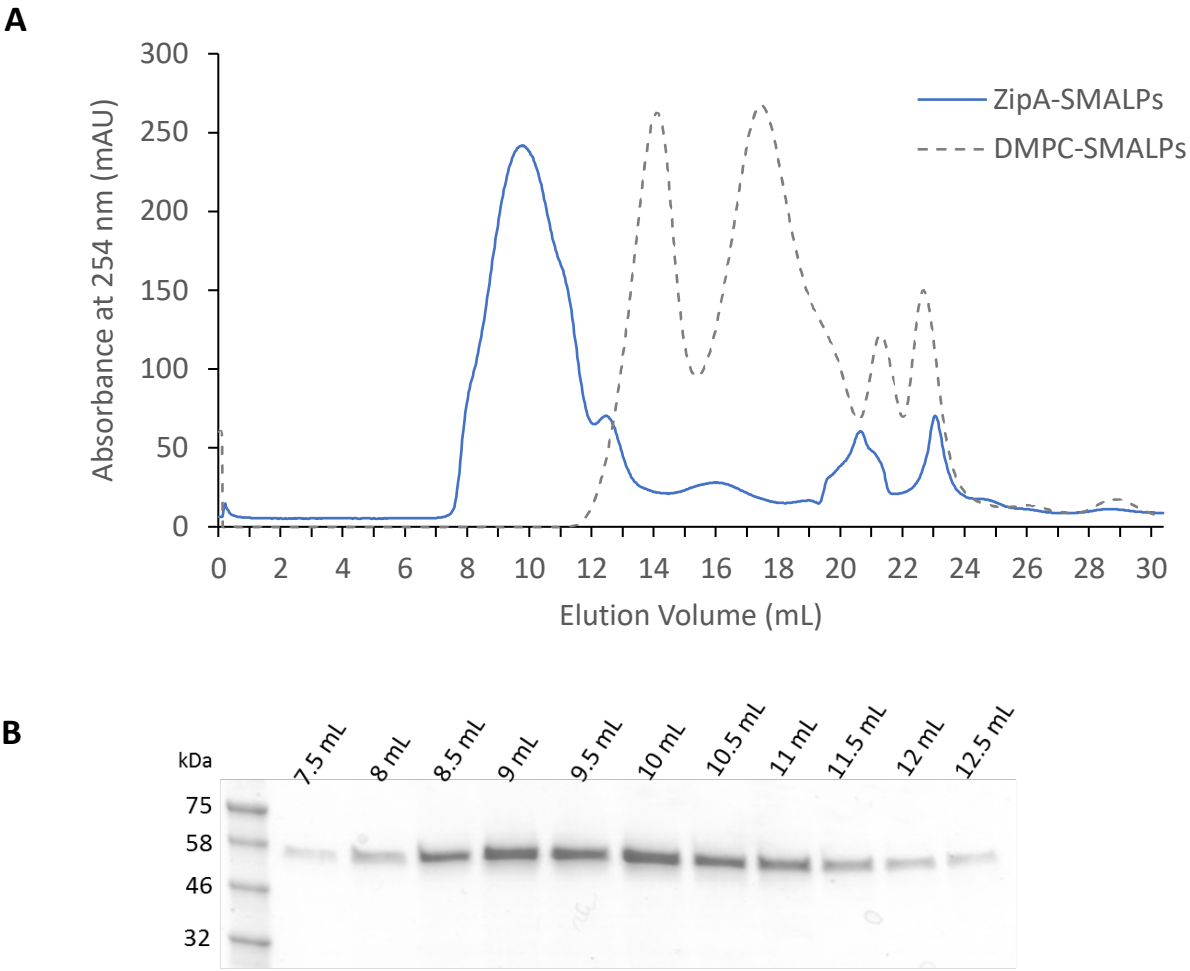

Figure 6.7 **Size exclusion chromatography (SEC) of SMA solubilised ZipA.** Elution fractions from Ni-NTA purification were pooled and injected onto a Superdex 200 Increase 10/300 GL column. The column was run at 0.5 mL/min for 30 mL collecting 0.5 mL fractions. (A) SEC elution profile. Elution of protein from the column was monitored by absorbance at 280 nm. The elution profile of DMPC-SMALPs is overlaid for comparison. (B) SDS-PAGE of elution profile. Elution fractions at the given volumes were analysed by electrophoresis on an 18% SDS-PAGE gel and protein bands visualised by Coomassie staining.

When the same fractions were analysed by BN-PAGE bands at multiple molecular weights were seen, suggesting the presence of multiple oligomerisation states within the SMALPs (figure 6.8). The lowest molecular weight bands, eluting at 12.5 mL, migrate to approximately 40 kDa, 80 kDa and 200 kDa.

However, the staining of Native-PAGE produces diffuse bands which are often overlapping making accurate size analysis difficult, therefore analysis by AUC would provide more detailed molecular weight analysis.

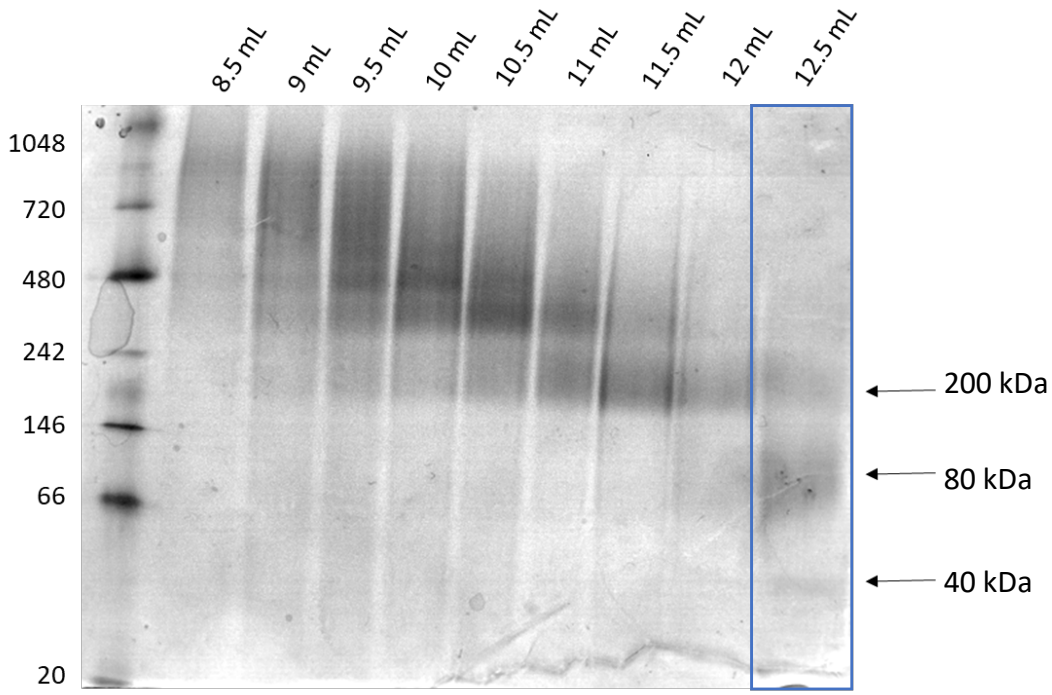

Figure 6.8 **Blue Native-PAGE ZipA-SMALPs.** SEC elution fractions at the given volumes were analysed by BN-PAGE on a 4-16% Bis-Tris gel and protein bands visualised by Coomassie staining.

The 12.5 mL SEC elution fraction chosen for AUC analysis as this fraction clearly contained three populations on the BN-PAGE. The sample was diluted at a 1:1 ratio with either H_2O or D_2O and analysed by AUC at a rotor speed of 30,000 rpm, measuring absorbance at 280 nm. The sedimentation distribution for deuterated and non-deuterated DMPC-SMALPs are shown in figure 6.9. For both samples, three peaks were seen along the sedimentation distribution, with the middle peak having the largest intensity. This major peak showed a shift from a sedimentation coefficient of 5.21 S in non-deuterated solvent, down to 4.34 S in deuterated solvent.

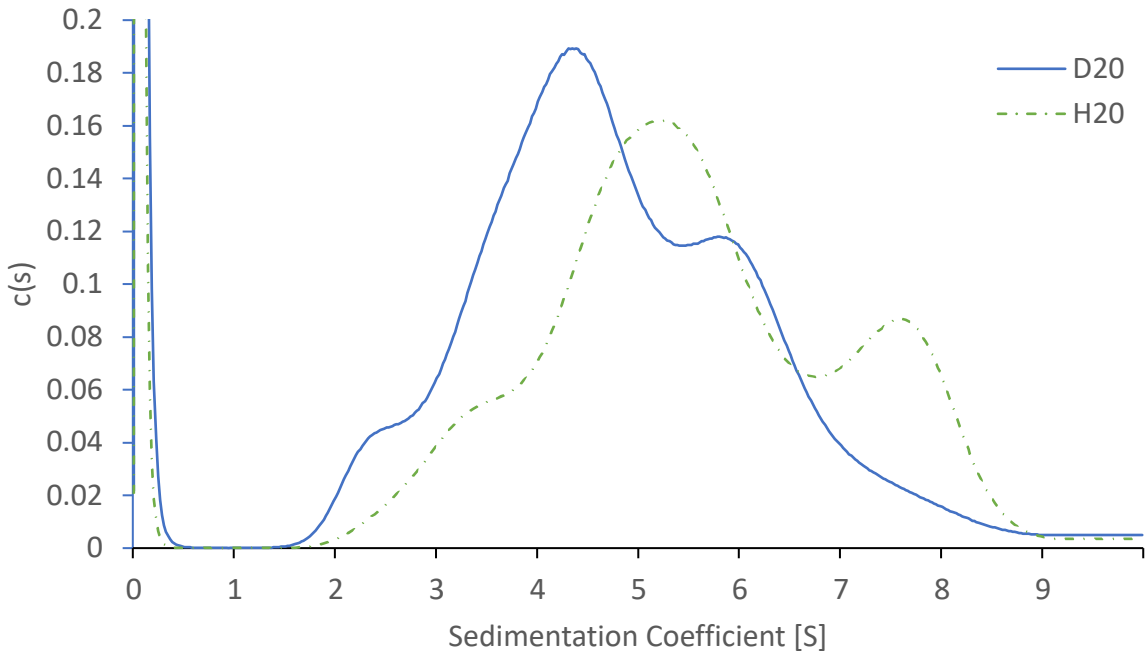

Figure 6.9 **Differential sedimentation of ZipA-SMALPs.** ZipA-SMALPs were prepared in either 50% deuterated solvent (D_20) or non-deuterated solvent (H_20). A sedimentation velocity experiment was performed at 20°C, 40,000 rpm, monitoring the samples by absorbance at 280 nm. Data was analysed in SEDFIT (Schuck, 2000) applying the continuous c(s) distribution model.

The calculated s values were then used to calculate the partial specific volume of ZipA-SMALPs using equation 6.7. The κ value for the ZipA-SMALPs was calculated by determining the number of labile hydrogens in ZipA and SMALPs. The κ value for ZipA is 1.016 while the κ for SMALPs is 1.004 therefore 1.016 was used as it will encompass the exchange by ZipA and the disc itself. The partial specific volume of ZipA-SMALPs was calculated to be 0.743. The values for ρ and η were found using SEDNTERP, correcting for the increase of density and viscosity by the addition of deuterium. The frictional ratio f/f_0 was calculated by SEDFIT during data analysis, by allowing the program to fit the most likely f/f_0. The calculated values are outlined in table 6.3.

κ	ρ_H	ρ_D	η_H	η_D	s_H	s_D	f/f_0
1.016	1.000814	1.0535	0.9243	1.0096	5.21	4.34	1.80

Table 6.3 **Parameters for the estimation of ZipA-SMALP partial specific volume.** $\bar{v}$, η, S, and ρ represent partial specific volume, buffer viscosity, sedimentation coefficient, and buffer density respectively. Subscript $_D$ denotes D_2O samples and subscript $_H$ denotes H_2O samples. κ represents the molar mass ratio of the sample in deuterated compared to non-deuterated solvent.

The parameters for the H_2O samples in table 6.3 and the calculated partial specific volume could then be used to calculate the mass of the particle using equation 6.8. The first, second and third peaks were calculated to be 75,000 Da, 125,000 Da and 220,000 Da respectively. Previous results with ZipA monomers in SMALPs found that monomers have a sedimentation coefficient around 4 S and that this equated to a molecular weight of 70 kDa with SMA and

lipid contributing ~30 kDa to the molecular weight of the disc (Lee *et al.*, 2016). Combining this information, it allows the prediction of all the oligomeric states of ZipA in this sample from the AUC analysis. The first peak, predicted to be 75 kDa, can be assigned as monomeric ZipA with 35 kDa molecular weight resulting from the SMALP disc. The second peak was predicted to be 125 kDa, an increased molecular weight of 50 kDa from the monomer and therefore most likely to result from the addition of another ZipA protein to form a dimer. Finally, the third peak was predicted to be ~220 kDa, an increase of 95 kDa from the dimer. This would suggest an additional ZipA dimer in the disc, whether as a tetramer or as two separate dimers within the same disc. These results agree with the BN-PAGE analysis, which for this elution fraction had bands migrating to 40 kDa, 80 kDa and 200 kDa. As SMALPs migrate to a molecular weight consistent with the protein molecular weight, with no additional weight from the SMALP disc (Pollock *et al.*, 2019), this would also suggest the presence of ZipA monomers, dimers and tetramers/two dimers.

6.5 Analytical Ultracentrifugation of FtsBL-SMALPs

The previous section demonstrated that when analysing ZipA-SMALPs, the partial specific volume of the sample matches that of the partial specific volume of the protein when calculated from the protein sequence. Therefore, this technique was applied to FtsBL-SMALPs to measure the molecular weight of the multiple oligomers purified by size exclusion chromatography. Three samples were chosen, which were the elution fractions at 13 mL, 14.5 mL and 16 mL, as outlined in figure 6.10a.

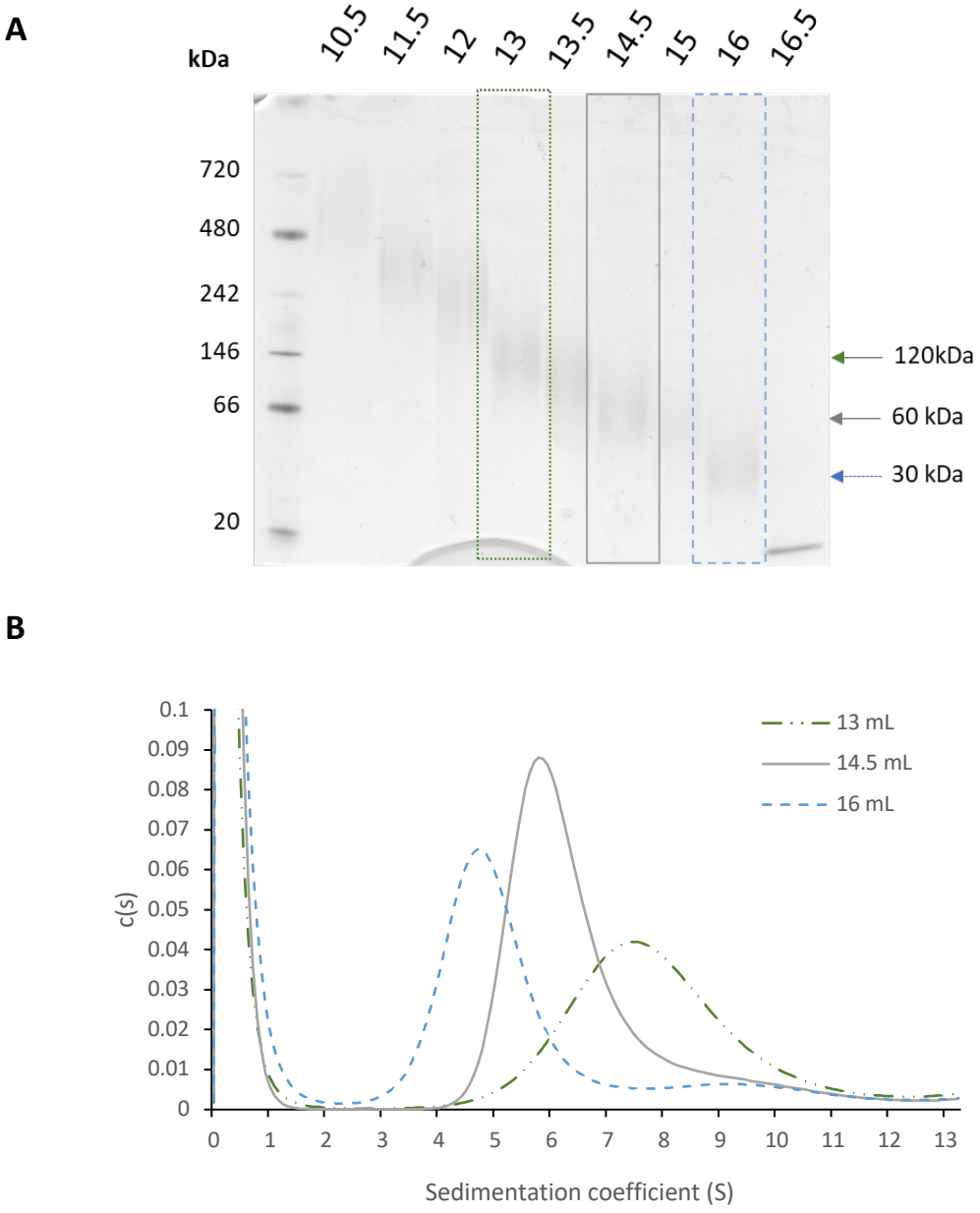

Figure 6.10 **Analytical ultracentrifugation of FtsBL-SMALPs.** (A) BN-PAGE of the FtsB/FtsL subcomplex. Elution fractions from Ni-NTA purification were pooled and injected onto a Superdex 200 Increase 10/300 GL column. The column was run at 0.5 mL/min for 25 mL, collecting 0.5 mL fractions. Elution was followed at 280 nm for detection of protein. Elution fractions at the given volumes were analysed by BN-PAGE electrophoresis on a 4-16% Bis-Tris gel and protein bands visualised by Coomassie staining. The highlighted fractions were analysed by AUC. (B) A sedimentation velocity experiment was performed at 20°C, 30,000 rpm, monitoring the sample by absorbance at 280 nm. Data was analysed in SEDFIT (Schuck, 2000) applying the continuous c(s) distribution model.

By BN-PAGE these fractions appeared to contain bands migrating to 120 kDa, 60 kDa and 30 kDa respectively. The samples were analysed by AUC at a rotor speed of 30,000 rpm, measuring absorbance at 280 nm. The sedimentation distributions for the FtsBL-SMALPs in figure 6.10b. Each distribution had only one major peak, confirming that each elution fraction had contained only one population of FtsBL-SMALPs.

The partial specific volume for FtsB alone, calculated by its protein sequence with SEDNTERP was 0.734, and for FtsL it was 0.748 therefore 0.74 was used as the partial specific volume. Using the sedimentation distributions, the molecular weight was calculated for each of the samples, outlined in table 6.4.

Elution volume (mL)	Predicted molecular weight by BN-PAGE (kDa)	Sedimentation coefficient (S)	Calculated molecular weight (kDa)
16	30	4.59	61.4
14.5	60	5.65	83.8
13	120	7.31	123.1

Table 6.4 **Analytical ultracentrifugation of FtsBL-SMALPs.**

The sample eluting at 16 mL was predicted to be dimeric FtsBL as it migrated to 30 kDa by BN-PAGE. By AUC this sample was calculated to be 61.4 kDa, which is in agreement with the finding that SMALPs contribute around 30 kDa to protein molecular weight estimates. Similarly, the elution volume at 14.5 mL contained a protein complex migrating to 60 kDa in BN-PAGE, an additional 30 kDa compared to the 13 mL elution and therefore predicted to be the presence of a tetramer or two dimers. This sample was calculated to be 84 kDa by AUC, an increase of 22 kDa compared to the 13 mL sample. As FtsB and FtsL are 11 kDa and 13

kDa respectively, this is also likely to be the addition of a dimer to the SMALP. These calculations therefore demonstrate that AUC can be used to accurately measure the molecular weight of protein complexes within SMALPs, and that BN-PAGE is a useful tool for validating these calculations.

6.6 Discussion

The aim of this chapter was to use differential sedimentation to characterise a range of SMALP samples by analytical ultracentrifugation. To first test the method of differential sedimentation on a well-defined protein, commercial BSA was used as a model. The low cost and high availability of the material also allow analysis to be performed at high concentrations with multiple repeats to ensure results were reproducible. BSA is a 66.4 kDa water soluble protein which is known to dimerise in solution, with a monomer to dimer ratio of around 6 at concentrations below 10 mg/mL (Molodenskiy *et al.*, 2017). The sedimentation coefficient profile of BSA reflected this, displaying two well defined peaks with the lower molecular weight peak having a relative height of around 6 times the higher molecular weight peak. The first and second peak were therefore assigned as monomer and dimer respectively. In order to calculate the partial specific volume ($\bar{\upsilon}$) of BSA, samples were sedimented in both non-deuterated and deuterated solvent, and the resulting sedimentation coefficients compared. BSA peaks showed a significant reduction in sedimentation coefficient in deuterated solvent compared to non-deuterated solvent. The equation of Martin, Cook and Winkler (1956) could then be applied to calculate $\bar{\upsilon}$. To adjust for the additional weight of samples in deuterated solvent due to H-D exchange, a κ value was calculated by identifying labile hydrogens in the

protein sequence and predicting the molecular weight increase of exchange at these positions. These calculations were made assuming 100% H-D exchange, as predicting the rate of exchange was not possible. Protein folding will affect accessibility of hydrogens for exchange (Li and Woodward, 1999), and intramolecular hydrogen bonding will also slow exchange rates (Bai *et al.*, 1995), thus H-D exchange may not be 100%. To allow an H-D exchange rate as close to 100% as possible, samples were diluted into D_2O and allowed to equilibrate for at least 16 hours. H_2O^{18} offers a solution to the difficulties of calculating κ values as it provides the same density contrast as D_2O but no exchange takes place. The use of H_2O^{18} was successfully applied to $\bar{\upsilon}$ determination by differential sedimentation by (Brown *et al.*, 2011), however the cost of H_2O^{18} prohibited its use in these experiments.

By the above methods, the $\bar{\upsilon}$ for BSA was calculated to be 0.73, in agreement with the published $\bar{\upsilon}$ for BSA of 0.733 (Oncley, Scatchard and Brown, 1947), obtained by classical density methods. This figure was then used to estimate the molecular weights of monomer and dimer peaks, predicting weights of 65 kDa and 120 kDa. For both peaks this method predicted molecular weight within a 2% error. These results demonstrate that differential sedimentation provides a methodology for calculating partial specific volume using small sample volumes and low protein concentration.

To simplify the analysis of SMALPs containing proteins, lipid only SMALPs were assessed first. DMPC lipid vesicles were solubilised with SMA and DMPC-SMALPs purified from excess polymer and lipid. These SMALPs were then analysed by AUC in deuterated and non-deuterated solvent. Just as in the BSA samples, deuterated solvent resulted in a decrease in sedimentation coefficient, which was used to calculate the samples $\bar{\upsilon}$. To determine the κ

value for DMPC-SMALPs, the separate κ values for DMPC and SMA were first found. As DMPC does not have any labile hydrogens and SMA has a κ of 1.003, the value of 1 was used, assuming that DMPC makes up most of the molecular weight of the SMALP. The $\bar{\upsilon}$ for DMPC-SMALPs was calculated to be 0.857. In a similar technique where lipid bilayers are stabilised in a disc by membrane scaffold proteins, discs are also ~12 nm and were found to have a partial specific volume of 0.89 (Inagaki, Ghirlando and Grisshammer, 2013). Using this value of $\bar{\upsilon}$, DMPC-SMALPs were estimated to be 135 kDa, in agreement with their predicted weight from the SEC elution. Structural analysis of DMPC SMALPs by Jamshad, Grimard, *et al.* (2015) found that disc on average contained around 140 DMPC molecules per disc, which would equate to 95 kDa of the disc weight. The additional molecular weight of SMA can then be considered, which with an M_n of 7 kDa would be around 5-6 SMA polymers per disc, a value in line with the current estimates of 3-10 SMA per disc (Timothy Dafforn, personal communication). These results demonstrate that differential sedimentation can be used to calculate the partial specific volume of lipid only discs, and this value can be used to accurately predict SMALP molecular weight.

These methods were then applied to SMALP discs containing protein. The divisomal protein ZipA was chosen for this work as it has been previously purified in SMA and there is a range of literature on its structure and lipid environment within SMALPs (Lee *et al.*, 2016; Teo *et al.*, 2019). ZipA was overexpressed in *E. coli* and successfully solubilised from membranes using SMA. Purification using the C-terminal His-Tag resulted in samples with high purity, migrating as a single protein band in SDS-PAGE. For improved purity and separation by molecular weight, samples were then purified by SEC. When SEC samples were analysed by SDS-PAGE, ZipA

appeared as single bands along the elution profile. However, when the same samples were analysed by Native-PAGE, a non-denaturing, non-reducing electrophoresis method, protein bands at multiple molecular weights were seen across the elution profile. This demonstrated that while the samples are pure ZipA, these samples contain multiple different assemblies of this protein. While these results also allowed rudimentary analysis of molecular weight, suggesting MWs of 90 kDa, 180 kDa and 360 kDa, these bands were diffuse and difficult to accurately measure. Previously published molecular weight estimation by Native-PAGE for protein-SMALPs reported errors of up to 22% (Pollock *et al.*, 2019), and considering that ZipA has been shown to run erroneously under electrophoresis (Hale, Rhee and de Boer, 2000), AUC was applied to these samples to verify these predicted molecular weights.

ZipA samples from along the elution peak were then pooled and analysed by AUC, in both deuterated and non-deuterated solvent. Sedimentation analysis resulted in three sedimentation peaks, at 3.55 S, 5.21 S and 7.62 S, with the second peak representing the highest proportion of sample. By comparing the s value of the second peak in deuterated and non-deuterated solvent, a partial specific volume of 0.743 was calculated for ZipA-SMALPs. Using this value, the molecular weight for the three peaks was calculated to be 75,000 Da, 125,000 Da and 220,000 Da respectively. This result was surprising, as when the SEC elution traces of DMPC-SMALPs and ZipA-SMALPs were overlaid, it appeared that ZipA-SMALPs eluted at an earlier volume than DMPC-SMALPs, indicating they had a higher molecular weight, however the smallest ZipA peak had been calculated to be ~60 kDa smaller than the DMPC discs. However, the ZipA samples has sedimented at a higher s value than DMPC discs, thus suggesting that it was the influence of the partial specific volume that resulted in this lower

molecular weight value for ZipA. Interestingly, the $\bar{\upsilon}$ for ZipA calculated by its protein sequence with SEDNTERP is 0.731, a value very close to that of the $\bar{\upsilon}$ calculated by differential sedimentation. This suggested these results may be due to the specific volume of the lipids becoming disregarded.

To further investigate this, it was important to calculate the partial specific volumes of the lipids within each sample. However, the partial specific volumes of many lipids are not available. Instead the method of Koenig and Gawrisch (2005) was used, which allows the prediction of lipid specific volume from the sum of the volumes of its CH, CH_2 and CH_3 group and a constant volume for the polar head region. Using this method, DMPC was calculated to have a $\bar{\upsilon}$ of 0.97, in line with published values (Petrache, Tristram-Nagle and Nagle, 1998). For ZipA-SMALPs, published lipidomic data was used to assess lipid content of discs obtained by solubilising *E. coli* membranes. Teo *et al.* (2019) analysed the lipid content of ZipA-SMALPs and found that 70% of the lipids in the disc were phosphatidylethanolamines (PE), with the most common species being PE(32:1), PE(33:1), PE(34:1). The remaining lipid was found to be 20% phosphatidylglycerol (PG), particularly PG(32:1) and PG (34:1) and 10% cardiolipin. Using the methods of Koenig and Gawrisch (2005), the partial specific volume of these lipids was found to be 1.005 on average for the PE species and 0.998 for PG species. Considering that $M = \frac{sf\eta}{(1-\bar{\upsilon}\rho)}$ (equation 6.8), for DMPC in non-deuterated buffer (1-$\bar{\upsilon}\rho$) ≈ 0.07 and therefore DMPC will increase the mass estimate of the disc. However, for *E. coli* lipids (1-$\bar{\upsilon}\rho$) approaches zero or becomes negative. This means that when using *E. coli* lipids, the lipids either do not affect the mass estimate and therefore are effectively “invisible”, or they reduce mass estimates slightly. These results may explain why the partial specific volume of ZipA-SMALPs

was calculated to be 0.743, as at the buffer density used the only effective partial specific volumes are that from ZipA ($\bar{\upsilon}$=0.731 by SEDNTERP) and a small proportion from SMA ($\bar{\upsilon}$=0.847). To further investigate this difference between lipid-only and protein SMALPs, it would be useful to conduct further experiments of lipid only SMALPs containing a range of lipids, for example, SMALP-solubilised *E. coli* lipids.

Previous AUC analysis of ZipA-SMALPs similarly found that ZipA monomers sedimenting ~4 S were calculated to an apparent molecular weight of 70 kDa (Lee *et al.*, 2016), which translates to a 40 kDa protein with an additional 30 kDa from another component. Considering that, it would follow that in the case of ZipA-SMALPs, only the protein and SMA weight is measured, while lipid does not contribute to molecular weight estimations. Therefore, the molecular weight estimates of 75,000 Da, 125,000 Da and 220,000 Da would represent ZipA monomers, dimers and tetramers/two dimers respectively. By this method it is not possible to differentiate between multiple monomers or oligomeric states, but as ZipA has previously been reported to dimerise (Skoog and Daley, 2012) and molecular weight estimates did not find any evidence for a situation with 3 ZipA proteins within a disc, it is most likely that these proteins have dimerised. In the case of the 220 kDa disc, this could be either two dimers in the same disc, or a tetramer. Tetrameric ZipA has not been reported and there is no evidence of binding interfaces for a tetrameric association, however the data is inconclusive.

Finally, these methods were applied to FtsB/FtsL-SMALPs. BN-PAGE analysis of the SEC elution fractions had predicted the presence of dimers and tetramers, and this was corroborated by AUC analysis. These results are in line with the predictions made by Villanelo *et al.* (2011). Previous AUC analysis by Glas *et al.* (2015) only found evidence for dimerisation of FtsB/FtsL,

therefore these results demonstrate that SMALP solubilisation allowed for the purification of a range of quaternary structures which are not found when the periplasmic regions are studied in isolation.

CHAPTER 7: SUMMARY

"Le rêve d'une bactérie doit devenir deux bactéries"

(The dream of a bacterium is to become two bacteria)

François Jacob, 1965

The proteins of the *E. coli* divisome are essential for bacterial viability, and have attracted increasing interest as potential targets for new antibiotics. While some divisomal proteins such as FtsZ have been studied in great detail, the structure and function of many of the components are yet to be fully elucidated. The FtsB/FtsL/FtsQ complex has been postulated to perform a central role in modulating the onset of constriction, inhibiting the activity of PBPs until the rise in FtsN levels signals the completion of divisome assembly, however very little is known about the structure and activity of the complex. A major hurdle faced by previous studies of this complex has been the solubilisation of FtsB/FtsL/FtsQ from the *E. coli* membrane. The development of the use of styrene-maleic acid (SMA) as a solubilisation technique over the past decade offers an alternative strategy for the solubilisation of the FtsB/FtsL/FtsQ complex. The aim of this study was to investigate the potential utility of SMA in the characterisation of this complex, and the following sections are a summary of the key findings.

7.1 Styrene-maleic acid successfully solubilised the components of the FtsBLQ subcomplex

Chapter 3 investigated the use of SMA to solubilise the individual components of the FtsB/FtsL/FtsQ complex. This "bottom-up" approach was chosen because understanding each

of the components in isolation would simplify data analysis, and allow for the complex to be pieced together in a well-defined manner. After cloning and expression trials, each of the three proteins was successfully solubilised from the *E. coli* membrane using SMA. Significant challenges were faced in purifying the target SMALPs away from contaminants, as the presence of the SMALP disc appeared to interfere with the efficient binding of the His-Tag of each protein to Ni-NTA resin. This limited the amount of protein yielded from each purification. It was predicted that this may be due to the short length of the protein compared to the large volume of the SMALP disc, therefore future studies may benefit from employing linkers to increase the distance of the affinity tag from the disc. Despite these challenges, this chapter demonstrated the first use of SMA to solubilise full-length FtsB/FtsL/FtsQ, and additionally identified a possible binding partner, CGG synthase, that has not been previously identified.

7.2 Full-length components of the FtsBLQ complex were characterised in SMALPs

Chapter 4 focused on the characterisation of the individual FtsB, FtsL, and FtsQ proteins in SMALPs. Circular dichroism analysis demonstrated that these proteins are folded within SMALPs, and that they demonstrate improved thermal stability compared to other solubilisation methods. Due to the aforementioned difficulties in purifying high yields of protein, the range of techniques available for further characterisation were limited. However, native-PAGE allows for the measurement of protein quaternary structure using a very small

amount of sample, and has recently been shown to be compatible with SMALPs. This method was applied to FtsB-, FtsL- and FtsQ-SMALPs and results showed that multiple quaternary structures for each protein could be identified. These findings give clarity to the debate surrounding whether FtsB, FtsL and FtsQ self-associate, and do so in the context of the proteins surrounded by the native lipid environment. It was also shown that the lipids surrounding FtsB within SMALPs can be successfully extracted and analysed by thin layer chromatography. To date, no studies have been conducted on the specific lipid environment of the FtsB/FtsL/FtsQ complex despite evidence that divisomal proteins can display specific lipid preferences. Therefore, future studies could build off of the SMALP mass-spectroscopy work of Teo *et al.* (2019) to further develop this technique and fully assess the lipid composition of FtsB/FtsL/FtsQ SMALPs.

7.3 The FtsBL subcomplex within SMALPs was determined to be tetrameric

The aim of chapter 5 was to investigate whether SMA can also solubilise hetero-complexes. These experiments focused on the FtsB/FtsL subcomplex, as these proteins have been shown to associate in the absence of FtsQ. SMA successfully solubilised co-expressed FtsB and FtsL, and further analysis demonstrated that these proteins co-purified. Using native-PAGE, the quaternary structure of the FtsB/FtsL complexes were investigated, which suggested the presence of an FtsB/FtsL tetramer. Whether these proteins form a tetrameric structure had been debated in the literature, therefore these techniques added to the data supporting a 2:2 oligomerisation state. Further structural analysis was attempted using small angle X-ray scattering, however, the low protein yield and increased complexity of SMALPs made the

refinement of a low resolution model unattainable. Due to time limitations of the project, the FtsB/FtsL/FtsQ complex was not characterised, however, the technique presented here outlines a framework for studying complexes within SMALPs, and therefore this could be extended to the FtsB/FtsL/FtsQ complex in future work.

7.4 The partial specific volume of SMALPs was successfully determined using differential sedimentation

Finally, chapter 6 focussed on the application of analytical ultracentrifugation as technique for the determination of SMALP molecular weight. To date, there have been no in-depth studies of SMALPs by AUC, and there has been no published figure for the partial specific volume of SMALPs. Differential sedimentation was applied to a range of samples, and this allowed for the determination of a partial specific volume for lipid-only SMALPs. The analysis of SMA-solubilised proteins was more complex, and the partial specific volume was significantly different to that of lipid-only SMALPs, suggesting that the lipid disc is not the main factor in the sedimentation of these samples. However, this initial study has added a significant amount of data to the current knowledge surrounding SMALPs and AUC, and future studies can apply these methods to a wider range of samples for a more accurate picture of how to analyse SMALP AUC data.

7.5 Conclusions

In conclusion, this study has shown that SMA allows for the solubilisation of membrane proteins that are full-length, supported by the local lipid environment and does not require the use of any detergents. This has been demonstrated to improve the thermal stability of the proteins and produces a wide range of quaternary structures within the SMALP disc. However, SMA solubilisation adds an extra layer of complexity to protein purification and downstream analysis. The presence of an approximately 135 kDa disc of lipid and polymer, which has been shown to be rapidly exchange lipid with the aqueous environment, has implications for structural studies, especially when considering low molecular weight proteins that are a fraction of the size of the disc. Therefore, further work to define the assembly and structure of SMALPs would allow more accurate analysis of SMA solubilisation proteins.

CHAPTER 8: SUPPLEMENTARY FIGURES

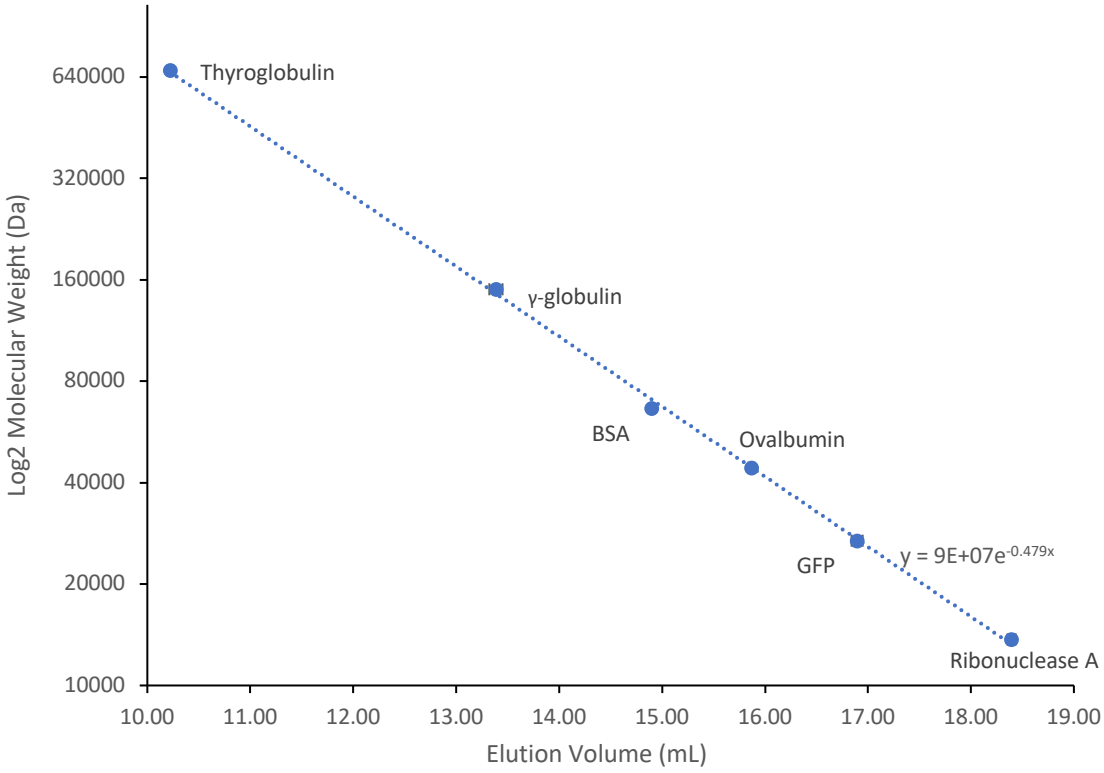

Figure 8.1 **Superdex® 200 Increase 10/300 Calibration Curve**.
A commercial protein standard mix was injected onto a Superdex 200 Increase 10/300 GL column. The column was run at 0.5 mL/min for 25 mL and the elution of protein from the column was monitored by absorbance at 280nm. 1 mg/mL bovine serum albumin and 1 mg/mL green fluorescent were similarly analysed. Each sample was individually prepared and analysed three times, and the results were plotted on a scatter graph using Microsoft Excel. An exponential trend line was fitted to the data and the equation of this line is shown.

CHAPTER 9: REFERENCES

ADAM, M., FRAIPONT, C., RHAZI, N., NGUYEN-DISTÈCHE, M., LAKAYE, B., FRÈRE, J. M., DEVREESE, B., VAN BEEUMEN, J., VAN HEIJENOORT, Y., VAN HEIJENOORT, J. AND GHUYSEN, J. M. (1997) 'The bimodular G57-V577 polypeptide chain of the class B penicillin-binding protein 3 of Escherichia coli catalyzes peptide bond formation from thiolesters and does not catalyze glycan chain polymerization from the lipid II intermediate.', *Journal of Bacteriology*, 179(19), pp. 6005–6009. doi: 10.1128/jb.179.19.6005-6009.1997.
ADDINALL, S. G., CAO, C. AND LUTKENHAUS, J. (1997) 'FtsN, a late recruit to the septum in Escherichia coli', *Molecular Microbiology*, 25(02), pp. 303–309. doi: 10.1046/j.1365-2958.1997.4641833.x.
ADDINALL, S. G. AND LUTKENHAUS, J. (1996) 'FtsA is localized to the septum in an FtsZ-dependent manner.', *Journal of Bacteriology*, 178(24), pp. 7167–7172. doi: 10.1128/jb.178.24.7167-7172.1996.
ANDERSSON, K. M. AND HOVMÖLLER, S. (1998) 'The average atomic volume and density of proteins', *Zeitschrift für Kristallographie - Crystalline Materials*, 213(7–8). doi: 10.1524/zkri.1998.213.7-8.369.
ARENDS, S. J. R., KUSTUSCH, R. J. AND WEISS, D. S. (2009) 'ATP-Binding Site Lesions in FtsE Impair Cell Division', *Journal of Bacteriology*, 191(12), pp. 3772–3784. doi: 10.1128/JB.00179-09.
BAAS, B. J., DENISOV, I. G. AND SLIGAR, S. G. (2004) 'Homotropic cooperativity of monomeric cytochrome P450 3A4 in a nanoscale native bilayer environment.', *Archives of biochemistry and biophysics*. United States, 430(2), pp. 218–28. doi: 10.1016/j.abb.2004.07.003.
BAI, Y., ENGLANDER, J. J., MAYNE, L., MILNE, J. S. AND ENGLANDER, S. W. B. T.-M. IN E. (1995) 'Thermodynamic parameters from hydrogen exchange measurements', in *Energetics of Biological Macromolecules*. Academic Press, pp. 344–356. doi: https://doi.org/10.1016/0076-6879(95)59051-X.
BAKER, T. A. AND BELL, S. P. (1998) 'Polymerases and the Replisome: Machines within Machines', *Cell*, 92(3), pp. 295–305. doi: 10.1016/S0092-8674(00)80923-X.
BATES, D. AND KLECKNER, N. (2005) 'Chromosome and Replisome Dynamics in E. coli: Loss of Sister Cohesion Triggers Global Chromosome Movement and Mediates Chromosome Segregation', *Cell*, 121(6), pp. 899–911. doi: 10.1016/j.cell.2005.04.013.
BAYBURT, T. H., GRINKOVA, Y. V. AND SLIGAR, S. G. (2006) 'Assembly of single bacteriorhodopsin trimers in bilayer nanodiscs', *Archives of Biochemistry and Biophysics*, 450(2), pp. 215–222. doi: 10.1016/j.abb.2006.03.013.
BAYBURT, T. H., GRINKOVA, Y. V AND SLIGAR, S. G. (2002) 'Self-Assembly of Discoidal Phospholipid Bilayer Nanoparticles with Membrane Scaffold Proteins', *Nano Letters*. American Chemical Society, 2(8), pp. 853–856. doi: 10.1021/nl025623k.
VAN DEN BERG VAN SAPAROEA, H. B., GLAS, M., VERNOOIJ, I. G. W. H., BITTER, W., DEN BLAAUWEN, T. AND LUIRINK, J. (2013) 'Fine-mapping the Contact Sites of the Escherichia coli Cell Division Proteins FtsB and FtsL on the FtsQ Protein', *Journal of Biological Chemistry*, 288(34), pp. 24340–24350. doi: 10.1074/jbc.M113.485888.
BERNHARDT, T. G. AND DE BOER, P. A. J. (2005) 'SlmA, a Nucleoid-Associated, FtsZ Binding Protein Required for Blocking Septal Ring Assembly over Chromosomes in E. coli', *Molecular Cell*, 18(5), pp. 555–564. doi: 10.1016/j.molcel.2005.04.012.
DE BOER, P. A. J., CROSSLEY, R. E. AND ROTHFIELD, L. I. (1989) 'A division inhibitor and a topological specificity factor coded for by the minicell locus determine proper placement of the division

septum in E. coli', *Cell*, 56(4), pp. 641–649. doi: 10.1016/0092-8674(89)90586-2.
BOES, A., OLATUNJI, S., BREUKINK, E. AND TERRAK, M. (2019) 'Regulation of the Peptidoglycan Polymerase Activity of PBP1b by Antagonist Actions of the Core Divisome Proteins FtsBLQ and FtsN', *mBio*. Edited by T. den Blaauwen and N. R. Salama, 10(1). doi: 10.1128/mBio.01912-18.
BOTTA, G. A. AND PARK, J. T. (1981) 'Evidence for involvement of penicillin-binding protein 3 in murein synthesis during septation but not during cell elongation', *Journal of Bacteriology*.
BOUHSS, A., TRUNKFIELD, A. E., BUGG, T. D. H. AND MENGIN-LECREULX, D. (2008) 'The biosynthesis of peptidoglycan lipid-linked intermediates', *FEMS Microbiology Reviews*, 32(2), pp. 208–233. doi: 10.1111/j.1574-6976.2007.00089.x.
BOWIE, J. U. (2011) 'Membrane protein folding: How important are hydrogen bonds?', *Current Opinion in Structural Biology*. doi: 10.1016/j.sbi.2010.10.003.
BRAMHILL, D. AND KORNBERG, A. (1988) 'Duplex opening by dnaA protein at novel sequences in initiation of replication at the origin of the E. coli chromosome', *Cell*, 52(5), pp. 743–755. doi: 10.1016/0092-8674(88)90412-6.
BRAMKAMP, M., WESTON, L., DANIEL, R. A. AND ERRINGTON, J. (2006) 'Regulated intramembrane proteolysis of FtsL protein and the control of cell division in Bacillus subtilis', *Molecular Microbiology*, 62(2), pp. 580–591. doi: 10.1111/j.1365-2958.2006.05402.x.
BREYTON, C., TRIBET, C., OLIVE, J., DUBACQ, J.-P. AND POPOT, J.-L. (1997) 'Dimer to Monomer Conversion of the Cytochrome b 6 f Complex', *Journal of Biological Chemistry*, 272(35), pp. 21892–21900. doi: 10.1074/jbc.272.35.21892.
BROECKER, J., EGER, B. T. AND ERNST, O. P. (2017) 'Crystallogenesis of Membrane Proteins Mediated by Polymer-Bounded Lipid Nanodiscs', *Structure*, 25(2), pp. 384–392. doi: 10.1016/j.str.2016.12.004.
BROWN, P. H., BALBO, A., ZHAO, H., EBEL, C. AND SCHUCK, P. (2011) 'Density Contrast Sedimentation Velocity for the Determination of Protein Partial-Specific Volumes', *PLoS ONE*. Edited by V. N. Uversky, 6(10), p. e26221. doi: 10.1371/journal.pone.0026221.
BUDDELMEIJER, N. AND BECKWITH, J. (2002) 'Assembly of cell division proteins at the E. coli cell center', *Current Opinion in Microbiology*, 5(6), pp. 553–557. doi: 10.1016/S1369-5274(02)00374-0.
BUDDELMEIJER, N. AND BECKWITH, J. (2004) 'A complex of the Escherichia coli cell division proteins FtsL, FtsB and FtsQ forms independently of its localization to the septal region', *Molecular Microbiology*. Blackwell Science Ltd, 52(5), pp. 1315–1327. doi: 10.1111/j.1365-2958.2004.04044.x.
BUDDELMEIJER, N., JUDSON, N., BOYD, D., MEKALANOS, J. J. AND BECKWITH, J. (2002) 'YgbQ, a cell division protein in Escherichia coli and Vibrio cholerae, localizes in codependent fashion with FtsL to the division site', *Proceedings of the National Academy of Sciences*. The National Academy of Sciences, 99(9), pp. 6316–6321. doi: 10.1073/pnas.092128499.
BUSIEK, K. K., ERASO, J. M., WANG, Y. AND MARGOLIN, W. (2012) 'The Early Divisome Protein FtsA Interacts Directly through Its 1c Subdomain with the Cytoplasmic Domain of the Late Divisome Protein FtsN', *Journal of Bacteriology*, 194(8), pp. 1989–2000. doi: 10.1128/JB.06683-11.
CHAE, P. S. *ET AL.* (2010) 'Maltose-neopentyl glycol (MNG) amphiphiles for solubilization, stabilization and crystallization of membrane proteins', *Nature Methods*. doi:

10.1038/nmeth.1526.
CHAE, P. S., CHO, K. H., WANDER, M. J., BAE, H. E., GELLMAN, S. H. AND LAIBLE, P. D. (2014) 'Hydrophobic variants of ganglio-tripod amphiphiles for membrane protein manipulation', *Biochimica et Biophysica Acta - Biomembranes*. doi: 10.1016/j.bbamem.2013.09.011.
CHAE, P. S., RANA, R. R., GOTFRYD, K., RASMUSSEN, S. G. F., KRUSE, A. C., CHO, K. H., CAPALDI, S., KOBILKA, B., LOLAND, C. J., GETHER, U., BANERJEE, S., BYRNE, B., LEE, J. K. AND GELLMAN, S. H. (2013) 'Glucose-Neopentyl Glycol (GNG) amphiphiles for membrane protein study', *Chemical Communications*. doi: 10.1039/c2cc36844g.
CHAE, P. S., WANDER, M. J., BOWLING, A. P., LAIBLE, P. D. AND GELLMAN, S. H. (2008) 'Glycotripod amphiphiles for solubilization and stabilization of a membrane-protein superassembly: Importance of branching in the hydrophilic portion', *ChemBioChem*. doi: 10.1002/cbic.200800169.
CHARLTON, J. (2016) *Solubilisation and characterisation of G-protein-coupled receptors using styrene maleic acid polymer*. University of Birmingham. Available at: http://etheses.bham.ac.uk//id/eprint/6525/.
CHEN, G. C. AND YANG, J. T. (1977) 'Two-Point Calibration of Circular Dichrometer with d-10-Camphorsulfonic Acid', *Analytical Letters*, 10(14), pp. 1195–1207. doi: 10.1080/00032717708067855.
CHEN, J. C. AND BECKWITH, J. (2001) 'FtsQ, FtsL and FtsI require FtsK, but not FtsN, for co-localization with FtsZ during Escherichia coli cell division.', *Molecular microbiology*. England, 42(2), pp. 395–413. Available at: http://www.ncbi.nlm.nih.gov/pubmed/11703663.
CHEN, X., ZARO, J. L. AND SHEN, W. C. (2013) 'Fusion protein linkers: Property, design and functionality', *Advanced Drug Delivery Reviews*. doi: 10.1016/j.addr.2012.09.039.
CHOI, Y., KIM, J., YOON, H.-J., JIN, K. S., RYU, S. AND LEE, H. H. (2018) 'Structural Insights into the FtsQ/FtsB/FtsL Complex, a Key Component of the Divisome', *Scientific Reports*, 8(1), p. 18061. doi: 10.1038/s41598-018-36001-2.
COLUMBUS, L., LIPFERT, J., JAMBUNATHAN, K., FOX, D. A., SIM, A. Y. L., DONIACH, S. AND LESLEY, S. A. (2009) 'Mixing and matching detergents for membrane protein NMR structure determination', *Journal of the American Chemical Society*. doi: 10.1021/ja808776j.
CONDON, S. G. F., MAHBUBA, D.-A., ARMSTRONG, C. R., DIAZ-VAZQUEZ, G., CRAVEN, S. J., LAPOINTE, L. M., KHADRIA, A. S., CHADDA, R., CROOKS, J. A., RANGARAJAN, N., WEIBEL, D. B., HOSKINS, A. A., ROBERTSON, J. L., CUI, Q. AND SENES, A. (2018) 'The FtsLB subcomplex of the bacterial divisome is a tetramer with an uninterrupted FtsL helix linking the transmembrane and periplasmic regions.', *The Journal of biological chemistry*, 293(5), pp. 1623–1641. doi: 10.1074/jbc.RA117.000426.
COOPER, S. AND HELMSTETTER, C. E. (1968) 'Chromosome replication and the division cycle of Escherichia coli', *Journal of Molecular Biology*, 31(3), pp. 519–540. doi: 10.1016/0022-2836(68)90425-7.
CORBIN, B. D. (2002) 'Exploring intracellular space: function of the Min system in round-shaped Escherichia coli', *The EMBO Journal*, 21(8), pp. 1998–2008. doi: 10.1093/emboj/21.8.1998.
D'ULISSE, V., FAGIOLI, M., GHELARDINI, P. AND PAOLOZZI, L. (2007) 'Three functional subdomains of the Escherichia coli FtsQ protein are involved in its interaction with the other division proteins', *Microbiology*, 153(1), pp. 124–138. doi: 10.1099/mic.0.2006/000265-0.

DAJKOVIC, A., PICHOFF, S., LUTKENHAUS, J. AND WIRTZ, D. (2010) 'Cross-linking FtsZ polymers into coherent Z rings', *Molecular Microbiology*, 78(3), pp. 651–668. doi: 10.1111/j.1365-2958.2010.07352.x.
DANILOVA, O., REYES-LAMOTHE, R., PINSKAYA, M., SHERRATT, D. AND POSSOZ, C. (2007) 'MukB colocalizes with the oriC region and is required for organization of the two Escherichia coli chromosome arms into separate cell halves', *Molecular Microbiology*, 65(6), pp. 1485–1492. doi: 10.1111/j.1365-2958.2007.05881.x.
DIAGNE, C. T., SALHI, M., CROZAT, E., SALOMÉ, L., CORNET, F., ROUSSEAU, P. AND TARDIN, C. (2014) 'TPM analyses reveal that FtsK contributes both to the assembly and the activation of the XerCD-dif recombination synapse', *Nucleic Acids Research*, 42(3), pp. 1721–1732. doi: 10.1093/nar/gkt1024.
DONACHIE, W. D. (1968) 'Relationship between Cell Size and Time of Initiation of DNA Replication', *Nature*, 219(5158), pp. 1077–1079. doi: 10.1038/2191077a0.
DÖRR, J. M., KOORENGEVEL, M. C., SCHÄFER, M., PROKOFYEV, A. V, SCHEIDELAAR, S., VAN DER CRUIJSEN, E. A. W., DAFFORN, T. R., BALDUS, M. AND KILLIAN, J. A. (2014) 'Detergent-free isolation, characterization, and functional reconstitution of a tetrameric K + channel: The power of native nanodiscs', *Proceedings of the National Academy of Sciences*, 111(52), pp. 18607–18612. doi: 10.1073/pnas.1416205112.
DRAPER, G. C., MCLENNAN, N., BEGG, K., MASTERS, M. AND DONACHIE, W. D. (1998) 'Only the N-terminal domain of FtsK functions in cell division', *Journal of Bacteriology*.
DU, S., HENKE, W., PICHOFF, S. AND LUTKENHAUS, J. (2019) 'How FtsEX localizes to the Z ring and interacts with FtsA to regulate cell division', *Molecular Microbiology*. doi: 10.1111/mmi.14324.
DU, S. AND LUTKENHAUS, J. (2014) 'SlmA Antagonism of FtsZ Assembly Employs a Two-pronged Mechanism like MinCD', *PLoS Genetics*. Edited by L. Søgaard-Andersen, 10(7), p. e1004460. doi: 10.1371/journal.pgen.1004460.
DU, S., PICHOFF, S. AND LUTKENHAUS, J. (2016) 'FtsEX acts on FtsA to regulate divisome assembly and activity', *Proceedings of the National Academy of Sciences*, 113(34), pp. E5052–E5061. doi: 10.1073/pnas.1606656113.
DUBARRY, N., POSSOZ, C. AND BARRE, F.-X. (2010) 'Multiple regions along the Escherichia coli FtsK protein are implicated in cell division', *Molecular Microbiology*, 78(5), pp. 1088–1100. doi: 10.1111/j.1365-2958.2010.07412.x.
EHSAN, M., GHANI, L., DU, Y., HARIHARAN, P., MORTENSEN, J. S., RIBEIRO, O., HU, H., SKINIOTIS, G., LOLAND, C. J., GUAN, L., KOBILKA, B. K., BYRNE, B. AND CHAE, P. S. (2017) 'New penta-saccharide-bearing tripod amphiphiles for membrane protein structure studies', *Analyst*. doi: 10.1039/c7an01168g.
VAN DEN ENT, F., VINKENVLEUGEL, T. M. F., IND, A., WEST, P., VEPRINTSEV, D., NANNINGA, N., DEN BLAAUWEN, T. AND LÖWE, J. (2008) 'Structural and mutational analysis of the cell division protein FtsQ', *Molecular Microbiology*, 68(1), pp. 110–123. doi: 10.1111/j.1365-2958.2008.06141.x.
ERICKSON, H. P. AND OSAWA, M. (2017) 'FtsZ Constriction Force – Curved Protofilaments Bending Membranes', in, pp. 139–160. doi: 10.1007/978-3-319-53047-5_5.
FLETCHER, J. M., BARTLETT, G. J., BOYLE, A. L., DANON, J. J., RUSH, L. E., LUPAS, A. N. AND WOOLFSON, D. N. (2017) 'N@ a and N@ d : Oligomer and Partner Specification by Asparagine in Coiled-Coil

Interfaces', *ACS Chemical Biology*, 12(2), pp. 528–538. doi: 10.1021/acschembio.6b00935.
FOTIADIS, D., HARDER, D. AND FOTIADIS, D. (2012) 'Preparation of detergent-solubilized membranes from Escherichia coli', *Protocol Exchange*. doi: 10.1038/protex.2012.033.
FRANKE, D. AND SVERGUN, D. I. (2009) 'DAMMIF , a program for rapid ab-initio shape determination in small-angle scattering', *Journal of Applied Crystallography*, 42(2), pp. 342–346. doi: 10.1107/S0021889809000338.
GAUTHIER, M. (1995) *Engineered Materials Handbook, Desk Edition*. 1st edn, *ASM International*. 1st edn.
GE HEALTHCARE (2018) *Superdex 200 Increase 3.2/300*. Available at: https://cdn.gelifesciences.com/dmm3bwsv3/AssetStream.aspx?mediaformatid=10061&destinationid=10016&assetid=16444 (Accessed: 20 March 2019).
GERDING, M. A., LIU, B., BENDEZU, F. O., HALE, C. A., BERNHARDT, T. G. AND DE BOER, P. A. J. (2009) 'Self-Enhanced Accumulation of FtsN at Division Sites and Roles for Other Proteins with a SPOR Domain (DamX, DedD, and RlpA) in Escherichia coli Cell Constriction', *Journal of Bacteriology*, 191(24), pp. 7383–7401. doi: 10.1128/JB.00811-09.
GLAS, M., AB, E., HOLLANDER, J., SIEGAL, G., LUIRINK, J. AND DE ESCH, I. (2019) 'Interrogating the Essential Bacterial Cell Division Protein FtsQ with Fragments Using Target Immobilized NMR Screening (TINS)', *International Journal of Molecular Sciences*. doi: 10.3390/ijms20153684.
GLAS, M., VAN DEN BERG VAN SAPAROEA, H. B., MCLAUGHLIN, S. H., ROSEBOOM, W., LIU, F., KONINGSTEIN, G. M., FISH, A., DEN BLAAUWEN, T., HECK, A. J. R., DE JONG, L., BITTER, W., DE ESCH, I. J. P. AND LUIRINK, J. (2015) 'The Soluble Periplasmic Domains of Escherichia coli Cell Division Proteins FtsQ/FtsB/FtsL Form a Trimeric Complex with Submicromolar Affinity', *Journal of Biological Chemistry*. 11200 Rockville Pike, Suite 302, Rockville, MD 20852-3110, U.S.A.: American Society for Biochemistry and Molecular Biology, 290(35), pp. 21498–21509. doi: 10.1074/jbc.M115.654756.
GOEHRING, N. W., GONZALEZ, M. D. AND BECKWITH, J. (2006) 'Premature targeting of cell division proteins to midcell reveals hierarchies of protein interactions involved in divisome assembly', *Molecular Microbiology*, 61(1), pp. 33–45. doi: 10.1111/j.1365-2958.2006.05206.x.
GONZALEZ, M. D., AKBAY, E. A., BOYD, D. AND BECKWITH, J. (2010) 'Multiple Interaction Domains in FtsL, a Protein Component of the Widely Conserved Bacterial FtsLBQ Cell Division Complex', *Journal of Bacteriology*, 192(11), pp. 2757–2768. doi: 10.1128/JB.01609-09.
GONZALEZ, M. D. AND BECKWITH, J. (2009) 'Divisome under Construction: Distinct Domains of the Small Membrane Protein FtsB Are Necessary for Interaction with Multiple Cell Division Proteins', *Journal of Bacteriology*. American Society for Microbiology (ASM), 191(8), pp. 2815–2825. doi: 10.1128/JB.01597-08.
GRAHAM, J. E., SIVANATHAN, V., SHERRATT, D. J. AND ARCISZEWSKA, L. K. (2010) 'FtsK translocation on DNA stops at XerCD-dif', *Nucleic Acids Research*, 38(1), pp. 72–81. doi: 10.1093/nar/gkp843.
GRAINGE, I., LESTERLIN, C. AND SHERRATT, D. J. (2011) 'Activation of XerCD-dif recombination by the FtsK DNA translocase', *Nucleic Acids Research*, 39(12), pp. 5140–5148. doi: 10.1093/nar/gkr078.
GRENGA, L., LUZI, G., PAOLOZZI, L. AND GHELARDINI, P. (2008) 'The Escherichia coli FtsK functional domains involved in its interaction with its divisome protein partners', *FEMS Microbiology Letters*. doi: 10.1111/j.1574-6968.2008.01317.x.

GULATI, S., JAMSHAD, M., KNOWLES, T. J., MORRISON, K. A., DOWNING, R., CANT, N., COLLINS, R., KOENDERINK, J. B., FORD, R. C., OVERDUIN, M., KERR, I. D., DAFFORN, T. R. AND ROTHNIE, A. J. (2014) 'Detergent-free purification of ABC (ATP-binding-cassette) transporters', *Biochemical Journal*. England, 461(2), pp. 269–278. doi: 10.1042/BJ20131477.
HALE, C. A., RHEE, A. C. AND DE BOER, P. A. J. (2000) 'ZipA-Induced Bundling of FtsZ Polymers Mediated by an Interaction between C-Terminal Domains', *Journal of Bacteriology*, 182(18), pp. 5153–5166. doi: 10.1128/JB.182.18.5153-5166.2000.
HALL, S. C. L., TOGNOLONI, C., CHARLTON, J., BRAGGINTON, É. C., ROTHNIE, A. J., SRIDHAR, P., WHEATLEY, M., KNOWLES, T. J., ARNOLD, T., EDLER, K. J. AND DAFFORN, T. R. (2018) 'An acid-compatible co-polymer for the solubilization of membranes and proteins into lipid bilayer-containing nanoparticles', *Nanoscale*, 10(22), pp. 10609–10619. doi: 10.1039/C8NR01322E.
HANEY, S. A., GLASFELD, E., HALE, C., KEENEY, D., HE, Z. AND DE BOER, P. (2001) 'Genetic Analysis of the Escherichia coli FtsZ·ZipA Interaction in the Yeast Two-hybrid System', *Journal of Biological Chemistry*, 276(15), pp. 11980–11987. doi: 10.1074/jbc.M009810200.
HAZELL, G., ARNOLD, T., BARKER, R. D., CLIFTON, L. A., STEINKE, N. J., TOGNOLONI, C. AND EDLER, K. J. (2016) 'Evidence of Lipid Exchange in Styrene Maleic Acid Lipid Particle (SMALP) Nanodisc Systems', *Langmuir*. doi: 10.1021/acs.langmuir.6b02927.
HEIDRICH, C., URSINUS, A., BERGER, J., SCHWARZ, H. AND HÖLTJE, J. V. (2002) 'Effects of multiple deletions of murein hydrolases on viability, septum cleavage, and sensitivity to large toxic molecules in Escherichia coli', *Journal of Bacteriology*. doi: 10.1128/JB.184.22.6093-6099.2002.
HILL, N. S., KADOYA, R., CHATTORAJ, D. K. AND LEVIN, P. A. (2012) 'Cell Size and the Initiation of DNA Replication in Bacteria', *PLoS Genetics*. Edited by W. F. Burkholder, 8(3), p. e1002549. doi: 10.1371/journal.pgen.1002549.
HILL, T. M., HENSON, J. M. AND KUEMPEL, P. L. (1987) 'The terminus region of the Escherichia coli chromosome contains two separate loci that exhibit polar inhibition of replication.', *Proceedings of the National Academy of Sciences*, 84(7), pp. 1754–1758. doi: 10.1073/pnas.84.7.1754.
HITSCHERICH, C., ALLAMAN, M., WIENCEK, J., KAPLAN, J. AND LOLL, P. J. (2000) 'Static light scattering studies of OmpF porin: Implications for integral membrane protein crystallization', *Protein Science*. doi: 10.1110/ps.9.8.1559.
HU, Z., GOGOL, E. P. AND LUTKENHAUS, J. (2002) 'Dynamic assembly of MinD on phospholipid vesicles regulated by ATP and MinE', *Proceedings of the National Academy of Sciences*, 99(10), pp. 6761–6766. doi: 10.1073/pnas.102059099.
HU, Z., SAEZ, C. AND LUTKENHAUS, J. (2003) 'Recruitment of MinC, an inhibitor of Z-ring formation, to the membrane in Escherichia coli: Role of minD and minE', *Journal of Bacteriology*. doi: 10.1128/JB.185.1.196-203.2003.
HUGHES, G. W. *ET AL.* (2019) 'Evidence for phospholipid export from the bacterial inner membrane by the Mla ABC transport system', *Nature Microbiology*. doi: 10.1038/s41564-019-0481-y.
INAGAKI, S., GHIRLANDO, R. AND GRISSHAMMER, R. (2013) 'Biophysical characterization of membrane proteins in nanodiscs', *Methods*, 59(3), pp. 287–300. doi: 10.1016/j.ymeth.2012.11.006.
ISHIHARA, G., GOTO, M., SAEKI, M., ITO, K., HORI, T., KIGAWA, T., SHIROUZU, M. AND YOKOYAMA, S.

(2005) ‘Expression of G protein coupled receptors in a cell-free translational system using detergents and thioredoxin-fusion vectors’, *Protein Expression and Purification*. doi: 10.1016/j.pep.2005.01.013.
JACOB, F., BRENNER, S. AND CUZIN, F. (1963) ‘On the Regulation of DNA Replication in Bacteria’, *Cold Spring Harbor Symposia on Quantitative Biology*, 28, pp. 329–348. doi: 10.1101/SQB.1963.028.01.048.
JAMSHAD, M., CHARLTON, J., LIN, Y.-P., ROUTLEDGE, S. J., BAWA, Z., KNOWLES, T. J., OVERDUIN, M., DEKKER, N., DAFFORN, T. R., BILL, R. M., POYNER, D. R. AND WHEATLEY, M. (2015) ‘G-protein coupled receptor solubilization and purification for biophysical analysis and functional studies, in the total absence of detergent.’, *Bioscience reports*, 35(2), pp. 1–10. doi: 10.1042/BSR20140171.
JAMSHAD, M., GRIMARD, V., IDINI, I., KNOWLES, T. J., DOWLE, M. R., SCHOFIELD, N., SRIDHAR, P., LIN, Y., FINKA, R., WHEATLEY, M., THOMAS, O. R. T., PALMER, R. E., OVERDUIN, M., GOVAERTS, C., RUYSSCHAERT, J.-M., EDLER, K. J. AND DAFFORN, T. R. (2015) ‘Structural analysis of a nanoparticle containing a lipid bilayer used for detergent-free extraction of membrane proteins’, *Nano Research*, 8(3), pp. 774–789. doi: 10.1007/s12274-014-0560-6.
JOSHI, M. C., BOURNIQUEL, A., FISHER, J., HO, B. T., MAGNAN, D., KLECKNER, N. AND BATES, D. (2011) ‘Escherichia coli sister chromosome separation includes an abrupt global transition with concomitant release of late-splitting intersister snaps’, *Proceedings of the National Academy of Sciences*, 108(7), pp. 2765–2770. doi: 10.1073/pnas.1019593108.
JOSHI, M. C., MAGNAN, D., MONTMINY, T. P., LIES, M., STEPANKIW, N. AND BATES, D. (2013) ‘Regulation of Sister Chromosome Cohesion by the Replication Fork Tracking Protein SeqA’, *PLoS Genetics*. Edited by W. F. Burkholder, 9(8), p. e1003673. doi: 10.1371/journal.pgen.1003673.
JUN, S. AND MULDER, B. (2006) ‘Entropy-driven spatial organization of highly confined polymers: Lessons for the bacterial chromosome’, *Proceedings of the National Academy of Sciences*, 103(33), pp. 12388–12393. doi: 10.1073/pnas.0605305103.
KALMBACH, R., CHIZHOV, I., SCHUMACHER, M. C., FRIEDRICH, T., BAMBERG, E. AND ENGELHARD, M. (2007) ‘Functional Cell-free Synthesis of a Seven Helix Membrane Protein: In situ Insertion of Bacteriorhodopsin into Liposomes’, *Journal of Molecular Biology*. doi: 10.1016/j.jmb.2007.05.087.
KHADRIA, A. S. AND SENES, A. (2013) ‘The Transmembrane Domains of the Bacterial Cell Division Proteins FtsB and FtsL Form a Stable High-Order Oligomer’, *Biochemistry*, 52(43), pp. 7542–7550. doi: 10.1021/bi4009837.
KIELEC, J. M., VALENTINE, K. G. AND WAND, A. J. (2010) ‘A method for solution NMR structural studies of large integral membrane proteins: Reverse micelle encapsulation’, *Biochimica et Biophysica Acta - Biomembranes*. doi: 10.1016/j.bbamem.2009.07.027.
KIKHNEY, A. G. AND SVERGUN, D. I. (2015) ‘A practical guide to small angle X-ray scattering (SAXS) of flexible and intrinsically disordered proteins’, *FEBS Letters*. doi: 10.1016/j.febslet.2015.08.027.
KLAMMT, C., LÖHR, F., SCHÄFER, B., HAASE, W., DÖTSCH, V., RÜTERJANS, H., GLAUBITZ, C. AND BERNHARD, F. (2004) ‘High level cell-free expression and specific labeling of integral membrane proteins’, *European Journal of Biochemistry*. doi: 10.1111/j.1432-1033.2003.03959.x.
KNOWLES, T. J., FINKA, R., SMITH, C., LIN, Y.-P., DAFFORN, T. AND OVERDUIN, M. (2009) ‘Membrane Proteins Solubilized Intact in Lipid Containing Nanoparticles Bounded by Styrene Maleic Acid

Copolymer', *Journal of the American Chemical Society*, 131(22), pp. 7484–7485. doi: 10.1021/ja810046q.
KOENIG, B. W. AND GAWRISCH, K. (2005) 'Specific volumes of unsaturated phosphatidylcholines in the liquid crystalline lamellar phase', *Biochimica et Biophysica Acta (BBA) - Biomembranes*, 1715(1), pp. 65–70. doi: 10.1016/j.bbamem.2005.07.006.
KOPPAKA, V., SILVESTRO, L., ENGLER, J. A., BROUILLETTE, C. G. AND AXELSEN, P. H. (1999) 'The structure of human lipoprotein A-I. Evidence for the "belt" model', *Journal of Biological Chemistry*. doi: 10.1074/jbc.274.21.14541.
KRAFT, A. R., PRABHU, J., URSINUS, A. AND HÖLTJE, J. V. (1999) 'Interference with murein turnover has no effect on growth but reduces beta-lactamase induction in Escherichia coli.', *Journal of bacteriology*, 181(23), pp. 7192–8. Available at: http://www.ncbi.nlm.nih.gov/pubmed/10572120.
KRUPKA, M., SOBRINOS-SANGUINO, M., JIMÉNEZ, M., RIVAS, G. AND MARGOLIN, W. (2018) 'Escherichia coli ZipA Organizes FtsZ Polymers into Dynamic Ring-Like Protofilament Structures', *mBio*. Edited by R. Losick, 9(3). doi: 10.1128/mBio.01008-18.
KUREISAITE-CIZIENE, D., VARADAJAN, A., MCLAUGHLIN, S. H., GLAS, M., MONTÓN SILVA, A., LUIRINK, R., MUELLER, C., DEN BLAAUWEN, T., GROSSMANN, T. N., LUIRINK, J. AND LÖWE, J. (2018) 'Structural Analysis of the Interaction between the Bacterial Cell Division Proteins FtsQ and FtsB', *mBio*. Edited by J. Lutkenhaus and R. Losick, 9(5). doi: 10.1128/mBio.01346-18.
LALOUX, G. AND JACOBS-WAGNER, C. (2014) 'How do bacteria localize proteins to the cell pole?', *Journal of Cell Science*, 127(1), pp. 11–19. doi: 10.1242/jcs.138628.
LAPOINTE, L. M., TAYLOR, K. C., SUBRAMANIAM, S., KHADRIA, A., RAYMENT, I. AND SENES, A. (2013) 'Structural Organization of FtsB, a Transmembrane Protein of the Bacterial Divisome', *Biochemistry*, 52(15), pp. 2574–2585. doi: 10.1021/bi400222r.
LARENTIS, A. L., NICOLAU, J. F. M. Q., ESTEVES, G. D. S., VARESCHINI, D. T., DE ALMEIDA, F. V. R., DOS REIS, M. G., GALLER, R. AND MEDEIROS, M. A. (2014) 'Evaluation of pre-induction temperature, cell growth at induction and IPTG concentration on the expression of a leptospiral protein in E. coli using shaking flasks and microbioreactor', *BMC Research Notes*. doi: 10.1186/1756-0500-7-671.
LAUE, T. M., SHAH, B. D., RIDGEWAY, T. M. AND PELLETIER, S. L. (1992) 'Computer-aided interpretation of analytical sedimentation data for proteins', in Harding, S., Rowe, A., and Horton, J. C. (eds) *Analytical ultracentrifugation in biochemistry and polymer science*. Cambridge: The Royal Society of Chemistry, pp. 90–125. doi: 10.1016/0003-2670(95)90401-8.
LEE, A. G. (2004) 'How lipids affect the activities of integral membrane proteins', *Biochimica et Biophysica Acta - Biomembranes*. doi: 10.1016/j.bbamem.2004.05.012.
LEE, S. C., KNOWLES, T. J., POSTIS, V. L. G., JAMSHAD, M., PARSLOW, R. A., LIN, Y., GOLDMAN, A., SRIDHAR, P., OVERDUIN, M., MUENCH, S. P. AND DAFFORN, T. R. (2016) 'A method for detergent-free isolation of membrane proteins in their local lipid environment.', *Nature protocols*, 11(7), pp. 1149–62. doi: 10.1038/nprot.2016.070.
LEE, Y.-C. *ET AL.* (2018) 'Impact of Detergents on Membrane Protein Complex Isolation', *Journal of Proteome Research*, 17(1), pp. 348–358. doi: 10.1021/acs.jproteome.7b00599.
LEITZ, A. J., BAYBURT, T. H., BARNAKOV, A. N., SPRINGER, B. A. AND SLIGAR, S. G. (2006) 'Functional reconstitution of Beta2-adrenergic receptors utilizing self-assembling Nanodisc technology.',

BioTechniques. United States, 40(5), pp. 601–2, 604, 606, passim. doi: 10.2144/000112169.
LI, R. AND WOODWARD, C. (1999) 'The hydrogen exchange core and protein folding', *Protein Science*, 8(8), pp. 1571–1590. doi: 10.1110/ps.8.8.1571.
LIN, Y.-P. (2011) *Over-expression and Biophysical Characterisation of Membrane Proteins Solubilised in a Styrene Maleic Acid Polymer*. University of Birmingham.
LIU, B., PERSONS, L., LEE, L. AND DE BOER, P. A. J. (2015) 'Roles for both FtsA and the FtsBLQ subcomplex in FtsN-stimulated cell constriction in E scherichia coli', *Molecular Microbiology*, 95(6), pp. 945–970. doi: 10.1111/mmi.12906.
LIU, Z., MUKHERJEE, A. AND LUTKENHAUS, J. (1999) 'Recruitment of ZipA to the division site by interaction with FtsZ', *Molecular Microbiology*, 31(6), pp. 1853–1861. doi: 10.1046/j.1365-2958.1999.01322.x.
LOGEZ, C., DAMIAN, M., LEGROS, C., DUPRÉ, C., GUÉRY, M., MARY, S., WAGNER, R., M'KADMI, C., NOSJEAN, O., FOULD, B., MARIE, J., FEHRENTZ, J.-A., MARTINEZ, J., FERRY, G., BOUTIN, J. A. AND BANÈRES, J.-L. (2016) 'Detergent-free Isolation of Functional G Protein-Coupled Receptors into Nanometric Lipid Particles.', *Biochemistry*, 55(1), pp. 38–48. doi: 10.1021/acs.biochem.5b01040.
LOVERING, A. L., SAFADI, S. S. AND STRYNADKA, N. C. J. (2012) 'Structural Perspective of Peptidoglycan Biosynthesis and Assembly', *Annual Review of Biochemistry*, 81(1), pp. 451–478. doi: 10.1146/annurev-biochem-061809-112742.
LUND-KATZ, S. AND PHILLIPS, M. C. (2010) 'High Density Lipoprotein Structure-Function and Role in Reverse Cholesterol Transport', *Sub-Cellular Biochemistry*. doi: 10.1007/978-90-481-8622-8_7.
LUPAS, A., VAN DYKE, M. AND STOCK, J. (1991) 'Predicting coiled coils from protein sequences', *Science*, 252(5009), pp. 1162–1164. doi: 10.1126/science.252.5009.1162.
LE MAIRE, M., CHAMPEIL, P. AND MØLLER, J. V. (2000) 'Interaction of membrane proteins and lipids with solubilizing detergents', *Biochimica et Biophysica Acta - Biomembranes*. doi: 10.1016/S0304-4157(00)00010-1.
MALHOTRA, K. AND ALDER, N. N. (2014) 'Advances in the use of nanoscale bilayers to study membrane protein structure and function', *Biotechnology and Genetic Engineering Reviews*, 30(1), pp. 79–93. doi: 10.1080/02648725.2014.921502.
MARTIN, W. G., COOK, W. H. AND WINKLER, C. A. (1956) 'THE DETERMINATION OF PARTIAL SPECIFIC VOLUMES BY DIFFERENTIAL SEDIMENTATION', *Canadian Journal of Chemistry*, 34(6), pp. 809–814. doi: 10.1139/v56-104.
MARTIN, W. G., WINKLER, C. A. AND COOK, W. H. (1959) 'PARTIAL SPECIFIC VOLUME MEASUREMENTS BY DIFFERENTIAL SEDIMENTATION', *Canadian Journal of Chemistry*. NRC Research Press, 37(10), pp. 1662–1670. doi: 10.1139/v59-241.
MASSON, S., KERN, T., LE GOUËLLEC, A., GIUSTINI, C., SIMORRE, J.-P., CALLOW, P., VERNET, T., GABEL, F. AND ZAPUN, A. (2009) 'Central Domain of DivIB Caps the C-terminal Regions of the FtsL/DivIC Coiled-coil Rod', *Journal of Biological Chemistry*, 284(40), pp. 27687–27700. doi: 10.1074/jbc.M109.019471.
MCCARTY, R. M., SOMOGYI, A., LIN, G., JACOBSEN, N. E. AND BANDARIAN, V. (2009) 'The Deazapurine Biosynthetic Pathway Revealed: In Vitro Enzymatic Synthesis of PreQ 0 from Guanosine 5'-Triphosphate in Four Steps', *Biochemistry*, 48(18), pp. 3847–3852. doi: 10.1021/bi900400e.
MCQUADE, D. T., QUINN, M. A., YU, S. M., POLANS, A. S., KREBS, M. P. AND GELLMAN, S. H. (2000)

'Rigid Amphiphiles for Membrane Protein Manipulation', *Angewandte Chemie International Edition*. doi: 10.1002/(sici)1521-3773(20000218)39:4<758::aid-anie758>3.0.co;2-v.
MEESKE, A. J., RILEY, E. P., ROBINS, W. P., UEHARA, T., MEKALANOS, J. J., KAHNE, D., WALKER, S., KRUSE, A. C., BERNHARDT, T. G. AND RUDNER, D. Z. (2016) 'SEDS proteins are a widespread family of bacterial cell wall polymerases', *Nature*, 537(7622), pp. 634–638. doi: 10.1038/nature19331.
MEINHARDT, H. AND DE BOER, P. A. J. (2001) 'Pattern formation in Escherichia coli: A model for the pole-to-pole oscillations of Min proteins and the localization of the division site', *Proceedings of the National Academy of Sciences*, 98(25), pp. 14202–14207. doi: 10.1073/pnas.251216598.
MERCER, K. L. N. AND WEISS, D. S. (2002) 'The Escherichia coli cell division protein FtsW is required to recruit its cognate transpeptidase, FtsI (PBP3), to the division site', *Journal of Bacteriology*. doi: 10.1128/jb.184.4.904-912.2002.
MICHELSEN, O. (2003) 'Precise determinations of C and D periods by flow cytometry in Escherichia coli K-12 and B/r', *Microbiology*, 149(4), pp. 1001–1010. doi: 10.1099/mic.0.26058-0.
MILES, A. J. AND WALLACE, B. A. (2016) 'Circular dichroism spectroscopy of membrane proteins', *Chemical Society Reviews*, 45(18), pp. 4859–4872. doi: 10.1039/C5CS00084J.
MILEYKOVSKAYA, E. AND DOWHAN, W. (2000) 'Visualization of phospholipid domains in Escherichia coli by using the cardiolipin-specific fluorescent dye 10-N-nonyl acridine orange', *Journal of Bacteriology*. doi: 10.1128/JB.182.4.1172-1175.2000.
MOHAMMADI, T., VAN DAM, V., SIJBRANDI, R., VERNET, T., ZAPUN, A., BOUHSS, A., DIEPEVEEN-DE BRUIN, M., NGUYEN-DISTÈCHE, M., DE KRUIJFF, B. AND BREUKINK, E. (2011) 'Identification of FtsW as a transporter of lipid-linked cell wall precursors across the membrane', *The EMBO Journal*, 30(8), pp. 1425–1432. doi: 10.1038/emboj.2011.61.
MOLODENSKIY, D., SHIRSHIN, E., TIKHONOVA, T., GRUZINOV, A., PETERS, G. AND SPINOZZI, F. (2017) 'Thermally induced conformational changes and protein–protein interactions of bovine serum albumin in aqueous solution under different pH and ionic strengths as revealed by SAXS measurements', *Physical Chemistry Chemical Physics*, 19(26), pp. 17143–17155. doi: 10.1039/C6CP08809K.
MORAIS, M. C., KANAMARU, S., BADASSO, M. O., KOTI, J. S., OWEN, B. A. L., MCMURRAY, C. T., ANDERSON, D. L. AND ROSSMANN, M. G. (2003) 'Bacteriophage ϕ29 scaffolding protein gp7 before and after prohead assembly', *Nature Structural & Molecular Biology*, 10(7), pp. 572–576. doi: 10.1038/nsb939.
MOUTINHO, I. M. T., FERREIRA, P. J. T. AND FIGUEIREDO, M. L. (2007) 'Impact of Surface Sizing on Inkjet Printing Quality', *Industrial & Engineering Chemistry Research*, 46(19), pp. 6183–6188. doi: 10.1021/ie070356k.
MÜHLMANN, M., FORSTEN, E., NOACK, S. AND BÜCHS, J. (2017) 'Optimizing recombinant protein expression via automated induction profiling in microtiter plates at different temperatures', *Microbial Cell Factories*. doi: 10.1186/s12934-017-0832-4.
MUKHERJEE, A. (1998) 'Dynamic assembly of FtsZ regulated by GTP hydrolysis', *The EMBO Journal*, 17(2), pp. 462–469. doi: 10.1093/emboj/17.2.462.
NASR, M. L. AND SINGH, S. K. (2014) 'Radioligand Binding to Nanodisc-Reconstituted Membrane Transporters Assessed by the Scintillation Proximity Assay', *Biochemistry*, 53(1), pp. 4–6. doi: 10.1021/bi401412e.

ONCLEY, J. L., SCATCHARD, G. AND BROWN, A. (1947) 'Physical-chemical Characteristics of Certain of the Proteins of Normal Human Plasma.', *The Journal of Physical and Colloid Chemistry*, 51(1), pp. 184–198. doi: 10.1021/j150451a014.
PARK, K.-T., DAJKOVIC, A., WISSEL, M., DU, S. AND LUTKENHAUS, J. (2018) 'MinC and FtsZ mutant analysis provides insight into MinC/MinD-mediated Z ring disassembly', *Journal of Biological Chemistry*, 293(16), pp. 5834–5846. doi: 10.1074/jbc.M117.815894.
PARMAR, M., RAWSON, S., SCARFF, C. A., GOLDMAN, A., DAFFORN, T. R., MUENCH, S. P. AND POSTIS, V. L. G. (2018) 'Using a SMALP platform to determine a sub-nm single particle cryo-EM membrane protein structure', *Biochimica et Biophysica Acta (BBA) - Biomembranes*, 1860(2), pp. 378–383. doi: 10.1016/j.bbamem.2017.10.005.
PENG, Y., LUO, Y., YU, T., XU, X., FAN, K., ZHAO, Y. AND YANG, K. (2011) 'A Blue Native-PAGE analysis of membrane protein complexes in Clostridium thermocellum', *BMC Microbiology*, 11(1), p. 22. doi: 10.1186/1471-2180-11-22.
PETRACHE, H. I., TRISTRAM-NAGLE, S. AND NAGLE, J. F. (1998) 'Fluid phase structure of EPC and DMPC bilayers', *Chemistry and Physics of Lipids*, 95(1), pp. 83–94. doi: 10.1016/S0009-3084(98)00068-1.
PICHOFF, S. (2002) 'Unique and overlapping roles for ZipA and FtsA in septal ring assembly in Escherichia coli', *The EMBO Journal*, 21(4), pp. 685–693. doi: 10.1093/emboj/21.4.685.
PICHOFF, S. AND LUTKENHAUS, J. (2005) 'Tethering the Z ring to the membrane through a conserved membrane targeting sequence in FtsA', *Molecular Microbiology*, 55(6), pp. 1722–1734. doi: 10.1111/j.1365-2958.2005.04522.x.
PICHOFF, S., SHEN, B., SULLIVAN, B. AND LUTKENHAUS, J. (2012) 'FtsA mutants impaired for self-interaction bypass ZipA suggesting a model in which FtsA's self-interaction competes with its ability to recruit downstream division proteins', *Molecular Microbiology*, 83(1), pp. 151–167. doi: 10.1111/j.1365-2958.2011.07923.x.
POLLOCK, N. L. *ET AL.* (2019) 'SMA-PAGE: A new method to examine complexes of membrane proteins using SMALP nano-encapsulation and native gel electrophoresis', *Biochimica et Biophysica Acta (BBA) - Biomembranes*, 1861(8), pp. 1437–1445. doi: 10.1016/j.bbamem.2019.05.011.
POPOT, J.-L. *ET AL.* (2003) 'Amphipols: polymeric surfactants for membrane biology research', *Cellular and Molecular Life Sciences (CMLS)*. Birkhäuser-Verlag, 60(8), pp. 1559–1574. doi: 10.1007/s00018-003-3169-6.
POPOT, J.-L. (2010) 'Amphipols, Nanodiscs, and Fluorinated Surfactants: Three Nonconventional Approaches to Studying Membrane Proteins in Aqueous Solutions', *Annual Review of Biochemistry*. doi: 10.1146/annurev.biochem.052208.114057.
POSTIS, V., RAWSON, S., MITCHELL, J. K., LEE, S. C., PARSLOW, R. A., DAFFORN, T. R., BALDWIN, S. A. AND MUENCH, S. P. (2015) 'The use of SMALPs as a novel membrane protein scaffold for structure study by negative stain electron microscopy.', *Biochimica et biophysica acta*. Elsevier B.V., 1848(2), pp. 496–501. doi: 10.1016/j.bbamem.2014.10.018.
PRIVÉ, G. G. (2007) 'Detergents for the stabilization and crystallization of membrane proteins', *Methods*. doi: 10.1016/j.ymeth.2007.01.007.
PROVERBIO, D., ROOS, C., BEYERMANN, M., ORBÁN, E., DÖTSCH, V. AND BERNHARD, F. (2013) 'Functional properties of cell-free expressed human endothelin A and endothelin B receptors in artificial membrane environments', *Biochimica et Biophysica Acta - Biomembranes*. doi:

10.1016/j.bbamem.2013.05.031.
RASKIN, D. M. AND DE BOER, P. A. (1999) 'Rapid pole-to-pole oscillation of a protein required for directing division to the middle of Escherichia coli.', *Proceedings of the National Academy of Sciences of the United States of America*, 96(9), pp. 4971–6. doi: 10.1073/pnas.96.9.4971.
RATH, A., GLIBOWICKA, M., NADEAU, V. G., CHEN, G. AND DEBER, C. M. (2009) 'Detergent binding explains anomalous SDS-PAGE migration of membrane proteins', *Proceedings of the National Academy of Sciences of the United States of America*. doi: 10.1073/pnas.0813167106.
READING, E., HALL, Z., MARTENS, C., HAGHIGHI, T., FINDLAY, H., AHDASH, Z., POLITIS, A. AND BOOTH, P. J. (2017) 'Interrogating Membrane Protein Conformational Dynamics within Native Lipid Compositions', *Angewandte Chemie - International Edition*. doi: 10.1002/anie.201709657.
RENNER, L. D. AND WEIBEL, D. B. (2011) 'Cardiolipin microdomains localize to negatively curved regions of Escherichia coli membranes', *Proceedings of the National Academy of Sciences of the United States of America*. doi: 10.1073/pnas.1015757108.
RODRÍGUEZ-DÍAZ, J., RUBIO-DEL-CAMPO, A. AND YEBRA, M. J. (2012) 'Regulatory insights into the production of UDP-N-acetylglucosamine by Lactobacillus casei.', *Bioengineered*, 3(6), pp. 339–42. doi: 10.4161/bioe.21271.
ROHS, P. D. A., BUSS, J., SIM, S. I., SQUYRES, G. R., SRISUKNIMIT, V., SMITH, M., CHO, H., SJODT, M., KRUSE, A. C., GARNER, E. C., WALKER, S., KAHNE, D. E. AND BERNHARDT, T. G. (2018) 'A central role for PBP2 in the activation of peptidoglycan polymerization by the bacterial cell elongation machinery', *PLOS Genetics*. Edited by P. H. Viollier, 14(10), p. e1007726. doi: 10.1371/journal.pgen.1007726.
ROMANTSOV, T., HELBIG, S., CULHAM, D. E., GILL, C., STALKER, L. AND WOOD, J. M. (2007) 'Cardiolipin promotes polar localization of osmosensory transporter ProP in Escherichia coli', *Molecular Microbiology*, 64(6), pp. 1455–1465. doi: 10.1111/j.1365-2958.2007.05727.x.
ROSENBUSCH, J. P. (2001) 'Stability of membrane proteins: Relevance for the selection of appropriate methods for high-resolution structure determinations', *Journal of Structural Biology*. doi: 10.1006/jsbi.2001.4431.
RUIZ, N. (2008) 'Bioinformatics identification of MurJ (MviN) as the peptidoglycan lipid II flippase in Escherichia coli', *Proceedings of the National Academy of Sciences*, 105(40), pp. 15553–15557. doi: 10.1073/pnas.0808352105.
SÁNCHEZ-PULIDO, L., DEVOS, D., GENEVROIS, S., VICENTE, M. AND VALENCIA, A. (2003) 'POTRA: a conserved domain in the FtsQ family and a class of β-barrel outer membrane proteins', *Trends in Biochemical Sciences*, 28(10), pp. 523–526. doi: 10.1016/j.tibs.2003.08.003.
SCHÄGGER, H. AND VON JAGOW, G. (1991) 'Blue native electrophoresis for isolation of membrane protein complexes in enzymatically active form', *Analytical Biochemistry*, 199(2), pp. 223–231. doi: 10.1016/0003-2697(91)90094-A.
SCHEIDELAAR, S., KOORENGEVEL, M. C., PARDO, J. D., MEELDIJK, J. D., BREUKINK, E. AND KILLIAN, J. A. (2015) 'Molecular model for the solubilization of membranes into nanodisks by styrene maleic Acid copolymers.', *Biophysical journal*. Biophysical Society, 108(2), pp. 279–90. doi: 10.1016/j.bpj.2014.11.3464.
SCHEIDELAAR, S., KOORENGEVEL, M. C., VAN WALREE, C. A., DOMINGUEZ, J. J., DÖRR, J. M. AND KILLIAN, J. A. (2016) 'Effect of Polymer Composition and pH on Membrane Solubilization by Styrene-Maleic Acid Copolymers', *Biophysical Journal*, 111(9), pp. 1974–1986. doi:

10.1016/j.bpj.2016.09.025.
SCHLAGER, B., STRAESSLE, A. AND HAFEN, E. (2012) 'Use of anionic denaturing detergents to purify insoluble proteins after overexpression', *BMC Biotechnology*. doi: 10.1186/1472-6750-12-95.
SCHMIDT, K. L., PETERSON, N. D., KUSTUSCH, R. J., WISSEL, M. C., GRAHAM, B., PHILLIPS, G. J. AND WEISS, D. S. (2004) 'A Predicted ABC Transporter, FtsEX, Is Needed for Cell Division in Escherichia coli', *Journal of Bacteriology*, 186(3), pp. 785–793. doi: 10.1128/JB.186.3.785-793.2004.
SCHUCK, P. (2000) 'Size-Distribution Analysis of Macromolecules by Sedimentation Velocity Ultracentrifugation and Lamm Equation Modeling', *Biophysical Journal*, 78(3), pp. 1606–1619. doi: 10.1016/S0006-3495(00)76713-0.
SEDDON, A. M., CURNOW, P. AND BOOTH, P. J. (2004) 'Membrane proteins, lipids and detergents: not just a soap opera', *Biochimica et Biophysica Acta (BBA) - Biomembranes*, 1666(1–2), pp. 105–117. doi: 10.1016/j.bbamem.2004.04.011.
SHAM, L.-T., BUTLER, E. K., LEBAR, M. D., KAHNE, D., BERNHARDT, T. G. AND RUIZ, N. (2014) 'MurJ is the flippase of lipid-linked precursors for peptidoglycan biogenesis', *Science*, 345(6193), pp. 220–222. doi: 10.1126/science.1254522.
SKOOG, K. AND DALEY, D. O. (2012) 'The Escherichia coli Cell Division Protein ZipA Forms Homodimers Prior to Association with FtsZ', *Biochemistry*, 51(7), pp. 1407–1415. doi: 10.1021/bi2015647.
SPRATT, B. G. (1975) 'Distinct penicillin binding proteins involved in the division, elongation, and shape of Escherichia coli K12.', *Proceedings of the National Academy of Sciences of the United States of America*, 72(8), pp. 2999–3003. doi: 10.1073/pnas.72.8.2999.
STAUBACH, S. AND HANISCH, F.-G. (2011) 'Lipid rafts: signaling and sorting platforms of cells and their roles in cancer', *Expert Review of Proteomics*, 8(2), pp. 263–277. doi: 10.1586/epr.11.2.
STETSENKO, A. AND GUSKOV, A. (2017) 'An overview of the top ten detergents used for membrane protein crystallization', *Crystals*. doi: 10.3390/cryst7070197.
STOUF, M., MEILE, J.-C. AND CORNET, F. (2013) 'FtsK actively segregates sister chromosomes in Escherichia coli', *Proceedings of the National Academy of Sciences*, 110(27), pp. 11157–11162. doi: 10.1073/pnas.1304080110.
STROUD, Z., HALL, S. C. L. AND DAFFORN, T. R. (2018) 'Purification of membrane proteins free from conventional detergents: SMA, new polymers, new opportunities and new insights', *Methods*, 147, pp. 106–117. doi: 10.1016/j.ymeth.2018.03.011.
SUN, C., BENLEKBIR, S., VENKATAKRISHNAN, P., WANG, Y., HONG, S., HOSLER, J., TAJKHORSHID, E., RUBINSTEIN, J. L. AND GENNIS, R. B. (2018) 'Structure of the alternative complex III in a supercomplex with cytochrome oxidase', *Nature*. doi: 10.1038/s41586-018-0061-y.
SZETO, T. H., ROWLAND, S. L., HABRUKOWICH, C. L. AND KING, G. F. (2003) 'The MinD Membrane Targeting Sequence Is a Transplantable Lipid-binding Helix', *Journal of Biological Chemistry*, 278(41), pp. 40050–40056. doi: 10.1074/jbc.M306876200.
TAGUCHI, A., WELSH, M. A., MARMONT, L. S., LEE, W., SJODT, M., KRUSE, A. C., KAHNE, D., BERNHARDT, T. G. AND WALKER, S. (2019) 'FtsW is a peptidoglycan polymerase that is functional only in complex with its cognate penicillin-binding protein', *Nature Microbiology*, 4(4), pp. 587–594. doi: 10.1038/s41564-018-0345-x.
TAM, Y., ALLAUDIN, Z., LILA, M. A., BAHAMAN, A., TAN, J. AND REZAEI, M. (2012) 'Enhanced cell disruption strategy in the release of recombinant hepatitis B surface antigen from Pichia pastoris using response surface methodology', *BMC Biotechnology*, 12(1), p. 70. doi:

10.1186/1472-6750-12-70.
TEO, A. C. K., LEE, S. C., POLLOCK, N. L., STROUD, Z., HALL, S., THAKKER, A., PITT, A. R., DAFFORN, T. R., SPICKETT, C. M. AND ROPER, D. I. (2019) 'Analysis of SMALP co-extracted phospholipids shows distinct membrane environments for three classes of bacterial membrane protein', *Scientific Reports*, 9(1), p. 1813. doi: 10.1038/s41598-018-37962-0.
TONGE, S. (2006) 'Compositions Comprising a Lipid and Copolymer of Styrene and Maleic Acid'.
TONGE, S. . AND TIGHE, B. . (2001) 'Responsive hydrophobically associating polymers: a review of structure and properties', *Advanced Drug Delivery Reviews*, 53(1), pp. 109–122. doi: 10.1016/S0169-409X(01)00223-X.
TONGE, S. AND TIGHE, B. (2003) 'Lipid-containing Compositions and Uses Therefore'. EP.
TONTHAT, N. K., AROLD, S. T., PICKERING, B. F., VAN DYKE, M. W., LIANG, S., LU, Y., BEURIA, T. K., MARGOLIN, W. AND SCHUMACHER, M. A. (2011) 'Molecular mechanism by which the nucleoid occlusion factor, SlmA, keeps cytokinesis in check', *The EMBO Journal*, 30(1), pp. 154–164. doi: 10.1038/emboj.2010.288.
TRIBET, C., AUDEBERT, R. AND POPOT, J.-L. (1996) 'Amphipols: Polymers that keep membrane proteins soluble in aqueous solutions', *Proceedings of the National Academy of Sciences*, 93(26), pp. 15047–15050. doi: 10.1073/pnas.93.26.15047.
TYPAS, A., BANZHAF, M., GROSS, C. A. AND VOLLMER, W. (2012) 'From the regulation of peptidoglycan synthesis to bacterial growth and morphology', *Nature Reviews Microbiology*, 10(2), pp. 123–136. doi: 10.1038/nrmicro2677.
UEHARA, T., PARZYCH, K. R., DINH, T. AND BERNHARDT, T. G. (2010) 'Daughter cell separation is controlled by cytokinetic ring-activated cell wall hydrolysis', *The EMBO Journal*, 29(8), pp. 1412–1422. doi: 10.1038/emboj.2010.36.
VEGA, D. E. AND MARGOLIN, W. (2019) 'Direct interaction between the two Z ring membrane anchors FtsA and ZipA', *Journal of Bacteriology*. doi: 10.1128/JB.00579-18.
DI VENTURA, B., KNECHT, B., ANDREAS, H., GODINEZ, W. J., FRITSCHE, M., ROHR, K., NICKEL, W., HEERMANN, D. W. AND SOURJIK, V. (2014) 'Chromosome segregation by the Escherichia coli Min system', *Molecular Systems Biology*, 9(1), pp. 686–686. doi: 10.1038/msb.2013.44.
VILLANELO, F., ORDENES, A., BRUNET, J., LAGOS, R. AND MONASTERIO, O. (2011) 'A model for the Escherichia coli FtsB/FtsL/FtsQ cell division complex.', *BMC structural biology*, 11, p. 28. doi: 10.1186/1472-6807-11-28.
VINELLA, D., CASHEL, M. AND D'ARI, R. (2000) 'Selected amplification of the cell division genes ftsQ-ftsA-ftsZ in Escherichia coli.', *Genetics*. United States, 156(4), pp. 1483–92. Available at: http://www.ncbi.nlm.nih.gov/pubmed/11102351.
VOLKOV, V. V. AND SVERGUN, D. I. (2003) 'Uniqueness of ab initio shape determination in small-angle scattering', in *Journal of Applied Crystallography*. doi: 10.1107/S0021889803000268.
VOLLMER, W., BLANOT, D. AND DE PEDRO, M. A. (2008) 'Peptidoglycan structure and architecture', *FEMS Microbiology Reviews*, 32(2), pp. 149–167. doi: 10.1111/j.1574-6976.2007.00094.x.
VOLLMER, W., JORIS, B., CHARLIER, P. AND FOSTER, S. (2008) 'Bacterial peptidoglycan (murein) hydrolases', *FEMS Microbiology Reviews*, 32(2), pp. 259–286. doi: 10.1111/j.1574-6976.2007.00099.x.
WADENPOHL, I. AND BRAMKAMP, M. (2010) 'DivIC stabilizes FtsL against RasP cleavage.', *Journal of bacteriology*, 192(19), pp. 5260–3. doi: 10.1128/JB.00287-10.

WELSH, M. A., SCHAEFER, K., TAGUCHI, A., KAHNE, D. AND WALKER, S. (2019) 'The direction of chain growth and substrate preferences of SEDS-family peptidoglycan glycosyltransferases', *Journal of the American Chemical Society*. American Chemical Society, p. jacs.9b06358. doi: 10.1021/jacs.9b06358.
WILLIAMS, J. J. (2007) 'Formulation of Carpet Cleaners', in *Handbook for Cleaning/Decontamination of Surfaces*. Elsevier, pp. 103–123. doi: 10.1016/B978-044451664-0/50004-8.
YADAVALLI, S. S., CAREY, J. N., LEIBMAN, R. S., CHEN, A. I., STERN, A. M., ROGGIANI, M., LIPPA, A. M. AND GOULIAN, M. (2016) 'Antimicrobial peptides trigger a division block in Escherichia coli through stimulation of a signalling system', *Nature Communications*, 7(1), p. 12340. doi: 10.1038/ncomms12340.
YAHASHIRI, A., JORGENSON, M. A. AND WEISS, D. S. (2017) 'The SPOR Domain, a Widely Conserved Peptidoglycan Binding Domain That Targets Proteins to the Site of Cell Division', *Journal of Bacteriology*. Edited by W. Margolin, 199(14). doi: 10.1128/JB.00118-17.
YANG, D. C., PETERS, N. T., PARZYCH, K. R., UEHARA, T., MARKOVSKI, M. AND BERNHARDT, T. G. (2011) 'An ATP-binding cassette transporter-like complex governs cell-wall hydrolysis at the bacterial cytokinetic ring', *Proceedings of the National Academy of Sciences*, 108(45), pp. E1052–E1060. doi: 10.1073/pnas.1107780108.
YU, X. C., TRAN, A. H., SUN, Q. AND MARGOLIN, W. (1998) 'Localization of cell division protein FtsK to the Escherichia coli septum and identification of a potential N-Terminal targeting domain', *Journal of Bacteriology*.
ZHOU, Y. (2001) 'Inactivation mechanism of the membrane protein diacylglycerol kinase in detergent solution', *Protein Science*. doi: 10.1110/ps.34201.
EL ZOEIBY, A., SANSCHAGRIN, F. AND LEVESQUE, R. C. (2003) 'Structure and function of the Mur enzymes: Development of novel inhibitors', *Molecular Microbiology*. doi: 10.1046/j.1365-2958.2003.03289.x.
ZOONENS, M. AND POPOT, J. L. (2014) 'Amphipols for Each Season', *Journal of Membrane Biology*. doi: 10.1007/s00232-014-9666-8.